RECENT ADVANCES IN CARDIOTOXICITY TESTING

EDITED BY: Tamer M. A. Mohamed, Javid Moslehi and Jonathan Satin
PUBLISHED IN: Frontiers in Pharmacology

frontiers Research Topics

ISSN 1664-8714
ISBN 978-2-88971-954-9
DOI 10.3389/978-2-88971-954-9

About Frontiers

Frontiers is more than just an open-access publisher of scholarly articles: it is a pioneering approach to the world of academia, radically improving the way scholarly research is managed. The grand vision of Frontiers is a world where all people have an equal opportunity to seek, share and generate knowledge. Frontiers provides immediate and permanent online open access to all its publications, but this alone is not enough to realize our grand goals.

Frontiers Journal Series

The Frontiers Journal Series is a multi-tier and interdisciplinary set of open-access, online journals, promising a paradigm shift from the current review, selection and dissemination processes in academic publishing. All Frontiers journals are driven by researchers for researchers; therefore, they constitute a service to the scholarly community. At the same time, the Frontiers Journal Series operates on a revolutionary invention, the tiered publishing system, initially addressing specific communities of scholars, and gradually climbing up to broader public understanding, thus serving the interests of the lay society, too.

Dedication to Quality

Each Frontiers article is a landmark of the highest quality, thanks to genuinely collaborative interactions between authors and review editors, who include some of the world's best academicians. Research must be certified by peers before entering a stream of knowledge that may eventually reach the public - and shape society; therefore, Frontiers only applies the most rigorous and unbiased reviews.
Frontiers revolutionizes research publishing by freely delivering the most outstanding research, evaluated with no bias from both the academic and social point of view.
By applying the most advanced information technologies, Frontiers is catapulting scholarly publishing into a new generation.

What are Frontiers Research Topics?

Frontiers Research Topics are very popular trademarks of the Frontiers Journals Series: they are collections of at least ten articles, all centered on a particular subject. With their unique mix of varied contributions from Original Research to Review Articles, Frontiers Research Topics unify the most influential researchers, the latest key findings and historical advances in a hot research area! Find out more on how to host your own Frontiers Research Topic or contribute to one as an author by contacting the Frontiers Editorial Office: frontiersin.org/about/contact

RECENT ADVANCES IN CARDIOTOXICITY TESTING

Topic Editors:

Tamer M. A. Mohamed, University of Louisville, United States
Javid Moslehi, Vanderbilt University Medical Center, United States
Jonathan Satin, University of Kentucky, United States

Citation: Mohamed, T. M. A., Moslehi, J., Satin, J., eds. (2021). Recent Advances in Cardiotoxicity Testing. Lausanne: Frontiers Media SA.
doi: 10.3389/978-2-88971-954-9

Table of Contents

frontiers in Pharmacology

EDITORIAL
published: 08 November 2021
doi: 10.3389/fphar.2021.798189

Editorial: Recent Advances in Cardiotoxicity Testing

Tamer M. A. Mohamed[1,2], Javid Moslehi[3] and Jonathan Satin[4]*

[1]Department of Medicine, The Institute of Molecular Cardiology, University of Louisville, Louisville, KY, United States, [2]Department of Medicine, Diabetes and Obesity Center, Envirome Institute, University of Louisville, Louisville, KY, United States, [3]Department of Cardio-oncology, University of California, San Francisco, San Francisco, CA, United States, [4]Department of Physiology, University of Kentucky, Lexington, KY, United States

Keywords: cancer, cardiooncology, heart, toxicity, hiPS cardiomycytes, heart slices

Editorial on the Research Topic

Recent Advances in Cardiotoxicity Testing

OPEN ACCESS

Edited and reviewed by:
Francesco Rossi,
University of Campania Luigi Vanvitelli,
Italy

****Correspondence:***
Tamer M. A. Mohamed
tamer.mohamed@louisville.edu

Specialty section:
This article was submitted to Cardiovascular and Smooth Muscle Pharmacology, a section of the journal Frontiers in Pharmacology

Received: *19 October 2021*
Accepted: *26 October 2021*
Published: *08 November 2021*

Citation:
Mohamed TMA, Moslehi J and Satin J (2021) Editorial: Recent Advances in Cardiotoxicity Testing. Front. Pharmacol. 12:798189. doi: 10.3389/fphar.2021.798189

INTRODUCTION

Drug induced cardiotoxicity is a major cause of market withdrawal (Onakpoya et al., 2016). In the last decade of the 20th century, eight non-cardiovascular drugs were withdrawn from clinical use because they prolonged the QT interval (Fermini and Fossa, 2003), resulting in ventricular arrhythmias and potentially sudden death. In particular, the last decade has seen an explosion of cancer therapies, which while effective can lead to several cardiovascular toxicities. Both traditional (e.g., anthracyclines and radiation) and targeted (e.g., trastuzumab) therapies can result in cardiovascular complications in a subset of patients (Groarke et al., 2013; Moslehi, 2016). A close collaboration between cardiologists and oncologists (via the emerging field of "cardio-oncology") had helped make these complications manageable ensuring that patients can be treated effectively (Campia et al., 2019). An explosion of novel therapies which include newer kinase inhibitors, proteolysis-targeting chimera (PROTAC) and immune-based therapies expand the oncology armamentarium, each drug with its own potential cardiovascular toxicity (Sheng et al., 2016; Fleming et al., 2021). Therefore, there is a growing need for reliable preclinical screening strategies for CV toxicities associated with emerging breast cancer therapies prior to human clinical trials. The most prevalently used cardiac physiology screening platform are animal models that have limited reliability in mirroring the effects of drugs in human hearts (Liu et al., 2006; Salama and Bett, 2014; Asnani et al., 2021). Additionally, the use of animal models to create a pharmacokinetic profile of drugs is relatively expensive at the early development stage since large amounts of the drugs are used (Guth et al., 2019). Ultimately, the ideal experimental cardiac tissue culture model is the one that demonstrates high sensitivity and specificity towards various therapeutic and pharmacological interventions while accurately replicating the physiology and pathophysiology of the human heart (Wang et al., 2008). The recent move towards the use of human induced pluripotent stem cell-derived cardiomyocytes (hiPS-CMs) (Burridge et al., 2016) and human heart slices (Ou et al., 2019; Miller et al., 2020; Ou et al., 2020) in cardiotoxicity testing provided a potential solution to address this issue. In this special issue we have 12 manuscripts, seven review articles and five original research articles summarizing the recent advances in cardiotoxicity testing.

Jaeger et al. used a novel computer simulation to identifying drug response through combining several assessments of the membrane potential, the cytosolic calcium concentration, and the extracellular potential in microphysiological systems. In another effort for in silico modeling of cardiotoxicity, Paci et al., assessed the response of three human stem cell derived cardiomyocytes (hSC-CMs) in silico models to simulate drug action, and compare simulation results against *in vitro* data for 15 drugs. Furthermore, in an effort to create a novel high-throughput platform to detect cardiotoxicity for atrial arrhythmias, Honda et al. (2021) created and validated a high-throughput drug screening system based on hiPS-derived-atrial myocytes. In the same vein, Verkerk et al. optimized a dynamic clamp system to obtain patch-clamp recordings of action potentials from adult primary human atrial myocytes. This technology will be useful in detecting arrhythmogenic cardiotoxins on adult human hearts. The same first author, Dr. Verkerk with other team of collaborators have modeled a prominent cause of arrhythmia in patients with a deficiency in very long-chain acyl-CoA dehydrogenase (VLCAD), an enzyme that is involved in the mitochondrial beta-oxidation of long-chain fatty acids. They generated hiPSC-CMs from VLCAD deficiency patients and they tested the effect of carnitine supplement on attenuating the arrhythmic potential; however, it was not effective.

This special issue includes seven great reviews and perspectives of different topics related to cardiotoxicity testing. Szabo et al. provided a perspective regarding novel anticancer therapeutics to prevent tumorigenesis without cardiotoxic effects highlighting a new family of therapeutics including ERK dimerization inhibitors and BAX allosteric inhibitors. Campana et al. provided a perspective regarding the role of inflammation in cardiotoxicity and how inflammation should be accounted for during drug screening in early stages of drug development. Thomas et al., Keung et al., and Orsolits et al. have provided three comprehensive reviews for the cellular and tissue models derived from hiPS cells and their recent uses to assess cardiotoxicity of cancer therapies. Furthermore, Tu et al. wrote a mini review regarding the use of hiPS-derived cells as a screening platform for drug-induced vascular toxicity. hiPSC-CM systems are ideal for high-throughput testing and for proof-of-principle evaluations of patient-specific genetic backgrounds or disease mutations; however, the incomplete maturation and lack of multicellularity creates caveats. The use of slice preparations is an exciting advance in test platforms because this native tissue preparation retains phenotypic properties *in vitro* (Ou et al., 2019; Miller et al., 2020; Ou et al., 2020). Finally, Meki et al. reviewed the use of adult human and pig heart slices in cardiotoxicity testing.

Overall, this special issue provides an overview of the novel platforms used for cardiotoxicity testing. This field of research is evolving rapidly, and it ultimately holds promise for more reliable and sensitive drug and chemical screening.

AUTHOR CONTRIBUTIONS

All authors listed have made a substantial, direct, and intellectual contribution to the work and approved it for publication.

FUNDING

TM is supported by NIH grants R01HL147921 and P30GM127607 and American Heart Association grant 16SDG29950012. We also acknowledge the United States Department of Defense for the grant W81XWH-20-1-0419 (JS and TM).

REFERENCES

Asnani, A., Moslehi, J. J., Adhikari, B. B., Baik, A. H., Beyer, A. M., de Boer, R. A., et al. (2021). Preclinical Models of Cancer Therapy-Associated Cardiovascular Toxicity: A Scientific Statement from the American Heart Association. *Circ. Res.* 129, e21–e34. doi:10.1161/RES.0000000000000473

Burridge, P. W., Li, Y. F., Matsa, E., Wu, H., Ong, S. G., Sharma, A., et al. (2016). Human Induced Pluripotent Stem Cell-Derived Cardiomyocytes Recapitulate the Predilection of Breast Cancer Patients to Doxorubicin-Induced Cardiotoxicity. *Nat. Med.* 22, 547–556. doi:10.1038/nm.4087

Campia, U., Moslehi, J. J., Amiri-Kordestani, L., Barac, A., Beckman, J. A., Chism, D. D., et al. (2019). Cardio-Oncology: Vascular and Metabolic Perspectives: A Scientific Statement from the American Heart Association. *Circulation* 139, e579–e602. doi:10.1161/CIR.0000000000000641

Fermini, B., and Fossa, A. A. (2003). The Impact of Drug-Induced QT Interval Prolongation on Drug Discovery and Development. *Nat. Rev. Drug Discov.* 2, 439–447. doi:10.1038/nrd1108

Fleming, M. R., Xiao, L., Jackson, K. D., Beckman, J. A., Barac, A., and Moslehi, J. J. (2021). Vascular Impact of Cancer Therapies: The Case of BTK (Bruton Tyrosine Kinase) Inhibitors. *Circ. Res.* 128, 1973–1987. doi:10.1161/CIRCRESAHA.121.318259

Groarke, J. D., Cheng, S., and Moslehi, J. (2013). Cancer-drug Discovery and Cardiovascular Surveillance. *N. Engl. J. Med.* 369, 1779–1781. doi:10.1056/NEJMp1313140

Guth, B. D., Engwall, M., Eldridge, S., Foley, C. M., Guo, L., Gintant, G., et al. (2019). Considerations for an *In Vitro*, Cell-Based Testing Platform for Detection of Adverse Drug-Induced Inotropic Effects in Early Drug Development. Part 1: General Considerations for Development of Novel Testing Platforms. *Front. Pharmacol.* 10, 884. doi:10.3389/fphar.2019.00884

Honda, Y., Li, J., Hino, A., Tsujimoto, S., and Lee, J. K. (2021). High-Throughput Drug Screening System Based on Human Induced Pluripotent Stem Cell-Derived Atrial Myocytes ∼ A Novel Platform to Detect Cardiac Toxicity for Atrial Arrhythmias. *Front. Pharmacol.* 12, 680618. doi:10.3389/fphar.2021.680618

Liu, W., Ashford, M. W., Chen, J., Watkins, M. P., Williams, T. A., Wickline, S. A., et al. (2006). MR Tagging Demonstrates Quantitative Differences in Regional Ventricular wall Motion in Mice, Rats, and Men. *Am. J. Physiol. Heart Circ. Physiol.* 291, H2515–H2521. doi:10.1152/ajpheart.01016.2005

Miller, J. M., Meki, M. H., Ou, Q., George, S. A., Gams, A., Abouleisa, R. R. E., et al. (2020). Heart Slice Culture System Reliably Demonstrates Clinical Drug-Related Cardiotoxicity. *Toxicol. Appl. Pharmacol.* 406, 115213. doi:10.1016/j.taap.2020.115213

Moslehi, J. J. (2016). Cardiovascular Toxic Effects of Targeted Cancer Therapies. *N. Engl. J. Med.* 375, 1457–1467. doi:10.1056/NEJMra1100265

Onakpoya, I. J., Heneghan, C. J., and Aronson, J. K. (2016). Post-marketing Withdrawal of 462 Medicinal Products Because of Adverse Drug Reactions: a Systematic Review of the World Literature. *BMC Med.* 14, 10. doi:10.1186/s12916-016-0553-2

Ou, Q., Abouleisa, R. R. E., Tang, X. L., Juhardeen, H. R., Meki, M. H., Miller, J. M., et al. (2020). Slicing and Culturing Pig Hearts under Physiological Conditions. *J. Vis. Exp.* 20 (157). doi:10.3791/60913

Ou, Q., Jacobson, Z., Abouleisa, R. R. E., Tang, X. L., Hindi, S. M., Kumar, A., et al. (2019). Physiological Biomimetic Culture System for Pig and Human Heart Slices. *Circ. Res.* 125, 628–642. doi:10.1161/CIRCRESAHA.119.314996

Salama, G., and Bett, G. C. (2014). Sex Differences in the Mechanisms Underlying Long QT Syndrome. *Am. J. Physiol. Heart Circ. Physiol.* 307, H640–H648. doi:10.1152/ajpheart.00864.2013

Sheng, C. C., Amiri-Kordestani, L., Palmby, T., Force, T., Hong, C. C., Wu, J. C., et al. (2016). 21st Century Cardio-Oncology: Identifying Cardiac Safety Signals in the Era of Personalized Medicine. *JACC Basic Transl Sci.* 1, 386–398. doi:10.1016/j.jacbts.2016.05.008

Wang, D., Patel, C., Cui, C., and Yan, G. X. (2008). Preclinical Assessment of Drug-Induced Proarrhythmias: Role of the Arterially Perfused Rabbit Left Ventricular Wedge Preparation. *Pharmacol. Ther.* 119, 141–151. doi:10.1016/j.pharmthera.2008.02.009

Conflict of Interest: TM holds equities in Tenaya Therapeutics.

The remaining authors declare that the research was conducted in the absence of any commercial or financial relationships that could be construed as a potential conflict of interest.

frontiers in Pharmacology

ORIGINAL RESEARCH
published: 12 January 2021
doi: 10.3389/fphar.2020.616834

Electrophysiological Abnormalities in VLCAD Deficient hiPSC-Cardiomyocytes Do not Improve with Carnitine Supplementation

Arie O. Verkerk[1,2†], Suzan J. G. Knottnerus[3,4†], Vincent Portero[1], Jeannette C. Bleeker[3,4], Sacha Ferdinandusse[3], Kaomei Guan[5], Lodewijk IJlst[3], Gepke Visser[3,4], Ronald J. A. Wanders[3], Frits A. Wijburg[6], Connie R. Bezzina[1], Isabella Mengarelli[1] and Riekelt H. Houtkooper[3]**

[1]Department of Clinical and Experimental Cardiology, Heart Center, Amsterdam Cardiovascular Sciences, Amsterdam UMC, University of Amsterdam, Amsterdam, Netherlands, [2]Department of Medical Biology, Amsterdam Cardiovascular Sciences, Amsterdam UMC, University of Amsterdam, Amsterdam, Netherlands, [3]Laboratory Genetic Metabolic Diseases, Amsterdam UMC, University of Amsterdam, Amsterdam Gastroenterology and Metabolism, Amsterdam Cardiovascular Sciences, Amsterdam, Netherlands, [4]Department of Pediatric Metabolic Diseases, Wilhelmina Children's Hospital, University Medical Center Utrecht, Utrecht, Netherlands, [5]Institute of Pharmacology and Toxicology, Technische Universität Dresden, Dresden, Germany, [6]Department of Pediatric Metabolic Diseases, Emma Children's Hospital, Amsterdam UMC, University of Amsterdam, Amsterdam, Netherlands

Edited by:
Tamer M. A. Mohamed,
University of Louisville, United States

Reviewed by:
Jerry Vockley,
University of Pittsburgh, United States
Lukas Cyganek,
University Medical Center Göttingen, Germany
Eric Stephen Goetzman,
University of Pittsburgh, United States

***Correspondence:**
Connie R. Bezzina
c.r.bezzina@amsterdamumc.nl
Riekelt H. Houtkooper
r.h.houtkooper@amsterdamumc.nl

†These authors have contributed equally to this work.

Specialty section:
This article was submitted to Cardiovascular and Smooth Muscle Pharmacology, a section of the journal Frontiers in Pharmacology

Received: 13 October 2020
Accepted: 24 November 2020
Published: 12 January 2021

Citation:
Verkerk AO, Knottnerus SJG, Portero V, Bleeker JC, Ferdinandusse S, Guan K, IJlst L, Visser G, Wanders RJA, Wijburg FA, Bezzina CR, Mengarelli I and Houtkooper RH (2021) Electrophysiological Abnormalities in VLCAD Deficient hiPSC-Cardiomyocytes Do not Improve with Carnitine Supplementation. Front. Pharmacol. 11:616834. doi: 10.3389/fphar.2020.616834

Patients with a deficiency in very long-chain acyl-CoA dehydrogenase (VLCAD), an enzyme that is involved in the mitochondrial beta-oxidation of long-chain fatty acids, are at risk for developing cardiac arrhythmias. In human induced pluripotent stem cell derived cardiomyocytes (hiPSC-CMs), VLCAD deficiency (VLCADD) results in a series of abnormalities, including: 1) accumulation of long-chain acylcarnitines, 2) action potential shortening, 3) higher systolic and diastolic intracellular Ca^{2+} concentrations, and 4) development of delayed afterdepolarizations. In the fatty acid oxidation process, carnitine is required for bidirectional transport of acyl groups across the mitochondrial membrane. Supplementation has been suggested as potential therapeutic approach in VLCADD, but its benefits are debated. Here, we studied the effects of carnitine supplementation on the long-chain acylcarnitine levels and performed electrophysiological analyses in VLCADD patient-derived hiPSC-CMs with a *ACADVL* gene mutation (p.Val283Ala/p.Glu381del). Under standard culture conditions, VLCADD hiPSC-CMs showed high concentrations of long-chain acylcarnitines, short action potentials, and high delayed afterdepolarizations occurrence. Incubation of the hiPSC-CMs with 400 µM L-carnitine for 48 h led to increased long-chain acylcarnitine levels both in medium and cells. In addition, carnitine supplementation neither restored abnormal

Abbreviations: AP, action potential; APA, maximal action potential amplitude; APD_{20}, action potential duration at 20% repolarization; APD_{50}, action potential duration at 50% repolarization; APD_{90}, action potential duration at 90% repolarization; Ca_i^{2+}, intracellular Ca^{2+}; C_m, cell membrane capacitance; DAD, delayed afterdepolarization; EAD, early afterdepolarization; hiPSC-CMs, human induced pluripotent stem cell derived cardiomyocytes; hiPSCs, human induced pluripotent stem cells; $I_{Ca,L}$, L-type Ca^{2+} current; I_{K1}, inward rectifying K^+ current; I_{to1}, transient outward K^+ current; KO, knock out; LCAC, long-chain acylcarnitines; LCAD, long-chain acyl-CoA dehydrogenase; MDP, maximum diastolic potential; VLCAD, very long-chain acyl-CoA dehydrogenase; VLCADD, VLCAD deficiency; V_{max}, maximum upstroke velocity.

action potential parameters nor the increased occurrence of delayed afterdepolarizations in VLCADD hiPSC-CMs. We conclude that long-chain acylcarnitine accumulation and electrophysiological abnormalities in VLCADD hiPSC-CMs are not normalized by carnitine supplementation, indicating that this treatment is unlikely to be beneficial against cardiac arrhythmias in VLCADD patients.

Keywords: very long-chain acyl-CoA dehydrogenase, arrhythmia < cardiovascular, acylcarnitines, action potential, human induced pluripotent stem cell derived cardiomyocytes, patients, treatment, carnitine

INTRODUCTION

Patients with a deficiency in very long-chain acyl-CoA dehydrogenase (VLCAD; EC 1.3.99.3), the enzyme catalyzing the first step of the mitochondrial beta-oxidation of long-chain fatty acids (Houten and Wanders, 2010; Knottnerus et al., 2018), are at risk for developing liver, skeletal, and heart muscle dysfunction (Ribas and Vargas, 2020; Wanders et al., 2020), including cardiac arrhythmias (Bonnet et al., 1999). Traditionally patients with VLCAD deficiency (VLCADD; OMIM 609575) are treated with dietary restriction of long-chain triglycerides, supplementation of medium-chain triglycerides, and prevention of catabolic state (Yamada and Taketani, 2019). Carnitine supplementation had also been proposed for patients with VLCADD in order to treat secondary carnitine deficiency and to increase the transport of acyl compounds out of the mitochondria (Treem et al., 1991; Winter, 2003).

Carnitine is required for the transport of activated long-chain fatty acids into the mitochondrial matrix, by formation of long-chain acylcarnitines (LCAC) from acyl-CoA esters, and is therefore essential for fatty acid oxidation (Houten and Wanders, 2010). In humans, carnitine is mainly derived from the diet, but can also be synthesized by the liver, kidney and brain (Vaz and Wanders, 2002; Reuter and Evans, 2012; Wanders et al., 2020). Tissues like skeletal muscle and the heart acquire carnitine from the circulation. Its indispensable role in metabolism is illustrated by patients who suffer from primary carnitine deficiency (OMIM 212140) due to excessive urinary carnitine wasting (Longo et al., 2006). So far, the evidence for a beneficial effect of carnitine supplementation in VLCADD patients is not conclusive (Nasser et al., 2012; (Spiekerkoetter et al., 2010; Ribas and Vargas, 2020). A major concern may be the potential increased formation in LCACs (Spiekerkoetter et al., 2009; Ribas and Vargas, 2020), especially since LCACs are associated with the development of cardiac arrhythmia (Corr et al., 1989). On the other hand, extremely low free carnitine levels, as seen in patients with primary carnitine deficiency, are also linked to abnormalities in electrical morphology of the heart (Roussel et al., 2016). Therefore, more insight on effects and safety of carnitine supplementation on electrophysiological abnormalities for VLCADD treatment is needed.

So far, the cardiac effects of carnitine supplementation have been studied in mice. In VLCADD murine models, it was found that supplementation of carnitine can indeed lead to a more pronounced accumulation of LCACs (Liebig et al., 2006; Primassin et al., 2008) without replenishment of free carnitine in cardiac tissue (Liebig et al., 2006). This is in contrast with the findings in a long-chain acyl-CoA dehydrogenase (LCAD) knock out (KO) murine model, in which carnitine supplementation did not lead to increased long-chain acylcarnitine levels and even normalized myocardial triglycerides (Bakermans et al., 2013). However, mice are considerably different from humans with respect to fatty acid oxidation as well as carnitine metabolism (Chegary et al., 2009), and therefore it is uncertain whether findings in these murine models can be directly extrapolated to the human situation and be applied to formulation of a human therapy. Very recently, we generated a human-based cardiac VLCADD model by generation of human induced pluripotent stem cells (hiPSCs) from patients carrying mutations in the VLCAD-encoding *ACADVL* gene and differentiated them into cardiomyocytes (hiPSC-CMs) (Knottnerus et al., 2020). We found that VLCAD deficiency in this hiPSC-CMs model results in accumulation of LCACs, higher systolic and diastolic intracellular Ca^{2+} (Ca_i^{2+}) concentrations, action potential (AP) shortening, and development of delayed afterdepolarizations (DADs). Furthermore, we found that pre-incubation of VLCADD hiPSC-CMs with either resveratrol or etomoxir–compounds that give rise to an enhanced mitochondrial biogenesis or inhibit fatty acid transport into the mitochondria, respectively (Lopaschuk et al., 2010; Houtkooper et al., 2012)– led to the normalization of the acylcarnitine levels and restored electrophysiological and Ca_i^{2+} abnormalities (Knottnerus et al., 2020). Importantly, these findings suggest that treatment with such compounds may be beneficial for VLCADD patients. In addition, these findings also indicate that our hiPSC-CM model is suitable for drug discovery studies of this metabolic disorder. In the present study, we used the VLCADD hiPSC-CM model to study the effects of carnitine supplementation on the LCAC profile and cellular electrophysiology.

MATERIALS AND METHODS

Human Induced Pluripotent Stem Cell Derived Cardiomyocytes Generation

hiPSC-CMs were generated from the hiPSC line, iVLCADD1, which was derived from skin fibroblasts of a VLCADD-affected woman with mutations (p.Val283Ala/p.Glu381del) in the *ACADVL* gene (Knottnerus et al., 2020). Differentiation of the hiPSCs into hiPSC-CMs was performed in RPMI 1,640 medium supplemented with B27 (Gibco), initiated with CHIR99021, Activin A and BMP4, followed by Wnt-pathway inhibition by IWP4, differentiation proceeded in presence of RPMI medium supplemented with B27 and insulin until day 30 as we have previously described in detail (Knottnerus et al., 2020). Next, we performed a metabolic selection-based enrichment for hiPSC-CMs by applying glucose-depleted RPMI medium containing 4 mM lactate for six days, thereby removing a large proportion of non-cardiomyocytes (Tohyama et al., 2013). During the whole process, no serum was supplied to the culture medium. Finally, 36 days after the start of the differentiation process, hiPSC-CMs were dissociated to single cells using a two-step procedure starting with 5× TrypLE Select Enzyme (Gibco) to detach the cells from culture flasks, followed by a combination of liberase (Roche Chemicals) and Elastase (Serva) to obtain single cells (Knottnerus et al., 2020). The cells were seeded on matrigel-coated glass coverslips and cultured for 10 days in RPMI medium supplemented with 2% B27, 50 U/ml penicillin, and 50 µg/ml streptomycin and 48 h prior to measurement 400 µM L-carnitine (C0158, Sigma-Aldrich) was added to the culture medium in paired experiments. hiPSC-CMs generated from a control hiPSC line, iCTRL (Dudek et al., 2013), were used as control and were cultured in the absence of carnitine.

Acylcarnitine Profiling

The intracellular acylcarnitine profile of the hiPSC-CMs was assessed after 30 days of differentiation as described previously (Knottnerus et al., 2020). In short, hiPSC-CMs from the iCTRL and VLCADD1 line, here named iCTRL-CMs and iVLACDD1-CMs respectively, were harvested with trypsin and cell pellets or 50 µL of culture medium were extracted in 500 µL acetonitrile with 10 µL internal standards ($^2H_3$-C3-carnitine, $^2H_3$-C8 carnitine, $^2H_3$-C16 carnitine) and measured with high performance liquid chromatography mass spectrometry on a Q-ExactiveTM mass spectrometer (Thermo Scientific). Data was normalized to level of protein per well, determined using bicinchonic acid (BCA) assay with human serum albumin (HSA) in 0.4 mmol/L NaOH used as a standard (Knottnerus, et al., 2020).

Patch-Clamp Measurements

Data Acquisition

APs and afterdepolarizations were recorded at 36 ± 0.2°C using the perforated patch-clamp technique and an Axopatch 200B amplifier (Molecular Devices, Sunnyvale, CA, United States). Data acquisition, voltage control, and analysis were accomplished using custom software. Signals were low-pass filtered with a cut-off frequency of 5 kHz and digitized at 40 and 3 kHz for APs and DADs, respectively. Cell membrane capacitance (C_m, in pF) was estimated by dividing the time constant of the decay of the capacitive transient in response to 5 mV hyperpolarizing voltage clamp steps from −40 mV by the series resistance. C_m of hiPSC-CMs was 23.9 ± 1.3 pF (mean ± SEM, n = 41), and did not differed significantly between iCTRL-CMs, untreated iVLCADD1-CMs, and carnitine-treated iVLCADD1-CMs. Patch pipettes with a resistance of 2–3 MΩ were pulled from borosilicate glass (Harvard Apparatus) and filled with solution containing (in mM): 125 K-gluconate, 20 KCl, 5 NaCl, 0.44 Amphotericin-B, 10 HEPES; pH set to 7.2 (KOH). Cells were superfused with modified Tyrode's solution containing (in mM): 140 NaCl, 5.4 KCl, 1.8 $CaCl_2$, 1.0 $MgCl_2$, 5.5 D-glucose, 5 HEPES; pH set to 7.4 (NaOH). All potentials were corrected for the estimated liquid junction potential of −15 mV (Barry and Lynch, 1991).

Action Potential Recordings

hiPSC-CMs offer a great human-based model for cardiac disease modeling (Hoekstra et al., 2012), and drug discovery and cardiotoxicity screenings (Mordwinkin et al., 2013), but a major limitation for electrophysiological studies is that they have a small or even complete lack of the inward rectifying K^+ current (I_{K1}) (Veerman et al., 2015). I_{K1} plays a major role in maintaining a stable resting membrane potential in cardiomyocytes (Nerbonne and Kass, 2005), and consequent to its absence, hiPSC-CMs have a depolarized maximal diastolic potential and are frequently spontaneously active. To overcome this limitation, we injected an in silico I_{K1} with kinetics of Kir2.1 channels and a 2 pA/pF current density through dynamic clamp, as previously described in detail (Meijer van Putten et al., 2015). The dynamic clamp injected I_{K1} resulted in quiescent hiPSC-CMs and we elicited APs at 0.2–4 Hz by 3 ms, ≈1.2× threshold current pulses through the patch pipette. Susceptibility to DADs was tested by applying a 3 Hz pacing episode (10 s) followed by an 8 s pause. After the pause, a single AP was evoked to test the inducibility of early afterdepolarizations (EADs). DADs were defined as depolarizations that occurred after the fast pacing and which were larger than 1 mV. EADs were defined as oscillations in membrane potential which interrupt or retard repolarization of the AP were defined as EADs accordingly to the definition of Cranefield (1977). The AP parameters analyzed were maximum diastolic potential (MDP, in mV), maximal AP amplitude (APA, in mV), maximum upstroke velocity (V_{max}, in V/s) AP duration at 20, 50, and 90% repolarization (APD_{20}, APD_{50}, and APD_{90}, respectively, in ms). Parameters from 10 consecutive APs were averaged and number of DADs and EADs was counted and averaged over five fast pacing recording traces.

Statistical Analysis

Statistical analysis was carried out with SigmaStat 3.5 software (Systat Software, Inc., San Jose, CA, United States). Normality and equal variance assumptions were tested with the Kolmogorov-Smirnov and the Levene median test, respectively. Group comparisons were performed with unpaired t-test, One-Way ANOVA followed by Holm-Sidak post hoc test, Two-Way Repeated Measures ANOVA followed by pairwise comparison using the Student–Newman–Keuls test or Fisher Exact Test with Freeman-Halton extension.

In case of non-normally distributed parameters, Kruskal-Wallis tests followed by pairwise comparisons with Dunn's methods were applied. Data are presented as mean ± SEM or as boxplots, in which boxes represent lower quartile, median and upper quartile, and whiskers 1.5× interquartile range. $p < 0.05$ was considered statistically significant.

RESULTS

Long-Chain Acylcarnitine Concentrations

First, we measured the acylcarnitine profiles in iCTRL-CMs and iVLCADD1-CMs cultured under standard culture conditions

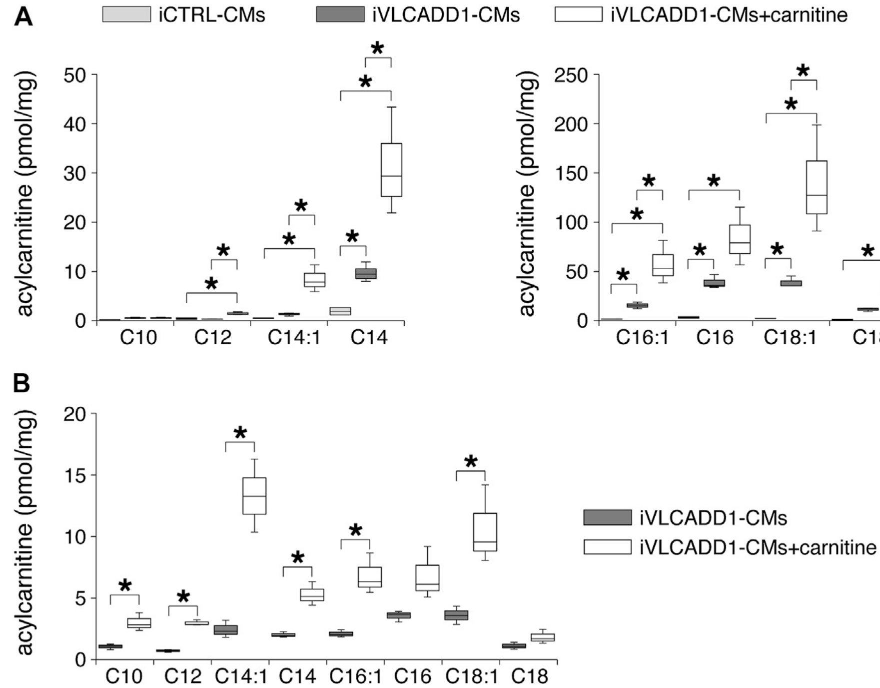

FIGURE 1 | Box plots of acylcarnitine profiles in cell pellets and culture medium. **(A)** Box plots of acylcarnitine profiles in cell pellets of iCTRL-CMs and iVLCADD1-CMs cultured in absence or in presence of 400 µM carnitine for 48 h. Asterisks indicate significant differences between groups (One-Way ANOVA followed by Holm-Sidak post hoc test or Kruskal-Wallis tests followed by pairwise comparisons with Dunn's methods). Data from three differentiations obtained from cell pellets 30 days after differentiation. **(B)** Box plots of acylcarnitine profiles measured in culture medium of VLCADD1-CMs cultured under standard culture conditions or in presence of 400 µM carnitine for 48 h. Asterisks indicate significant differences between groups (Unpaired t-test; data from three differentiations measured 30 days after differentiation.

and in the presence of 400 μM carnitine for 48 h. Compared to iCTRL-CMs, LCAC concentrations were higher in iVLCADD1-CMs cultured in the absence of carnitine (**Figure 1A**). Culturing the iVLCADD1-CMs in the presence of carnitine resulted even in a further increase (**Figure 1A**). For example, C18:1-acylcarnitine increased from 38.8 ± 4.0 pmol/mg (three replicates) in iVLCADD1-CMs cultured in standard medium without additional carnitine to 138.5 ± 38.9 pmol/mg (three replicates) in iVLCADD1-CMs cultured with carnitine. In iVLCADD1-CMs, carnitine also resulted in a significant increase in LCACs levels in the culture medium with most prominent effects on C14: 1-acylcarnitine (**Figure 1B**). This indicates that the hiPSC-CMs are able to excrete the accumulating LCACs.

Carnitines Incubation Does Not Affect Action Potentials

Next, we assessed the AP parameters of the iCTRL-CMs and compared them to those of the iVLCADD1-CMs cultured in the absence or presence of carnitine. The AP parameters were analyzed as depicted in **Figure 2A**. **Figure 2B** shows a typical AP at 1 Hz stimulation of an iCTRL-CMs as well as typical 1 Hz stimulated APs recorded from an iVLCADD1-CMs cultured in the absence or presence of carnitine. Average AP parameters obtained from a total of 16 iCTRL-CMs, 11 iVLCADD1-CMs cultured in standard conditions, and 14 iVLCADD1-CMs cultured in the presence of carnitine are summarized in **Figure 2C**. The average MDP was around −80 mV and the V_{max} was between 50 and 150 V/s, but both MDP and V_{max} did not differ significantly between the three hiPSC-CMs groups. In all cell lines, APs overshot the 0 mV level, but the APA was significantly lower in the iVLCADD1-CMs in the absence as well as in the presence of carnitine compared to the iCTRL-CMs. iCTRL-CMs had an APA of 120 ± 2.7 mV (n = 16), while the iVLCADD1-CMs lines showed an APA of 99 ± 3.9 mV (n = 11) and 102 ± 3.4 mV (n = 14) in the absence and presence of carnitine, respectively. APs of both iVLCADD1-CMs groups repolarized earlier and faster than iCTRL-CMs (**Figure 2A**), resulting in a significantly shorter APD_{20}, APD_{50}, and APD_{90}. For example, APD_{90} was 190 ± 9.7 mV (n = 16) in iCTRL-CMs and 127 ± 12.2 mV (n = 11) and 126 ± 21.0 mV (n = 14) in the iVLCADD1-CMs in absence and presence of carnitine. Neither APA nor the APDs differ significantly between iVLCADD1-CMs cultured in the presence of 400 μM carnitine and iVLCADD1-CMs cultured under standard conditions.

Cardiac APs show a frequency dependence in morphology (Carmeliet, 2004) and the iVLCADD1-CM electrical phenotype as well as potential effects of carnitine may be frequency-related. For this reason, we studied the AP characteristics at 0.2–4 Hz stimulation. **Figure 3A** shows typical APs and **Figure 3B** summarizes the average AP parameters that were significantly

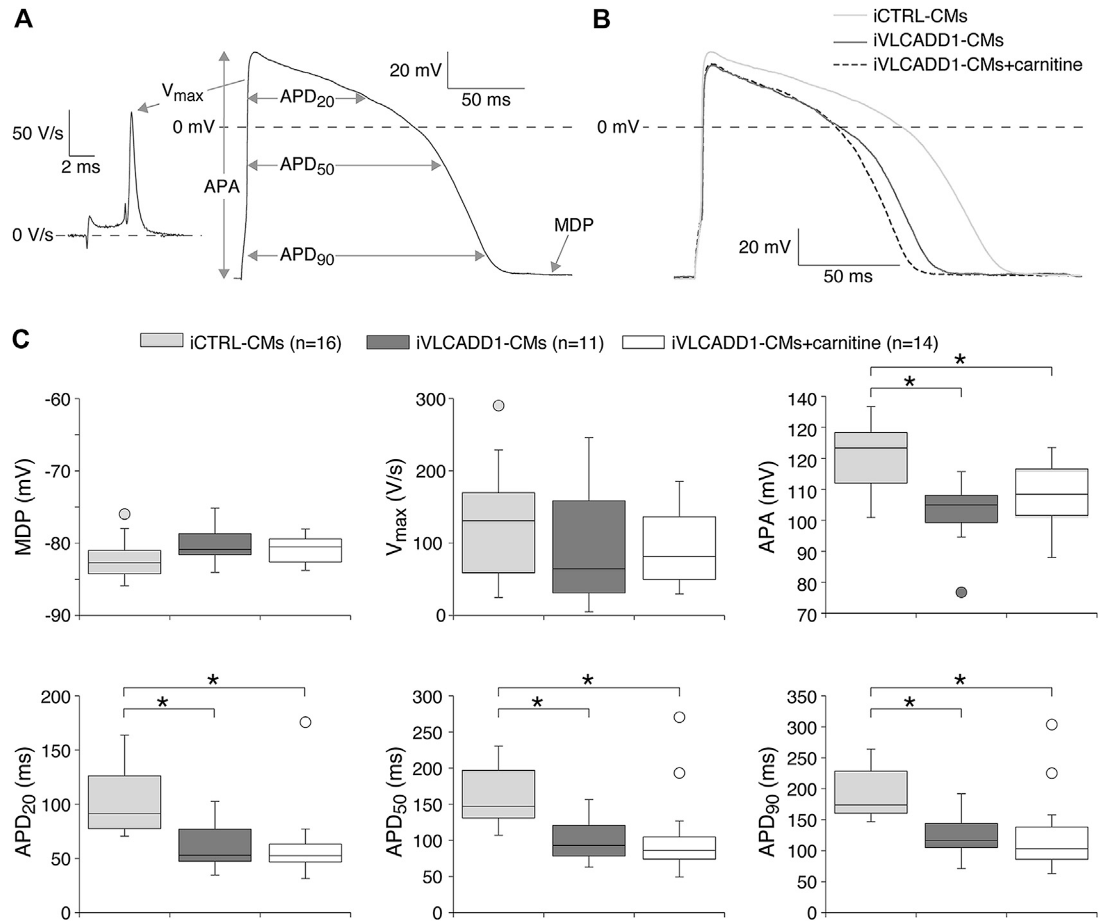

FIGURE 2 | Action potential (AP) characteristics at 1 Hz of single iCTRL-CMs and iVLCADD1-CMs cultured in absence or presence of carnitine. **(A)** Illustration of the analyzed AP parameters, i.e., maximum diastolic potential (MDP), AP amplitude (APA), maximum upstroke velocity (V_{max}), and AP duration at 20, 50, and 90% repolarization (APD_{20}, APD_{50}, and APD_{90}, respectively). **(B)** Typical APs of iCTRL-CMs and iVLCADD1-CMs cultured in absence or presence of carnitine. **(C)** Box plots of the APs characteristics. Asterisks indicate significant differences between groups (One-Way ANOVA followed by Holm-Sidak post hoc test or Kruskal-Wallis tests followed by pairwise comparisons with Dunn's methods). iCTRL-CM and iVLCADD1-CM data are from five to four differentiations, respectively, and were measured 46 and 47 days after differentiation.

different between iCTRL-CMs and iVLCADD1-CMs at 1 Hz. APA, APD_{20}, APD_{50}, and APD_{90} of iCTRL-CMs were significantly different from iVLCADD1-CMs cultured without and in the presence of carnitine at all frequencies, with exception of the APDs at 4 Hz in absence of carnitine (**Figure 3B**). As illustrated in **Figure 3**, the APs of iCTRL-CMs shows a clear frequency dependency with a decrease in APA and APDs upon both slower and faster pacing frequencies compared to the 1 Hz pacing frequency. This is depicted in more detail in **Figure 4A**, in which the iCTRL-CMs data presented in **Figure 3B** are replotted, but now with asterisks which indicate the significant differences between stimulus frequencies. In the VLCADD1 lines on the other hand, frequency dependence, especially those of the APDs, was less prominent as can be seen from the limited number of significant differences (**Figures 4B,C**). Thus, in iVLCADD1-CMs, APA and APDs are decreased at all frequencies compared to iCTRL-CMs, whereas the frequency dependence of AP parameters is hardly present in iVLCADD1-CMs. In addition, these data demonstrate that carnitine does not prevent these effects.

Carnitines Incubation Does Not Affect the Occurrence of Afterdepolarizations

We also assessed the effects of carnitine on the occurrence of DADs and EADs, both important cellular electrophysiological triggers for cardiac arrhythmias (Hoffman and Rosen, 1981; Wit, 2018). Susceptibility to DADs was tested by applying a fast, 3-Hz pacing episode (10-s) followed by an 8-s pause (**Figure 5B**). After the pause, we evoked a single AP (**Figure 5B**) to test the inducibility of EADs. In addition, we counted the occurrence of EADs during continuous 0.2 Hz stimulation. The results of DADs and EADS are shown in **Figures 5A,B**, respectively.

As illustrated in the typical examples of **Figures 5A**, fast pacing resulted in DADs (indicated with arrows) in the post-pacing pause in both iVLCADD1-CMs groups and not in the

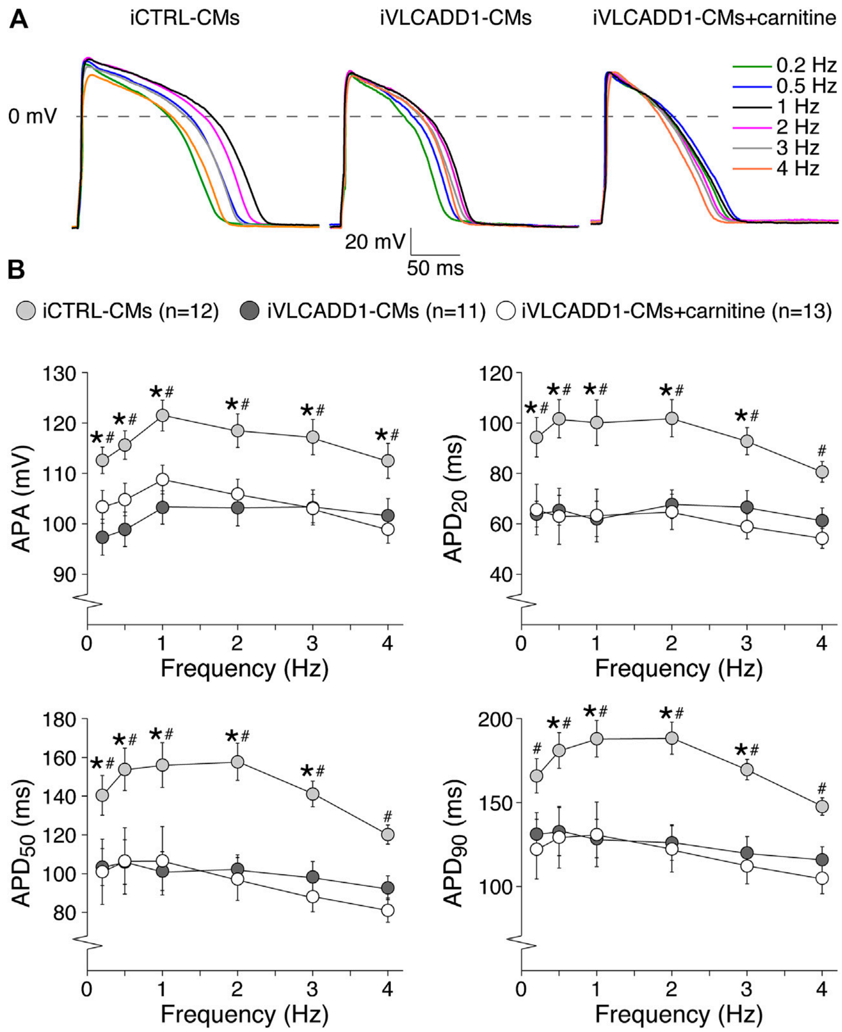

FIGURE 3 | AP parameters at 0.2–4 Hz pacing of iCTRL-CMs and iVLCADD1-CMs cultured in absence or presence of carnitine. **(A)** Typical APs of iCTRL-CMs and iVLCADD1-CMs cultured in absence or presence of carnitine stimulated at 0.2, 0.5, 1, 2, 3, and 4 Hz. **(B)** APA, APD_{20}, APD_{50}, and APD_{90} at 0.2–4 Hz. Asterisks indicate significant differences between groups (Two-way Repeated Measures ANOVA). iCTRL-CM and iVLCADD1-CM data are from five to four differentiations, respectively, and were measured 46 and 47 days after differentiation.

iCTRL-CMs. **Figure 5C** summarizes the occurrence of DADs for a total of 10 iCTRL-CMs, 11 iVLCADD1-CMs cultured in the absence, and 13 iVLCADD1-CMs cultured in the presence of carnitine. As already observed in the typical examples of **Figure 5A**, and confirming our previous findings (Knottnerus et al., 2020), there is a significant increase of DADs in the iVLCADD1-CMs lines (**Figure 5C**). However, the number of DADs was not significantly different between the iVLCADD1-CMs cultured in absence and presence of carnitine. EADs were never observed during the single AP evoked after the 8-s pause. In addition to the experiments presented in **Figure 5A**, we re-analyzed the experiments in which we paced the hiPSC-CMs continuously at a slow 0.2 Hz stimulus frequency for the occurrence of EADs. The data, obtained from a total of 12 iCTRL-CMs, 11 iVLCADD1-CMs cultured in standard conditions, and 13 iVLCADD1-CMs cultured in the presence of carnitine, further demonstrates that the presence of EADs was rare (**Figures 5D,E**). In iVLCADD1-CMs cultured without as well as in iVLCADD1-CMs cultured in the presence of carnitine, we only observed EADs in one cell (**Figures 5D,E**) and the EADs occurred once every three to five APs. No EADs were ever observed in the iCTRL-CMs. Thus, these experiments demonstrate a high incidence of DADs in iVLCADD1-CMs, but highlight the lack of protective effect of carnitine supplementation in afterdepolarization occurrence.

DISCUSSION

In recent years, supplementation of L-carnitine to patients with a lcFAO disorder has remained a topic of debate (Spiekerkoetter et al., 2010; Pena et al., 2016; Yamada and Taketani, 2019). The main argument against L-carnitine supplementation is the suspicion that high levels of intrinsic and/or circulating

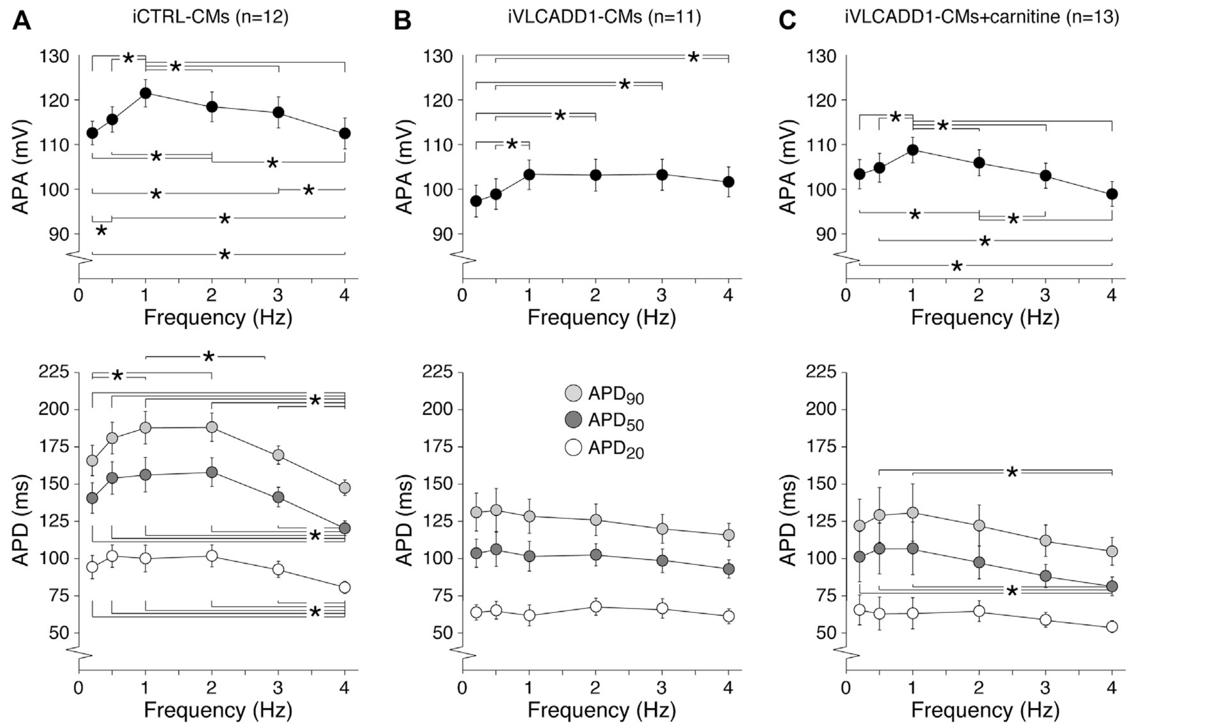

FIGURE 4 | (A–C) Frequency dependence of APA, APD_{20}, APD_{50}, and APD_{90} in iCTRL-CMs **(A)** and iVLCADD1-CMs cultured in absence **(B)** or presence of carnitine **(C)**. Asterisks indicate significant differences between stimulus frequencies (Two-way Repeated Measures ANOVA). iCTRL-CM and iVLCADD1-CM data are from five to four differentiations, respectively, and were measured 46 and 47 days after differentiation.

LCACs may cause cardiac arrhythmias (Corr et al., 1989). Here, we studied the effects of L-carnitine supplementation in hiPSC-CMs generated from a VLCADD patient. We observed an increase in intracellular levels of LCACs, as well as an increase in excreted LCACs. There was neither an improvement in AP parameters nor in the occurrence of afterdepolarizations after L-carnitine supplementation. We conclude that LCACs accumulation and electrophysiological abnormalities in VLCADD hiPSC-CMs are not restored by carnitine supplementation, which suggests that carnitine treatment is not beneficial against cardiac arrhythmias in VLCADD patients.

iVLCADD1-CMs cultured under standard conditions exhibit a lower APA and shorter AP at a wide range of stimulus frequencies compared to iCTRL-CMs (**Figures 2**, **3**). The exact mechanism is unknown, but is likely related to the LCAC accumulation (**Figure 1A**) and the consequent L-type Ca^{2+} current ($I_{Ca,L}$) decrease (Wu and Corr, 1992) and increased systolic Ca_i^{2+} concentrations resulting in enhanced Ca^{2+}-induced $I_{Ca,L}$ inactivation and increased K^+ currents (Knottnerus et al., 2020). Indeed, reducing LCAC concentrations with either resveratrol or etomoxir restored APA and APDs in VLCADD hiPSC-CMs (Knottnerus et al., 2020). This pharmacological rescue of the metabolic and electrical phenotypes further indicates that these electrical abnormalities were not due to different genetic backgrounds in our used cell lines. The latter is also supported by experiments with a second control hiPSC line (for details, see Veerman et al., 2016), which show almost identical AP parameters (and the absence of DADs and EADs) as the presently used iCTRL-CMs (data not shown). While the iCTRL-CMs showed a clear frequency dependency of APA and APDs, this was less pronounced in the standard cultured iVLCADD1-CMs (**Figure 4**). The APA and APD decrease in iCTRL-CMs at faster stimulus frequencies is likely due to a combination of incomplete recovery of $I_{Ca,L}$ and accumulation of repolarizing delayed rectifier K^+ currents (Carmeliet, 2004). The AP shortening at slow stimulus frequencies in iCTRL-CMs, on the other hand, is likely due the repolarizing transient outward K^+ current, I_{to1}. In hiPSC-CMs, I_{to1} has an extremely slow recovery from inactivation (Cordeiro et al., 2013) and consequently plays only a role in AP repolarizing at low stimulus frequencies (Ma et al., 2018). The loss of frequency dependency of APA and APDs observed in iVLCADD1-CMs may be related to the already above mentioned decrease in $I_{Ca,L}$ function and the obvious fast AP repolarization in iVLCADD1-CMs, which can mask subtle changes in net currents (Gaur et al., 2020). We found a high incidence of DADs in iVLCADD1-CMs cultured under standard conditions (**Figures 5A,C**), consistent with our previous study (Knottnerus et al., 2020). In human CMs, DADs are due to Ca_i^{2+} overload-induced spontaneous Ca^{2+} release from the sarcoplasmic reticulum (SR), which activates an inward current carried by the Na^+-Ca^{2+} exchanger (Verkerk et al., 2001). Ca_i^{2+} overload was previously observed in hiPSC-CMs from VLCADD patients (Knottnerus et al., 2020). EADs in

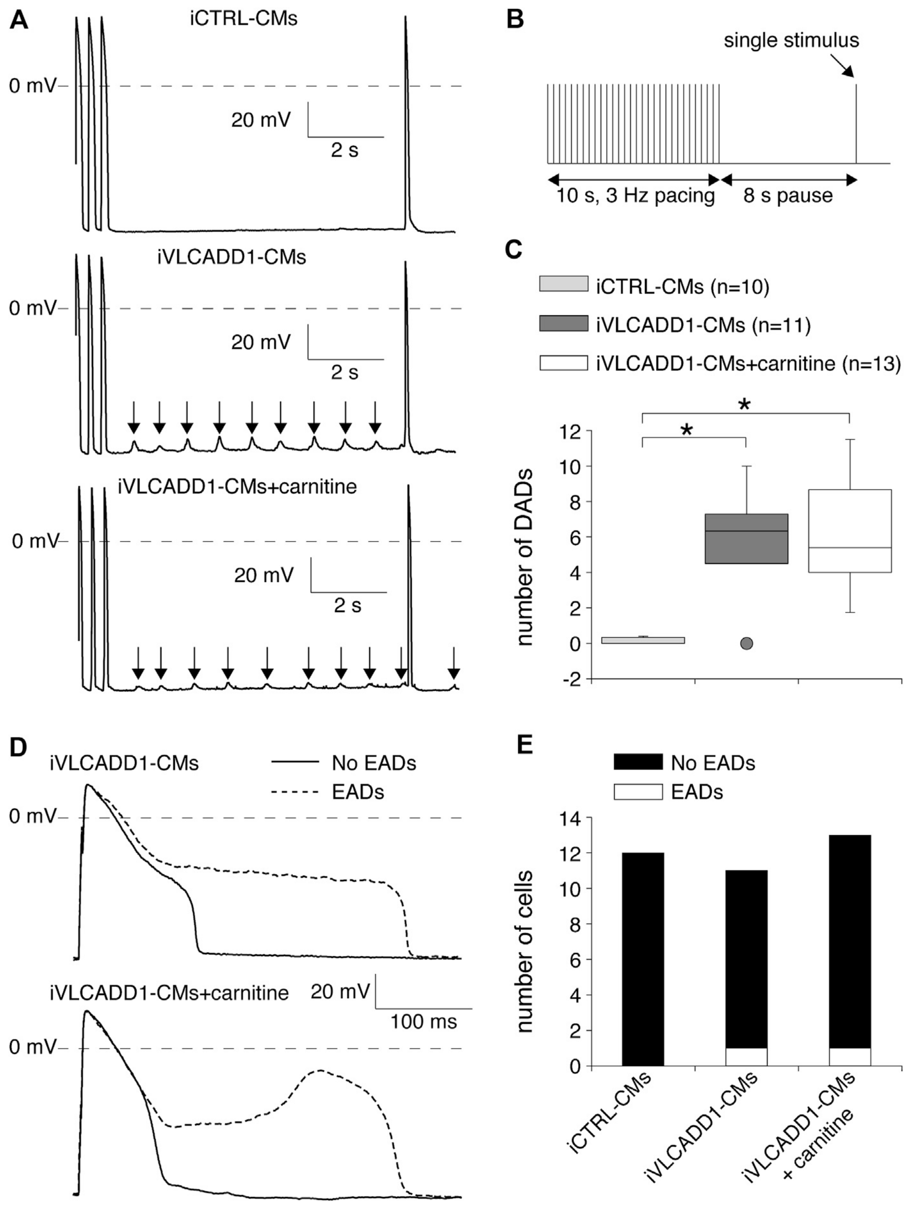

FIGURE 5 | Delayed and early afterdepolarization (DAD and EAD, respectively) inducibility of iCTRL-CMs and/or iVLCADD1-CMs cultured in absence or presence of carnitine. **(A)** Typical DAD examples of an iCTRL-CM and iVLCADD1-CMs cultured in absence or presence of carnitine. The arrows indicate the DADs. **(B)** Illustration of the protocol to induce DADs. **(C)** Average occurrence of DADs. **(D)** APs at 0.2 Hz pacing of an iVLCADD1-CM cultured in absence and an iVLCADD1-CM cultured in presence of carnitine. EADs were only present once every three to five APs and the APs exhibiting an EAD are indicated by dashed lines. **(E)** EADs occurrence at 0.2 Hz in iCTRL-CMs and iVLCADD1-CMs cultured in absence or presence of carnitine. Asterisks indicate significant differences between groups (Kruskal-Wallis test followed by pairwise comparisons with Dunn's methods). iCTRL-CM and iVLCADD1-CM data are from five to four differentiations, respectively, and were measured 46 and 47 days after differentiation.

iCTRL-CMs were absent and rare in iVLCADD-CMs (**Figures 5D,E**). EADs can be divided in the so-called phase 2 and late-phase 3 EADs which are supposed to be due to different mechanisms (Qu et al., 2013). Phase 2 EADs are caused by re-activation of $I_{Ca,L}$ which may occur during prolonged APs, while late-phase 3 EADs are likely due to the Na^+-Ca^{2+} exchange current when the AP is substantially shortened such that the Ca^{2+} transient outlast the AP repolarization (Qu et al., 2013). It is tempting to define the observed EADs as late-phase 3 EADs based on the observed AP shortening (**Figure 2**) and previously observed increased systolic Ca_i^{2+} (Knottnerus et al., 2020) which may result in a larger Na^+-Ca^{2+} exchange current, but further studies are required to address this issue in detail.

The electrophysiological properties of the iVLCADD1-CMs cultured for 48 h in the presence of carnitine supplementation were not different from iVLCADD1-CMs cultured under standard conditions (**Figures 2–5**), demonstrating that the lack of effect of carnitine in restoring electrophysiological abnormalities. Supplementation of carnitine for 48 h was sufficient to increase the LCAC concentrations (**Figure 1A**), indicating that the absence of electrophysiological effects is not related to the length of the exposure time to the drugs in this particular hiPSC-CM model. In addition, we have previously observed that 48 h of drug treatment is sufficient to affect mitochondrial function in our iVLCADD1-CMs model, therefore indicating that this hiPSC-CMs model is useful for metabolic disorder drug studies (Knottnerus et al., 2020), even though hiPSC-CMs may have a less developed mitochondrial system for FAO flux compared to adult cardiomyocytes due to their immaturity (Chen et al., 2016). While the carnitine treatment increased the LCAC concentrations, electrophysiological abnormalities were not aggravated. This suggests that there is not a simple linear relationship between AP shortening and incidence of DADs and the LCACs. In addition, it indicates that carnitine treatment can be used for other, non-cardiac VLCADD-induced dysfunctions without increasing the risk for cardiac arrhythmias.

Secondary carnitine deficiency may occur in patients with VLCADD as a result of acylcarnitine formation from high levels of non-degraded acyl-CoAs. The pathophysiological relevance of carnitine depletion for the signs and symptoms observed in this disorder is not clear. Still, carnitine supplementation is often part of the treatment of VLCADD, especially when low (plasma) carnitine concentrations are found in patients (Pena et al., 2016). Evaluation of the efficacy of this intervention is very complex, due to the low numbers of patients and heterogeneous phenotypic presentations. In addition, acylcarnitine profiles measured in plasma do not correlate well with profiles measured in tissue (muscle tissue or white adipose tissue) (Schooneman et al., 2014). We found in iVLCADD1-CMs an increased LCAC accumulation as well as an increased LCAC secretion after carnitine supplementation. So far, there is limited knowledge on the cellular export mechanisms of acylcarnitines (Kim et al., 2017), but the increased LCAC accumulation induced by carnitine supplementation is in agreement with findings in mouse models for VLCADD (Liebig et al., 2006; Primassin et al., 2008; Bakermans et al., 2013). Bakermans and colleagues (Bakermans et al., 2013), however, only observed an increase of C16 and C18:1-carnitine whereas C14:1 levels were not affected in bloodspots after carnitine supplementation.

The heart lacks enzymes for carnitine synthesis and is therefore dependent on carnitine import from the circulation via the sodium dependent organic cation transporter (OCTN2). In a recent study, it was shown that haploinsufficiency of OCTN2 in lcFAO disorder mice results in decreased free carnitine levels and subsequently decrease in tissue and plasma LCAC accumulation but does not significantly affect clinically relevant outcome parameters (hypoglycemia, heart weight or liver weight) (Ranea-Robles et al., 2020). However, it should be noted that the C14:1-acylcarnitine levels were still higher in lcFAO disorder with OCTN2 haploinsufficiency when compared to wild type in heart, liver and plasma. Therefore, toxicity of acylcarnitines cannot be excluded.

In the present study, we have tested the effects of carnitine treatment on single VLCADD hiPSC-CMs and not on iCTRL-CMs. Whereas this approach allows a detailed study of the effects of a well-controlled dose of carnitine on the intrinsic LCAC concentrations, AP configuration and afterdepolarizations of the VLCADD hiPSC-CMs, it does not take into account the metabolic and structural complexity and heterogeneity of the intact myocardium or body. Therefore, caution is warranted when translating our *in vitro* results to the *in vivo* situation. Furthermore, although our VLCADD model has a human background thereby avoiding potential species differences, our study was limited to one patient-specific hiPSC line with *ACADVL* gene mutation. This provided us the opportunity to investigate the effects of carnitine on cardiomyocytes derived from this patient-specific hiPSC line in detail, but further studies are needed to test the carnitine effects on other VLCADD models. In the present study, we focused on LCAC concentrations and electrophysiology in hiPSC-CMs but VLCADD has a broad clinical spectrum (Ribas and Vargas, 2020; Wanders et al., 2020). In future studies, our VLCADD hiPSC line may also be differentiated to a liver and skeletal muscle cell fate (van der Wall et al., 2018; Corbett and Duncan, 2019) to assesses the effects of VLCADD and potential treatment in these cell types.

In conclusion, carnitine enhanced LCAC concentrations in hiPSC-CMs with *ACADVL* gene mutations and did not improve the electrophysiological abnormalities. This indicates that carnitine treatment is unlikely to be beneficial against cardiac arrhythmias in patients with *ACADVL* gene mutations.

DATA AVAILABILITY STATEMENT

The raw data supporting the conclusions of this article will be made available by the authors, without undue reservation.

AUTHOR CONTRIBUTIONS

SK, CB, and RH conceived and designed the study. KG generated the hiPSC lines. IM. maintained the hiPSC lines and differentiated them to cardiomyocytes. IM, SK, SF and JB dissociated cells and performed biochemical experiments. AV and VP performed electrophysiology measurements. SK and AV analyzed and interpreted the data and drafted the manuscript. LIJ, GV, RW, and FW contributed to scientific discussions. All authors critically revised the manuscript and gave final approval of the version to be published.

FUNDING

KG was supported by the Free State of Saxony and the European Union EFRE (SAB project "PhänoKard") and by the DFG (GU595/3-1, IRTG2251). CB was supported by the Dutch Heart Foundation (CVON PREDICT2 project), Netherlands Organization for Scientific Research (VICI fellowship, 016.150.610) and Fondation Leducq. RH was supported by a VIDI grant from ZonMw (no. 91715305) and a grant from the Velux Stiftung (no. 1063).

REFERENCES

Bakermans, A. J., van Weeghel, M., Denis, S., Nicolay, K., Prompers, J. J., and Houten, S. M. (2013). Carnitine supplementation attenuates myocardial lipid accumulation in long-chain acyl-CoA dehydrogenase knockout mice. *J. Inherit. Metab. Dis*. 36 (6), 973–981. doi:10.1007/s10545-013-9604-4

Barry, P. H., and Lynch, J. W. (1991). Liquid junction potentials and small cell effects in patch-clamp analysis. *J. Membr. Biol*. 121, 101–117. doi:10.1007/BF01870526

Bonnet, D., Martin, D., de Lonlay, P., Villain, E., Jouvet, P., Rabier, D., et al. (1999). Arrhythmias and conduction defects as presenting symptoms of fatty acid oxidation disorders in children. *Circulation*. 100 (22), 2248–2253. doi:10.1161/01.cir.100.22.2248

Carmeliet, E. (2004). Intracellular Ca^{2+} concentration and rate adaptation of the cardiac action potential. *Cell. Calcium*. 35 (6), 557–573. doi:10.1016/j.ceca.2004.01.010

Chegary, M., te Brinke, H., Ruiter, J. P., Wijburg, F. A., Stoll, M. S., Minkler, P. E., et al. (2009). Mitochondrial long chain fatty acid beta-oxidation in man and mouse. *Biochim. Biophys. Acta*. 1791 (8), 806–815. doi:10.1016/j.bbalip.2009.05.006

Corbett, J. L., and Duncan, S. A. (2019). IPSC-derived hepatocytes as a platform for disease modeling and drug discovery. *Front. Med. (Lausanne)*. 6, 265. doi:10.3389/fmed.2019.00265

Cordeiro, J. M., Nesterenko, V. V., Sicouri, S., Goodrow, Jr, R. J., Treat, J. A., Desai, J. A., et al. (2013). Identification and characterization of a transient outward K+ current in human induced pluripotent stem cell-derived cardiomyocytes. *J. Mol. Cell Cardiol*. 60: 36–46. doi:10.1016/j.yjmcc.2013.03.014

Corr, P. B., Creer, M. H., Yamada, K. A., Saffitz, J. E., and Sobel, B. E. (1989). Prophylaxis of early ventricular fibrillation by inhibition of acylcarnitine accumulation. *J. Clin. Invest*. 83 (3), 927–936. doi:10.1172/JCI113978

Cranefield, P. F. (1977). Action potentials, afterpotentials, and arrhythmias. *Circ. Res*. 41 (4), 415–423. doi:10.1161/01.res.41.4.415

Dudek, J., Cheng, I.-F., Balleininger, M., Vaz, F. M., Streckfuss-Bömeke, K., Hübscher, D., et al. (2013). Cardiolipin deficiency affects respiratory chain function and organization in an induced pluripotent stem cell model of Barth syndrome. *Stem Cell Res*. 11 (2), 806–819. doi:10.1016/j.scr.2013.05.005

Gaur, N., Ortega, F., Verkerk, A. O., Mengarelli, I., Krogh-Madsen, T., Christini, D. J., et al. (2020). Validation of quantitative measure of repolarization reserve as a novel marker of drug induced proarrhythmia. *J. Mol. Cell. Cardiol*. 145, 122–132. doi:10.1016/j.yjmcc.2020.04.019

Hoekstra, M., Mummery, C. L., Wilde, A. A. M., Bezzina, C. R., and Verkerk, A. O. (2012). Induced pluripotent stem cell derived cardiomyocytes as models for cardiac arrhythmias. *Front. Physiol*. 3, 346. doi:10.3389/fphys.2012.00346

Hoffman, B. F., and Rosen, M. R. (1981). Cellular mechanisms for cardiac arrhythmias. *Circ. Res*. 49 (1), 1–15. doi:10.1161/01.res.49.1.1

Houten, I. Y., Matsa, E., and Wu, J. C. (2016). Induced pluripotent stem cells: at the heart of cardiovascular precision medicine. *Nat. Rev. Cardiol*. 13 (6), 333–349. doi:10.1038/nrcardio.2016.36

Houten, S. M., and Wanders, R. J. A. (2010). A general introduction to the biochemistry of mitochondrial fatty acid β-oxidation. *J. Inherit. Metab. Dis*. 33 (5), 469–477. doi:10.1007/s10545-010-9061-2

Houtkooper, R. H., Pirinen, E., and Auwerx, J. (2012). Sirtuins as regulators of metabolism and healthspan. *Nat. Rev. Mol. Cell Biol*. 13 (4), 225–238. doi:10.1038/nrm3293

Kim, H. I., Raffler, J., Lu, W., Lee, J. J., Abbey, D., Saleheen, D., et al. (2017). Fine mapping and functional analysis reveal a role of SLC22A1 in acylcarnitine transport. *Am. J. Hum. Genet*. 101 (4), 489–502. doi:10.1016/j.ajhg.2017.08.008

Knottnerus, S. J. G., Bleeker, J. C., Wüst, R. C. I., Ferdinandusse, S., IJlst, L., Wijburg, F. A., et al. (2018). Disorders of mitochondrial long-chain fatty acid oxidation and the carnitine shuttle. *Rev. Endocr. Metab. Disord*. 19 (1), 93–106. doi:10.1007/s11154-018-9448-1

Knottnerus, S. J. G., Mengarelli, I., Wüst, R. C. I., Baartscheer, A., Bleeker, J. C., Coronel, R., et al. (2020). Electrophysiological abnormalities in VLCAD deficient hiPSC-cardiomyocytes can be improved by lowering accumulation of fatty acid oxidation intermediates. *Int. J. Mol. Sci*. 21 (7), 2589. doi:10.3390/ijms21072589

Liebig, M., Gyenes, M., Brauers, G., Ruiter, J. P., Wendel, U., Mayatepek, E., et al. (2006). Carnitine supplementation induces long-chain acylcarnitine production: studies in the VLCAD-deficient mouse. *J. Inherit. Metab. Dis*. 29 (2-3), 343–344. doi:10.1007/s10545-006-0249-4

Longo, N., di San Filippo, C. A., and Pasquali, M. (2006). Disorders of carnitine transport and the carnitine cycle. *Am. J. Med. Genet. C*. 142 (2), 77–85. doi:10.1002/ajmg.c.30087

Lopaschuk, G. D., Ussher, J. R., Folmes, C. D., Jaswal, J. S., and Stanley, W. C. (2010). Myocardial fatty acid metabolism in health and disease. *Physiol. Rev*. 90 (1), 207–258. doi:10.1152/physrev.00015.2009

Ma, D., Liu, Z., Loh, L. J., Zhao, Y., Li, G., Liew, R., et al. (2018). Identification of an I_{Na}-dependent and I_{to}-mediated proarrhythmic mechanism in cardiomyocytes derived from pluripotent stem cells of a Brugada syndrome patient. *Sci. Rep*. 8 (1), 11246. doi:10.1038/s41598-018-29574-5

Meijer van Putten, R. M. E., Mengarelli, I., Guan, K., Zegers, J. G., van Ginneken, A. C. G., Verkerk, A. O., et al. (2015). Ion channelopathies in human induced pluripotent stem cell derived cardiomyocytes: a dynamic clamp study with virtual I_{k1}. *Front. Physiol*. 6, 7. doi:10.3389/fphys.2015.00007

Mordwinkin, N. M., Burridge, P. W., and Wu, J. C. (2013). A review of human pluripotent stem cell-derived cardiomyocytes for high-throughput drug discovery, cardiotoxicity screening, and publication standards. *J. Cardiovasc. Transl. Res*. 6 (1), 22–30. doi:10.1007/s12265-012-9423-2

Nasser, M., Javaheri, H., Fedorowicz, Z., and Noorani, Z. (2012). Carnitine supplementation for inborn errors of metabolism. *Cochrane Database Syst. Rev*. 15 (2), Cd006659. doi:10.1002/14651858.CD006659.pub3

Nerbonne, J. M., and Kass, R. S. (2005). Molecular physiology of cardiac repolarization. *Physiol. Rev*. 85, 1205–1253. doi:10.1152/physrev.00002.2005

Pena, L. D., van Calcar, S. C., Hansen, J., Edick, M. J., Walsh-Vockley, C., Leslie, N., et al. (2016). Outcomes and genotype-phenotype correlations in 52 individuals with VLCAD deficiency diagnosed by NBS and enrolled in the IBEM-IS database. *Mol. Genet. Metab*. 118 (4), 272–281. doi:10.1016/j.ymgme.2016.05.007

Primassin, S., Ter Veld, F., Mayatepek, E., and Spiekerkoetter, U. (2008). Carnitine supplementation induces acylcarnitine production in tissues of very long-chain acyl-CoA dehydrogenase-deficient mice, without replenishing low free carnitine. *Pediatr. Res*. 63 (6), 632–637. doi:10.1203/PDR.0b013e31816ff6f0

Qu, Z., Xie, L. H., Olcese, R., Karagueuzian, H. S., Chen, P. S., Garfinkel, A., et al. (2013). Early afterdepolarizations in cardiac myocytes: beyond reduced repolarization reserve. *Cardiovasc. Res*. 99 (1), 6–15. doi:10.1093/cvr/cvt104

Ranea-Robles, P., Yu, C., van Vlies, N., Vaz, F. M., and Houten, S. M. (2020). Slc22a5 haploinsufficiency does not aggravate the phenotype of the long-chain acyl-CoA dehydrogenase KO mouse. *J. Inherit. Metab. Dis*. 43 (3), 486–495. doi:10.1002/jimd.12204

Reuter, S. E., and Evans, A. M. (2012). Carnitine and acylcarnitines: pharmacokinetic, pharmacological and clinical aspects. *Clin. Pharmacokinet*. 51 (9), 553–572. doi:10.1007/BF03261931

Ribas, G. S., and Vargas, C. R. (2020). Evidence that oxidative disbalance and mitochondrial dysfunction are involved in the pathophysiology of fatty acid oxidation disorders. *Cell. Mol. Neurobiol*. [in Press]. doi:10.1007/s10571-020-00955-7

Roussel, J., Labarthe, F., Thireau, J., Ferro, F., Farah, C., Roy, J., et al. (2016). Carnitine deficiency induces a short QT syndrome. *Heart Rhythm*. 13 (1), 165–174. doi:10.1016/j.hrthm.2015.07.027

Schooneman, M. G., Achterkamp, N., Argmann, C. A., Soeters, M. R., and Houten, S. M. (2014). Plasma acylcarnitines inadequately reflect tissue acylcarnitine metabolism. *Biochim. Biophys. Acta*. 1841 (7), 987–994. doi:10.1016/j.bbalip.2014.04.001

Spiekerkoetter, U., Bastin, J., Gillingham, M., Morris, A., Wijburg, F., and Wilcken, B. (2010). Current issues regarding treatment of mitochondrial fatty acid oxidation disorders. *J Inherit. Metab. Dis*. 33 (5), 555–561. doi:10.1007/s10545-010-9188-1

Spiekerkoetter, U., Lindner, M., Santer, R., Grotzke, M., Baumgartner, M. R., Boehles, H., et al. (2009). Treatment recommendations in long-chain fatty acid oxidation defects: consensus from a workshop. *J. Inherit. Metab. Dis*. 32 (4), 498–505. doi:10.1007/s10545-009-1126-8

Tohyama, S., Hattori, F., Sano, M., Hishiki, T., Nagahata, Y., Matsuura, T., et al. (2013). Distinct metabolic flow enables large-scale purification of mouse and human pluripotent stem cell-derived cardiomyocytes. *Cell. Stem. Cell*. 12, 127–137. doi:10.1016/j.stem.2012.09.013

Treem, W. R., Stanley, C. A., Hale, D. E., Leopold, H. B., and Hyams, J. S. (1991). Hypoglycemia, hypotonia, and cardiomyopathy: the evolving clinical picture of long-chain acyl-CoA dehydrogenase deficiency. *Pediatrics*. 87 (3), 328–333.

van der Wall, E., Herrero-Hernandez, P., Wan, R., Broeders, M., in't Groen, S. L. M., van Gestel, T. J. M., et al. (2018). Large-scale expansion of human iPSC-derived skeletal muscle cells for disease modeling and cell-based therapeutic strategies. *Stem Cell Rep*. 10, 1975–1990. doi:10.1016/j.stemcr.2018.04.002

Vaz, F. M., and Wanders, R. J. A. (2002). Carnitine biosynthesis in mammals. *Biochem J*. 361 (Pt 3), 417–429. doi:10.1042/0264-6021:3610417

Veerman, C. C., Kosmidis, G., Mummery, C. L., Casini, S., Verkerk, A. O., and Bellin, M. (2015). Immaturity of human stem-cell-derived cardiomyocytes in culture: fatal flaw or soluble problem? *Stem Cells Dev*. 24 (9), 1035–1052. doi:10.1089/scd.2014.0533

Veerman, C. C., Mengarelli, I., Guan, K., Stauske, M., Barc, J., Tan, H. L., et al. (2016). hiPSC-derived cardiomyocytes from Brugada Syndrome patients without identified mutations do not exhibit clear cellular electrophysiological abnormalities. *Sci. Rep*. 6, 30967. doi:10.1038/srep30967

Verkerk, A. O., Veldkamp, M. W., Baartscheer, A., Schumacher, C. A., Klöpping, C., van Ginneken, A. C. G., et al. (2001). Ionic mechanism of delayed afterdepolarizations in ventricular cells isolated from human end-stage failing hearts. *Circulation*. 104 (22), 2728–2733. doi:10.1161/hc4701.099577

Wanders, R. J. A., Visser, G., Ferdinandusse, S., Vaz, F. M., and Houtkooper, R. H. (2020). Mitochondrial fatty acid oxidation disorders: laboratory diagnosis, pathogenesis, and the complicated route to treatment. *J. Lipid Atheroscler*. 9 (3), 313–333. doi:10.12997/jla.2020.9.3.313

Winter, S. C. (2003). Treatment of carnitine deficiency. *J. Inherit. Metab. Dis*. 26 (2), 171–180. doi:10.1023/a:1024433100257

Wit, A. L. (2018). Afterdepolarizations and triggered activity as a mechanism for clinical arrhythmias. *Pacing Clin. Electrophysiol*. 41 (8), 883–896. doi:10.1111/pace.13419

Wu, J., and Corr, P. B. (1992). Influence of long-chain acylcarnitines on voltage-dependent calcium current in adult ventricular myocytes. *Am. J. Physiol*. 263 (2), H410–H417. doi:10.1152/ajpheart.1992.263.2.H410

Yamada, K., and Taketani, T. (2019). Management and diagnosis of mitochondrial fatty acid oxidation disorders: focus on very-long-chain acyl-CoA dehydrogenase deficiency. *J. Hum. Genet*. 64 (2), 73–85. doi:10.1038/s10038-018-0527-7

Conflict of Interest: The authors declare that the research was conducted in the absence of any commercial or financial relationships that could be construed as a potential conflict of interest.

frontiers in Pharmacology

MINI REVIEW
published: 04 February 2021
doi: 10.3389/fphar.2021.617922

Heart Slices to Model Cardiac Physiology

*Moustafa H. Meki[1,2†], Jessica M. Miller[1,2†] and Tamer M. A. Mohamed[1,3,4]**

[1]From the Institute of Molecular Cardiology, Department of Medicine, University of Louisville, Louisville, KY, United States, [2]Department of Bioengineering, University of Louisville, Louisville, KY, United States, [3]Department of Pharmacology and Toxicology, University of Louisville, Louisville, KY, United States, [4]Institute of Cardiovascular Sciences, University of Manchester, Manchester, United Kingdom

Translational research in the cardiovascular field is hampered by the unavailability of cardiac models that can recapitulate organ-level physiology of the myocardium. Outside the body, cardiac tissue undergoes rapid dedifferentiation and maladaptation in culture. There is an ever-growing demand for preclinical platforms that allow for accurate, standardized, long-term, and rapid drug testing. Heart slices is an emerging technology that solves many of the problems with conventional myocardial culture systems. Heart slices are thin (<400 µm) slices of heart tissue from the adult ventricle. Several recent studies using heart slices have shown their ability to maintain the adult phenotype for prolonged periods in a multi cell-type environment. Here, we review the current status of cardiac culture systems and highlight the unique advantages offered by heart slices in the light of recent efforts in developing physiologically relevant heart slice culture systems.

Keywords: heart, cardiotoxicity, cardiomyocytes, iPS-cell derived cardiomyocytes, heart slices

Edited by:
Xinkang Wang, Agennix, United States

Reviewed by:
Julio Aleman, University of Pittsburgh, United States
Nazish Sayed, Stanford University, United States

****Correspondence:***
Tamer M A Mohamed
tamer.mohamed@louisville.edu

†These authors have contributed equally to this work

Specialty section:
This article was submitted to Cardiovascular and Smooth Muscle Pharmacology, a section of the journal Frontiers in Pharmacology

Received: *15 October 2020*
Accepted: *05 January 2021*
Published: *04 February 2021*

Citation:
Meki MH, Miller JM and Mohamed TMA (2021) Heart Slices to Model Cardiac Physiology. Front. Pharmacol. 12:617922. doi: 10.3389/fphar.2021.617922

INTRODUCTION

Before clinical studies, there is a need for reliable experimental systems that can accurately replicate the human heart's physiological environment. Such systems should model altered mechanical loading, heart rate, and electrophysiological properties. The most prevalently used cardiac physiology screening platform are animal models that have limited reliability in mirroring the effects of drugs in human hearts (Liu et al., 2006; Salama and Bett, 2014). Additionally, the use of animal models to create a pharmacokinetic profile of drugs is relatively expensive at the early development stage since large amounts of the drugs are used (Guth et al., 2019). Ultimately, the ideal experimental cardiac model is one that demonstrates high sensitivity and specificity toward various therapeutic and pharmacological interventions while accurately replicating the physiology and pathophysiology of the human heart (Wang et al., 2008).

IN-VITRO MODELING OF THE HUMAN MYOCARDIUM

In-vitro systems using a controlled culture environment have the unique advantage of quantitatively characterizing drug-related changes at the cellular level with relatively lower cost. These systems' success depends on how much clinically relevant information can be detected through the system. This includes contractility measurements, protein expression (e.g., gap junction proteins and contractile proteins), accurate transcriptional profile, calcium homeostasis, and electrophysiology. Additionally, the applicability of the system to human cells is of paramount importance. Guth et al. (Guth et al., 2019) summarized the most relevant features and considerations for *in-vivo* drug testing platforms.

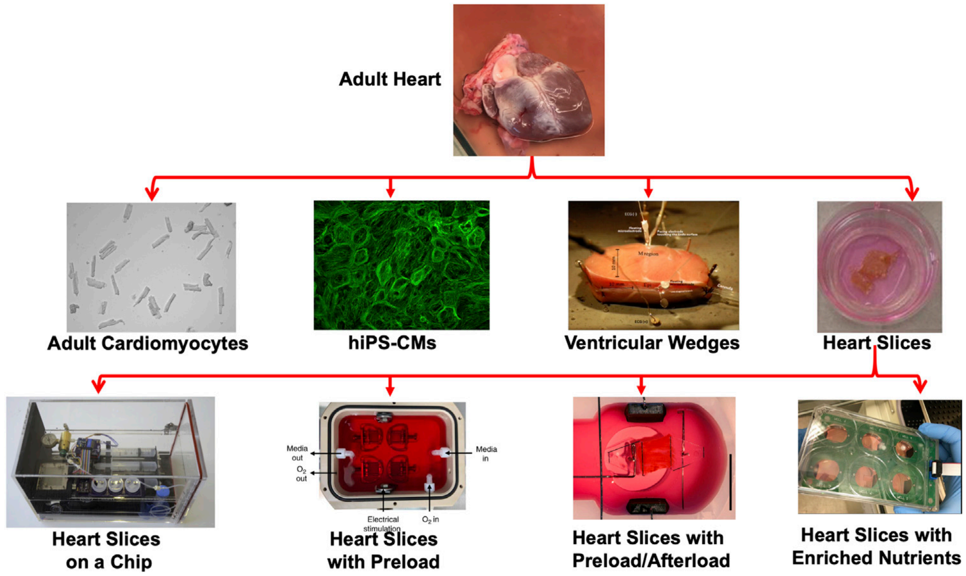

FIGURE 1 | Modeling heart tissue in cultures. Representation of the various platforms used to model cardiac physiology in culture including adult cardiomyocytes (Mohamed et al., 2017), hiPS-CMs (Mohamed et al., 2018), Ventricular wedges (Di Diego et al., 2013) and heart slices (Brandenburger et al., 2012). Recently, several groups advanced the heart slice technology by developing heart slices on-a-chip (Qiao et al., 2019), including preload (Watson et al., 2019), including preload/afterload (Fischer et al., 2019), or enriching the culture medium with nutrients (Ou et al., 2019).

Nonetheless, 28% of drug withdrawals are owed to unanticipated cardiotoxicity (Gwathmey et al., 2009). This only shows that current cardiac models are unsuitable for preclinical drug testing and development. To this end, there have been many efforts to develop reliable preclinical models to mimic the human heart tissue. This review will focus on the most relevant cardiac physiology models: isolated adult cardiomyocytes, human induced pluripotent stem cell-derived cardiomyocytes, arterially perfused left ventricular wedge preparations, and subsequently, compare them to heart slices.

Thin heart slices are a relatively new technology that has emerged in recent years and has shown promise in providing a system of adequate complexity and viability to allow for drug screening (Miller et al., 2020). They retain the adult phenotype, including the adult heart's multicellularity and extracellular structure, and have been produced from human cardiac tissue and large mammals.

While each of these models has its advantages, each model has shortcomings in modeling the physiology/pathophysiology of an adult human heart. This is owed to the heart tissue's complex environment where multiple cell types interact under chronic neurohormonal stimulation to maintain normal heart homeostasis. It is thus understandable that there are many challenges in reproducing this multiplexed system in culture.

This review article will highlight each of these models and discuss their potential to model cardiac physiology in culture (**Figure 1**).

ANIMAL/HUMAN ISOLATED ADULT CARDIOMYOCYTE

One of the oldest and most simplistic cardiac models is the use of isolated human cardiomyocytes. The first isolated cardiomyocyte from adult hearts failed to last for a reasonable time in culture and lacked proper phenotypic characteristics (Harary and Farley, 1963; Halbert and Bruderer, 1971; Halbert et al., 1973). Successful isolation and culture of adult cardiomyocytes were performed first by Powell and Twist in 1976 (Powell and Twist, 1976). Since then, cultured adult isolated cardiomyocytes have been primarily used to study cardiac electrophysiology (Beuckelmann and Wier, 1988; Ke et al., 2007), response to sepsis (Celes et al., 2013), Ca^{+2} dynamics (Beuckelmann et al., 1992; Gorski et al., 2018), gene transfer (Judd et al., 2016), and contractile function (Parikh et al., 1993; Monte et al., 1999). Indeed, the simplistic unicellularity of isolated primary cardiomyocytes provides experimental strength by avoiding extraneous influences from other tissue components (Gilsbach et al., 2014). Moreover, when cultured adhering to a coated plastic surface, they will retain many adult cardiomyocyte phenotype characteristics including cell-cell coupling, t-tubule organization, and rod-shaped morphology (Mitcheson, 1998). While having been instrumental to cellular level research, adult isolated cardiomyocytes' appropriateness for predicting cardiotoxicity and macrolevel response to drugs and therapies is restricted. Although isolated cardiomyocytes can survive for weeks, the single cell-type culture will rapidly dedifferentiate and lose function within 48 h of culture (Bird et al., 2003). Additionally, the low cell yield with currently used enzymatic isolation protocols and cellular damage limit their use in high throughput screening (Tytgat, 1994; Dipla et al., 1998; Dobrev et al., 2000). Adult isolated primary cardiomyocytes may be unsuitable for long-term drug screening due to their limited life span in culture and its nature of replicating only a single cell type out of the multiplexed heart cell types. Nevertheless, recent efforts have focused on improving isolation protocols to improve cell yield and lowered the damage to the cardiac tissue (Guo et al., 2018). Notably, Callaghan et al. (Callaghan et al., 2020) have shown that Geltrex and blebbistatin using adult mouse cardiomyocytes enhanced survival in culture with maintained cellular function. However, the inhibition of cardiomyocyte contraction using blebbistatin may limit the model's use to study cardiomyocyte contractility.

HUMAN-INDUCED PLURIPOTENT STEM CELL-DERIVED CARDIOMYOCYTES (HIPSC-CMS)

Human-induced pluripotent stem cells (hiPSC) reprogramming was first demonstrated in 2007 (Takahashi et al., 2007), and hiPSC-cardiomyocytes (hiPSC-CMs) have since been extensively used to determine drug cardiotoxicity, arrhythmogenicity (Sirenko et al., 2013; Pointon et al., 2015; Sharma et al., 2018), and cardiac disease modeling (Jung and Bernstein, 2014; Yang et al., 2015) due to the relative simplicity of hiPSC-CMs generation and culture process (Denning et al., 2016). However, it is well known that hiPSC-CMs are structurally and functionally similar to fetal cardiomyocytes due to their lack of cell-cell coupling, under-developed sarcoplasmic reticulum, and no T-tubules; hence slow excitation-contraction coupling (Denning et al., 2016).

With these apparent limitations in mind, several efforts have been conducted to promote their maturation, discussed in detail in Ahmed et al. review (Ahmed et al., 2020). These studies aim to mimic certain cardiac milieu stimuli using integrated heart-on-chip systems to include extracellular matrix (Roberts et al., 2016), 3-D structure (Zhang et al., 2013; Zhang et al., 2016), electrical (Tandon et al., 2009; Nunes et al., 2013), and electro-mechanical stimulation (Jackman et al., 2016; Ruan et al., 2016; Ronaldson-Bouchard et al., 2018). Notably, Kroll et al., (Kroll et al., 2017) developed a force stretch system that can apply synchronized mechanical stress and electrical stimulation on hiPSC-CMs cultured on a flexible PDMS membrane. They have shown enhanced N-cadherin signal, stress fiber formation, sarcomere shortening, and contractile protein expression with hiPSC-CMs conditioning, indicating a trend toward maturation. We suggest the following comprehensive reviews for details (Benam et al., 2015; Ronaldson-Bouchard and Vunjak-Novakovic, 2018; Zhang et al., 2018; Zhao et al., 2020). These advancements allow the hiPS-CMs to become the most widely used platform for drug screening due to their stability in culture for a long time and their physiological resemblance to the human heart.

ANIMAL-DERIVED ARTERIALLY PERFUSED LEFT VENTRICULAR WEDGE PREPARATIONS

Arterially perfused left ventricular wedges were developed by Yan and Antzelevitch in 1996 (Yan and Antzelevitch, 1996; Yan et al., 1998) using canine hearts. Since then, ventricular wedge preparations have been expanded to other animal models, including humans, and have been extensively used in studying heart electrophysiology, conduction velocity, and the development of arrhythmia (Chen et al., 2006; Glukhov et al., 2010; Lou et al., 2011; O'Shea et al., 2019). The advantage of this model is producing 3-dimensional tissue-level insight into cardiac physiology and pathophysiology.

However, where ventricular wedges fall short is the relatively low throughput of the preparation due to the coronary system's complexity and, therefore, low sample yield per heart, (Qiao et al., 2019) limiting their use in drug testing. Furthermore, the preparations can only remain viable for a few hours in perfusion before suffering a similar fate to isolated cardiomyocytes (Kang et al., 2016) restricting their use in subacute and chronic studies. Such a system as a drug screening platform would be challenging due to the short life in culture and the low throughput.

ANIMAL/HUMAN-DERIVED HEART SLICES TO MODEL CARDIAC PHYSIOLOGY

The first thin (<400 μm) heart slices were developed in 1992 (Parrish et al., 1992) in the advent of tissue slicing technology with relatively high precision and reproducible slice thicknesses. In this study, rat ventricular heart slices were cultured for 24 h with maintained viability and metabolism (Parrish et al., 1992). The key feature was the use of continuously oxygenated media while rotating the culture within a cylinder. Brandenburger et al., (Brandenburger et al., 2012) 10 years later developed a more simplistic approach to overcome the inadequacies with isolated cardiomyocytes and ventricular wedge preparations. Brandenburger and colleagues used a transwell membrane to allow for a liquid-air interface.

Thin heart tissue slices (300 μm) have since been shown to achieve high viability, retain typical tissue architecture, contractility, calcium handling, and conduction velocity for 24 h (Kang et al., 2016; Watson et al., 2017). Additionally, heart slices maintain a 3-dimensional structure with the multi cell-type environment and the presence of extracellular matrix (ECM). This allows for other cellular components in the heart slices and ECM to interact with the cardiomyocytes through direct cellular contact or paracrine secretion, which is essential to maintain a mature cardiomyocyte phenotype (Talman and Kivelä, 2018; Yoshida et al., 2018). It is important to note that heart slices and ventricular wedge preparations are different. Thin heart slices could remain viable and functional in culture for 24 h, do not require external perfusion, and obtain oxygen and nutrients directly from culture media. These unique advantages make them adequate for medium to high throughput systems for drug discovery.

Since their inception, heart slices have been prepared from several animals as well as human hearts. Detailed protocols for preparing heart slices have been described by our group and others (Brandenburger et al., 2012; Watson et al., 2017; Watson et al., 2019; Ou et al., 2020). While multiple factors control the maturation and regulation of the adult cardiac phenotype, the structural fidelity of heart slices provides cell-cell interactions, transmembrane regulation and maintains standard tissue stiffness. These heart slices' thinness simplifies nutrient and oxygen diffusion through the tissue and provides a "pseudo" 3-dimensional model that can allow for multiplexed cellular-level studies. Pseudo-3-dimensional model refers to the large surface area to thickness ratio of the heart tissue slices, which does not compromise the tissue's 3-D structure while maintaining proper substrate exchange.

RECENT ADVANCEMENTS IN HEART SLICES

Early transwell culture of cardiac slices by Brandenburger et al. maintained viability, ß-adrenergic response, and many electrophysiological properties for 28 days (Brandenburger et al., 2012). However, the prolonged culture of heart slices in transwell systems produced an observable loss in the tissue's structural and functional integrity after 24 h in culture shown by a >90% drop in contractility. The observed tissue remodeling reaffirmed this with a dedifferentiated cardiomyocyte phenotype and a significant reduction in mRNA expression of MLC2 and α-actin (Brandenburger et al., 2012). Subsequent efforts used the same culture transwell system to culture heart slices 24 h using human and other vertebrate hearts (Kang et al., 2016; Watson et al., 2017). Indeed, the heterogeneous heart slice preparation incorporates many organotypic characteristics of the myocardium, and they will undergo dedifferentiation due to the non-physiological environment in culture (Parrish et al., 1992; Brandenburger et al., 2012; Perbellini et al., 2018).

The native heart experiences several hemodynamic and neurohormonal factors which precisely compose its ideal environment for functional integrity (Barton et al., 2005). Disruption of this balance in culture will ultimately promote some level of adaptive remodeling within the heart. This highlights the importance of incorporating biomimetic stimulants to maintain cardiac phenotype properly. But given the cardiovascular system's complexity, it is difficult to define all the cardiac milieu constituents responsible for this balance.

In 2019, several efforts were taken to prolong further the functional viability of the heart slices in culture. The most relevant factors addressed in these efforts are biophysical stimulation through electrical pacing, mechanical loading (preload and afterload), and proper oxygenation and nutrient support (Fischer et al., 2019; Ou et al., 2019; Qiao et al., 2019; Watson et al., 2019).

Electrical impulse propagation in the heart is regulated through the gap junctions, which synchronize action potential progress and contraction (Ye and Black, 2011). The disruption of the gap junction protein connexin 43, localization, or expression can trigger arrhythmias. Continuous electrical stimulation of hiPSCs has been shown to improve connexin abundance and improve sarcomere ultrastructure (Hirt et al., 2014). The other side of the coin is the mechanical loading condition in culture. Mechanical cues in the native heart play an essential role in steering physiological/pathological remodeling such as dilated or hypertrophic cardiomyopathy (Barton et al., 2005). The absence of electrical stimulation, preload, and afterload in static transwell culture may partially explain the loss of contractility and contractile protein expression after 24 h in culture (Brandenburger et al., 2012). Furthermore, the high metabolic demand of the myocardium necessitates the incorporation of rich nutrient media. Several media supplements have been previously used to support hiPSC-CMs in culture (Yamakawa et al., 2015; Mohamed et al., 2017; Mohamed et al., 2018). Likewise, oxygenation of the media has proven crucial to prevent tissue hypoxia since the slice thickness (300–400 µm) approaches the diffusion limit of oxygen of the myocardium and can heavily impact cardiac gene expression (Giordano, 2005).

In this context, we review four recent studies from different laboratories that have made significant efforts to emulate the cardiac milieu (Fischer et al., 2019; Ou et al., 2019; Qiao et al., 2019; Watson et al., 2019).

HEART TISSUE SLICE ON A CHIP CULTURE CHAMBER

Qiao et al. (Qiao et al., 2019), developed an automated heart-on-a-chip culture system that uses heart tissue slices and supports accurately controlled culture conditions with continuous O_2/CO_2 control, an orbital shaker, media circulation, static mechanical loading, and electrical stimulation. The system was tested using murine atrial and human ventricular slices. The culture system itself offered some unique advantages, including optical mapping, contraction rate using far-field pseudo ECG electrodes, and integrated pacing electrodes. Human heart slices preserved electrophysiology for four days in culture with uniform repolarization, average transverse conduction velocity, and anisotropic conduction. While this culture system is innovative, the study presented did not apply electrical stimulation or mechanical loading in the smart tissue culture chamber. Additionally, it was only used to test the cultured slices' electrophysiology, which was more stable in early static transwell cultures than the drastic drop in contractility and phenotype on the functional and transcriptional levels in extended culture (Brandenburger et al., 2012). Hence, further validation to confirm any implied reduction in dedifferentiation or maintenance of heart slices functionality in culture is needed.

INTRODUCTION OF PRELOAD AND AFTERLOAD

Watson et al. (Watson et al., 2019), investigated the application of simultaneous electrical stimulation and preload on rat, rabbit, and failing human heart slices. The system used a hand-operated screw and nut post to progressively stretch the tissue to different sarcomeric lengths and achieved sub-micrometer resolution. The study compared this system to static transwell culture and fresh tissue. Rat heart slices cultured for 24 h with an increased sarcomeric length of 2.2 µm showed maintained contractile function, normal electrophysiology, conduction velocity, calcium handling, and action potential compared to fresh tissue. Interestingly, this model showed an upregulation of hypertrophic genes and increased calcium transient amplitude within 24 h in culture compared to fresh heart slices. At the same time, cardiomyocyte size did not vary for all preloading conditions tested. Five days culture with rabbit heart showed no deterioration in contractile function. Heart failure slices from human hearts showed some degree of preserved contractility after 24 h in culture.

There are obvious limitations when using slices from rat hearts since their high metabolic rates make them more susceptible to dedifferentiation. Moreover, the short culture time leaves unanswered questions regarding the long-term performance of static preload. Nevertheless, the improvement in functionality with stretching heart slices underlined the undeniable mechanical stimulation role in regulating the cardiac phenotype *in vitro*. Additionally, the upregulation seen in some hypertrophic genes may be related to the isometric contraction of the tissue slices with theoretically infinite afterload (Pitoulis et al., 2020).

A reasonably similar system was developed by Fischer et al. (Fischer et al., 2019). In this system, slices from normal and failing human hearts were stretched between two posts in culture with electrical stimulation. The heart slice was fixed at one end, while the other end was connected to a spring cantilever to provide a linear mechanical afterload. A small magnet coupled with a magnetic field sensor was used to detect the movement of the free end of the tissue slice, and the contractile force was calculated in real-time using the spring constant. While using a low stimulation pace (0.2 Hz) for up to 4 months, the study showed preserved contractility, preserved tissue elasticity, connexin localization, and α-actinin. But there is severe downregulation of cardiac gene expression at the first assessed time point (8 days). Unlike the culture system by Watson et al. (Watson et al., 2019), this system allowed for active tissue contraction and shortening. Nevertheless, as noted by Pitoulis et al. (Pitoulis et al., 2020) this mode of contraction is still short of the physiological force-length loop where relaxation and contraction are separated by periods of isometric relaxation and contraction.

OPTIMIZATION OF NUTRIENTS AND ELECTRICAL STIMULATION

Our group has shown that through optimized proprietary culture media, frequent oxygenation, and electrical stimulation, tissue slices can preserve viability, functionality, and cardiomyocyte structure for up to 6 days (Ou et al., 2019; Ou et al., 2020). The 300 µm human and pig heart slices were cultured at a physiological rate (1.2 Hz, 72 beats/min) and showed normal viability, gene expression profile, calcium homeostasis, contractility, twitch force generation, and response to ß-adrenergic stimulation over the first six days. However, by day 10, dedifferentiation was evident by the disruption of gene expression of more than 500 genes, connexin-43 delocalization, and loss of contractility. Nonetheless, prolonging functionality and maintaining cardiac phenotype for six days is a significant advancement compared to the early transwell culture systems. However, the critical element missing is the addition of synchronized mechanical loading of the heart tissue.

APPLICATIONS OF HEART SLICES AS A CARDIOTOXICITY SCREENING PLATFORM

To date, the perfect human cardiac tissue model does not exist. The suitability of the testing platform is dependent on the level of complexity and experimental question which needs to be answered for each specific application. Engineered 3-dimensional tissue culture of hiPSC-CMs have shown promise in producing heterogeneous, relatively mature cardiac constructs that suit a wide range of applications (e.g., regenerative medicine, personalized assays, and basic science) (Lemoine et al., 2017; Goldfracht et al., 2019; Ahmed et al., 2020). Nevertheless, the recent advancements in biomimetic heart slice technology discussed above show that this technology is progressing in the right direction and may soon provide a medium/high throughput platform to recapitulate drug effects on myocardial mechanics, electrophysiology at a cellular level that does not compromise organ level complexity.

The most immediate application of organotypic heart slices is in the field of drug screening and cardiotoxicity. Current preclinical cardiotoxicity systems are failing to detect the cardiotoxicity of many drugs (Gwathmey et al., 2009). We have recently shown that our optimized heart slice system (Ou et al., 2019) can reliably detect drug-related cardiotoxicity (Miller et al., 2020). Three medications from three different anticancer categories were tested (doxorubicin, trastuzumab, and sunitinib). Cardiac slices demonstrated toxic effects in response to all treatments and were superior to hiPSC-CMs in detecting sunitinib at 0.1–1 µM concentration. These results provide evidence of the clinical relevance of heart slices as an essential tool in drug development.

CURRENT LIMITATIONS AND FUTURE PERSPECTIVE OF THE CARDIAC SLICE TECHNOLOGY

There are several limitations for the heart slice culture, which will need to be addressed in further studies. First, the exact nutrients needed to further maintain the metabolic activities and mitochondrial utilization rates in the presence of several nutrients such as fatty acids, glucose, fructose, corticosteroids, and hormones of heart slices. Our lab has performed the only study to provide a proof of concept study to show that heart slices can reflect clinical phenotypes of cardiotoxins (Miller et al., 2020). This study used three known cardiotoxins at three different concentrations and assessed effects at one time point (48 h). Further studies are needed to address a more in-depth time course and test other cardiotoxins and cardiac therapeutics. Furthermore, studies to test cardiotoxicity in enhanced cardiac function models are required.

Another limitation of the heart slices is the inability to record conduction velocity and electrophysiological properties within the culture. Considering that electrophysiology is highly relevant for predicting arrhythmogenic drug potential, action potential recordings from the whole tissue would be informative. In comparison, Integrated and miniaturized technologies that use hiPSC-CMs, such as heart-on-a-chip systems, have been used to record accurate electrophysiological data and other quantitative data due to the ease with which microsensors can be integrated within the system (Cohen-Karni et al., 2009; Nunes et al., 2013; Stoehr et al., 2016). Indeed, a recent study established a glass microelectrode technique to perform patch clamping on the whole heart (Barbic et al., 2017). However, further research is required to adapt this microelectrode technology for recording action potentials in heart slices. Another limitation is that heart slice technology is technically and financially demanding, limiting its general or widespread use. To this end, several groups have recently published detailed video protocols to promote this technology (George et al., 2020; Ou et al., 2020). Another major limitation of the heart slice technology is the relatively short functional viability in culture (6 days), making it suitable for only acute and subacute cardiotoxicity testing but not for chronic toxicity testing. Further efforts to prolong the viability in culture are needed. Moreover, access to fresh human heart tissue is limited to a few research groups, limiting the spread of the technology. Research for preserving the human heart tissue should be conducted to facilitate the spread of the technology.

AUTHOR CONTRIBUTIONS

JM, MM, TM: manuscript writing, and final approval of manuscript.

FUNDING

TMAM is supported by NIH grants R01HL147921 and P30GM127607 and American Heart Association grant 16SDG29950012, USA department of Defense grant number W81XWH-20-1-0419.

REFERENCES

Ahmed, R. E., Anzai, T., Chanthra, N., and Uosaki, H. (2020). A brief review of current maturation methods for human induced pluripotent stem cells-derived cardiomyocytes. *Front. Cell Dev. Biol.* 8, 178. doi:10.3389/fcell.2020.00178

Barbic, M., Moreno, A., Harris, T. D., and Kay, M. W. (2017). Detachable glass microelectrodes for recording action potentials in active moving organs. *Am. J. Physiol. Heart Circ. Physiol.* 312, H1248–H1259. doi:10.1152/ajpheart.00741.2016

Barton, P. J. R., Felkin, L. E., Birks, E. J., Cullen, M. E., Banner, N. R., Grindle, S., et al. (2005). Myocardial insulin-like growth factor-I gene expression during recovery from heart failure after combined left ventricular assist device and clenbuterol therapy. *Circulation* 112, I46–I50. doi:10.1161/01.CIRCULATIONAHA.105.525873

Benam, K. H., Dauth, S., Hassell, B., Herland, A., Jain, A., Jang, K.-J., et al. (2015). Engineered in vitro disease models. *Annu. Rev. Pathol.* 10, 195–262. doi:10.1146/annurev-pathol-012414-040418

Beuckelmann, D. J., and Wier, W. G. (1988). Mechanism of release of calcium from sarcoplasmic reticulum of Guinea-pig cardiac cells. *J. Physiol. (Lond.)* 405, 233–255. doi:10.1113/jphysiol.1988.sp017331

Beuckelmann, D. J., Näbauer, M., and Erdmann, E. (1992). Intracellular calcium handling in isolated ventricular myocytes from patients with terminal heart failure. *Circulation* 85, 1046–1055. doi:10.1161/01.cir.85.3.1046

Bird, S. D., Doevendans, P. A., Van Rooijen, M. A., Brutel De La Riviere, A., Hassink, R. J., Passier, R., et al. (2003). The human adult cardiomyocyte phenotype. *Cardiovasc. Res.* 58, 423–434. doi:10.1016/s0008-6363(03)00253-0

Brandenburger, M., Wenzel, J., Bogdan, R., Richardt, D., Nguemo, F., Reppel, M., et al. (2012). Organotypic slice culture from human adult ventricular myocardium. *Cardiovasc. Res.* 93, 50–59. doi:10.1093/cvr/cvr259

Callaghan, N. I., Lee, S.-H., Hadipour-Lakmehsari, S., Lee, X. A., Ahsan Siraj, M., Driouchi, A., et al. (2020). Functional culture and *in vitro* genetic and small-molecule manipulation of adult mouse cardiomyocytes. *Commun. Biol.* 3, 229. doi:10.1038/s42003-020-0946-9

Celes, M. R. N., Malvestio, L. M., Suadicani, S. O., Prado, C. M., Figueiredo, M. J., Campos, E. C., et al. (2013). Disruption of calcium homeostasis in cardiomyocytes underlies cardiac structural and functional changes in severe sepsis. *PloS One* 8, e68809. doi:10.1371/journal.pone.0068809

Chen, X., Cordes, J. S., Bradley, J. A., Sun, Z., and Zhou, J. (2006). Use of arterially perfused rabbit ventricular wedge in predicting arrhythmogenic potentials of drugs. *J. Pharmacol. Toxicol. Methods* 54, 261–272. doi:10.1016/j.vascn.2006.02.005

Cohen-Karni, T., Timko, B. P., Weiss, L. E., and Lieber, C. M. (2009). Flexible electrical recording from cells using nanowire transistor arrays. *Proc. Natl. Acad. Sci. U.S.A.* 106, 7309–7313. doi:10.1073/pnas.0902752106

Denning, C., Borgdorff, V., Crutchley, J., Firth, K. S., George, V., Kalra, S., et al. (2016). Cardiomyocytes from human pluripotent stem cells: from laboratory curiosity to industrial biomedical platform. *Biochim. Biophys. Acta* 1863, 1728–1748. doi:10.1016/j.bbamcr.2015.10.014

Di Diego, J. M., Sicouri, S., Myles, R. C., Burton, F. L., Smith, G. L., and Antzelevitch, C. (2013). Optical and electrical recordings from isolated coronary-perfused ventricular wedge preparations. *J. Mol. Cell. Cardiol.* 54, 53–64. doi:10.1016/j.yjmcc.2012.10.017

Dipla, K., Mattiello, J. A., Jeevanandam, V., Houser, S. R., and Margulies, K. B. (1998). Myocyte recovery after mechanical circulatory support in humans with end-stage heart failure. *Circulation* 97, 2316–2322. doi:10.1161/01.cir.97.23.2316

Dobrev, D., Wettwer, E., Himmel, H. M., Kortner, A., Kuhlisch, E., Schüler, S., et al. (2000). G-Protein beta(3)-subunit 825T allele is associated with enhanced human atrial inward rectifier potassium currents. *Circulation* 102, 692–697. doi:10.1161/01.cir.102.6.692

Fischer, C., Milting, H., Fein, E., Reiser, E., Lu, K., Seidel, T., et al. (2019). Long-term functional and structural preservation of precision-cut human myocardium under continuous electromechanical stimulation *in vitro*. *Nat. Commun.* 10, 117. doi:10.1038/s41467-019-08510-9

George, S. A., Brennan, J. A., and Efimov, I. R. (2020). Preclinical cardiac electrophysiology assessment by dual voltage and calcium optical mapping of human organotypic cardiac slices. *JoVE* 16, e60781. doi:10.3791/60781

Gilsbach, R., Preissl, S., Grüning, B. A., Schnick, T., Burger, L., Benes, V., et al. (2014). Dynamic DNA methylation orchestrates cardiomyocyte development, maturation and disease. *Nat. Commun.* 5, 5288. doi:10.1038/ncomms6288

Giordano, F. J. (2005). Oxygen, oxidative stress, hypoxia, and heart failure. *J. Clin. Invest.* 115, 500–508. doi:10.1172/JCI24408

Glukhov, A. V., Fedorov, V. V., Lou, Q., Ravikumar, V. K., Kalish, P. W., Schuessler, R. B., et al. (2010). Transmural dispersion of repolarization in failing and nonfailing human ventricle. *Circ. Res.* 106, 981–991. doi:10.1161/CIRCRESAHA.109.204891

Goldfracht, I., Efraim, Y., Shinnawi, R., Kovalev, E., Huber, I., Gepstein, A., et al. (2019). Engineered heart tissue models from hiPSC-derived cardiomyocytes and cardiac ECM for disease modeling and drug testing applications. *Acta Biomater.* 92, 145–159. doi:10.1016/j.actbio.2019.05.016

Gorski, P. A., Kho, C., and Oh, J. G. (2018). Measuring cardiomyocyte contractility and calcium handling in vitro. *Methods Mol. Biol.* 1816, 93–104. doi:10.1007/978-1-4939-8597-5_7

Guo, G. R., Chen, L., Rao, M., Chen, K., Song, J. P., and Hu, S. S. (2018). A modified method for isolation of human cardiomyocytes to model cardiac diseases. *J. Transl. Med.* 16, 288. doi:10.1186/s12967-018-1649-6

Guth, B. D., Engwall, M., Eldridge, S., Foley, C. M., Guo, L., Gintant, G., et al. (2019). Considerations for an in vitro, cell-based testing platform for detection of adverse drug-induced inotropic effects in early drug development. Part 1: general considerations for development of novel testing platforms. *Front. Pharmacol.* 10, 884. doi:10.3389/fphar.2019.00884

Gwathmey, J. K., Tsaioun, K., and Hajjar, R. J. (2009). Cardionomics: a new integrative approach for screening cardiotoxicity of drug candidates. *Expet Opin. Drug Metabol. Toxicol.* 5, 647–660. doi:10.1517/17425250902932915

Halbert, S., and Bruderer, R. (1971). Studies on in-vitro growth of dissociated beating rat and human heart cells. *Circulation* 5, 174.

Halbert, S. P., Bruderer, R., and Thompson, A. (1973). Growth of dissociated beating human heart cells in tissue culture. *Life Sci.* 13, 969–975. doi:10.1016/0024-3205(73)90087-8

Harary, I., and Farley, B. (1963). *In vitro* studies on single beating rat heart cells. I. Growth and organization. *Exp. Cell Res.* 29, 451–465. doi:10.1016/s0014-4827(63)80008-7

Hirt, M. N., Boeddinghaus, J., Mitchell, A., Schaaf, S., Börnchen, C., Müller, C., et al. (2014). Functional improvement and maturation of rat and human engineered heart tissue by chronic electrical stimulation. *J. Mol. Cell. Cardiol.* 74, 151–161. doi:10.1016/j.yjmcc.2014.05.009

Jackman, C., Carlson, A. L., and Bursac, N. (2016). Dynamic culture yields engineered myocardium with near-adult functional output. *Biomaterials* 111, 66–79. doi:10.1016/j.biomaterials.2016.09.024

Judd, J., Lovas, J., and Huang, G. N. (2016). Isolation, culture and transduction of adult mouse cardiomyocytes. *JoVE* 28, 66–79. doi:10.3791/54012

Jung, G., and Bernstein, D. (2014). hiPSC modeling of inherited cardiomyopathies. *Curr. Treat. Options Cardiovasc. Med.* 16, 320. doi:10.1007/s11936-014-0320-7

Kang, C., Qiao, Y., Li, G., Baechle, K., Camelliti, P., Rentschler, S., et al. (2016). Human organotypic cultured cardiac slices: new platform for high throughput preclinical human trials. *Sci. Rep.* 6, 28798. doi:10.1038/srep28798

Ke, Q., Xiao, Y.-F., Bradbury, J. A., Graves, J. P., Degraff, L. M., Seubert, J. M., et al. (2007). Electrophysiological properties of cardiomyocytes isolated from CYP2J2 transgenic mice. *Mol. Pharmacol.* 72, 1063–1073. doi:10.1124/mol.107.035881

Kroll, K., Chabria, M., Wang, K., Häusermann, F., Schuler, F., and Polonchuk, L. (2017). Electro-mechanical conditioning of human iPSC-derived cardiomyocytes for translational research. *Prog. Biophys. Mol. Biol.* 130, 212–222. doi:10.1016/j.pbiomolbio.2017.07.003

Lemoine, M. D., Mannhardt, I., Breckwoldt, K., Prondzynski, M., Flenner, F., Ulmer, B., et al. (2017). Human iPSC-derived cardiomyocytes cultured in 3D engineered heart tissue show physiological upstroke velocity and sodium current density. *Sci. Rep.* 7, 5464. doi:10.1038/s41598-017-05600-w

Liu, W., Ashford, M. W., Chen, J., Watkins, M. P., Williams, T. A., Wickline, S. A., et al. (2006). MR tagging demonstrates quantitative differences in regional ventricular wall motion in mice, rats, and men. *Am. J. Physiol. Heart Circ. Physiol.* 291, H2515–H2521. doi:10.1152/ajpheart.01016.2005

Lou, Q., Fedorov, V. V., Glukhov, A. V., Moazami, N., Fast, V. G., and Efimov, I. R. (2011). Transmural heterogeneity and remodeling of ventricular excitation-contraction coupling in human heart failure. *Circulation* 123, 1881–1890. doi:10.1161/CIRCULATIONAHA.110.989707

Miller, J. M., Meki, M. H., Ou, Q., George, S. A., Gams, A., Abouleisa, R. R. E., et al. (2020). Heart slice culture system reliably demonstrates clinical drug-related cardiotoxicity. *Toxicol. Appl. Pharmacol.* 406, 115213. doi:10.1016/j.taap.2020.115213

Mitcheson, J. (1998). Cultured adult cardiac myocytes: future applications, culture methods, morphological and electrophysiological properties. *Cardiovasc. Res.* 39, 280–300. doi:10.1016/s0008-6363(98)00128-x

Mohamed, T. M. A., Ang, Y. S., Radzinsky, E., Zhou, P., Huang, Y., Elfenbein, A., et al. (2018). Regulation of cell cycle to stimulate adult cardiomyocyte proliferation and cardiac regeneration. *Cell* 173, 104–e12. doi:10.1016/j.cell.2018.02.014

Mohamed, T. M., Stone, N. R., Berry, E. C., Radzinsky, E., Huang, Y., Pratt, K., et al. (2017). Chemical enhancement of in vitro and in vivo direct cardiac reprogramming. *Circulation* 135, 978–995. doi:10.1161/CIRCULATIONAHA.116.024692

Monte, F. D., Harding, S. E., Schmidt, U., Matsui, T., Kang, Z. B., Dec, G. W., et al. (1999). Restoration of contractile function in isolated cardiomyocytes from failing human hearts by gene transfer of SERCA2a. *Circulation* 100, 2308–2311. doi:10.1161/01.cir.100.23.2308

Nunes, S. S., Miklas, J. W., Liu, J., Aschar-Sobbi, R., Xiao, Y., Zhang, B., et al. (2013). Biowire: a platform for maturation of human pluripotent stem cell-derived cardiomyocytes. *Nat. Methods* 10, 781–787. doi:10.1038/nmeth.2524

Ou, Q., Jacobson, Z., Abouleisa, R. R. E., Tang, X. L., Hindi, S. M., Kumar, A., et al. (2019). Physiological biomimetic culture system for pig and human heart slices. *Circ. Res.* 125, 628–642. doi:10.1161/CIRCRESAHA.119.314996

Ou, Q., Abouleisa, R. R. E., Tang, X. L., Juhardeen, H. R., Meki, M. H., Miller, J. M., et al. (2020). Slicing and culturing pig hearts under physiological conditions. *JoVE* 20, 60913. doi:10.3791/60913

O'shea, C., Holmes, A. P., Winter, J., Correia, J., Ou, X., Dong, R., et al. (2019). Cardiac optogenetics and optical mapping–overcoming spectral congestion in all-optical cardiac electrophysiology. *Front. Physiol.* 10, 182. doi:10.3389/fphys.2019.00182

Parikh, S. S., Zou, S. Z., and Tung, L. (1993). Contraction and relaxation of isolated cardiac myocytes of the frog under varying mechanical loads. *Circ. Res.* 72, 297–311. doi:10.1161/01.res.72.2.297

Parrish, A. R., Shipp, N. G., Spall, R. D., Dorr, R. T., Krumdieck, C. L., Gandolfi, A. J., et al. (1992). Organ culture of rat myocardial slices: an alternative *in Vitro* tool in organ-specific toxicology. *Toxicol. Mech. Methods* 2, 101–111. doi:10.3109/15376519209087715

Perbellini, F., Watson, S. A., Scigliano, M., Alayoubi, S., Tkach, S., Bardi, I., et al. (2018). Investigation of cardiac fibroblasts using myocardial slices. *Cardiovasc. Res.* 114, 77–89. doi:10.1093/cvr/cvx152

Pitoulis, F. G., Watson, S. A., Perbellini, F., and Terracciano, C. M. (2020). Myocardial slices come to age: an intermediate complexity *in vitro* cardiac model for translational research. *Cardiovasc. Res.* 116, 1275–1287. doi:10.1093/cvr/cvz341

Pointon, A., Harmer, A. R., Dale, I. L., Abi-Gerges, N., Bowes, J., Pollard, C., et al. (2015). Assessment of cardiomyocyte contraction in human-induced pluripotent stem cell-derived cardiomyocytes. *Toxicol. Sci.* 144, 227–237. doi:10.1093/toxsci/kfu312

Powell, T., and Twist, V. W. (1976). A rapid technique for the isolation and purification of adult cardiac muscle cells having respiratory control and a tolerance to calcium. *Biochem. Biophys. Res. Commun.* 72, 327–333. doi:10.1016/0006-291x(76)90997-9

Qiao, Y., Dong, Q., Li, B., Obaid, S., Miccile, C., Yin, R. T., et al. (2019). Multiparametric slice culture platform for the investigation of human cardiac tissue physiology. *Prog. Biophys. Mol. Biol.* 144, 139–150. doi:10.1016/j.pbiomolbio.2018.06.001

Roberts, M. A., Tran, D., Coulombe, K. L. K., Razumova, M., Regnier, M., Murry, C. E., et al. (2016). Stromal cells in dense collagen promote cardiomyocyte and microvascular patterning in engineered human heart tissue. *Tissue Eng.* 22, 633–644. doi:10.1089/ten.TEA.2015.0482

Ronaldson-Bouchard, K., Ma, S. P., Yeager, K., Chen, T., Song, L., Sirabella, D., et al. (2018). Advanced maturation of human cardiac tissue grown from pluripotent stem cells. *Nature* 556, 239–243. doi:10.1038/s41586-018-0016-3

Ronaldson-Bouchard, K., and Vunjak-Novakovic, G. (2018). Organs-on-a-Chip: a fast track for engineered human tissues in drug development. *Cell stem cell* 22, 310–324. doi:10.1016/j.stem.2018.02.011

Ruan, J. L., Tulloch, N. L., Razumova, M. V., Saiget, M., Muskheli, V., Pabon, L., et al. (2016). Mechanical stress conditioning and electrical stimulation promote contractility and force maturation of induced pluripotent stem cell-derived human cardiac tissue. *Circulation* 134, 1557–1567. doi:10.1161/CIRCULATIONAHA.114.014998

Salama, G., and Bett, G. C. (2014). Sex differences in the mechanisms underlying long QT syndrome. *Am. J. Physiol. Heart Circ. Physiol.* 307, H640–H648. doi:10.1152/ajpheart.00864.2013

Sharma, A., Mckeithan, W. L., Serrano, R., Kitani, T., Burridge, P. W., Del Álamo, J. C., et al. (2018). Use of human induced pluripotent stem cell-derived cardiomyocytes to assess drug cardiotoxicity. *Nat. Protoc.* 13, 3018–3041. doi:10.1038/s41596-018-0076-8

Sirenko, O., Cromwell, E. F., Crittenden, C., Wignall, J. A., Wright, F. A., and Rusyn, I. (2013). Assessment of beating parameters in human induced pluripotent stem cells enables quantitative *in vitro* screening for cardiotoxicity. *Toxicol. Appl. Pharmacol.* 273, 500–507. doi:10.1016/j.taap.2013.09.017

Stoehr, A., Hirt, M. N., Hansen, A., Seiffert, M., Conradi, L., Uebeler, J., et al. (2016). Spontaneous formation of extensive vessel-like structures in murine engineered heart tissue. *Tissue Eng.* 22, 326–335. doi:10.1089/ten.TEA.2015.0242

Takahashi, K., Tanabe, K., Ohnuki, M., Narita, M., Ichisaka, T., Tomoda, K., et al. (2007). Induction of pluripotent stem cells from adult human fibroblasts by defined factors. *Cell* 131, 861–872. doi:10.1016/j.cell.2007.11.019

Talman, V., and Kivelä, R. (2018). Cardiomyocyte-endothelial cell interactions in cardiac remodeling and regeneration. *Front. Cardiovasc. Med.* 5, 101. doi:10.3389/fcvm.2018.00101

Tandon, N., Cannizzaro, C., Chao, P. H., Maidhof, R., Marsano, A., Au, H. T. H., et al. (2009). Electrical stimulation systems for cardiac tissue engineering. *Nat. Protoc.* 4, 155–173. doi:10.1038/nprot.2008.183

Tytgat, J. (1994). How to isolate cardiac myocytes. *Cardiovasc. Res.* 28, 280–283. doi:10.1093/cvr/28.2.280

Wang, D., Patel, C., Cui, C., and Yan, G. X. (2008). Preclinical assessment of drug-induced proarrhythmias: role of the arterially perfused rabbit left ventricular wedge preparation. *Pharmacol. Ther.* 119, 141–151. doi:10.1016/j.pharmthera.2008.02.009

Watson, S. A., Duff, J., Bardi, I., Zabielska, M., Atanur, S. S., Jabbour, R. J., et al. (2019). Biomimetic electromechanical stimulation to maintain adult myocardial slices *in vitro*. *Nat. Commun.* 10, 2168. doi:10.1038/s41467-019-10175-3

Watson, S. A., Scigliano, M., Bardi, I., Ascione, R., Terracciano, C. M., and Perbellini, F. (2017). Preparation of viable adult ventricular myocardial slices from large and small mammals. *Nat. Protoc.* 12, 2623–2639. doi:10.1038/nprot.2017.139

Yamakawa, H., Muraoka, N., Miyamoto, K., Sadahiro, T., Isomi, M., Haginiwa, S., et al. (2015). Fibroblast growth factors and vascular endothelial growth factor promote cardiac reprogramming under defined conditions. *Stem Cell Reports* 5, 1128–1142. doi:10.1016/j.stemcr.2015.10.019

Yan, G.-X., and Antzelevitch, C. (1996). Cellular basis for the electrocardiographic J wave. *Circulation* 93, 372–379. doi:10.1161/01.cir.93.2.372

Yan, G. X., Shimizu, W., and Antzelevitch, C. (1998). Characteristics and distribution of M cells in arterially perfused canine left ventricular wedge preparations. *Circulation* 98, 1921–1927. doi:10.1161/01.cir.98.18.1921

Yang, C., Al-Aama, J., Stojkovic, M., Keavney, B., Trafford, A., Lako, M., et al. (2015). Concise review: cardiac disease modeling using induced pluripotent stem cells. *Stem Cell.* 33, 2643–2651. doi:10.1002/stem.2070

Ye, K. Y., and Black, L. D., 3rd (2011). Strategies for tissue engineering cardiac constructs to affect functional repair following myocardial infarction. *J Cardiovasc Transl Res.* 4, 575–591. doi:10.1007/s12265-011-9303-1

Yoshida, S., Miyagawa, S., Fukushima, S., Kawamura, T., Kashiyama, N., Ohashi, F., et al. (2018). Maturation of human induced pluripotent stem cell-derived cardiomyocytes by soluble factors from human mesenchymal stem cells. *Mol. Ther.* 26, 2681–2695. doi:10.1016/j.ymthe.2018.08.012

Zhang, B., Korolj, A., Lai, B., and Radisic, M. (2018). Advances in organ-on-a-chip engineering. *Nat. Rev. Mater.* 3, 257–278. doi:10.1038/s41578-018-0034-7

Zhang, D., Shadrin, I. Y., Lam, J., Xian, H. Q., Snodgrass, H. R., and Bursac, N. (2013). Tissue-engineered cardiac patch for advanced functional maturation of human ESC-derived cardiomyocytes. *Biomaterials* 34, 5813–5820. doi:10.1016/j.biomaterials.2013.04.026

Zhang, Y. S., Arneri, A., Bersini, S., Shin, S. R., Zhu, K., Goli-Malekabadi, Z., et al. (2016). Bioprinting 3D microfibrous scaffolds for engineering endothelialized myocardium and heart-on-a-chip. *Biomaterials* 110, 45–59. doi:10.1016/j.biomaterials.2016.09.003

Zhao, Y., Rafatian, N., Wang, E. Y., Wu, Q., Lai, B. F. L., Lu, R. X., et al. (2020). Towards chamber specific heart-on-a-chip for drug testing applications. *Adv. Drug Deliv. Rev.* 165-166, 60–76. doi:10.1016/j.addr.2019.12.002

Conflict of Interest: TM holds equities in Tenaya Therapeutics.

The remaining authors declare that the research was conducted in the absence of any commercial or financial relationships that could be construed as a potential conflict of interest.

frontiers in Pharmacology

ORIGINAL RESEARCH
published: 08 February 2021
doi: 10.3389/fphar.2020.569489

Identifying Drug Response by Combining Measurements of the Membrane Potential, the Cytosolic Calcium Concentration, and the Extracellular Potential in Microphysiological Systems

Karoline Horgmo Jæger[1]*, *Verena Charwat*[2], *Samuel Wall*[1], *Kevin E. Healy*[2,3] and *Aslak Tveito*[1,4]

[1]Simula Research Laboratory, Oslo, Norway, [2]Department of Bioengineering, University of California, Berkeley, CA, United States, [3]Department of Material Science and Engineering, University of California, Berkeley, CA, United States, [4]Department of Informatics, University of Oslo, Oslo, Norway

OPEN ACCESS

Edited by:
Tamer M. A. Mohamed,
University of Louisville, United States

Reviewed by:
Jong-Kook Lee,
Osaka University, Japan
Tomoharu Osada,
LSI Medience Corporation, Japan

***Correspondence:**
Karoline Horgmo Jæger
karolihj@simula.no

Specialty section:
This article was submitted to Cardiovascular and Smooth Muscle Pharmacology,
a section of the journal Frontiers in Pharmacology

Received: 04 June 2020
Accepted: 16 November 2020
Published: 08 February 2021

Citation:
Jæger KH, Charwat V, Wall S, Healy KE and Tveito A (2020) Identifying Drug Response by Combining Measurements of the Membrane Potential, the Cytosolic Calcium Concentration, and the Extracellular Potential in Microphysiological Systems. Front. Pharmacol. 11:569489. doi: 10.3389/fphar.2020.569489

Cardiomyocytes derived from human induced pluripotent stem cells (hiPSC-CMs) offer a new means to study and understand the human cardiac action potential, and can give key insight into how compounds may interact with important molecular pathways to destabilize the electrical function of the heart. Important features of the action potential can be readily measured using standard experimental techniques, such as the use of voltage sensitive dyes and fluorescent genetic reporters to estimate transmembrane potentials and cytosolic calcium concentrations. Using previously introduced computational procedures, such measurements can be used to estimate the current density of major ion channels present in hiPSC-CMs, and how compounds may alter their behavior. However, due to the limitations of optical recordings, resolving the sodium current remains difficult from these data. Here we show that if these optical measurements are complemented with observations of the extracellular potential using multi electrode arrays (MEAs), we can accurately estimate the current density of the sodium channels. This inversion of the sodium current relies on observation of the conduction velocity which turns out to be straightforwardly computed using measurements of extracellular waves across the electrodes. The combined data including the membrane potential, the cytosolic calcium concentration and the extracellular potential further opens up for the possibility of accurately estimating the effect of novel drugs applied to hiPSC-CMs.

Keywords: action potential model, bidomain model, computational inversion, human induced pluripotent stem cell derived cardiomyocytes, multielectrode array recording, conduction velocity, ion channel block

1 INTRODUCTION

In recent reports (Tveito et al., 2018; Jæger et al., 2020a) we have demonstrated how microphysiological systems utilizing human induced pluripotent stem cell derived cardiomyocytes (hiPSC-CMs) (Mathur et al., 2015; Mathur et al., 2016) can be used to estimate drug induced changes to the cardiac action potential using computational approaches. These methods use optical measurements of the membrane potential and the cytosolic calcium concentration to quantitate changes in underlying ion channel conductances and calcium handling pathways using a mathematical model of the hiPSC-CM dynamics. We have further shown how these estimates, at least in principle, carry over from immature cells to adult cardiomyocytes. This methodology provides information on a number of the major ion channels and when compared to data presented in (Mohammad et al., 1997; Di Stilo et al., 1998; Zhang et al., 1999; Zhabyeyev et al., 2000; Mirams et al., 2011; Kramer et al., 2013; Crumb et al., 2016), the method is able to provide reasonable estimates of the IC50 values of well-known drugs like Nifedipine, Lidocaine, Cisapride, Flecainide and Verapamil; see Table 2 of (Jæger et al., 2020a). These drug affects the I_{CaL}, I_{NaL} or I_{Kr} currents and the effect is well estimated by our methodology.

However, difficulties remain in the characterization of the fast sodium current, I_{Na}. This is a major issue since this current more or less completely governs the rapid upstroke of the action potential and thus also the conduction velocity. Therefore, it is of great importance to characterize the effect of drugs on this current. The reason for this deficiency in our methodology is the time resolution of the data obtained by fluorescence; the data used in the inversions are provided with a resolution of 10 ms and this is far too coarse to be able to estimate the strength of I_{Na}. Time resolution can be improved but at the cost of less accurate data and therefore another experimental technique is needed to pin down the channel density of and drug effects on I_{Na}. It is well known that the extracellular potential can be measured in microphysical systems using multielectrode arrays; see, e.g., (Zwi et al., 2009; Clements and Thomas, 2014; Asakura et al., 2015; Bouyssier and Zemzemi, 2017; Tixier et al., 2018). In this report we will show that the extracellular data can be used to determine the sodium current. And therefore, by combining imaging data for the membrane potential (V) and the cytosolic calcium concentration (Ca) with data for the extracellular potential (U), we are able to identify both the fast sodium current and other major currents characterizing the action potential of the hiPSC-CMs.

The main challenge in combining V, Ca and U data is that a spatial problem needs to be resolved. When the data are given by V and Ca only, we have simply used a data trace obtained by taking the average over the whole chip (see Mathur et al., 2015; Tveito et al., 2018) and the inversion of the data has amounted to estimating parameters describing a system of ordinary differential equations. But when U is added to the data, the extracellular potential needs to be calculated. In our present implementation, we use the bidomain model (see, e.g., Franzone et al., 2014) for this purpose. The bidomain model has already been used for inversion of U data (but not V and Ca) by several authors; see (Bouyssier and Zemzemi, 2017; Raphel et al., 2017; Abbate et al., 2018; Tixier et al., 2018; Raphel et al., 2020). However, it is demonstrated in (Abbate et al., 2018) that the bidomain model does not provide an extracellular repolarization wave. Such a wave is clearly present in the experimental data and inhomogeneities have to be introduced in the bidomain model in order to enforce a repolarization wave. These inhomogeneities are difficult to obtain from measurements, and therefore we choose to use U only to estimate the currents involved in generating the upstroke and not the whole action potential. This turns out to determine I_{Na} accurately, - at least in data generated by simulations.

2 METHODS

In this section, we describe the methods applied to identify drug response by combining measurements of the membrane potential, the cytosolic calcium concentration and the extracellular potential in microphysiological systems of hiPSC-CMs.

2.1 Bidomain-Base Model Simulations

In order to represent the electrical properties of a microphysiological system, we conduct simulations of the bidomain model of the form

$$\chi C_m\left(\frac{\partial v}{\partial t} + I_{\mathrm{ion}}(v,s) + I_{\mathrm{stim}}\right) = \nabla\cdot(\sigma_i\nabla v) + \nabla\cdot(\sigma_i\nabla u_e), \quad (1)$$

$$0 = \nabla\cdot(\sigma_i\nabla v) + \nabla\cdot[(\sigma_i+\sigma_e)\nabla u_e], \quad (2)$$

$$\frac{\partial s}{\partial t} = F(v,s) \quad (3)$$

(see, e.g., Tung, 1978; Sundnes et al., 2007; Keener and James, 2009; Franzone et al., 2014). Here, v and u_e are the membrane potential and the extracellular potential, respectively. In addition, σ_i and σ_e are the bidomain conductivities of the extracellular and intracellular spaces, respectively, C_m is the specific membrane capacitance, and χ is the surface-to-volume ratio of the cell membrane. The values chosen for these parameters are given in **Table 1**.

Furthermore, I_{ion} represents the density of currents through different types of ion channels, pumps and exchangers on the cell membrane. We use an adjusted version of the hiPSC-CM base model introduced in (Jæger et al., 2020a) to represent these currents. The current density is then given on the form

$$I_{\mathrm{ion}}(v,s) = \sum_i I_i(v,s), \quad (4)$$

TABLE 1 | Parameter values used in the bidomain-base model simulations.

Parameter	Value
C_m	1 μF/cm^2
σ_i	0.4 mS/cm
σ_e	10 mS/cm
X	1,400 cm^{-1}
Domain size	1,600 μm × 1,600 μm
Electrode size	50 μm × 50 μm
Electrode distance	100 μm
Δx, Δy	50 μm
Δt (recordings of V and Ca)	10 ms
Δt (extracellular recordings)	0.05 ms
Δt (simulations)	0.05 ms for $t \le 50$ ms 0.2 ms for $t > 50$ ms

TABLE 2 | Parameter values used in the hiPSC-CM base model. The remaining parameter values are the same as specified in (Jæger et al., 2020a).

Parameter	Value	Parameter	Value
$[Ca^{2+}]_e$	0.42 mM	$\bar{I}_{NaK}$	1.9 μA/μF
$[K^+]_e$	5 mM	$\bar{I}_{NaCa}$	9.4 μA/μF
$[Na^+]_e$	140 mM	$\bar{I}_{pCa}$	0.12 μA/μF
g_{Na}	2.6 mS/μF	$\bar{J}_{SERCA}$	0.00016 mM/ms
g_{NaL}	0.03 mS/μF	α_{RyR}	0.0052 ms^{-1}
g_{to}	0.21 mS/μF	β_{RyR}	0.0265 mM
g_{Kr}	0.075 mS/μF	α_d^c	0.0027 ms^{-1}
g_{Ks}	0.0127 mS/μF	α_{sl}^c	0.3 ms^{-1}
g_{KI}	0.05 mS/μF	α_n^s	0.0093 ms^{-1}
g_f	0.012 mS/μF	B_{tot}^c	0.063 mM
g_{bCl}	0.0001 mS/μF	B_{tot}^d	2.7 mM
g_{bCa}	0.0005 mS/μF	B_{tot}^{sl}	1.45 mM
g_{CaL}	1.8 nL/(μF ms)	B_{tot}^s	60 mM

where each I_i represents the current through a specific type of ion channel, pump or exchanger. The hiPSC-CM base model includes a number of additional state variables representing the gating of ion channels and intracellular Ca^{2+} concentrations. These variables are represented by s in the model above, and their dynamics are modeled by a set of ordinary differential equations (ODEs) given by $F(v, s)$. A number of parameters in the hiPSC-CM base model have been adjusted to make the size of eight currents of particular interest (I_{Kr}, I_{NaL}, I_{CaL}, I_{Na}, I_{to}, I_{Ks}, I_{K1}, and I_f) close to the size of the currents in the model described in (Kernik et al., 2019), which is fitted to recordings of hiPSC-CMs from several different studies. The adjusted parameter values of the hiPSC-CM base model are given in **Table 2**, and the base model is, for completeness, given in the **Supplementary Material**.

The geometry of the domain used to represent a microphysiological system is described in **Figure 1** and **Table 1**. We consider a two-dimensional domain, and initiate a traveling wave by stimulating the lower left corner. Furthermore, 8 × 8 electrodes are distributed in the center of the domain, and we record the extracellular potential in these electrodes. On the boundary of the domain, we apply the Dirichlet boundary condition $u_e = 0$.

In addition to the bidomain simulations, we in some cases conduct simulations in which the spatial variation of the variables are ignored. In that case, the system **Eqs 1–3** can be written as a pure ODE system of form

$$\frac{dv}{dt} = -\frac{1}{C_m}(I_{ion} + I_{stim}), \tag{5}$$

$$\frac{ds}{dt} = F(v, s). \tag{6}$$

Below, we refer to the system **Eqs 5** and **6** as the pure ODE system.

2.1.1 Adjustment Factors

In order to investigate whether we are able to identify drug responses from combined measurements of V, Ca and U data, we perform numerical simulations representing a number of different drugs reported in (Crumb et al., 2016). More specifically, we simulate ion channel blockers by introducing adjustment factors $-1 \le \lambda_i \le 0$, such that I_{ion} is given by

$$I_{ion}(v, s) = \sum_i (1 + \lambda_i) I_i(v, s). \tag{7}$$

In our simulation, we consider the drug effect on three major ionic currents, I_{Kr}, I_{CaL} and I_{Na}, believed to be of importance in evaluation of drug safety (see, e.g., Crumb et al., 2016), and we therefore introduce the four adjustment factors λ_{Kr}, λ_{CaL} and λ_{Na}.

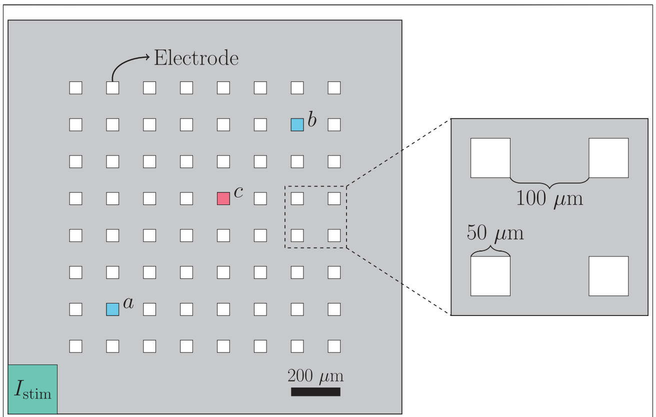

FIGURE 1 | Geometry used in the bidomain-base model simulations. The domain contains 8 × 8 evenly spaced electrodes, and the propagating wave is initiated by stimulating the lower left corner of the domain. The conduction velocity is computed between the electrodes marked as *a* and *b*, and when we plot the extracellular potential of just a single electrode, we consider the electrode marked as *c*.

2.1.2 Bidomain-Base Model Simulations Used to Generate Data

We wish to investigate how V, Ca and U data from a microphysiological system can be used to identify the effect of drugs. In order to generate data representing this type of recordings, we perform bidomain-base model simulations. The simulation procedure used to generate the data is illustrated in **Figure 2**.

As illustrated in the upper panel of **Figure 2**, for a given combination of λ-values, we first perform bidomain-base model simulations for the duration of an entire action potential and store the extracellular potential, the membrane potential, and the cytosolic calcium concentration in each mesh point for each time step. We then wish to convert these recorded solutions into corresponding measurements that may be performed in microphysiological systems.

The first considered type of measurement is optical measurements of voltage-sensitive dyes. This type of measurement is mimicked in the computations by extracting the mean membrane potential over the entire domain for each time step. Because the exact conversion factor between the pixel intensity of the optical measurements and the associated membrane potential (in mV) is not known for this type of optical measurement, we normalize the mean V-trace to

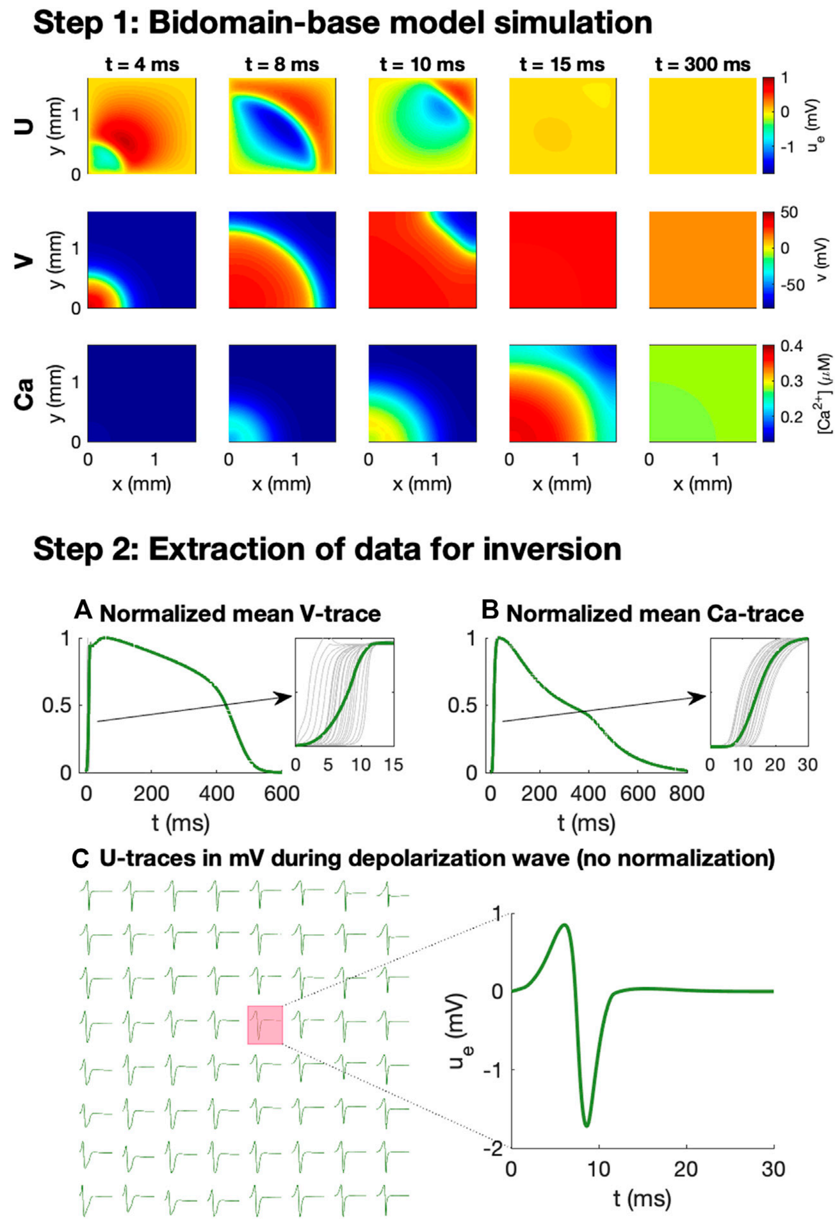

FIGURE 2 | Simulation procedure used to generate data for the inversions. In Step 1, we conduct bidomain-base model simulations, recording *V*, Ca and *U* for a number of time steps. In Step 2, we extract *V* and Ca data for inversion by recording the mean *V* and Ca over the domain at each time step and normalizing the traces to values between 0 and 1. In addition, *U* is recorded (in mV) in 8 × 8 electrodes at each time step during the depolarization wave.

values between 0 and 1. Moreover, because the time resolution of the measurement equipment for the optical measurements typically is quite limited (see, e.g., Tveito et al., 2018), we only store the membrane potential at relatively large time steps (every 10 ms). Traces representing optical measurements of the cytosolic calcium concentration is generated in exactly the same manner.

In addition to the optical measurements of V and Ca, the extracellular potential may also be measured in electrodes located in the microphysiological system. In the simulations, we extract this type of measurements by storing the mean extracellular potential in the grid points overlapping the location of the electrodes. We are primarily interested in the extracellular potential during the depolarization wave, and we therefore only store the extracellular potential in the beginning of the simulation (typically the first 50 ms).

2.1.3 Pure ODE Simplification Used in the Inversion Procedure

During the inversion procedure, we wish to identify the λ-values associated with some considered data, generated as explained in the previous section. In this inversion procedure, we need to conduct simulations using a large number of different λ-values for comparison to the data. As mentioned above, the repolarization wave is known to be poorly represented by the bidomain model when applied to small collections of hiPSC-CMs. Therefore, we perform spatial simulations only for the start of the action potential. The data from this part of the simulation is used to determine the conduction velocity, the Ca transient time to peak and the terms of the cost function related to the extracellular potential, U. By performing spatial simulations only for the beginning of the action potential, we save time by avoiding a full bidomain simulation for all of the different parameter combinations. To generate the full V and Ca traces, we instead run a simple pure ODE simulation of the form **Eqs 5** and **6** of the full action potential. The solution of this ODE simulation is used to compute all the terms in the cost function (see **Section 2.2.1**), except for the ones related to U, the Ca transient time to peak and the conduction velocity.

2.1.4 Stimulation Protocol and Update of Initial Conditions

In the pure ODE simulations, the cell is stimulated by a constant stimulus current of −5 μA/cm^2 until v is above −40 mV. In the bidomain simulations, we stimulate the domain in the lower left corner as illustrated in **Figure 1** by a 5-ms-long constant membrane stimulus current of −40 μA/cm^2. Note that after each parameter change, and before any bidomain or pure ODE simulation is performed, we conduct an ODE simulation for 10 AP cycles, stimulating at 1 Hz, to update the initial conditions.

2.1.5 Numerical Methods

The numerical simulations of the bidomain model are performed using an operator splitting procedure (see, e.g., Sundnes et al., 2005; Sundnes et al., 2007; Schroll et al., 2007). For each time step, we first solve the non-linear part of the system (i.e., **Eqs 1** and **3** with the left-hand side of **Eq. 1** set to zero), using the GRL2 method (Sundnes et al., 2009). Then, we solve the remaining linear part of the system (i.e., **Eqs 1** and **2** with $I_{\text{ion}} = 0$) using a finite difference discretization in space and a backward Euler discretization in time. The discretization parameters used in the numerical simulations are given in **Table 1**. In the pure ODE simulations used in the inversion procedure we apply the same GRL2 method as in the non-linear part of the bidomain simulations, and in the pure ODE simulations used to update the initial conditions after a parameter change, we use the *ode15s* ODE-solver in Matlab.

2.2 Inversion Procedure

In this section, we will describe the inversion procedure applied to identify the effect of drugs based on V, Ca and U data in the form of adjustment factors, λ (see **Section 2.1.1**).

2.2.1 Cost Function

In the inversion procedure, we wish to find appropriate adjustment factors, λ, such that the solution of the model specified by λ is as similar as possible to the considered data. To this end, we define a cost function $H(\lambda)$, measuring the difference between the data and the model solution. This cost function is defined as

$$H(\lambda) = \sum_j \left(w_j H_j(\lambda)^2 \right) + \delta \left(\sum_i |\lambda_i| \right)^2, \tag{8}$$

where each $H_j(\lambda)$ represent various differences between the data and the model solution specified by λ, and w_j are weights for each of these terms. In addition, δ is the weight of the regularization term $(\sum_i |\lambda_i|)^2$, which is included so that small adjustments, λ, are preferred if several choices of λ result in almost identical solutions. The individual cost function terms, $H_j(\lambda)$, are defined below.

2.2.1.1 Action Potential and Calcium Transient Durations

A number of terms in the cost function measure differences in the action potential and calcium transient durations. These terms take the form

$$H_{\text{APD}p}(\lambda) = \frac{\left|\text{APD}p(\lambda) - \text{APD}p^*\right|}{\left|\text{APD}p^*\right|}, \tag{9}$$

$$H_{\text{CaD}p}(\lambda) = \frac{\left|\text{CaD}p(\lambda) - \text{CaD}p^*\right|}{\left|\text{CaD}p^*\right|}, \tag{10}$$

for $p = 20, 30, \ldots, 70, 80$ The APDp value is measured as the time from V is p% below its maximum value during the upstroke of the action potential to the time at which V reaches a value below p% of the maximum during the repolarization phase; see **Figure 3**. APD$p(\lambda)$ is the value obtained from the solution of the model given by the parameter vector λ, whereas APDp^* is the value obtained from the data. The calcium transient durations, CaDp, are defined just like the action potential durations. Note also that the notation of a * marking the data values is used for all the terms in the cost function (see below).

2.2.1.2 Membrane Potential Integral

The cost function also includes a term of the form

$$H_{\text{Int30}}(\lambda) = \frac{\left|\text{Int30}(\lambda) - \text{Int30}^*\right|}{\left|\text{Int30}^*\right|}, \tag{11}$$

where Int30 is defined as

$$\text{Int30} = \int_{t_1}^{t_2} [v - v(t_1)] dt \tag{12}$$

and v is the membrane potential. The values t_1 and t_2 are here time points corresponding to when V is 30% below the maximum value during the depolarization and repolarization phases of the action potential (see **Figure 3**).

2.2.1.3 Calcium Transient Time to Peak

The typical time resolution of the V and Ca data (10 ms) is too coarse to be able to detect changes in the upstroke velocity of the action potential. However, the upstroke of the calcium transient is slower, and therefore, changes in the upstroke of the calcium transient may be detected. To measure this upstroke velocity, we include a term of the form

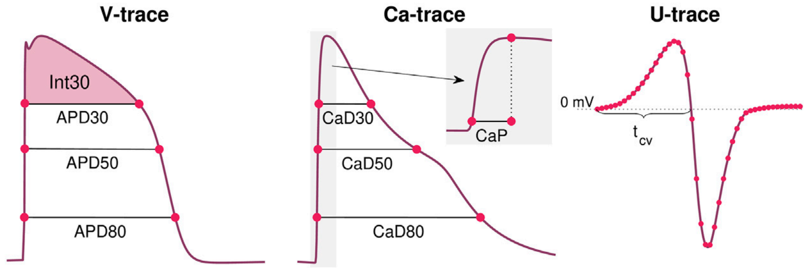

FIGURE 3 | Illustration of some of the properties included in the cost function **Eq. 8**. From the *V*-trace, we include a number of APD-values (see **Eq. 9**), and the integral of *V* above APD30 (see **Eq. 11**). From the Ca-trace, we include a number of CaD-values (see **Eq. 10**) in addition to the Ca transient time to peak, CaP (see **Eq. 13**). From the *U* data, we include the value in each time point and each electrode (see **Eq. 14**) and the conduction velocity computed using the time points in which *U* crosses 0 mV after the peak in different electrodes (see **Eq. 15** and **Figure 1**).

$$H_{t,\mathrm{Ca}}(\lambda) = \frac{|\mathrm{CaP}(\lambda) - \mathrm{CaP}^*|}{|\mathrm{CaP}^*|}, \tag{13}$$

where CaP is the time from Ca is 10% above its minimum value until it reaches its maximum (see **Figure 3**).

As mentioned above, we use a bidomain simulation instead of a pure ODE simulation to compute an estimate of CaP(λ) (and CaP* in the case of simulated data). We conduct this bidomain simulation for a rather short time interval (typically 50 ms) and record Ca in all the grid points. Then, we extract the grid points that have reached their peak Ca concentration during this simulation, and set up a normalized mean Ca-trace for these grid points. The value of CaP is then computed from this normalized mean Ca-trace. When the data is generated, we use the same procedure of considering the solution for only the first part of the simulation (e.g., 50 ms) when we compute CaP*.

2.2.1.4 Extracellular Potenial

In order to detect changes in U measured at the electrodes, we include a cost function term of the form

$$H_{\mathrm{U}}(\lambda) = \frac{\sum_k \left\| u_e^k(\lambda) - u_e^{k,*} \right\|_2}{\sum_k \left\| u_e^{k,*} \right\|_2}, \tag{14}$$

where u_e^k is a vector denoting U (in mV) in electrode k for each of the recorded time steps.

2.2.1.5 Average Conduction Velocity

In addition, the cost function includes a term for the average conduction velocity of the form

$$H_{\mathrm{cv}}(\lambda) = \frac{|\mathrm{cv}(\lambda) - \mathrm{cv}^*|}{|\mathrm{cv}^*|}, \tag{15}$$

where cv denotes the average conduction velocity (in cm/s) computed from U recorded in the electrodes. More specifically, the average conduction velocity is computed as the distance between the center of the two electrodes marked as a and b in **Figure 1** divided by the time between U crosses 0 mV after the peak in these two electrodes (see **Figure 3**).

2.2.1.6 Cost Function Weights

In the applications of the inversion procedure reported below, we have used the weight $w_j = 1$ for each of the cost function terms, except for H_{APD80} and H_{CaD80}, which are given the weight of 5. In addition, we use the value $\delta = 0.01$ for the regularization term. All terms of the cost function are scaled and thus have no unit, and therefore also w and δ are unit free.

2.2.2 Continuation-Based Optimization

In order to find the optimal λ-values minimizing the cost function H defined in **Eq. 8**, we apply a continuation-based minimization procedure. This approach is described in detail in (Jæger et al., 2020a). In short, we attempt to find the optimal λ-values by gradually moving from a known solution $\lambda^0 = 0$ to the final λ fitting the data as best possible. To this end, we introduce a parameter θ that is gradually increased from 0 to 1, and define an intermediate cost function

$$\overline{H}(\lambda, \theta) = \sum_j \left(w_j \overline{H}_j(\lambda, \theta)^2 \right) + \frac{\delta}{\max(\theta, \xi)} \left(\sum_i |\lambda_i| \right)^2, \tag{16}$$

where $\overline{H}_j(\lambda, \theta)$ are adjusted versions of each of the cost function terms defined above and ξ is some small number (e.g., 10^{-10}). In general, $\overline{H}_j(\lambda, \theta)$ is defined as

$$\overline{H}_j(\lambda, \theta) = \frac{\left| R_j(\lambda) - R_j^*(\theta) \right|}{\left| R_j^*(\theta) \right|}, \tag{17}$$

where R_j is some property of the solution, for example an action potential duration. Moreover, $R_j(\lambda)$ is the property computed in the solution of the model defined by λ, and $R_j^*(\theta)$ is defined as

$$R_j^*(\theta) = (1 - \theta) R_j(\lambda_0) + \theta R_j^*, \tag{18}$$

where $R_j(\lambda_0)$ is the property computed from the model solution defined by $\lambda^0 = 0$, and R_j^* is the property computed from the data we are trying to invert.

Considering the cost function terms, H_j, defined above, all the terms may straightforwardly be defined on the form **Eq. 17** except for the term H_U defined in **Eq. 14**. For this term, we instead define

$$\overline{H}_{\mathrm{U}}(\lambda,\theta) = (1-\theta)H_{\mathrm{U}}^{0} + \theta H_{\mathrm{U}}(\lambda), \tag{19}$$

where H_{U}^{0} is defined by **Eq. 14** with $u_e^{k,*}$ replaced by the model solution $u_e^k(\lambda_0)$, and $H_U(\lambda)$ is defined by **Eq. 14**.

From the definitions **Eqs 16–19**, we observe that for $\theta = 0$, $R_j^* = R_j(\lambda_0)$ and $\overline{H}_j(\lambda_0, 0) = 0$, implying that the known solution $\lambda = \lambda_0$ minimize **Eq. 16** for $\theta = 0$. Furthermore, for $\theta = 1$, $R_j^*(1) = R_j^*$ defined by the data, $\overline{H}_j(\lambda, 1) = H_j(\lambda)$, and $\overline{H}(\lambda, 1) = H(\lambda)$. Consequently, for $\theta = 1$, the minimum of $\overline{H}$ defined in **Eq. 16** is the same as the minimum of H defined in **Eq. 8**.

The advantage of the continuation algorithm is that we can move from the known optimal value λ_0 to the final optimal value λ gradually in a number of iterations, and that we for each iteration can assume that the new estimated λ is in the vicinity of the optimal λ from the previous iteration. In the applications of the inversion procedure reported below, we use four θ-iterations in the continuation algorithm ($\theta = 1/4$, $\theta = 1/2$, $\theta = 3/4$ and $\theta = 1$). In the first three iterations, m, we draw 63 random initial guesses of $\lambda(\theta_m)$ in the vicinity of $\lambda(\theta_{m-1})$, and in the last iteration, we draw 126 initial guesses. More specifically, the initial guesses for $\lambda_i(\theta_m)$ are drawn from $[\lambda_i(\theta_{m-1}) - 0.2, \lambda_i(\theta_{m-1}) + 0.2]$, where $\lambda_i(\theta_0)$ is defined to be 0. From these initial guesses we minimize the cost function $\overline{H}(\lambda, \theta)$ using the Nelder-Mead algorithm (Nelder and Mead, 1965). In the first three θ-iterations, we use 10 iterations of the Nelder-Mead algorithm for each initial guess, and in the last θ-iteration, we use 25 iterations.

2.3 Adjustment of Extracellular Concentrations

In order to better distinguish between different ion channel blockers, we consider the drug effects under different extracellular conditions. In particular, we vary the extracellular calcium concentration by introducing a number of known adjustment factors γ_{Ca} such that

$$[\mathrm{Ca}^{2+}]_e = (1+\gamma_{\mathrm{Ca}})[\mathrm{Ca}^{2+}]_e^*, \tag{20}$$

where $[\mathrm{Ca}^{2+}]_e$ is the extracellular calcium concentration and $[\mathrm{Ca}^{2+}]_e^*$ is the default extracellular calcium concentration reported in **Table 2**.

In the inversions reported below, we use the two values $\gamma_{\mathrm{Ca},1} = 0$ and $\gamma_{\mathrm{Ca},2} = 0.25$. We generate V, Ca and U data using the approach described in **Section 2.1.2** for both of these values of γ_{Ca}. Furthermore, for a given choice of λ in the inversion procedure, we compute a version of the solutions for each of these γ_{Ca}-values, and define the cost function

$$H(\lambda) = \sum_q \sum_j \left(w_j H_j\left(\lambda, \gamma_{\mathrm{Ca},q}\right)^2 \right) + \delta \left(\sum_i |\lambda_i| \right)^2, \tag{21}$$

where q counts the different extracellular conditions and $H_j(\lambda, \gamma_{\mathrm{Ca},q})$ represents the cost function terms computed using the extracellular calcium concentration defined by $\gamma_{\mathrm{Ca},q}$.

2.4 Measuring the Extracellular Potential

Experimentally, the extracellular potential was measured in a monolayer of cardiomyocytes using the microelectrode array system MED64-Basic with P515 electrode dishes. Cardiomyocytes (CM) were differentiated from the human induced-pluripotent stem cell (hiPSC) line Wild Type C (WTC, Coriell Repository, # GM25256) expressing the fluorescent calcium reporter GCaMP6f (Huebsch et al., 2015). Cells were differentiated into CM using a modified version of the Palecek protocol (Lian et al., 2012) applying 6 μm CHIR, 5 μM IWP4 and minus insulin media for 48 h each. PCR analysis of these cells, see (Huebsch et al., 2018), revealed MYL2 expression, which is indicative of an atrial phenotype, however at lower levels than found in adult atria. Similarly, the levels of MYL7 were higher than in adult atria but lower than in adult ventricles. Overall, MLY2 and MLY7 expression together with the ventricular-like action potential waveform indicate these are immature ventricular cardiomyocytes (Veevers et al., 2018). MED64 electrode dishes were coated with polyethyleneimine followed by Matrigel and handled as suggested in the vendor application notes (MED64 Application Note, 2015; MED64 Application Note, 2016). CM were seeded to form a confluent cell layer and allowed to stabilize for 30 days with media changes of RPMI 1640 + B27 supplement (Gibco) every 2–3 days. Flecainide (Abcam, ab120504) doses were prepared in RPMI 1640 + B27 from a 25 mM stock in DMSO. Each drug dose (0, 1, 2.5 and 10 μM flecainide) was incubated for at least 30 min before measurements. Extracellular potential recordings were performed using the Mobius software (Version Win 7 0.5.1) with the template for spontaneous QT recording. Traces of spontaneous beating activity were recorded on all 64 electrodes and directly exported as raw data without any pre-filtering or peak extraction. Recordings were performed on a heated stage (37°C sample temperature) in ambient atmosphere.

3 RESULTS

In this section, we report the results of some applications of the inversion procedure defined above. First, we investigate the sensitivity of the V, Ca and U data in response to perturbations of the I_{Kr}, I_{CaL} and I_{Na} currents, and how this sensitivity may be increased when data for several different extracellular calcium concentrations are included. Next, we show some examples of extracellular repolarization waves, and explain why we have chosen to only consider the extracellular depolarization waves in the inversion procedure. Afterward, we show some examples of how bidomain-base model simulations are able to reproduce measured drug induced effects on the average conduction velocity, illustrating that including U data in the inversion procedure improves the identifiability of drug effects on I_{Na}. Finally, we test the inversion procedure by using it to identify drug effects for a number of simulated drugs and investigate how the accuracy of the inversion is affected when noise is included in the simulated data.

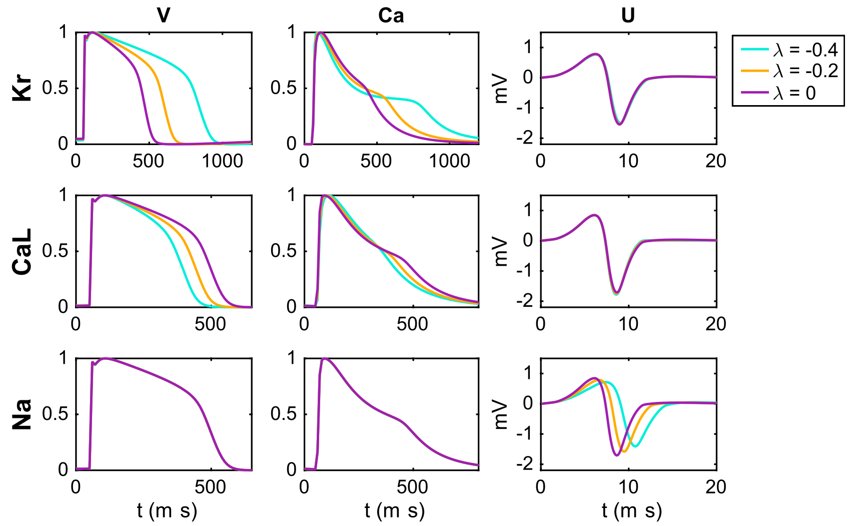

FIGURE 4 | Effect of perturbing I_{Kr}, I_{CaL} and I_{Na} on the *V*, Ca and *U* data. For the *U* data, we show the extracellular potential in the electrode marked as *c* in **Figure 1** and the time scale is zoomed in on the first 20 ms of the simulation.

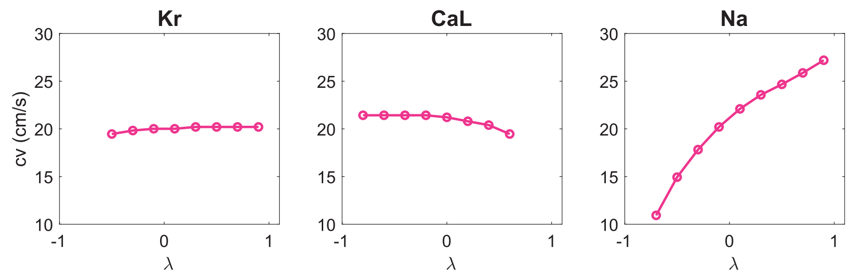

FIGURE 5 | Effect of perturbing I_{Kr}, I_{CaL} and I_{Na} on the computed conduction velocity. The conduction velocities are computed from the *U* data as explained in **Section 2.2.1**.

3.1 Sensitivity of Currents

In **Figure 4**, we investigate the effect on the simulated *V*, Ca and *U* data of perturbing the I_{Kr}, I_{CaL} and I_{Na} currents. We compute the data for the default base model ($\lambda = 0$) and for two perturbations $\lambda_i = -0.2$ and $\lambda_i = -0.4$ for each of the currents i = Kr, CaL, Na, corresponding to 20% and 40% block of the currents, respectively (see **Section 2.1.1**). Note that in the upper panel (investigating block of I_{Kr}), we have used a pacing frequency of 0.5 Hz instead of 1 Hz in order to allow for increased action potential durations resulting from block of I_{Kr}.

We observe that block of the I_{Kr} current results in increased action potential and calcium transient durations, whereas block of I_{CaL} results in decreased action potential and calcium transient durations. Moreover, no effects are visible in the *U* data resulting from block of I_{Kr} or I_{CaL} (recall that the *U* data is only considered for the first 20 ms). For block of the I_{Na} current, on the other hand, no effects on the action potential and calcium transient durations are visible, but there are clearly visible effects on the *U* data. Specifically, the amplitude of *U* is decreased and the timing of the peaks is delayed in response to block of the I_{Na} current.

Furthermore, in **Figure 5**, we report the conduction velocities computed from the *U* data in response to perturbations of the three currents. We observe that for perturbations of I_{Kr} and I_{CaL}, the effects on the conduction velocity are quite small, whereas block of I_{Na} results in a considerably decreased conduction velocity.

3.2 Adjustment of Extracellular Concentrations

Because the effect on the *V*, Ca and *U* data of blocking I_{Kr} is almost exactly the opposite of the effect of blocking I_{CaL} (see **Figure 4**), we expect that determining the correct combination of block for these two currents will be difficult. Therefore, it could be useful to consider drug effects under different extracellular conditions in order to increase the chance of identifying the correct block for the two currents.

Figure 6 shows the effect of block of the I_{Kr}, I_{CaL} and I_{Na} currents for three different extracellular calcium concentrations. We consider the default extracellular calcium concentration specified in **Table 2** ($\gamma_{Ca} = 0$), a 10% increased concentration

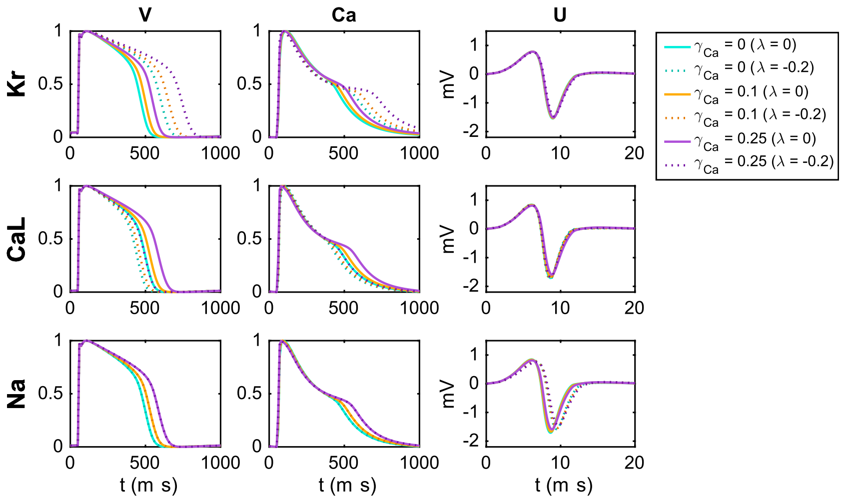

FIGURE 6 | Effect of perturbing I_{Kr}, I_{CaL} and I_{Na} on the V, Ca and U data for three different adjustments, γ_{Ca}, of the extracellular calcium concentration (see **Section 2.3**). For the U data, we show the extracellular potential in the electrode marked as c in **Figure 1** and the time scale is zoomed in on the first 20 ms of the simulation.

(γ_{Ca} = 0.1), and a 25% increased concentration (γ_{Ca} = 0.25). The solid lines show the default solutions for each of these extracellular environments, and we observe that the action potential and calcium transient durations are increased as the extracellular calcium concentration is increased. Furthermore, the dotted lines show the solutions corresponding to 20% block of the considered currents. For all the considered U data and for the V and Ca data for block of I_{Na}, the different extracellular calcium concentrations do not seem to have a significant effect. However, for the V and Ca data for block of I_{Kr} and I_{CaL}, we observe that the effect of the block varies for the different concentrations. For example, the effect of block of I_{Kr} is more prominent for an increased extracellular calcium concentration.

In **Figure 7**, we show an example of a case where including an additional extracellular calcium concentration could help identify the correct block of I_{Kr} and I_{CaL}. In the upper panel, we use the default extracellular calcium concentration of **Table 2**. The solid line shows V and Ca for the default base model, and the dotted line shows the solution for a case with 20% block of I_{Kr} and 33% block of I_{CaL}. We observe that V and Ca look very similar in these two cases. As a result, the inversion procedure might mistake the

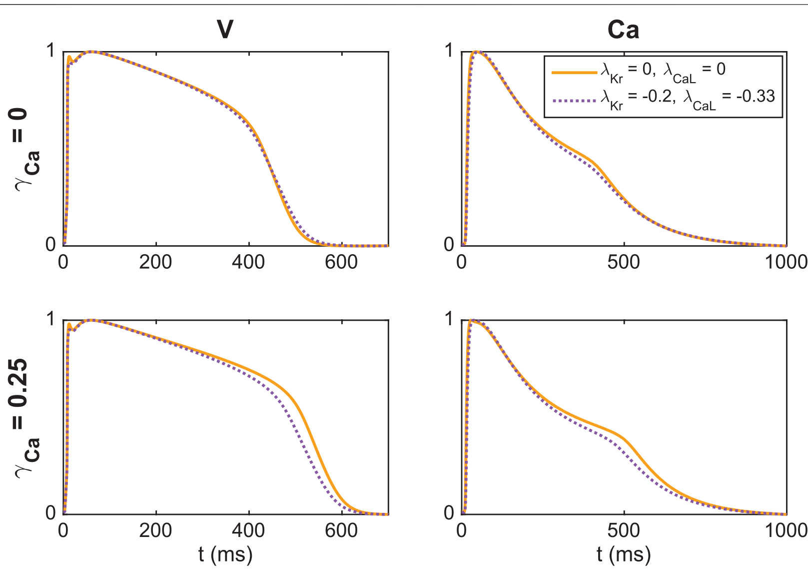

FIGURE 7 | Illustration of how including an extra extracellular calcium concentration adjustment may improve the identifiability of I_{Kr} and I_{CaL}. In the upper panel, we compare V and Ca for two different block combinations for the default extracellular calcium concentration (γ_{Ca} = 0), and in the lower panel we consider the solutions for a 25% increased extracellular calcium concentration (γ_{Ca} = 0.25). For γ_{Ca} = 0, the two solutions are very similar, but the difference is increased for γ_{Ca} = 0.25.

case of ($\lambda_{Kr} = -0.2$, $\lambda_{CaL} = -0.33$) to the case with no block. In the lower panel, however, we compare the two solutions for the case with an increased extracellular calcium concentration, and in this case, the difference between the solutions is more prominent. Consequently, the inversion procedure can more easily distinguish between the two cases when the solutions for both extracellular calcium concentrations are included.

3.3 Estimating the Action Potential Duration

Figure 8A shows measurements of the extracellular potential in 64 electrodes recorded for collections of hiPSC-CMs. In the upper panel, we observe that there is some early activity, corresponding to the time of the upstroke of the action potential, in addition to a weaker signal after some hundred milliseconds. This weaker signal occurs at the time of repolarization of the action potential and is therefore referred

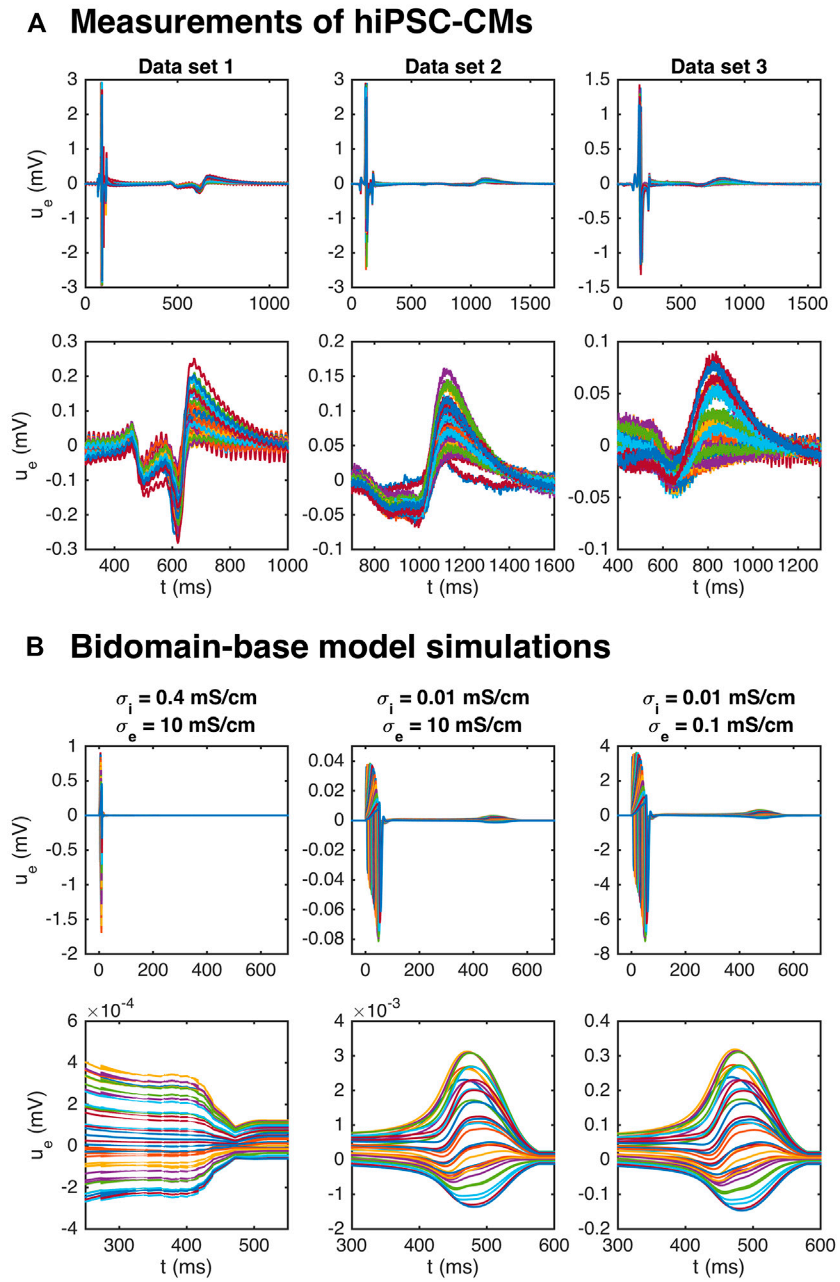

FIGURE 8 | Repolarization wave in hiPSC-CM data and bidomain-base model simulations. The upper panel shows measurements of U during an action potential for three different data sets. The traces for the 64 electrodes are overlaid in the plots. In the second panel, we zoom in on the repolarization wave. The third panel shows U in three bidomain-base model simulations, and the bottom panel shows the corresponding repolarization waves. The parameters used in the simulations are given in **Table 1**, except for σ_i and σ_e which are reported in the plot titles.

TABLE 3 | Effect of the drug Flecainide on the conduction velocity computed from the extracellular potential.

Dose	CV data	CV simulation ($IC50_{Na}$ = 2.2 μM, h_{Na} = 1)	CV simulation ($IC50_{Na}$ = 0.2 μM, h_{Na} = 0.4)
0 μM	23.7 cm/s	23.6 cm/s	23.7 cm/s
1 μM	17.9 cm/s	20.0 cm/s	14.2 cm/s
2.5 μM	11.7 cm/s	16.7 cm/s	12.0 cm/s
10 μM	9.3 cm/s	9.2 cm/s	8.9 cm/s

*The left panel reports values based on measurements of hiPSC-CMs and the center and right panels report values computed in bidomain-base model simulations with $IC50_{CaL}$ = 9 μM, $IC50_{NaL}$ = 47 μM, $IC50_{Kr}$ = 1.9 μM, and h_i = 1, for i = CaL, NaL, and Kr (see **Eq. 22**). The drug effect on I_{Na} is set to $IC50_{Na}$ = 2.2 μM, h_{Na} = 1 in the center column and $IC50_{Na}$ = 0.2 μM, h_{Na} = 0.4 in the right column. The parameters used in the simulations are given in **Tables 1** and **2**, and the default g_{Na} value is increased by 45% to match the conduction velocity in the control case.*

to as the repolarization wave. In the lower panel, we zoom in on this repolarization wave, and we observe that the extracellular potential reaches a magnitude of up to about 0.1–0.2 mV in this period.

It has been demonstrated (see, e.g., Abbate et al., 2018), that bidomain simulations of small collections of hiPSC-CMs tend to give rise to very weak or even non-exsisting repolarization waves. Indeed, in the leftmost panel of **Figure 8B**, we plot the extracellular potential in a bidomain-base model simulation using the default parameter values of **Table 1**, and we observe that the magnitude of the wave in this case is very small, and completely invisible in the upper plot over the entire action potential duration. If we decrease the intracellular conductivity, σ_i, on the other hand, a repolarization wave is visible, but the entire extracellular signal is quite weak (see the center panel of **Figure 8B**). However, if the extracellular conductivity, σ_e, is decreased as well, the size of both the depolarization wave and the repolarization wave are quite similar to the recorded data (see the rightmost panel of **Figure 8B**).

In theory, the repolarization waves observed in the data and simulations could be used to estimate the action potential duration in the inversion procedure. However, as observed in the lower panels of **Figure 8**, the repolarization waves are quite smooth, and it is not clear which time points represent different degrees of repolarization. For the V-traces on the other hand (see, e.g., **Figure 2**), it is straightforward to define accurate measures of different degrees of repolarization in the form of APD-values (see **Section 2.2.1** and **Figure 3**). Therefore, we use the optical measurements of V to define the action potential durations and only use the U data for information regarding the depolarization wave.

3.4 Estimating Drug Induced Effects on the Average Conduction Velocity

One of the advantages of including measurements of the extracellular potential in addition to optical measurements of V and Ca in the inversion procedure is that the extracellular measurements can be used to estimate the average conduction velocity of the cell collection. This information could be useful for determining drug effects on the I_{Na} current (see **Figure 5**). The left column of **Table 3** reports the conduction velocity computed from measurements of the extracellular potential in a collection of hiPSC-CMs exposed to different doses of the drug Flecainide (measured data, not simulated). We observe that as the drug dose is increased, the conduction velocity is decreased. This could indicate that the drug blocks the I_{Na} current, which has also been found in previous studies (Kramer et al., 2013; Crumb et al., 2016).

In the paper (Jæger et al., 2020a), we estimated IC50-values for I_{CaL}, I_{NaL} and I_{Kr} based on optical measurements of V and Ca of hiPSC-CMs exposed to Flecainide, but we were not able to estimate the effect on I_{Na} due to the low time resolution for the optical measurements. The IC50-values were estimated to $\mathrm{IC50}_{\mathrm{CaL}}$ = 9 μM, $\mathrm{IC50}_{\mathrm{NaL}}$ = 47 μM, and $\mathrm{IC50}_{\mathrm{Kr}}$ = 1.9 μM, where the conductance of each current was scaled according to

$$g_i^d = \left[\frac{1}{1 + \left(\frac{D}{\mathrm{IC50}_i}\right)^{h_i}}\right] \cdot g_i^c, \quad \text{for } i = \text{ CaL, NaL, Kr,} \tag{22}$$

where g_i^d is the conductance of current i in presence of the drug dose D and g_i^c is the conductance in the control case with no drug present. Furthermore, h_i is the so-called Hill coefficient, assumed to be one in (Jæger et al., 2020a). Incorporating these IC50-values in addition to some estimated IC50-values for I_{Na} in bidomain-base model simulations, we obtain the conduction velocities reported in the center and right columns of **Table 3**. In the center column we use $\mathrm{IC50}_{\mathrm{Na}}$ = 2.2 μM and h_{Na} = 1, and in the right column we use $\mathrm{IC50}_{\mathrm{Na}}$ = 0.2 μM and h_{Na} = 0.4. The $\mathrm{IC50}_{\mathrm{Na}}$ value in the case of h_{Na} = 1 compares relatively well with literature values; 6.7, 6.2 and 4.4 μM from Crumb et al., (2016), Kramer et al., (2013) and Qu and Vargas, (2015), respectively.

Note that since high doses of Flecainide result in increased action potential durations (see, e.g., Jæger et al., 2020a), we have used a pacing frequency of 0.5 Hz instead of 1 Hz when updating the initial conditions for these simulations. In addition, to match the conduction velocity in the control case, the default value of g_{Na} value of **Table 2** is increased by 45%. We observe that the bidomain-base model simulations are able to roughly reproduce the drug induced reduction in conduction velocity observed in the measurements, indicating that a comparison of measured and simulated conduction velocities could help identify drug effects on I_{Na}.

The data and model solutions are further compared in **Figure 9**. Here, we show the U solutions and the measured U data in the 64 electrodes for the control case and for the 10 μM dose case at some different points in time. In the simulations, we use $\mathrm{IC50}_{\mathrm{Na}}$ = 0.2 μM and h_{Na} = 0.4, and we have adjusted the stimulation location to correspond to the propagation direction observed in the measured data. In the control case, the wave moves in the y-direction from the lower part of the domain to the upper part, and in the drug case, the wave moves from the upper left corner to the lower right corner of the domain. In both the data and the simulations, we observe that the extracellular depolarization wave moves more slowly across the domain for 10 μM Flecainide than in the control case, consistent with the reduced conduction velocities observed in **Table 3**.

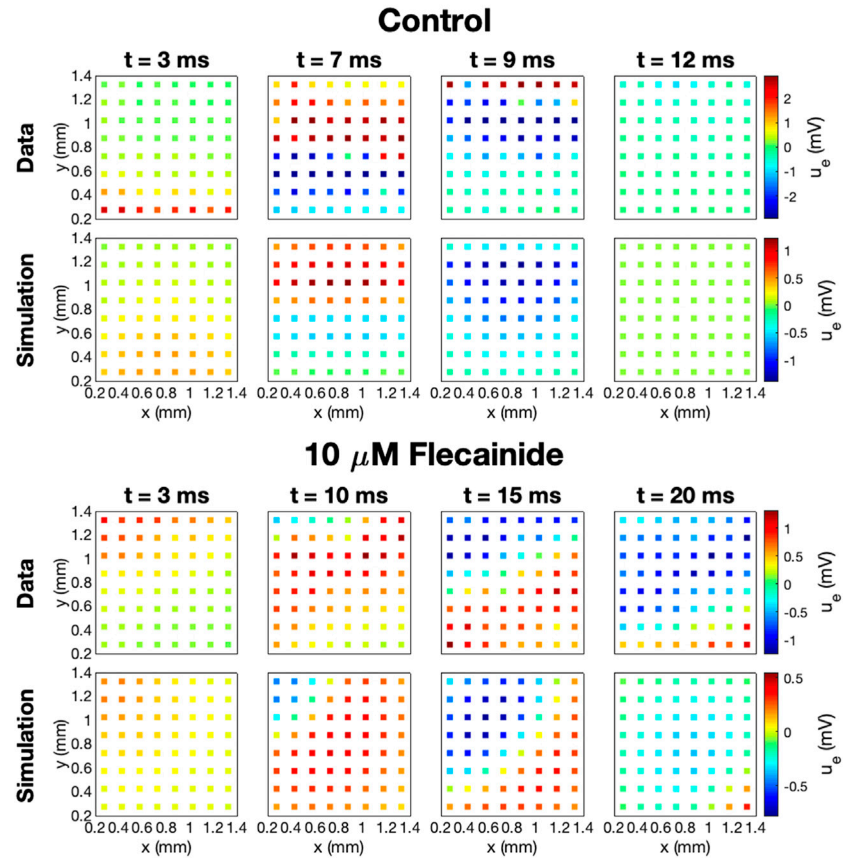

FIGURE 9 | Measured and simulated U data in 64 electrodes for the control case and for 10 μM Flecainide, modeled using $IC50_{CaL}$ = 9 μM, $IC50_{NaL}$ = 47 μM, $IC50_{Kr}$ = 1.9 μM, $IC50_{Na}$ = 0.2 μM, $h_i = 1$ for i = CaL, NaL, and Kr, and $h_{Na} = 0.4$. The parameters used in the simulations are given in **Tables 1** and **2**, and the default g_{Na} value is increased by 45%. The stimulation location is adjusted to correspond to the propagation direction in the data.

3.5 Inversion of Simulated Drugs

In order to investigate how well the inversion procedure outlined above is able to identify the effect of drugs on I_{Kr}, I_{CaL} and I_{Na}, we generate simulated data for twelve drugs whose effect on I_{Kr}, I_{CaL} and I_{Na} was investigated in (Crumb et al., 2016). The block percentages used to generate the data are based on the block percentages for drug concentrations corresponding to three times the free plasma C_{max} reported in (Crumb et al., 2016). However, large block percentages for I_{Kr} have been reduced in order to obtain reasonable V and Ca traces. In the inversions, we use two extracellular calcium concentrations, as explained in **Section 2.3**. Furthermore, we save U data and information about the Ca peak time extracted from the first 50 ms of the bidomain simulations for all the drugs, except for the drug Diltiazem. For Diltiazem we had to increase the bidomain simulation time to 100 ms in order to ensure that some of the grid points in the domain had reached their peak calcium concentration to compute the Ca peak time (see **Section 2.2.1**).

In **Figure 10**, we compare the block percentages estimated by the inversion procedure to those used to generate the data for the twelve drugs. We observe that for all the considered drugs, the inversion procedure is able to identify the block of the three currents quite accurately.

3.6 Effect of Noise

In **Figure 10**, we considered how well the inversion procedure was able to identify drugs based on data generated by bidomanbase model simulations, and we observed that the inversion procedure was able to identify the correct channel blocking quite accurately. However, when the V, Ca and U data are recorded from real measurements from microphysiological systems, the data will include some noise. In order to investigate how well the inversion procedure is able to identify the effect of drugs from data including noise, we include 5% noise in the V data, 3% noise in the Ca data and 1% noise in the U data and repeat the inversions shown in **Figure 10**. The noise is added by drawing a random number between $-p \cdot A$ and $p \cdot A$ for each point in time, where A is the difference between the maximum and minimum value of the considered data and p is the noise percentage. This random number is then added to the V, Ca and U traces.

The result of the inversions with noise included in the data is given in **Figure 11**. We observe that the inversion procedure is able to estimate the block percentage quite accurately in most cases, but that the accuracy is reduced compared to the case with no noise in **Figure 10**.

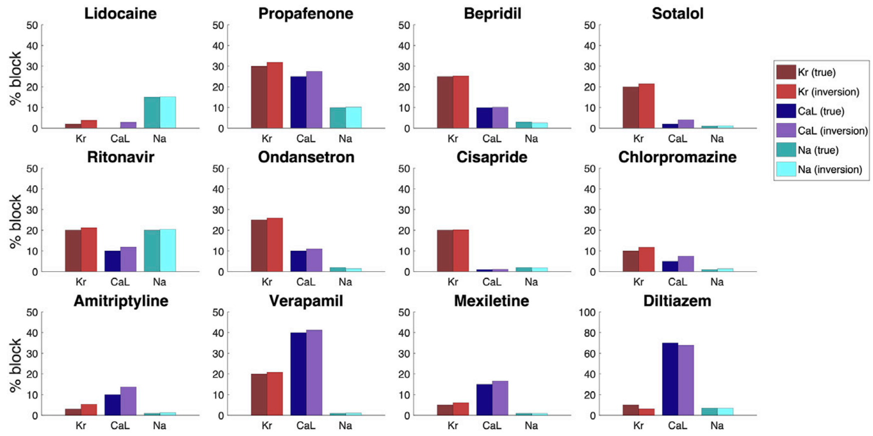

FIGURE 10 | Result of the inversion procedure applied to simulated data of twelve drugs, based on the block percentages corresponding to three times the free plasma C_{max} reported in (Crumb et al., 2016).

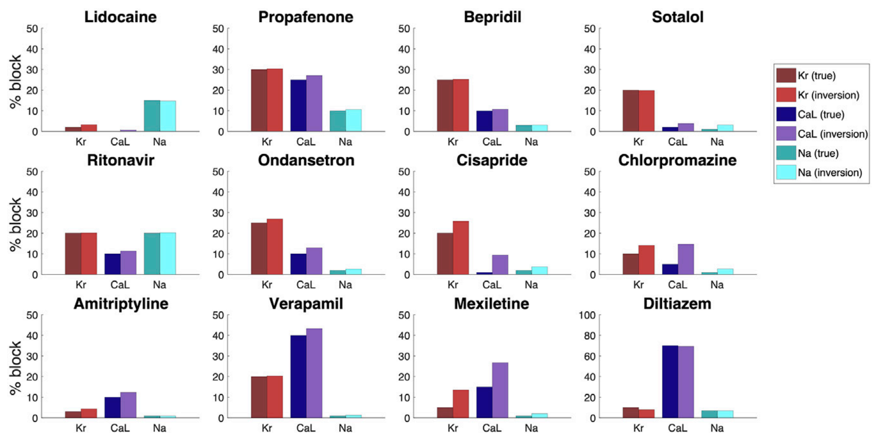

FIGURE 11 | Result of the inversion procedure applied to simulated data of the twelve drugs of **Figure 10**.We have here included 5% noise in the V data, 3% noise in the Ca data and 1% noise in the U data.

4 DISCUSSION

4.1 Sensitivity of Parameters Is Necessary for Identification

A generic problem in mathematical models of physiology is to determine the parameters included in the model. For models of the action potential of excitable cells, there is a large number of parameters that needs to be determined in order to use the model; see, e.g., (Sobie, 2009; Otte et al., 2016; Mora et al., 2017; Jæger et al., 2019b). If a model is insensitive to changes in a specific parameter, that parameter is impossible to determine by comparing experimental results and results of numerical simulations. Contrarily, if the model is sensitive to a parameter, numerical experiments can be used to match the model to the data by fine-tuning the parameter. In **Figure 4** above, we saw that the membrane potential is clearly sensitive to changes in the I_{Kr} and I_{CaL} currents. The upstroke is also sensitive to changes in the I_{Na} current, but since the upstroke is very fast, the sensitivity is difficult to see in the plot of the entire AP. Since optical measurements have a relatively coarse time resolution, we have been unable to identify the strength of the sodium current based solely on voltage and calcium traces. However, we note from **Figure 4** that the extracellular potential is indeed sensitive to changes in the sodium current. This sensitivity also carries over to sensitivity of the average conduction velocity (CV) with respect to changes in the sodium current, and this sensitivity is utilized in the cost function; see **Eq. 15**.

4.2 The Conduction Velocity Is Governed by the Sodium Current

The conduction of the electrochemical signal through the cardiac muscle is essential for the functioning of the heart. Surprisingly, the conduction process is still not completely understood; see, e.g., (Veeraraghavan et al., 2014), for a review of the development of the understanding of cardiac conduction. Globally (mm scale), cardiac conduction is usually modeled using homogenized models like the bidomain or monodomain models (see, e.g., Sundnes et al., 2007; Keener and James, 2009; Franzone et al., 2014), but locally (μm scale) more detailed models are used; see, e.g., (Kucera et al., 2002; Kucera et al., 2017; Jæger et al., 2019a). The microphysiological system is somewhere in between these scales (the size is about 1.2 mm × 1.2 mm) and we would have liked to use the detailed EMI model introduced for cardiac conduction in (Tveito et al., 2017). However, the EMI approach is challenging from a computational point of view and we have therefore used the much simpler bidomain model to consider how the CV depends on changing the different ion currents.

In **Figure 5** we observe that the CV is very sensitive to changes of the I_{Na} current, but almost insensitive to changes in the I_{Kr} and I_{CaL} currents. This means that we can use the measurements of U to identify the I_{Na} current first and then only look for the I_{Kr} and I_{CaL} currents based on the V- and Ca-traces.

4.3 Improving Visibility of Parameters by Changing the Extracellular Concentrations

In using experimental data to determine parameters of a computational model, it is desirable to use protocols designed to highlight the effect of different parameters. For instance, it is argued in (Groenendaal et al., 2015) that random stimulation protocols can improve visibility of the parameters, and this is confirmed in (Jæger et al., 2019b). Another experimental parameter that can be changed is the ionic concentrations of the extracellular environment. In **Figures 6** and **7** we show that using two different extracellular calcium concentration can improve identifiability of the model parameters. One particular important effect of this is that multiple extracellular calcium concentration can aid in distinguishing changes of the I_{Kr} and I_{CaL} currents. Since blocking I_{Kr} has more or less the same effect as increasing I_{CaL}, it is difficult to distinguish these effects in measurements of the AP. But it is apparent from **Figure 7** that the level of blocking changes with the extracellular calcium concentration, and this can be used to distinguish between different blocking combinations for these two currents.

4.4 Inversion of Simulated Drugs

Simulated data is often used as a proxy for real data when the real data are cumbersome to obtain. Here, we have used real data for U both for the case of no drug and when various doses of Flecainide have been applied. Furthermore, the base model used to represent the membrane dynamics has been parameterized using real data; see (Tveito et al., 2018; Jæger et al., 2020a). However, in order to study inversion for the range of data provided in the CIPA report (Crumb et al., 2016), we have used simulated data. One advantage of this is that we can get data to any desired accuracy and that we can control the level of noise inevitably introduced in the measurements. The disadvantage is clearly the reduced realism of the data and it is a priority of future work to use combined V, Ca, and U data to do inversion of both well characterized and novel drugs with hitherto unknown properties.

For simulated data, we notice that the inversion procedure provides quite accurate estimates. Systematically, we observe a tendency to overestimate the block of both the I_{Kr} and I_{CaL} currents. As alluded to above, it is notoriously difficult to distinguish reduced I_{Kr} from increased I_{CaL} and vice versa. This can be improved (**Figures 6** and **7**), by using several values of the extracellular calcium concentration, but the problem is not completely removed.

4.5 Repolarization Waves in Bidomain Simulations

As mentioned above, the bidoman model has been used by many authors (see, e.g., Abbate et al., 2018; Bouyssier and Zemzemi, 2017; Raphel et al., 2017; Raphel et al., 2020; Tixier et al., 2018) to simulate the electrophysiology of collections of hiPSC-CMs. One problem pointed out by several authors is the lack of a repolarization wave in the simulated results although the repolarization wave is clearly present in measurements of the extracellular potential; see, e.g., Figures 3 and 4 of (Abbate et al., 2018). This feature of the bidomain solution is repaired by introducing heterogeneities in the tissue which lead to a repolarization wave. In **Figure 8A**, we show that there is indeed a repolarization wave present in the extracellular data obtained from collections of hiPSC-CMs. The repolarization wave is also present in our bidomain simulations, but the strength of the wave depends critically on the intracellular conductivity, σ_i. The repolarization wave becomes stronger as σ_i is reduced. Since the intracellular conductivity represents the geometrical average of the intercellular conductivity (regulated by gap junctions) and the cytosolic conductivity, it is reasonable to use a reduced value of σ_i for immature cells, since the gap junctions are most likely less developed in collections of hiPSC-CMs than for collections of adult cardiomyocytes. Experimentally, this has been observed in these cells, with indications of incomplete maturity and underdeveloped gap junctions by connexin-43 staining that localized in small speckles (Huebsch et al., 2018) rather than distinct disks as found in the adult human heart. Furthermore, immature tissue geometry, in terms of cell alignment, shape, and orientation of connectivity may also change these dynamics, and while these cells have demonstrated good agreement of geometric cell parameters, such as alignment within a microphysiological system compared to the adult human heart (Huebsch et al., 2018), more study is needed on the relative effects of these features on conduction properties. In (Abbate et al., 2018), it is argued that it is reasonable to introduce heterogeneities in the tissue and we agree. However, our results indicate that it is not necessary in order to see a repolarization wave in the simulation results.

5 CONCLUSION

We have shown that by using data traces of the membrane potential, the intracellular calcium concentration and the extracellular potential, we can estimate the major sodium, calcium and potassium currents in the base model. It remains to enable concurrent observation of all three modalities, but when such data become available, the methodology described in the present report may be used to invert the data and thus obtain channel densities and estimate drug effects on the channels.

DATA AVAILABILITY STATEMENT

The raw data supporting the conclusions of this article will be made available by the authors, without undue reservation.

AUTHOR CONTRIBUTIONS

KJ and AT developed the mathematical framework, performed the numerical experiments and wrote the paper. SW carefully checked all parts of the paper and improved the wording of the paper. VC and KH generated data of hiPSC-CMs from microphysiological systems. All authors read and approved the final manuscript.

FUNDING

We would like to acknowledge the following funding sources: The Research Council of Norway funded INTPART Project 249885, the SUURPh program funded by the Norwegian Ministry of Education and Research, the Peder Sather Center for Advanced Study, NIH-NCATS UH3TR000487, NIH-NHLBI 2485 HL130417, and the California Institute for Regenerative Medicine DISC2-10090. The funders had no role in study design, data collection and analysis, decision to publish, or preparation of the manuscript.

ACKNOWLEDGMENTS

This manuscript has been released as a pre-print at *bioRxiv*, (Jæger et al., 2020b).

SUPPLEMENTARY MATERIAL

The Supplementary Material for this article can be found online at: https://www.frontiersin.org/articles/10.3389/fphar.2020.569489/full#supplementary-material.

REFERENCES

Abbate, E., Boulakia, M., Coudière, Y., Gerbeau, J. F., Zitoun, P., and Zemzemi, N. (2018). In silico assessment of the effects of various compounds in mea/hipsc-cm assays: modeling and numerical simulations. *J. Pharmacol. Toxicol. Methods* 89, 59–72. doi:10.1016/j.vascn.2017.10.005

Asakura, K., Hayashi, S., Ojima, A., Taniguchi, T., Miyamoto, N., Nakamori, C., et al. (2015). Improvement of acquisition and analysis methods in multi-electrode array experiments with ips cell-derived cardiomyocytes. *J. Pharmacol. Toxicol. Methods* 75, 17–26. doi:10.1016/j.vascn.2015.04.002

Bouyssier, J., and Zemzemi, N. (2017). "Parameters estimation approach for the mea/hipsc-cm asaays," in 2017 computing in cardiology (CinC), Rennes, France, September 24–27, 2017 (Lille, France: IEEE), 1–4.

Clements, M., and Thomas, N. (2014). High-throughput multi-parameter profiling of electrophysiological drug effects in human embryonic stem cell derived cardiomyocytes using multi-electrode arrays. *Toxicol. Sci* 140 (2), 445–461. doi:10.1093/toxsci/kfu084

Crumb, W. J., Vicente, J., Johannesen, L., and Strauss, D. G. (2016). An evaluation of 30 clinical drugs against the comprehensive *in vitro* proarrhythmia assay (CiPA) proposed ion channel panel. *J. Pharmacol. Toxicol. Methods* 81, 251–262. doi:10.1016/j.vascn.2016.03.009

Di Stilo, A., Visentin, S., Cena, C., Gasco, A. M., Ermondi, G., and Gasco, A. (1998). New 1,4-dihydropyridines conjugated to furoxanyl moieties, endowed with both nitric oxide-like and calcium channel antagonist vasodilator activities. *J. Med. Chem* 41 (27), 5393–5401. doi:10.1021/jm9803267

Franzone, P. C., Pavarino, L. F., and Scacchi, S. (2014). *Mathematical cardiac electrophysiology*. Cham, Switzerland: Springer.

Groenendaal, W., Ortega, F. A., Kherlopian, A. R., Zygmunt, A. C., Krogh-Madsen, T., and Christini, D. J. (2015). Cell-specific cardiac electrophysiology models. *PLoS Comput. Biol* 11 (4), e1004242. doi:10.1371/journal.pcbi.1004242

Huebsch, N., Loskill, P., Mandegar, M. A., Marks, N. C., Sheehan, A. S., Ma, Z., et al. (2015). Automated video-based analysis of contractility and calcium flux in human-induced pluripotent stem cell-derived cardiomyocytes cultured over different spatial scales. *Tissue Eng. C Methods* 21 (5), 467–479. doi:10.1089/ten.TEC.2014.0283

Huebsch, N., Charrez, B., Siemons, B., Boggess, S. C., Wall, S., Charwat, V., et al. (2018). Metabolically-driven maturation of hipsc-cell derived heart-on-a-chip. Available at: https://www.biorxiv.org/content/10.1101/485169v3.

Jæger, K. H., Edwards, A. G., McCulloch, A., and Tveito, A. (2019a). Properties of cardiac conduction in a cell-based computational model. *PLoS Comput. Biol* 15 (5), e1007042. doi:10.1371/journal.pcbi.1007042

Jæger, K. H., Wall, S., and Tveito, A. (2019b). Detecting undetectables: can conductances of action potential models be changed without appreciable change in the transmembrane potential? *Chaos* 29 (7), 073102. doi:10.1063/1.5087629

Jæger, K. H., Charwat, V., Charrez, B., Finsberg, H., Maleckar, M. M., and Wall, S. (2020a). Improved computational identification of drug response using optical measurements of human stem cell derived cardiomyocytes in microphysiological systems. *Front. Pharmacol.* 10, 1648. doi:10.3389/fphar.2019.01648

Jæger, K. H., Charwat, V., Wall, S., Healy, K. E., and Tveito, A. (2020b). Identifying drug response by combining measurements of the membrane potential, the cytosolic calcium concentration, and the extracellular potential in microphysiological systems. Available at: https://www.biorxiv.org/content/10.1101/2020.05.29.122747v1.

Keener, J. P., and James, S. (2009). *Mathematical physiology*. New York, NY: Springer.

Kernik, D. C., Morotti, S., Wu, H. D., Garg, P., Henry, J. D., Kurokawa, J., et al. (2019). A computational model of induced pluripotent stem-cell derived cardiomyocytes incorporating experimental variability from multiple data sources. *J. Physiol* 597 (17), 4533–4564. doi:10.1113/JP277724

Kramer, J., Obejero-Paz, C. A., Myatt, G., Kuryshev, Y. A., Bruening-Wright, A., et al. (2013). MICE models: superior to the HERG model in predicting Torsade de Pointes. *Sci. Rep* 3, 2100. doi:10.1038/srep02100

Kucera, J. P., Rohr, S., and Kleber, A. G. (2017). Microstructure, cell-to-cell coupling, and ion currents as determinants of electrical propagation and arrhythmogenesis. *Circ. Arrhythm. Electrophysiol* 10 (9), e004665. doi:10.1161/CIRCEP.117.004665

Kucera, J. P., Rohr, S., and Rudy, Y. (2002). Localization of sodium channels in intercalated disks modulates cardiac conduction. *Circ. Res* 91 (12), 1176–1182. doi:10.1161/01.res.0000046237.54156.0a

Lian, X., Hsiao, C., Wilson, G., Zhu, K., Hazeltine, L. B., Azarin, S. M., et al. (2012). Robust cardiomyocyte differentiation from human pluripotent stem cells via temporal modulation of canonical wnt signaling. *Proc. Natl. Acad. Sci. U.S.A* 109 (27), E1848–E1857. doi:10.1073/pnas.1200250109

Mathur, A., Loskill, P., Shao, K., Huebsch, N., Hong, S., Marcus, S. G., et al. (2015). Human iPSC-based cardiac microphysiological system for drug screening applications. *Sci. Rep* 5, 8883. doi:10.1038/srep08883

Mathur, A., Ma, Z., Loskill, P., Jeeawoody, S., and Healy, K. E. (2016). *In vitro* cardiac tissue models: current status and future prospects. *Adv. Drug Deliv. Rev* 96, 203–213. doi:10.1016/j.addr.2015.09.011

MED64 Application Note (2015). Cellartis® cardiomyocytes. Available at: http://www.med64.com/support/Application_Note_Cellartis_hPSC-CM.pdf.

MED64 Application Note (2016). Human stem cell-derived cardiomyocytes. Available at: http://www.med64.com/wp-content/uploads/2016/04/Application_Note_hSC-CMs.pdf.

Mirams, G. R., Cui, Y., Sher, A., Fink, M., Cooper, J., Heath, B. M., et al. (2011). Simulation of multiple ion channel block provides improved early prediction of compounds' clinical torsadogenic risk. *Cardiovasc. Res* 91 (1), 53–61. doi:10.1093/cvr/cvr044

Mohammad, S., Zhou, Z., Gong, Q., and January, C. T. (1997). Blockage of the HERG human cardiac K+ channel by the gastrointestinal prokinetic agent cisapride. *Am. J. Physiol* 273 (5), H2534–H2538. doi:10.1152/ajpheart.1997.273.5.H2534

Mora, M. T., Ferrero, J. M., Romero, L., and Trenor, B. (2017). Sensitivity analysis revealing the effect of modulating ionic mechanisms on calcium dynamics in simulated human heart failure. *PloS One* 12 (11), e0187739. doi:10.1371/journal.pone.0187739

Nelder, J. A., and Mead, R. (1965). A simplex method for function minimization. *Comput. J* 7 (4), 308–313. doi:10.1093/comjnl/7.4.308

Otte, S., Berg, S., Luther, S., and Ulrich, P. (2016). Bifurcations, chaos, and sensitivity to parameter variations in the sato cardiac cell model. *Commun. Nonlinear Sci. Numer. Simulat* 37, 265–281. doi:10.1016/j.cnsns.2016.01.014

Qu, Y., and Vargas, H. M. (2015). Proarrhythmia risk assessment in human induced pluripotent stem cell-derived cardiomyocytes using the maestro mea platform. *Toxicol. Sci* 147 (1), 286–295. doi:10.1093/toxsci/kfv128

Raphel, F., Boulakia, M., Zemzemi, N., Coudière, Y., Guillon, J. M., Zitoun, P., et al. (2017). Identification of ion currents components generating field potential recorded in mea from hipsc-cm. *IEEE Trans. Biomed. Eng* 65 (6), 1311–1319. doi:10.1109/TBME.2017.2748798

Raphel, F., de Korte, T., Lombardi, D., Braam, S., and Gerbeau, J.-F. (2020). A greedy classifier optimisation strategy to assess ion channel blocking activity and pro-arrhythmia in hipsc-cardiomyocytes. *PLoS Comput. Biol* 16, e1008203. doi:10.1371/journal.pcbi.1008203

Schroll, H. J., Lines, G. T., and Tveito, A. (2007). On the accuracy of operator splitting for the monodomain model of electrophysiology. *Int. J. Comput. Math* 84 (6), 871–885. doi:10.1080/00207160701458724

Sobie, E. A. (2009). Parameter sensitivity analysis in electrophysiological models using multivariable regression. *Biophys. J* 96 (4), 1264–1274. doi:10.1016/j.bpj.2008.10.056

Sundnes, J., Artebrant, R., Skavhaug, O., and Tveito, A. (2009). A second-order algorithm for solving dynamic cell membrane equations. *IEEE Trans. Biomed. Eng* 56 (10), 2546–2548. doi:10.1109/TBME.2009.2014739

Sundnes, J., Lines, G. T., and Tveito, A. (2005). An operator splitting method for solving the bidomain equations coupled to a volume conductor model for the torso. *Math. Biosci* 194 (2), 233–248. doi:10.1016/j.mbs.2005.01.001

Sundnes, J., Lines, G. T., Cai, X., Nielsen, B. F., Mardal, K.-A., and Tveito, A. (2007). *Computing the electrical activity in the heart*. Cham, Switzerland: Springer Science and Business Media.

Tixier, E., Raphel, F., Lombardi, D., and Gerbeau, J. F. (2017). Composite biomarkers derived from micro-electrode array measurements and computer simulations improve the classification of drug-induced channel block. *Front. Physiol* 8, 1096. doi:10.3389/fphys.2017.01096

Tung, L. (1978). A bi-domain model for describing ischemic myocardial dc potentials. PhD thesis. Cambridge, MA: Massachusetts Institute of Technology.

Tveito, A., Jæger, K. H., Huebsch, N., Charrez, B., Edwards, A. G., Wall, S., et al. (2018). Inversion and computational maturation of drug response using human stem cell derived cardiomyocytes in microphysiological systems. *Sci. Rep* 8 (1), 17626. doi:10.1038/s41598-018-35858-7

Tveito, A., Karoline, H., Kuchta, M., Mardal, K.-A., and Rognes, M. E. (2017). A cell-based framework for numerical modeling of electrical conduction in cardiac tissue. *Front. Phys* 5, 48. doi:10.3389/fphy.2017.00048

Veeraraghavan, R., Gourdie, R. G., and Poelzing, S. (2014). Mechanisms of cardiac conduction: a history of revisions. *Am. J. Physiol. Heart Circ. Physiol* 306 (5), H619–H627. doi:10.1152/ajpheart.00760.2013

Veevers, J., Farah, E. N., Corselli, M., Witty, A. D., Palomares, K., Vidal, J. G., et al. (2018). Cell-surface marker signature for enrichment of ventricular cardiomyocytes derived from human embryonic stem cells. *Stem Cell Rep* 11 (3), 828–841. doi:10.1016/j.stemcr.2018.07.007

Zhabyeyev, P., Missan, S., Jones, S. E., and McDonald, T. F. (2000). Low-affinity block of cardiac K(+) currents by nifedipine. *Eur. J. Pharmacol* 401 (2), 137–143. doi:10.1016/s0014-2999(00)00413-1

Zhang, S., Zhou, Z., Gong, Q., Makielski, J. C., and January, C. T. (1999). Mechanism of block and identification of the verapamil binding domain to HERG potassium channels. *Circ. Res* 84 (9), 989–998. doi:10.1161/01.res.84.9.989

Zwi, L., Caspi, O., Arbel, G., Huber, I., Gepstein, A., Park, I. H., et al. (2009). Cardiomyocyte differentiation of human induced pluripotent stem cells. *Circulation* 120 (15), 1513. doi:10.1161/CIRCULATIONAHA.109.868885

Conflict of Interest: KJ, AT, SW, and KH have financial relationships with Organos Inc., and the company may benefit from commercialization of the results of this research.

The remaining author declares that the research was conducted in the absence of any commercial or financial relationships that could be construed as a potential conflict of interest.

frontiers in Pharmacology

PERSPECTIVE
published: 10 February 2021
doi: 10.3389/fphar.2020.569955

Two Targets, One Hit: new Anticancer Therapeutics to Prevent Tumorigenesis Without Cardiotoxicity

*Zoltán Szabó[1], Lilla Hornyák[2], Márton Miskei[2] and Lóránt Székvölgyi[2,3]**

[1]*Department of Emergency Medicine, Faculty of Medicine, University of Debrecen, Debrecen, Hungary,* [2]*MTA-DE Momentum Genome Architecture and Recombination Research Group, Department of Biochemistry and Molecular Biology, Faculty of Medicine, University of Debrecen, Doctoral School of Molecular Cell and Immune Biology, Debrecen, Hungary,* [3]*Faculty of Pharmacy, University of Debrecen, Debrecen, Hungary*

A serious adverse effect of cancer therapies is cardiovascular toxicity, which significantly limits the widespread use of antineoplastic agents. The promising new field of cardio-oncology offers the identification of potent anti-cancer therapeutics that effectively inhibit cancer cell proliferation without causing cardiotoxicity. Future introduction of recently identified cardio-safe compounds into clinical practice (including ERK dimerization inhibitors or BAX allosteric inhibitors) is expected to help oncologists avoid unwanted cardiological complications associated with therapeutic interventions.

Keywords: MAPK/ERK pathway, bax, cancer therapy, clinical trial, cardiotoxicity

OPEN ACCESS

Edited by:
Jonathan Satin,
University of Kentucky, United States

Reviewed by:
Xingrong Du,
St. Jude Children's Research Hospital, United States
Michele Russo,
University of Turin, Italy

****Correspondence:***
Lóránt Székvölgyi
lorantsz@med.unideb.hu

Specialty section:
This article was submitted to Cardiovascular and Smooth Muscle Pharmacology, a section of the journal Frontiers in Pharmacology

Received: *05 June 2020*
Accepted: *08 December 2020*
Published: *10 February 2021*

Citation:
Szabó Z, Hornyák L, Miskei M and Székvölgyi L (2021) Two Targets, One Hit: new Anticancer Therapeutics to Prevent Tumorigenesis Without Cardiotoxicity. Front. Pharmacol. 11:569955. doi: 10.3389/fphar.2020.569955

1 INTRODUCTION

One of the most devastating adverse effects of anticancer treatments is cardiovascular toxicity, which significantly restricts the effective use of conventional and targeted tumor therapeutics (Cameron and Chen, 2018; Herrmann, 2020). Therapy-related cardiovascular diseases involve a wide range of disorders from thromboembolism, stroke, systemic and pulmonary hypertension, myocarditis, cardiac arrhythmias to even sudden cardiac death, which collectively contribute to an increased morbidity and mortality of cancer patients. In addition to cardiovascular damage, a significant fraction of cancer patients suffers from acute or chronic kidney disease, requiring renal replacement therapies (Czifra et al., 2013; Barta et al., 2014), resulting in an increased risk of atrial and ventricular arrhythmias, heart failure and other adverse effects (Szabó et al., 2020). Nevertheless, increased prevalence of cancer among patients with heart failure indicates common molecular triggers and risk factors that contribute to both diseases (de Boer et al., 2019; Meijers and De Boer, 2019). Regardless of hemodynamic impairment, heart failure stimulates tumor development by secreting various circulating factors (Meijers et al., 2018; Richards, 2018), suggesting a causal relationship between heart failure and tumorigenesis. These associations encourage the development of new cardio-safe strategies to increase the effectiveness of cancer therapies (Hetey et al., 2017; Boros-oláh et al., 2019).

The MAPK/ERK pathway is one of the major targets of anti-tumor therapies in several malignancies as gain-of-function mutations of this pathway are collectively associated with more than 90% of cancers (Nissan et al., 2013; Smorodinsky-Atias et al., 2020). The cascade involves the sequential activation of receptor tyrosine kinases (RTK), RAS GTPases, RAF kinases (MAP3K), MEK (MAP2K), which ultimately phosphorylates ERK (MAPK) (Lee et al., 2020). Activated ERK (extracellular signal-regulated kinase) is located at the bottom of the cascade phosphorylating hundreds of cytosolic and nuclear targets (Plotnikov et al., 2015) that mediate opposing signaling pathways leading to cell survival, apoptosis, cancer growth or cardiac disfunction (**Figure 1**).

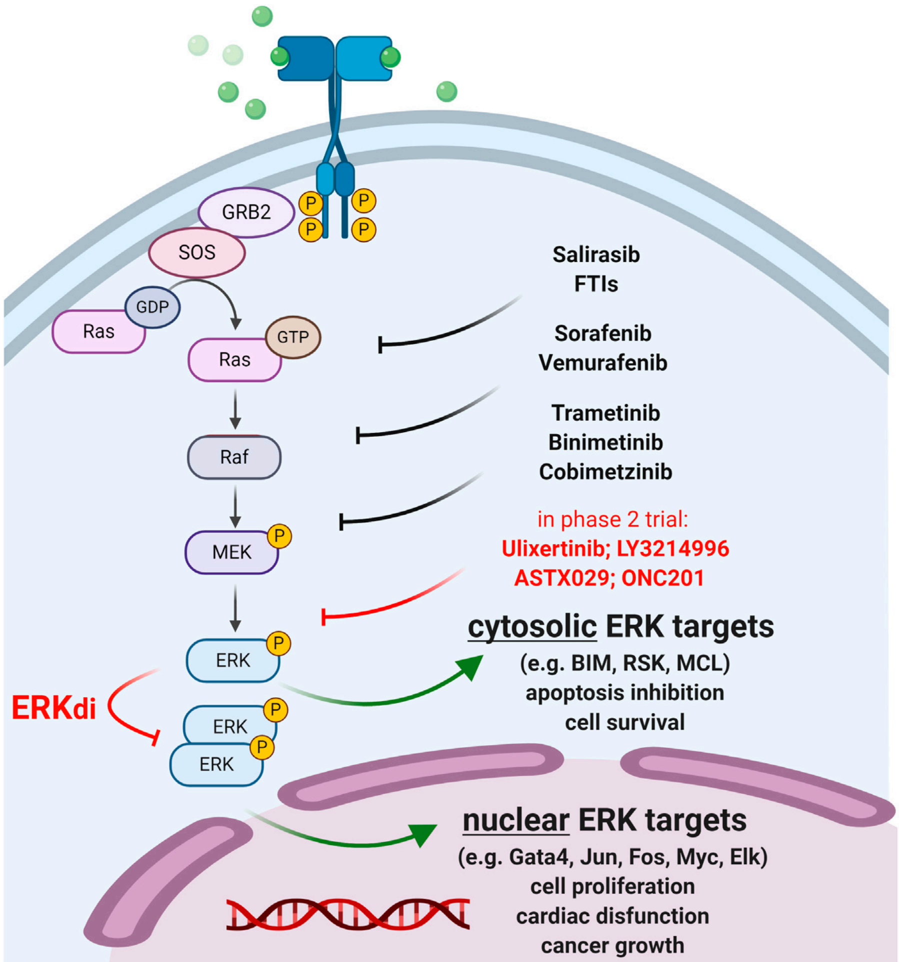

FIGURE 1 | Therapeutic targeting of the MAPK/ERK pathway. Approved anti-cancer compounds targeting RAS/RAF/MEK are indicated in black. ERK inhibitors (ERKi) in phase 2 clinical trials are shown in red. Newly developed ERK dimerization inhibitors (ERKdi) are currently in pre-clinical phases. ERKdi compounds prevent nuclear translocation of ERK, thereby inhibiting the activation of transcription factors that cause tumor cell proliferation and mediate cardiac disfunction in normal cardiac tissue.

Therapeutic targeting of ERK is of key interest since ERK inhibitors (ERKi) have the potential to overcome common drug resistance to "upstream" MEK/RAF/RAS inhibitors (Ryan and Corcoran, 2018; Smorodinsky-Atias et al., 2020). Indeed, ERKi therapies are expected to show greater antitumor efficacy in advanced metastatic and multidrug-resistant tumors with reactivated MAPK signaling, however, their broad clinical use is limited (Lee et al., 2020). This is because ERK is associated with many diseases, such as heart failure, and thus ERKi therapy may cause severe cardiotoxic side effects. Multiple ERK inhibitors are currently in clinical trials for the treatment of RAS/RAF-mutated and BRAFi/MEKi-resistant tumors (**Supplementary Table S1**); however, new cardio-safe strategies need to be developed to overcome acquired resistance to MAPK inhibitor therapies.

In this respect, recently developed ERK-dimerization inhibitors (ERKdi) show potential to prevent tumorigenesis in preclinical models, without causing severe cardiotoxicity (Herrero et al., 2015; Tomasovic, 2020). The latest compound (Tomasovic, 2020) specifically blocks ERK1/2 dimer formation and consequent Thr188 phosphorylation (that is a prerequisite for ERK nuclear translocation, oncogenic activation and cardiotoxic side effects (Tomasovic, 2020)), preventing heart failure while preserving ERK1/2 catalytic activity and cytosolic survival signaling. This dual consequence of ERKdi treatment is in sharp contrast with the adverse effect of "upstream" MAPK/RAS inhibitors (e.g., MEKi, RAFi), which severely compromise cardiomyocyte mitochondria function and often lead to cardiac injury. The newly developed ERKdi drug may also be relevant in other diseases that rely on intensive ERK signaling, such as secondary cardiac injuries (e.g., due to hypertension, oxidative damage, ischemia), which are expected to extend therapeutic modalities to tumors resistant to upstream MAPK inhibitors.

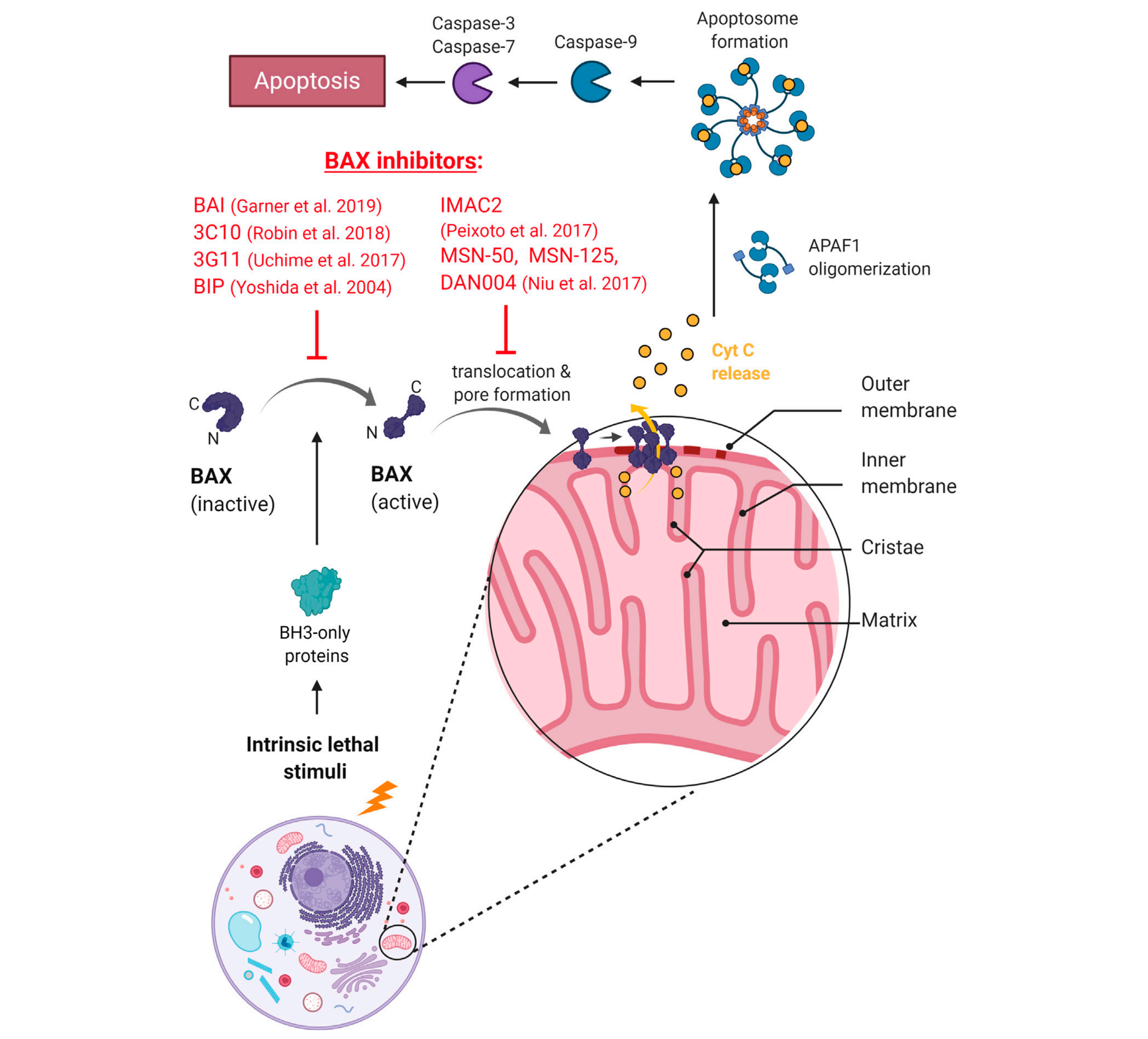

FIGURE 2 | The mechanism of action of BAX inhibitors. BAXi prevents conformational change and activation of BAX, or inhibits mitochondrial translocation and pore formation, preventing the release of cytochrome C and the onset of apoptosis.

In addition to MAPK inhibitors, doxorubicin (dox) is one of the most common anthracycline-based chemotherapeutics due to its broad spectrum and high efficacy; however, its applicability is highly limited by its severe cardiotoxic side-effects (Wallace et al., 2020). A recent study identified a new Sirt6–Tip60–Gata4 molecular axis that includes a histone deacetylase (Sirt6), a histone acetylase (Tip60), and a transcription factor (Gata4) that regulates an anti-apoptotic pathway and thus prevents dox-induced cardiotoxicity (Peng et al., 2020). Importantly, Gata4 is activated directly by ERK (via phosphorylation on serine 105 (Liang et al., 2001)) and thus inhibiting the deacetylase activity of Sirt6, which in turn disrupts the equilibrium in local histone acetylation. The resulting open chromatin allows the expression of cardiac-expressed genes involved in cardiac development and hypertrophy, as well as Bcl2 survival factors that suppress apoptosis and dox cardiotoxicity. Therefore, the Sirt6-Tip60-Gata4 axis represents a new therapeutic target to enhance the safety and efficacy of dox chemotherapy.

In another recent attempt, dox-based tumor therapy was made cardio-safe in combination with a specific Bax inhibitor (Amgalan et al., 2020). When dox was administered with a newly developed Bax allosteric inhibitor that modulate Bax function by conformational changes (BAI1 (Garner et al., 2019), **Figure 2**), cardiomyopathy was completely prevented without compromising the tumor-killing efficacy of dox treatment (Amgalan et al., 2020). The differential effect of Bax inhibition on cardiomyocytes vs. cancerous cells was attributed to the ubiquitously high Bax expression of cancer cells relative to the heart tissue (see e.g., https://www.proteinatlas.org/ENSG00000087088-BAX/pathology; (Thul et al., 2017)). High Bax levels in tumors may help suspend the inhibitory effect of the drug, promoting the apoptosis of cancer cells. These associations designate Bax as a potent tumor-selective drug target to prevent dox-induced cardiotoxicity. While it remains to be tested, the compound may also be used to prevent cardiomyopathies in other diseases in which Bax-mediated apoptotic and necrotic pathways are involved (e.g., infarction, stroke).

2 CONCLUSION

The above cardio-safe drugs (including ERK dimerization inhibitors or BAX allosteric inhibitors) are just the tip of the iceberg: superimposed on them, further research into new molecular pathways and anticancer therapeutics is needed to prevent tumorigenesis without instigating severe cardiotoxicity. BAXi data are still in the preclinical phase and ERKi human clinical trials are still preliminary. Classical ERK inhibitors have some common side effects that can be mild (e.g., diarrhea, nausea, fatigue, and rash) and severe, including neurotoxicity (CC-90003, NCT02313012) and myocardial infarction (Merchant et al., 2014; Sullivan et al., 2018; Chin et al., 2019; Weekes et al., 2020). In addition, tumors treated with ERKi often exhibit resistance to ERK inhibitors, just like upstream Ras/Raf/Mek kinases (Goetz et al., 2014; Jha et al., 2016; Jaiswal et al., 2018), which limits therapeutic efficacy. Whether the new generational ERK dimerization inhibitors (ERKdi) are better tolerable in combination with other cytostatic agents remains to be demonstrated. We also note that the ERK target GATA-4 is regulated by other post-translational modifications in myocardial cells involving e.g. p38 mitogen-activated protein kinase (p38 MAPK), small GTPase RhoA-associated coil-forming kinase (ROCK), glycogen synthase kinase-3beta (GSK-3beta) and cAMP-responsive element-binding protein binding protein (CBP) (Pikkarainen et al., 2004), which greatly increase the complexity of the system in terms of therapeutic options. This is a promising new field of cardio-oncology which is expected to improve the effectiveness of cancer treatments and help physicians avoid unexpected secondary effects related to therapeutic intervention.

AUTHOR CONTRIBUTIONS

Conceptualization: LS, ZS manuscript writing, LS, ZS, MM, and LH; supervision, LS; funding acquisition, LS. All authors have read and agreed to the published version of the manuscript.

FUNDING

This work was funded by NKFIH-NNE-130913, GINOP-2.3.2-15-2016-00024, and the Thematic Excellence Programme (TKP2020-IKA-04) of the Ministry for Innovation and Technology in Hungary. LS was supported by the Bolyai Janos fellowship of the Hungarian Academy of Sciences and the UNKP-20–5-DE-47 new national excellence program of the Ministry For Innovation and Technology from the source of the National Research, Development and Innovation Fund.

SUPPLEMENTARY MATERIAL

The Supplementary Material for this article can be found online at: https://www.frontiersin.org/articles/10.3389/fphar.2020.569955/full#supplementary-material.

REFERENCES

Amgalan, D., Garner, T. P., Pekson, R., Jia, X. F., Yanamandala, M., Paulino, V., et al. (2020). A small-molecule allosteric inhibitor of BAX protects against doxorubicin-induced cardiomyopathy. *Nat. Can.* 1, 315–328. doi:10.1038/s43018-020-0039-1

Barta, K., Czifra, Á., Kun, C., Páll, A., Kulcsár, J., Paragh, G., et al. (2014). Hemodiafiltration beneficially affects QT interval duration and dispersion compared to hemodialysis. *Clin. Exp. Nephrol.* 18, 952–959. doi:10.1007/s10157-014-0950-9

Boros-oláh, B., Dobos, N., Hornyák, L., Szabó, Z., Karányi, Z., Halmos, G., et al. (2019). Drugging the R-loop interactome : RNA-DNA hybrid binding proteins as targets for cancer therapy. *DNA Repair* 84, 102642. doi:10.1016/j.dnarep.2019.102642

Cameron, S. J., and Chen, H. (2018). Cardiotoxicity of anticancer therapeutics. *Front. Cardiovasc. Med.* 5, 9. doi:10.3389/fcvm.2018.00009

Chin, H., Lai, D., and Falchook, G. (2019). Extracellular signal-regulated kinase (ERK) inhibitors in oncology clinical trials. *J. Immunother. Precis. Oncol.* 2, 10. doi:10.4103/jipo.jipo_17_18

Czifra, Á., Páll, A., Kulcsár, J., Barta, K., Kertész, A., Paragh, G., et al. (2013). Hemodialysis and hemodiafiltration differently modulate left ventricular diastolic function. *BMC Nephrol.* 14, 74. doi:10.1186/1471-2369-14-76

de Boer, R. A., Meijers, W. C., van der Meer, P., and van Veldhuisen, D. J. (2019). *Cancer* and heart disease: associations and relations. *Eur. J. Heart Fail.* 21, 1515–1525. doi:10.1002/ejhf.1539

Garner, T. P., Amgalan, D., Reyna, D. E., Li, S., Kitsis, R. N., and Gavathiotis, E. (2019). Small-molecule allosteric inhibitors of BAX. *Nat. Chem. Biol.* 15, 322–330. doi:10.1038/s41589-018-0223-0

Goetz, E. M., Ghandi, M., Treacy, D. J., Wagle, N., and Garraway, L. A. (2014). ERK mutations confer resistance to mitogen-activated protein kinase pathway inhibitors. *Canc. Res.* 74, 7079–7089. doi:10.1158/0008-5472.CAN-14-2073

Herrero, A., Pinto, A., Colon-Bolea, P., Casar, B., Jones, M., Agudo-Ibanez, L., et al. (2015). Small molecule inhibition of ERK dimerization prevents tumorigenesis by RAS-ERK pathway oncogenes. *Canc. Cell* 28, 170–182. doi:10.1016/j.ccell.2015.07.001

Herrmann, J. (2020). Adverse cardiac effects of cancer therapies: cardiotoxicity and arrhythmia. *Nat. Rev. Cardiol.* 17 (8), 474–502. doi:10.1038/s41569-020-0348-1

Hetey, S., Boros-Oláh, B., Kuik-rózsa, T., Li, Q., Karányi, Z., Szabó, Z., et al. (2017). Biophysical characterization of histone H3.3 K27 M point mutation. *Biochem. Biophys. Res. Commun.* 490, 868–875. doi:10.1016/j.bbrc.2017.06.133

Jaiswal, B. S., Durinck, S., Stawiski, E. W., Yin, J., Wang, W., Lin, E., et al. (2018). ERK mutations and amplification confer resistance to ERK-inhibitor therapy. *Clin. Canc. Res.* 24, 4044–4055. doi:10.1158/1078-0432.CCR-17-3674

Jha, S., Morris, E. J., Hruza, A., Mansueto, M. S., Schroeder, G. K., Arbanas, J., et al. (2016). Dissecting therapeutic resistance to ERK inhibition. *Mol. Canc. Therapeut.* 15, 548–559. doi:10.1158/1535-7163.MCT-15-0172

Lee, S., Rauch, J., and Kolch, W. (2020). Targeting MAPK signaling in cancer: mechanisms of drug resistance and sensitivity. *Int. J. Mol. Sci.* 21, 1–29. doi:10.3390/ijms21031102

Liang, Q., Wiese, R. J., Bueno, O. F., Dai, Y.-S., Markham, B. E., and Molkentin, J. D. (2001). The transcription factor GATA4 is activated by extracellular signal-regulated kinase 1- and 2-mediated phosphorylation of serine 105 in cardiomyocytes. *Mol. Cell Biol.* 21, 7460–7469. doi:10.1128/mcb.21.21.7460-7469.2001

Meijers, W. C., and De Boer, R. A. (2019). Common risk factors for heart failure and cancer. *Cardiovasc. Res.* 115, 844–853. doi:10.1093/cvr/cvz035

Meijers, Wouter. C., Maglione, M., Bakker, S. J. L., Oberhuber, R., Kieneker, L. M., Jong, S. de., et al. (2018). Heart failure stimulates tumor growth by circulating factors. *Circulation* 138, 678–691. doi:10.1161/CIRCULATIONAHA.117.030816

Merchant, M., Chan, J., Orr, C., Cheng, J., Wang, X., Hunsaker, T., et al. (2014). 387 Combination of the ERK inhibitor GDC-0994 with the MEK inhibitor cobimetinib significantly enhances anti-tumor activity in KRAS and BRAF mutant tumor models. *Eur. J. Canc.* 50, 124. doi:10.1016/s0959-8049(14)70513-1

Nissan, M. H., Rosen, N., and Solit, D. B. (2013). ERK pathway Inhibitors: how low should we go? *Canc. Discov.* 3, 719–721. doi:10.1158/2159-8290.CD-13-0245

Peng, L., Qian, M., Liu, Z., Tang, X., Sun, J., Jiang, Y., et al. (2020). Deacetylase-independent function of SIRT6 couples GATA4 transcription factor and epigenetic activation against cardiomyocyte apoptosis. *Nucl. Acids Res.* 48, 4992–5005. doi:10.1093/nar/gkaa214

Pikkarainen, S., Tokola, H., Kerkelä, R., and Ruskoaho, H. (2004). GATA transcription factors in the developing and adult heart. *Cardiovasc. Res.* 63, 196–207. doi:10.1016/j.cardiores.2004.03.025

Plotnikov, A., Flores, K., Maik-rachline, G., Zehorai, E., Kapri-pardes, E., Berti, D. A., et al. (2015). The nuclear translocation of ERK1/2 as an anticancer target. *Nat. Commun.* 6, 6685. doi:10.1038/ncomms7685

Richards, A. M. (2018). Can heart failure cause cancer? *Nat. Rev. Cardiol.* 16, 7–8. doi:10.1038/s41569-018-0105-x

Ryan, M. B., and Corcoran, R. B. (2018). Therapeutic strategies to target RAS-mutant cancers. *Nat. Rev. Clin. Oncol.* 15, 709–720. doi:10.1038/s41571-018-0105-0

Smorodinsky-Atias, K., Soudah, N., and Engelberg, D. (2020). Mutations that confer drug-resistance, oncogenicity and intrinsic activity on the ERK MAP kinases–current state of the art. *Cells* 9, 129. doi:10.3390/cells9010129

Sullivan, R. J., Infante, J. R., Janku, F., Lee Wong, D. J., Sosman, J. A., Keedy, V., et al. (2018). First-in-class ERK1/2 inhibitor ulixertinib (BVD-523) in patients with MAPK mutant advanced solid tumors: results of a phase I dose-escalation and expansion study. *Canc. Discov.* 8, 184–195. doi:10.1158/2159-8290.CD-17-1119

Szabó, Z., Ujvárosy, D., Ötvös, T., Sebestyén, V., and Nánási, P. P. (2020). Handling of ventricular fibrillation in the emergency setting. *Front. Pharmacol.* 10, 1–18. doi:10.3389/fphar.2019.01640

Thul, P. J., Akesson, L., Wiking, M., Mahdessian, D., Geladaki, A., Ait Blal, H., et al. (2017). A subcellular map of the human proteome. *Science* 80–356, aal3321. doi:10.1126/science.aal3321

Tomasovic, A. (2020). Interference with ERK-dimerization at the nucleocytosolic interface targets pathological ERK1/2 signaling without cardiotoxic side-effects. *Natutre Commun* 11, 1733. doi:10.1038/s41467-020-15505-4

Wallace, K. B., Sardão, V. A., and Oliveira, P. J. (2020). Mitochondrial determinants of doxorubicin- induced cardiomyopathy. *Circ. Res.* 126, 926–941. doi:10.1161/CIRCRESAHA.119.314681

Weekes, C., Lockhart, A., LoRusso, P., Murray, E., Park, E., Tagen, M., et al. (2020). A phase ib study to evaluate the MEK inhibitor cobimetinib in combination with the ERK1/2 inhibitor GDC -0994 in patients with advanced solid tumors. *Oncol.* 25, 833. doi:10.1634/theoncologist.2020-0292

Conflict of Interest: The authors declare that the research was conducted in the absence of any commercial or financial relationships that could be construed as a potential conflict of interest.

frontiers in Pharmacology

REVIEW
published: 18 February 2021
doi: 10.3389/fphar.2021.607364

Building Multi-Dimensional Induced Pluripotent Stem Cells-Based Model Platforms to Assess Cardiotoxicity in Cancer Therapies

Dilip Thomas[1,2], *Sushma Shenoy*[1] *and Nazish Sayed*[1,2,3]*

[1]Stanford Cardiovascular Institute, Stanford, CA, United States, [2]Institute for Stem Cell Biology and Regenerative Medicine, Stanford, CA, United States, [3]Division of Vascular Surgery, Department of Surgery, Stanford University School of Medicine, Stanford, CA, United States

Cardiovascular disease (CVD) complications have contributed significantly toward poor survival of cancer patients worldwide. These complications that result in myocardial and vascular damage lead to long-term multisystemic disorders. In some patient cohorts, the progression from acute to symptomatic CVD state may be accelerated due to exacerbation of underlying comorbidities such as obesity, diabetes and hypertension. In such situations, cardio-oncologists are often left with a clinical predicament in finding the optimal therapeutic balance to minimize cardiovascular risks and maximize the benefits in treating cancer. Hence, prognostically there is an urgent need for cost-effective, rapid, sensitive and patient-specific screening platform to allow risk-adapted decision making to prevent cancer therapy related cardiotoxicity. In recent years, momentous progress has been made toward the successful derivation of human cardiovascular cells from induced pluripotent stem cells (iPSCs). This technology has not only provided deeper mechanistic insights into basic cardiovascular biology but has also seamlessly integrated within the drug screening and discovery programs for early efficacy and safety evaluation. In this review, we discuss how iPSC-derived cardiovascular cells have been utilized for testing oncotherapeutics to pre-determine patient predisposition to cardiovascular toxicity. Lastly, we highlight the convergence of tissue engineering technologies and precision medicine that can enable patient-specific cardiotoxicity prognosis and treatment on a multi-organ level.

Keywords: induced pluripotent stem cells, cardiomyocytes, cancer drugs, multicellular crosstalk, 3D platforms, cardio-oncology, drug testing

OPEN ACCESS

Edited by:
Tamer M. A. Mohamed, University of Louisville, United States

Reviewed by:
Tamer M. Mohamed, The University of Manchester, United Kingdom
Jiesi Luo, Yale University, United States
Sebastian Diecke, Helmholtz Association of German Research Centers (HZ), Germany

***Correspondence:**
Nazish Sayed
sayedns@stanford.edu

Specialty section:
This article was submitted to Cardiovascular and Smooth Muscle Pharmacology, a section of the journal Frontiers in Pharmacology

Received: *17 September 2020*
Accepted: *06 January 2021*
Published: *18 February 2021*

Citation:
Thomas D, Shenoy S and Sayed N (2021) Building Multi-Dimensional Induced Pluripotent Stem Cells-Based Model Platforms to Assess Cardiotoxicity in Cancer Therapies. Front. Pharmacol. 12:607364. doi: 10.3389/fphar.2021.607364

INTRODUCTION

There is a growing burden on the healthcare system with the rise in mortality rate associated with cardiovascular diseases (CVD) and cancer. A 2018 statistics reported ~17 million deaths globally from CVD and ~9 million deaths from cancer (Benjamin et al., 2019; Bray et al., 2018; Siegel et al., 2019). By 2040 these figures are expected to double due to a staggering increase in new cases. As of 2019, ~16 million individuals have been reported as cancer survivors, with nearly two-third of survivors above the age of 60, while 1 in 10 survivors younger than 50 years of age (Miller et al., 2019). It is becoming increasingly evident that cardiotoxicity in cancer patients arise from

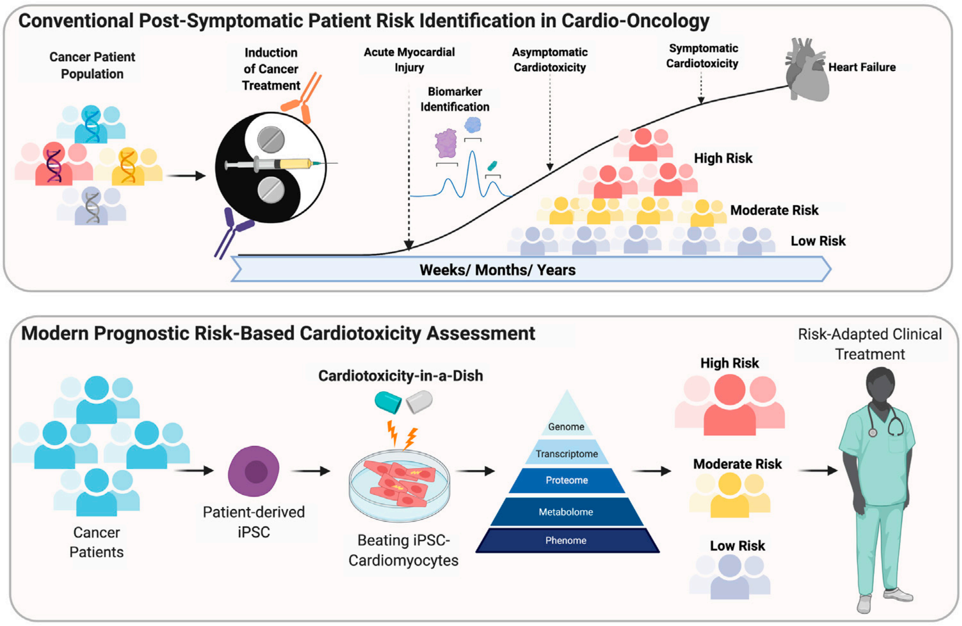

FIGURE 1 | Conventional post-Symptomatic patient risk indentification in Cardio-Oncology. Modern prognostic risk-based cardiotoxicity assessment.

chemotherapeutic drugs that inadvertently target the heart causing adverse effects such as ventricular systolic and diastolic dysfunction, arrhythmias, pericarditis, myocardial ischemia and heart failure (**Figure 1**). Indeed, these severe cardiovascular risks further contributes to the mortality rate seen in cancer patients (Sarfati et al., 2016; Miller et al., 2019). Even though, regulatory agencies such as the Food and Drug Administration (FDA) oversee a rigorous review process for new drugs, when it comes to life-threatening diseases such as cancer, the risk-benefit threshold may be higher. In a retrospective study, of all new drug approvals from 1997 to 2016, it was found that 48% had a higher rate of safety-related label changes (Mostaghim et al., 2017). Furthermore, between 2012 and 2017, approximately 95% of all cancer drugs were expedited through the approval process (Hwang et al., 2018). Due to lack of comprehensive testing and recent expedited approval process for many cancer drugs, there are always concerns regarding efficacy and safety. In order to faithfully predict the cardiotoxic side effects of investigational drugs, development of scalable testing platforms *in vitro* is essential. The discovery of human induced pluripotent stem (iPSC) technology has made it possible to regulate organ-specific switches in stem cells to generate any cell type outside the body in a highly controlled artificial environment (Sayed et al., 2016; Sayed and Wu, 2017). In the context of the heart, iPSC-derived cardiomyocytes (iPSC-CMs) has emerged as an attractive testing platform to not only understand basic biology of inherited and non-inherited cardiomyopathies, but also serve as a pharmacological barometer to understand drug-related toxicities and efficacy of new therapeutics (Sayed and Wu, 2017; Sayed et al., 2019; Rhee et al., 2020). In the context of oncotherapeutics, the primary goal is to retard cancerous growth and limit any bystander effects to other cell types of the body that share homologous intra and extracellular targets. Indirect effects of cancer drugs on the heart comprising of multiple cell types may trigger a complex integrated response leading to cardiotoxicity (Gintant et al., 2019). iPSC technology has not only enabled mass production of cardiovascular cell types but also recapitulate disease phenotypes and pharmacological responses. In the recent years, development of standalone engineered tissue systems and high-throughput screening modalities has gained immense interest due to their potential to serve as surrogate clinical trials *in vitro* for safety and efficacy (Fermini et al., 2018). In this review, we summarize the pre-clinical cardio-toxicology studies of chemotherapeutic agents on iPSC-CMs and current limitations associated with the use of iPSC-CMs. Finally, we cover the emerging *in vitro* models that have evolved over the recent decade, offering novel and more predictive alternative for mechanistic assessment of cardiotoxicity and efficacy of oncotherapeutics.

INDUCED PLURIPOTENT STEM CELLS CARDIOMYOCYTES IN CANCER DRUG CARDIOTOXICITY

Assessment of cardiovascular risks using conventional approaches such as non-clinical animal models have been challenging due to striking differences in both biochemical regulation and functional parameters such as beat rate and calcium handling (Sayed et al., 2016). In contrast, human iPSC-CMs share a higher resemblance to their non-human counterparts and offer higher sensitivity and specificity toward cardioactive or cardiotoxic drugs (Grimm et al., 2018). One of the key advantages of using iPSC-CMs is their ability to capture patient-specific drug responses, which may arise from a variety for underlying genetic or metabolic alterations. On a broader scale, iPSC-CMs have shown to exhibit inter-individual variability that enables us to extend our understanding to a larger group of individuals or population for better categorization into responders and non-responders toward a treatment (Burnett et al., 2019).

The potential of iPSC-CMs as an indispensable pre-clinical tool for drug screening assays have already been demonstrated with the Comprehensive *in vitro* Proarrhythmia Assay (CiPA) initiative. CiPA aims to evaluate the proarrhythmic risk of new drugs through a comprehensive mechanistic assessment and validation on human iPSC-CMs. These drug assessments occur in four distinct stages: 1) Characterization of the drug effects on human cardiac currents; 2) In silico reconstruction of the ventricular electrophysiology; 3) modeling the effects on iPSC or embryonic (ES)- derived ventricular cardiomyocytes; and 4) clinical evaluation of cardiac risk. The primary endpoint assay is detection of electrophysiological abnormalities that could be due to changes in repolarising or depolarising ionic currents (iNA, iTo, iCal, iKr, iKs, iK1). Electrophysiological abnormalities are often underreported in several drug induced toxicities but are key early indicators of potential drug-induced adverse effects (Doherty et al., 2013; Sharma et al., 2017). Therefore, systematic characterization and longitudinal assessments are required to understand acute, subacute and chronic toxicities observed in cancer drug-induced cardiac dysfunction. Indeed, several large scale, multi-centre studies have been conducted to detect ionotropic drug effects with well-defined ionic current parameters (Blinova et al., 2018). One of the major limitations of human iPSC-CMs is the immature phenotype that resemble the fetal stage of cardiac development (van den Berg et al., 2015). For example, iPSC-CMs lack morphological, metabolic and electrophysiological maturity when compared to adult cardiomyocytes. To overcome this, several techniques have been developed to enable higher degree of maturation. A comprehensive review of these methods is described elsewhere (Guo and Pu, 2020; Karbassi et al., 2020). Despite these limitations, iPSC-CMs due to their unlimited production capacity are preferred over human heart biopsy samples which are very limited and difficult to maintain *in vitro*. Traditional cell models for oncotherapeutic efficacy testing were created using cancer cell lines. The opportunity to use patient-derived iPSC-CMs and derivatives is a step toward in using the technology to capture the susceptibility of the cancer patients developing cardiotoxicity.

Current cancer drugs that are mainly studied for adverse cardiotoxic events belong to the class of 1) anthracyclines; 2) tyrosine kinase inhibitors; and 3) checkpoint inhibitors. The co-incidence of cardiotoxicity associated with chemotherapeutic drugs was first identified and reported in 1970s (Lefrak et al., 1973; Von Hoff et al., 1979). Since then studies have identified three common mechanisms by which cancer drugs induce cardiotoxicity. These include double stranded DNA breaks, targeting of DNA modifying enzymes to inhibit replication, and blocking of key prosurvival or metabolic signaling pathways.

Anthracyclines

The most widely used anthracyclines in the clinic are doxorubicin, daunorubicin, epirubicin and idarubicin. These anthracycline class of drugs induce "by-stander" cardiotoxic effects due to non-specificity on targets that are shared between both metabolically active cancerous cells and healthy cardiac cells. Doxorubicin (DOX), in particular have been shown to elicit a dose-dependent effect both in an acute or chronic setting (Doyle et al., 2005) (Sorensen et al., 2003). Indeed, chronic cardiotoxic effects have been reported in adults who were treated with doxorubicin in their childhood (Lipshultz et al., 2005). Multiple studies have been conducted in the past to understand the mechanisms that causes DOX induced cardiotoxicity. For example, mitochondrial oxidative stress caused due to rapid reduction of DOX, disruption of cytochrome enzymes, accumulation of iron and generation of free-radical ions is considered to be one of the modes of toxicity (Davies and Doroshow, 1986; Lebrecht et al., 2003; Ichikawa et al., 2014) (Papadopoulou and Tsiftsoglou, 1993). Similarly, the direct binding of DOX to topoisomerase 2 isoenzymes, which results in double stranded DNA breaks (Lyu et al., 2007; Zhang et al., 2012; Vejpongsa and Yeh, 2014) is considered to be another major factor contributing to cardiotoxicity. Dexrazoxane, an FDA-approved drug has shown to confer cardioprotective effects in DOX treated patients (Swain et al., 1997) by inhibiting the catalytic activity of topoisomerase II β (TOP2B) (Bureš et al., 2017; Jirkovský et al., 2018). Indeed, the iPSC-CM platform has also been employed to study the cardiotoxic effects of DOX. In a recent study, Burridge et al. derived iPSC-CMs from two groups of patients to evaluate the effects of DOX *in vitro* (Burridge et al., 2016). These included patients that developed cardiotoxicity following DOX treatment (DOXTOX) and patients that failed to show cardiotoxic symptoms (DOXCON). iPSC-CMs derived from DOXTOX patients showed poor survival with high oxidative stress and DNA damage when compared to DOXCON iPSC-CMs (Burridge et al., 2016). In another study, iPSC-CMs generated from 45 patients when exposed to varying concentrations of DOX revealed genetic basis for cardiotoxicity, wherein 477 expression variants that modulate signature transcriptomic profile were identified (Knowles et al., 2018). Indeed, genome-wide association studies (GWAS) among patient populations have revealed several significant variants that potentiate direct interaction with the TOP2B promoter region or mediate differential splicing of cardiac troponin gene (Aminkeng et al., 2015; Wang et al., 2016). Such patient stratification and inter-individual variability achieved using iPSC-CMs offer a strong basis for detecting patient-specific responses to cancer therapies based on their genotypic and phenotypic sensitivities.

Tyrosine Kinase Inhibitors

Human iPSC-CMs have been utilized to screen cardiovascular toxicities associated with tyrosine kinase inhibitors (TKIs) to mirror clinical phenotypes. TKI-associated cardiotoxicities in cancer patients include arrhythmias, myocardial infarction and reduced left ventricular ejection fraction (LVEF) (Force et al., 2007). While TKIs act by blocking tyrosine kinase receptors that stunts cell proliferation, survival and migration, their effects at the cellular level include increased reactive oxygen species (ROS) production, lipid and cholesterol accumulation, and activation of caspases (Doherty et al., 2013; Schwach et al., 2020).

One of the first large-scale studies looking at TKI-induced cardiotoxicity tested 21 FDA approved TKIs on iPSC-CMs derived from 11 healthy and two cancer patients on a high-throughput platform (Sharma et al., 2017). Six TKIs (regorafenib, vemurafenib, nilotinib, crizotinib, sorafenib and vandetanib) exposed to iPSC-CMs were found to exhibit varying degrees of cytotoxic and functional deficit. In particular, three TKIs (sorafenib, regorafenib and ponatinib) were found to be highly cytotoxic causing mitochondrial stress, contractility changes and cell death. In accordance with clinical findings (Lee et al., 2019), two of the TKIs, nilotinib and vandetanib were found to induce arrhythmias at a cellular level. Subsequent studies performed on iPSC-CMs revealed that cardiotoxicity associated with sorafenib is likely due to a metabolic shift from oxidative phosphorylation to glycolysis (Wang H. et al., 2019). Tyrosine kinase activity may also be reduced through blockade of human epidermal growth factor receptor 2 (HER2), a proto-oncogene upregulated mainly in breast cancer. Activation of HER-2 pathway is known to play an important role in cardiac development and drug-induced cardioprotection through endothelial-cardiomyocyte signaling (Lee et al., 1995; Lemmens et al., 2007; Galindo et al., 2014). In an iPSC-CM model, inhibition of HER2 signaling pathway with trastuzumab was shown to cause impairment in contractile and calcium handling properties which were reversed through metabolic modulation with AMP-activated protein kinase (AMPK) (Kitani et al., 2019). Similarly, exogenous treatment with neuregulin-1 (NRG-1) and heparin-binding epidermal growth factor (HB-EGF) has shown to confer cardioprotective effects in iPSC-CMs against DOX, however, co-treatment of DOX and trastuzumab were shown to partially negate the effect of NRG1 (Kurokawa et al., 2018).

Immunotherapies

Cancer immunotherapy drugs are targeted biologics aimed to reinvigorate the immune cells' capacity to target and eliminate cancer cells. In chimeric antigen receptor (CAR) T-cell therapy, patient's T cells are isolated and engineered to express receptors, which upon binding to cancer cells lead to cell death. Sporadic clinical cardiotoxicity has been reported mainly arising from co-expression of tumor targets or antigen cross-reactivity with cardiac proteins (Morgan et al., 2010; Cameron et al., 2013). One of the widely accepted adverse cardiac effects of CAR T-cell therapy is believed to be due to a "cytokine storm" caused by the activation of lymphocytes and the release of inflammatory cytokines. Cytokine storm also known as cytokine release syndrome (CRS) can lower cardiac ejection fraction and cause arrythmias (Neelapu et al., 2018). Immune checkpoint inhibitors (ICIs) are another class of T-cell modulators that prevent T-cells from being turned-off or remain in an anergic state. Several adverse cardiac events have been noted in patients treated with ICIs including myocarditis, vasculitis, electrophysiological abnormalities and arrhythmias (Mahmood et al., 2018; Moslehi et al., 2018). Even though mortality associated with such adverse events are disproportionately high, the incidence of such an event is rare. Target ligands of checkpoint inhibitors such as programmed cell death ligand 1 (PD-L1) expression has been reported in cardiomyocytes (Nishimura et al., 2001). Based on this, it can be speculated that possible underlying mechanisms of cardiotoxicity may be due to 1) homology in antigen expressed on tumor cells and cardiomyocytes, which are recognized by T-cells; 2) T-cell response toward unknown cardiac antigen; and 3) diverse T-cell receptor repertoire with distinct antigen binding on both tumor cell and cardiomyocytes followed by initiation of an effector response (Brown et al., 2020). Co-culture studies using iPSC-derived cardiovascular cells and primary T-cells or exposure to patient's serum may reveal more insights into active biomarkers or non-canonical molecular interactions that result in myocardial toxicities in these patients.

ADDRESSING FUNCTIONAL AND CELLULAR HETEROGENEITY IN CARDIOMYOCYTES DERIVED FROM INDUCED PLURIPOTENT STEM CELLS SOURCES

hiPSC-CMs have emerged as one of the important predictive tools is due to its ability to retain genetic identity of the patient for disease modeling and discovery of personalized medicine. However, somatic cell sources for pluripotency induction, differences in cardiomyocyte differentiation protocols and heterogeneity in myocyte composition can lead to inconsistencies in the outcomes of pharmacological studies. Several studies have indicated that differences in genetic background and iPSC-CM derivation methodologies can influence epigenetic landscape and consequently gene expression. For example, iPSCs derived from cardiac progenitor cells are shown to have higher cardiac differentiation potential compared to non-cardiac sources (Sanchez-Freire et al., 2014; Meraviglia et al., 2016). This suggests that although reprogramming erases most epigenetic modifications, some tissue-specific signatures may remain unaltered and thereby influence cardiac differentiation potential (Kim et al., 2011; Rouhani et al., 2014). From a drug testing point-of-view, epigenetic variations may alter cellular responses to drugs, overriding the phenotypic response. Such changes can be overcome by adopting uniform reprogramming methodology to reduce epigenetic alterations (Bar and Benvenisty, 2019). In addition to higher reproducibility, iPSC-CM drug responses can be validated by generation of artificial intelligence (AI) algorithms that can systematically compare endpoint measurements such as action potential (AP) or calcium handling parameters to extrapolate experimental outcome for a given class of drug (Juhola et al., 2018; Kernik et al., 2020). However, the full potential of such tools can only be exploited with data generated using iPSC-CMs of comparable quality. Integration of several such comprehensive data types will help distinguish the complex causal relationships from the noise introduced due to the quality of the cells.

To date several key optimizations in cardiac differentiation have been explored to derive iPSC-CMs using simple, cost-effective and xeno-free methods (Lian et al., 2012; Burridge et al., 2014). Despite these refinements, current differentiation protocols provide satisfactory yield for small-scale use. Furthermore, there is considerable variability in obtaining highly pure population of ventricular, atrial or pacemaker subtypes. To minimize batch-to-batch variability, reproducibility and functional quality of the cardiomyocytes generated, small-scale protocols need to be robustly tested in large scale culture devices and bioreactors. Currently, static two dimensional (2D) multi-layer flasks and dynamic three-dimensional (3D) microcarrier adherent systems are able to generate 1.5–2.8 billion cardiomyocytes in a single bioprocess (Correia et al., 2014; Tohyama et al., 2017). A recent report also demonstrated that iPSC-CMs can be expanded to a hundred-fold through inhibition of glycogen synthase kinase-3β (GSK-3β) pathway during early stages of cardiac differentiation. These cells obtained can be purified using non-genetic methods such as metabolic selection with lactate-containing medium or a dye to label mitochondria that occupy ~40% of the CM volume (Hattori et al., 2010; Tohyama et al., 2013).

With regard to function, in adult cardiomyocytes mature structural features are intertwined with functional regulation. Unlike adult cardiomyocytes, neonatal or iPSC cardiomyocytes do not show rectangular morphology, exhibit spontaneous generation of AP, have lower density of mitochondria and higher dependence on glycolytic metabolism over fatty acid oxidation. Several recently developed techniques help iPSC-CM maturation through metabolic supplementation (Parikh et al., 2017; Feyen et al., 2020), incremental pacing (Chan et al., 2013) and culture substrate modifications to promote higher contraction forces (Pandey et al., 2018). Currently, these culture procedures from somatic reprogramming to obtaining functionally mature iPSC-CMs require over a month's time, which may limit their use for point-of-care testing. Therefore, utilization of a single platform that enables rapid generation of functionally mature iPSC-CMs from the donor cells will accelerate the drug testing timeframe.

BUILDING PHYSIOLOGICALLY RELEVANT *IN VITRO* CARDIAC MODELS

Current drug discoveries and therapeutic testing takes place on conventional 2D tissue culture platforms. However, there are several limitations with using platforms that are non-physiological in a reductionist manner. 2D planar culture platforms offer flexibility and ease of use, however, fail to capture the structural complexities that are seen in 3D tissues and organ systems. These 3D tissues develop through gradients of biochemical and mechanical signaling, and multicellular crosstalk that contribute to the maintenance of tissue homeostasis. In a biological context, 2D platform offers the least resistance at a single-cell level wherein cellular turnover, metabolism, and protein synthesis occur in an accelerated manner. In contrast, in a 3D tissue-like architecture these processes occur in concert with changes in the local extracellular environment, receiving feedback responses from a multitude of cells that are tightly packed in a small volume (Baker and Chen, 2012; Thomas et al., 2018; Thomas et al., 2020). With the recent advancements in bioengineering tools, 3D culture systems with varying degrees of complexities have gained significant traction in the field of drug testing and drug discovery (**Figure 2**). Indeed, 3D cultures of iPSC-CMs in the form of engineered myocardium have been shown to enhance physiological hypertrophy, improve maturity, and enhance drug response (Karbassi et al., 2020).

Three Dimensional Cardiac Constructs for Drug Testing

iPSC-CMs have been used to generate 3D myocardium as self-assembled, scaffold-free, spontaneously beating clusters referred as cardiac spheroids. Alternatively, iPSC-CMs can also be embedded in natural or synthetic extracellular matrix (ECM) in form of engineered heart tissues (EHTs) that allow anisotropic tissue-like orientation and cellular alignment. iPSC-CMs in both scaffold-free cardiac spheroids and matrix assembled tissues have shown to exhibit more mature characteristics when compared to 2D cultures (Hoang et al., 2018). Maturity training in 3D cultures are conferred using biophysical stimulation with passive stretch and electromechanical conditioning (Ronaldson-Bouchard et al., 2018); whereas biochemical stimulation is induced by metabolic and hormonal programming (Parikh et al., 2017). Obtaining a "near" physiological maturation through such techniques can significantly improve drug responses. From a disease modeling perspective, EHTs fabricated from iPSC-CMs manifest a more clinically relevant phenotype in familial arrhythmogenic syndromes compared to iPSC-CMs at a single-cell level (Goldfracht et al., 2019). In two recent studies, EHTs derived from iPSC-CMs demonstrated a high force-frequency relationship and physiological response to ionotropic and chronotropic drugs (Mannhardt et al., 2017; Ronaldson-Bouchard et al., 2018).

As a platform technology for high-throughput screening, iPSC-CMs have been assembled into EHTs on a 24-well (Hansen et al., 2010) and 96-well formats (Mills et al., 2019) that are amenable to rapid screening of drugs to test safety and efficacy. For instance, EHTs derived from rat neonatal cardiomyocytes when treated with gefitinib (10 μM), lapatinib (150 μM), sunitinib (10 μM), imatinib (100 μM) and sorafenib (100 μM) showed significantly reduced tissue contractility; whereas vandetanib and lestaurtinib showed a dose-dependent decline in function (Jacob et al., 2016). In another study, EHTs derived from human iPSC-CMs were fabricated around soft and stiff posts to mimic pre-load and afterload conditions (Truitt et al., 2018). These EHTs when exposed to clinically relevant concentration (1–10 μmol/L) of sunitinib showed a significant increase in caspase-induced cardiotoxicity due to afterload. Here it is important to note that 3D platforms due to their higher tissue organization and slower diffusion kinetics may impart higher drug sensitivity thresholds similar to *in vivo*, unlike 2D culture systems. Furthermore, for the assessment of potential drug-induced toxicity, model systems that are relevant to human

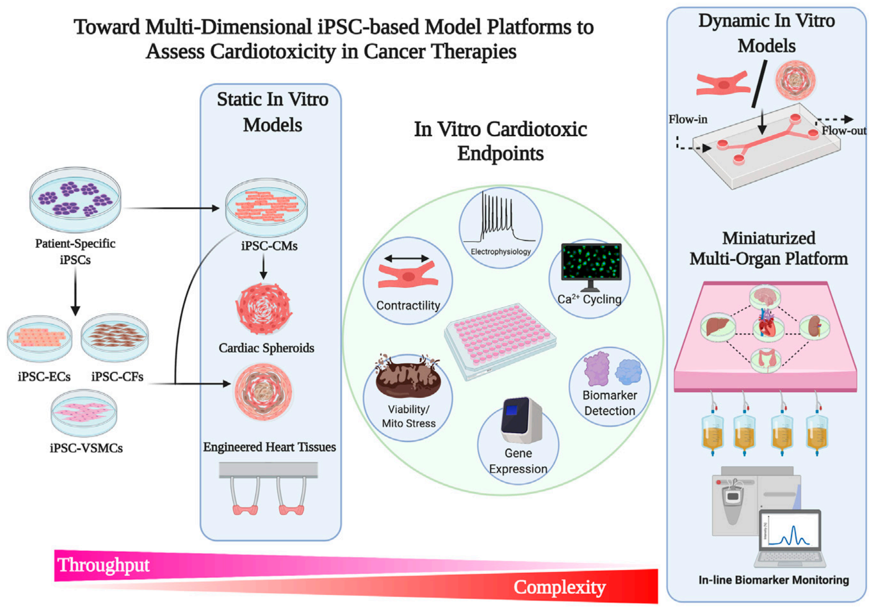

FIGURE 2 | Toward multi-dimensional iPSC-based model platform to access Cardiotoxicity in Cancer therapies.

cardiac physiology and diseases may be more suitable over other species due to inherent differences in function and drug sensitivity. An overview of 2D and 3D stem cell derived cardiomyocyte platforms used for chemotherapeutic testing on cardiovascular cells is summarized in **Table 1**.

At a cellular level, decreased contractile function due to mutational cardiac disorder or drug-induced toxicity is often associated with cytoskeletal disarray and poor structural integrity. These changes influence electromechanical coupling and biomechanical properties both at the cellular as well as tissue level. A combination of atomic force microscopy (AFM) coupled with MEA platform could be used to measure sensitive biological changes in topography and force (Caluori et al., 2019).

In an adult human heart, over 60% of the tissue comprises of non-myocytes, namely endothelial cells, vascular stromal cells, cardiac fibroblasts and a small fraction of immune cells (Pinto et al., 2016). Crosstalk between myocytes and non-myocytes are essential for maintaining a physiological balance and cardiovascular tone. Endothelial cells support cardiac metabolism, contractility and survival (Brutsaert, 2003; Sayed et al., 2020); whereas fibroblast play a key role in metabolic, structural, electrical and mechanical maturation (Giacomelli et al., 2017; Giacomelli et al., 2020). Therefore, it is intuitive that these major non-myocyte cell populations may play a significant role in disease and drug-related toxicities. Formation of multi-cell type scaffold-free cardiac clusters or spheroids offer higher surface area to volume ratio, and therefore have higher rates of diffusion and mass transport. However, unlike EHTs due to lack of structural guidance, cytoskeletal alignment is not observed. One of the benefits of using cardiac spheroids is their smaller size would allow easy integration into "tissue chips" or multi-well formats for high content imaging and toxicity profiling. Cardiac spheroids fabricated in 384-well format composed of iPSC-CMs, primary endothelial cells and fibroblasts have been utilized to demonstrate DOX-induced cytotoxicity at a concentration greater than 5 μM and sunitinib-induced cytotoxicity at a concentration greater than 10 μM (Archer et al., 2018). Similar studies have been performed to demonstrate DOX-mediated cytotoxicity in multicellular cardiac spheroids (Amano et al., 2016; Polonchuk et al., 2017; Beauchamp et al., 2020). These 3D *in vitro* cardiac models although offer very valuable insights in mimicking tissue complexities and multicellular interaction, they do not fully capture the dynamic pharmacokinetics and pharmacodynamics in volved in drug metabolism and absorption. Hence scaled-down models of interconnected multi-organ systems may provide additional insights that are not currently offered by static 3D *in vitro* models.

Microphysiological Devices: A New Age of Cardiotoxicity Testing

For research purposes, several ECM substrates are commercially available. Once a 3D framework is established, it is imperative to consider incorporation of modular interconnected multi-organ tissue assemblies on a single platform. 3D printing technologies and microfabrication of tissue chip devices are aimed toward engineering of scaffolds in spatially defined chambers for cell seeding and tissue assembly. Moreover, incorporation of channels in these devices provide essential nutrients and growth factors that help recreate a dynamic microenvironment that is far superior than static organotypic *in vitro* models. Furthermore, integrated platforms such as these combined with biosensors can enable continuous monitoring over long period of time. A fully

TABLE 1 | A summary of in vitro stem cell-based cardiac models for cancer drug testing.

Format	Drug class	Drug	Concentration	Cell type	Cell number	Cardiomyocyte age	Effect	Ref
2D	Anthracycline	Doxorubicin	1–10 μM	hiPSC-CM (mixture ventricular and atrial)	0.004–0.33$^{\times 10}$ 6/cm^2	3–4.5 weeks	Lower amplitude, beat frequency and decreased FPD	Burridge et al. (2016), Maillet et al. (2016)
2D	Anthracycline/TKI	Doxorubicin/ sunitinib/crizotinib	0.1–100 μM	hiPSC-CMs/iCell®	0.08$^{\times 10}$ 6/cm^2	-	Reduced cell viability, mitochondrial integrity, Increased cAMP formation and lower beat frequency	Grimm et al. (2015)
2D	Anthracycline	Doxorubicin	1–10 μmol/L	hiPSC-CM	0.26$^{\times 10}$ 6/cm^2	3.5–8 weeks	Dose and cell-age dependent apoptosis and ROS production. DNA damage via TOP2A	Cui et al. (2019)
2D	Anthracycline	Doxorubicin	0.05–0.45 μM	Cellartis® Pure hES-CM	0.2$^{\times 10}$ 6/cm^2	-	Increased cardiac Troponin T release at day 2, Increased expression of apoptosis and p53 signalling pathways	Holmgren et al. (2015)
2D	TKI	Vandetanib	0.1–1 μM	hiPSC-CM (mixture ventricular, atrial and nodal)	0.003$^{\times 10}$ 6/cm^2	4.5 weeks	Prolongation of repolarization and arrhythmia	Blinova et al. (2018)
2D	TKI	Sunitinib	0.3–10 μM	hiPSC-CM (mixture ventricular, atrialand nodal)	0.002$^{\times 10}$ 6/cm^2	4.5 weeks	FPD Prolongation and early afterdepolarization (EAD)	Nozaki et al. (2017)
2D	TKI	*niolotinib, Vandetanib (*21 TKIs tested)	0.1–100 μM	hiPSC-CM, hiPSC-ECs, hiPSC-CFs	0.44$^{\times 10}$ 6/cm^2	4–5 weeks	Prolonged FPD, alterations in CM contractility and calcium handling	Sharma et al. (2017)
2D	TKI	Lapatinib, Sorafenib, Erlotinib and Sunitinib	0.01–10 μM	Cor.4U hiPSCCMs	0.07$^{\times 10}$ 6/cm^2	-	Reduced mitochondrial potential and respiration, decreased troponin expression	Wang H. et al. (2019)
2D	Her2 monoclonalantibody/TKI	Trastuzumab/ Lapatinib	100 μg/ml/2 μM	hiPSC-CMs/iCell®	0.06$^{\times 10}$ 6/cm^2	-	Downregulation of ERBB2 with reduced media glucose levels after trastuzumab treatment. Both trastuzumab and lapatinib downregulated expression of PDK and upregulated PHLDA1	Necela et al. (2017)
2D	Her2 monoclonal antibody/Anthracycline	Trastuzumab - Doxorubicin co-treatment	1 μM	hiPSC-CMs/iCell®	0.06$^{\times 10}$ 6/cm^2	-	Concentration dependent reduction in cell impedance and ATP	Eldridge et al. (2014)
2D	Her2 monoclonal antibody/Anthracycline	Trastuzumab/ Doxorubicin	0.1–1μM/ 0.05–0.1 μM	hiPSC-CMs	0.12$^{\times 10}$ 6/cm^2	~2.5–3 weeks	Dose-dependent reduction in contractility, calcium handing and mitochondrial stress	Kitani et al. (2019)
2D	Her2 monoclonal antibody/Anthracycline	Trastuzumab/ Doxorubicin	1 μM/10 μM	hiPSC-CMs and primary ECs	0.16$^{\times 10}$ 6/cm^2	~4–5 weeks	Increased LDH release in doxorubicin only treatment compared to doxorubicin, trastuzumab and neuregulin-1	Kurokawa et al. (2018)
2D	Anthracycline	Doxorubicin	5 μM	Multi-organ on a chip in monolayer (hiPSC-CMs/iCell®,human HepG2 hepatocellular carcinoma cells , human skeletal muscle, hiPSC cortical neurons	0.1–0.16$^{\times 10}$ 6/cm^2	-	Concurrent dose-dependent toxicity in hepatocytes and cardiomyocytes, no action potential changes in neurons	Oleaga et al. (2016)
3D	Anthracycline	Doxorubicin	3.5–100 μM	hiPSC-derived cardiac bodies on a chip	-	-	Dose-dependent decline in beating frequency	Bergström et al. (2015)
3D	Anthracycline	Doxorubicin	1–40 μM	Cardiac spheroids composed of iPSC-CMs, iPSC-CFs and primary ECs	3,000–6,000/ construct	-	Dose-dependent reduction in cell viability and increase in endothelial nitric oxide	Polonchuk et al. (2017)

(Continued on following page)

TABLE 1 | (*Continued*) A summary of in vitro stem cell-based cardiac models for cancer drug testing.

Format	Drug class	Drug	Concentration	Cell type	Cell number	Cardiomyocyte age	Effect	Ref
3D	Anthracycline	Doxorubicin	0.5–20 μM	Cardiac spheroids composed of iPSC-CMs and fetal CFs	5,000/construct	-	Contractile dysfunction and irregular contractions with pacing	Beaucham p et al., 2020
3D	Anthracycline/TKI	Doxorubicin/ sunitinib	30μM/100 μM	Cardiac spheroids composed of hiPSC-CMs/iCellR , primary human microvascular ECs, and human primary CFs	500/construct	-	Reduced mitochondrial membrane potential and ATP. Elevated cTnI, CK-MB and FABP-3 after treatment. Reduced expression of cTnI, vimentin and α-actinin	Archer et al. (2018)
3D	TKI	Sunitinib	1.10 μM	Engineered Heart Tissue composed of hiPSC-CM and hMSC	-	2.5–4 weeks	Load induced increase in caspase3/7	Truitt et al. (2018)
3D	Anthracycline	Doxorubicin	1–1000 nM	Cardiac spheroids composed of hiPSC-CMs, primary CFs and primary microvascular ECs	100,000–5 × 106/construct	-	Decline in beat rate with increase in concentration and reduction vascular capilaries	Amano et al. (2016)
3D	Anthracycline	Doxorubicin	0.1–10 μM	Cardiac spheroids composed of hiPSC-CMs	5 × 105/construct	-	Concentration-dependent reduction in cell viability	Takeda et al. (2018)
3D	Anthracycline/Alkylating agent	Doxorubicin/ Oxaliplatin	0.1–10 μM/ 0.1–50 μM	Colon carcinoma SW620, hiPSCCM and hiPSCECs on a chip	0.3–1 × 108/ ml gel	4–6.5 weeks	Dose-dependent decline in viability, beat rate, conduction velocity	Weng et al. (2020)
3D	Anthracycline	Doxorubicin	5, 25 μM	Human HepG2 hepatocellular carcinoma cells and hiPSC-CM organoids on a chip	1 × 107/ml gel	-	Reduced viability, decrease in albumin secretion, increase in alpha glutathione s-transferase from hepatocytes, increase in creatine kinase MB in cardiomyocytes and decline in beat rate	Zhang et al. (2017)

integrated multi-organ platform developed by Zhang et al. demonstrated drug-induced organ toxicity using a liver-and-heart-on-a-chip comprising of human iPSC-derived cardiac spheroids and human primary hepatocyte-derived liver organoids (Zhang et al., 2017). The authors were able to model the conversion of capecitabine by the liver organoids to 5-fluorouracil (5-FU), a well-known cardiotoxic chemotherapeutic, which caused pronounced toxicity in cardiac spheroids. On the same platform, by replacing the lung organoids with hepatocellular carcinoma cells (HepG2/C3A), the authors demonstrated cytotoxic effect of DOX on cancer cells at 5 and 10 μM. The consequent toxicity-induced cell death in cardiac spheroids was measured using release of cardiac creatine kinase (CK-MB). A similar approach using human primary cardiomyocytes and HepG2 cells was demonstrated using DOX as a model drug (Kamei et al., 2017). In this study, liver cells were shown to generate doxorubicinol, a DOX metabolite, that is responsible for cytotoxicity rather than DOX itself in primary human cardiomyocytes.

Tissue chips with robust *in situ* monitoring of metabolic and functional parameters can be used to model both acute and chronic toxicity to drugs. Currently, there are several limitations with regard to the variability in cell sources used in these devices, such as the use of biopsies or immortalized cell lines. In order to achieve higher resemblance to patient phenotype, the organ specific cells used on the chips should be derived from patient's iPSCs. Secondly, assembly of cells into more organized hierarchical structures over random cell clusters may provide a deeper understanding of the tissue microenvironment (Thomas et al., 2018). Finally, significant efforts must be directed toward development of universal culture medium, which can be perfused through microchannels to support optimal function and maturation of tissues in these devices. The challenge of developing a universal medium can be overcome by segregated organ specific media reservoirs with an external loop for exchange of media metabolites. In the future, modular organ systems can be further simplified by adopting cartridge-based assemblies for testing synergistic effects of drug toxicity on a multi-organ platform.

INTEGRATIVE PANOMIC TECHNOLOGIES FOR MECHANISTIC INSIGHTS INTO CARDIOVASCULAR TOXICITY

High-throughput quantitative multiplex assays provide a comprehensive understanding of signal transduction networks and molecular signatures that emanate from oncogenes. Similarly, they can detect potential pathways that are activated in other somatic cells that contribute toward organ-specific or systemic toxicity. *In situ* integration of tissue chip devices with online analytical tools for quantitative gene expression or proteomic profiling can be powerful in deciphering intra and inter-cellular communications. Drug metabolism studies in liver slices on a chip, infused with substrates or inhibitors have been coupled with high-performance liquid chromatography with UV detection (HPLC-UV) for metabolite analyses. This on-line rapid detection of drug metabolites and inhibitors can be utilized to identify new biomarkers that can predict cardiotoxicities (van Midwoud et al., 2011). A key advantage of these platforms is their data acquisition and interpretation, which can be integrated within the system to allow feedback-dependent real-time changes in control parameters. In contrast, traditional approaches for transcriptomic profiling limits the understanding of cellular heterogeneity.

Advances in the latest single-cell analyses tools allow profiling of transcriptomic changes at a higher resolution (Tang et al., 2009). The technology since its inception has further evolved with a combination of spatial information, wherein tissue sections attached to a transcriptomic slide with barcoded primers bind and capture mRNAs from the adjacent cells or tissues (Ståhl et al., 2016). For example, using single-cell RNA sequencing (scRNA-seq), a recent study identified a novel gene expression signature (matrix Gla protein) in breast cancer patients treated with trastuzumab that can serve as a prognostic marker for long-term survival. Furthermore, the study revealed expression of 48 genes specifically associated with cardiotoxicity, which can serve as potential biomarkers for trastuzumab-induced cardiotoxicity (Wang J. et al., 2019). scRNA-seq has also been implicated in understanding the effects of novel immune based checkpoint inhibitors. A recent study employed a computational approach to identify interactions based on putative ligand-receptor expression in breast cancer tumor and immune cells. The study showed that radiosensitivity of the tumor played a key role in increased PDL-1 expression, resulting in immune cell inactivation due to their interaction via programmed cell death protein 1 (PD-1) (Jang et al., 2020). Such key findings in a clinical setting can be extremely valuable to devise combined therapeutic strategies followed by subsequent monitoring for cardiac immune-related adverse events (irAEs). On a 3D level, single cell transcriptomics can be applied to help resolve spatial transcriptomics while maintaining structural resolution at a tissue-level. Indeed, in a seminal study by Wang et al., the authors used STARmap approach to identify 23 distinct cell clusters from over 30,000 cells across six layers of mouse visual cortex (Wang et al., 2018). Most recently, a spatiotemporal transcriptomic atlas of a developing human heart was established to reveal developmental dynamics during cardiogenesis (Asp et al., 2019). Furthermore, power trajectory inference analyses can be applied to such large-scale transcriptomic data to understand the progression of each cell as a function of time (Saelens et al., 2019). Lastly, large-scale patient multi-omics data can be integrated into a systems pharmacogenomics approach to identify actionable biomarkers that can reduce cardiovascular risks in cancer patients and survivors (Menche et al., 2015).

CONCLUSION

Cardiovascular diseases and several types of cancers have common risk factors and share intricately related pathogenesis that are linked via common cellular pathways. Therefore, the negative consequences of cancer drugs on the cardiovascular system is inevitable. Although conventional toxicology studies in animal models have translational value, they can be cost ineffective and time intensive. As an alternative, iPSC technology can be harnessed to provide a comprehensive phenotypic and genotypic trait that can be used clinically to make therapeutic decisions. Derivation of cardiovascular cells from cancer patients can be utilized to characterize unique functional and genomic signatures that may influence potential adverse reactions to clinically approved drugs. However, with regard to cell maturity there are several milestones that still needs to be reached for minimizing the batch-to-batch variability and the time taken to generate cell or tissue models for a timely and accurate pharmacological prediction. Creation of multiple tissue types using iPSCs can be tested alongside tumors from the same patient in a microphysiological tissue chip devices to tease the mechanistic effects of onocotherapeutics on the body. Such "patient-on-a-chip" models will aid in stratification of cancer patients based on the sensitivity and efficacy of oncotherapeutics (Low et al., 2020). Currently, there are several challenges associated with using multi-organ tissue systems routinely. These are mainly due to complex fabrication process, inadequate physiological fluid flow, unavailability of universal medium for different organ types. Concerted efforts between academic and industry partners to solve these challenges, and further reduce the cost and increase availability will ensure reliability and readiness for clinical use. Finally, integration of analytical techniques with multi-dimensional platforms to obtain high-resolution genomic and proteomic biomarkers can further validate clinical signs of cancer drug-induced cardiotoxicity (Mandawat et al., 2017). Therefore, a multi-dimensional *in vitro* disease modeling approach that ensures reproducibility whilst capturing both acute and chronic effects will offer a boost in the predictive power and development of effective personalized cancer therapies.

AUTHOR CONTRIBUTIONS

DT made the figures and wrote the manuscript. SS contributed the table and wrote the manuscript. NS conceived, wrote the manuscript, gave financial support, and approved the final manuscript.

ACKNOWLEDGMENTS

We are grateful for the funding support from National Institutes of Health (NIH) K01 HL135455, Stanford TRAM scholar grant and Stanford Lyme Disease Seed Grant (N.S) and Tobacco-Related Disease Research Program of the University of California, Grant Number T29FT0380 (D.T). Figures were created with BioRender.com.

REFERENCES

Amano, Y., Nishiguchi, A., Matsusaki, M., Iseoka, H., Miyagawa, S., Sawa, Y., et al. (2016). Development of vascularized iPSC derived 3D-cardiomyocyte tissues by filtration Layer-by-Layer technique and their application for pharmaceutical assays. *Acta Biomater*. 33, 110–121. doi:10.1016/j.actbio.2016.01.033

Aminkeng, F., Bhavsar, A. P., Visscher, H., Rassekh, S. R., Li, Y., Lee, J. W., et al. (2015). A coding variant in RARG confers susceptibility to anthracycline-induced cardiotoxicity in childhood cancer. *Nat. Genet.* 47, 1079–1084. doi:10.1038/ng.3374

Archer, C. R., Sargeant, R., Basak, J., Pilling, J., Barnes, J. R., and Pointon, A. (2018). Characterization and validation of a human 3D cardiac microtissue for the assessment of changes in cardiac pathology. *Sci. Rep.* 8, 10160. doi:10.1038/s41598-018-28393-y

Asp, M., Giacomello, S., Larsson, L., Wu, C., Fürth, D., Qian, X., et al. (2019). A spatiotemporal organ-wide gene expression and cell atlas of the developing human heart. *Cell* 179, 1647–1660.e19. doi:10.1016/j.cell.2019.11.025

Baker, B. M., and Chen, C. S. (2012). Deconstructing the third dimension: how 3D culture microenvironments alter cellular cues. *J. Cell Sci.* 125, 3015–3024. doi:10.1242/jcs.079509

Bar, S., and Benvenisty, N. (2019). Epigenetic aberrations in human pluripotent stem cells. *EMBO J.* 38, 3. doi:10.15252/embj.2018101033

Beauchamp, P., Jackson, C. B., Ozhathil, L. C., Agarkova, I., Galindo, C. L., Sawyer, D. B., et al. (2020). 3D co-culture of hiPSC-derived cardiomyocytes with cardiac fibroblasts improves tissue-like features of cardiac spheroids. *Front. Mol. Biosci.* 7, 14. doi:10.3389/fmolb.2020.00014

Benjamin, E. J., Muntner, P., Alonso, A., Bittencourt, M. S., Callaway, C. W., Carson, A. P., et al. (2019). Heart disease and stroke statistics-2019 update: a report from the American Heart Association. *Circulation* 139, e56–e528. doi:10.1161/CIR.0000000000000659

Bergström, G., Christoffersson, J., Schwanke, K., Zweigerdt, R., and Mandenius, C. F. (2015). Stem cell derived in vivo-like human cardiac bodies in a microfluidic device for toxicity testing by beating frequency imaging. *Lab Chip* 15, 3242–3249. doi:10.1039/c5lc00449g

Blinova, K., Dang, Q., Millard, D., Smith, G., Pierson, J., Guo, L., et al. (2018). International multisite study of human-induced pluripotent stem cell-derived cardiomyocytes for drug proarrhythmic potential assessment. *Cell Rep.* 24, 3582–3592. doi:10.1016/j.celrep.2018.08.079

Bray, F., Ferlay, J., Soerjomataram, I., Siegel, R. L., Torre, L. A., and Jemal, A. (2018). Global cancer statistics 2018: GLOBOCAN estimates of incidence and mortality worldwide for 36 cancers in 185 countries. *CA Cancer J. Clin.* 68, 394–424. doi:10.3322/caac.21492

Brown, S. A., Ray, J. C., and Herrmann, J. (2020). Precision cardio-oncology: a systems-based perspective on cardiotoxicity of tyrosine kinase inhibitors and immune checkpoint inhibitors. *J. Cardiovasc. Transl. Res.* 13, 402–416. doi:10.1007/s12265-020-09992-5

Brutsaert, D. L. (2003). Cardiac endothelial-myocardial signaling: its role in cardiac growth, contractile performance, and rhythmicity. *Physiol. Rev.* 83, 59–115. doi:10.1152/physrev.00017.2002

Bureš, J., Jirkovská, A., Sestak, V., Jansova, H., Karabanovich, G., Roh, J., et al. (2017). Investigation of novel dexrazoxane analogue JR-311 shows significant cardioprotective effects through topoisomerase IIbeta but not its iron chelating metabolite. *Toxicology* 392, 1–10. doi:10.1016/j.tox.2017.09.012

Burnett, S. D., Blanchette, A. D., Grimm, F. A., House, J. S., Reif, D. M., Wright, F. A., et al. (2019). Population-based toxicity screening in human induced pluripotent stem cell-derived cardiomyocytes. *Toxicol. Appl. Pharmacol.* 381, 114711. doi:10.1016/j.taap.2019.114711

Burridge, P. W., Li, Y. F., Matsa, E., Wu, H., Ong, S. G., Sharma, A., et al. (2016). Human induced pluripotent stem cell-derived cardiomyocytes recapitulate the predilection of breast cancer patients to doxorubicin-induced cardiotoxicity. *Nat. Med.* 22, 547–556. doi:10.1038/nm.4087

Burridge, P. W., Matsa, E., Shukla, P., Lin, Z. C., Churko, J. M., Ebert, A. D., et al. (2014). Chemically defined generation of human cardiomyocytes. *Nat. Methods* 11, 855–860. doi:10.1038/nmeth.2999

Caluori, G., Pribyl, J., Pesl, M., Jelinkova, S., Rotrekl, V., Skladal, P., et al. (2019). Non-invasive electromechanical cell-based biosensors for improved investigation of 3D cardiac models. *Biosens. Bioelectron.* 124-125, 129–135. doi:10.1016/j.bios.2018.10.021

Cameron, B. J., Gerry, A. B., Dukes, J., Harper, J. V., Kannan, V., Bianchi, F. C., et al. (2013). Identification of a Titin-derived HLA-A1-presented peptide as a cross-reactive target for engineered MAGE A3-directed T cells. *Sci. Transl. Med.* 5, 197ra103. doi:10.1126/scitranslmed.3006034

Chan, Y. C., Ting, S., Lee, Y. K., Ng, K. M., Zhang, J., Chen, Z., et al. (2013). Electrical stimulation promotes maturation of cardiomyocytes derived from human embryonic stem cells. *J. Cardiovasc. Transl. Res.* 6, 989–999. doi:10.1007/s12265-013-9510-z

Correia, C., Serra, M., Espinha, N., Sousa, M., Brito, C., Burkert, K., et al. (2014). Combining hypoxia and bioreactor hydrodynamics boosts induced pluripotent stem cell differentiation towards cardiomyocytes. *Stem Cell Rev.* 10, 786–801. doi:10.1007/s12015-014-9533-0

Cui, N., Wu, F., Lu, W. J., Bai, R., Ke, B., Liu, T., et al. (2019). Doxorubicin-induced cardiotoxicity is maturation dependent due to the shift from topoisomerase IIα to IIβ in human stem cell derived cardiomyocytes. *J. Cell Mol. Med.* 23, 4627–4639. doi:10.1111/jcmm.14346

Davies, K. J., and Doroshow, J. H. (1986). Redox cycling of anthracyclines by cardiac mitochondria. I. Anthracycline radical formation by NADH dehydrogenase. *J. Biol. Chem.* 261, 3060–3067.

Doherty, K. R., Wappel, R. L., Talbert, D. R., Trusk, P. B., Moran, D. M., Kramer, J. W., et al. (2013). Multi-parameter *in vitro* toxicity testing of crizotinib, sunitinib, erlotinib, and nilotinib in human cardiomyocytes. *Toxicol. Appl. Pharmacol.* 272, 245–255. doi:10.1016/j.taap.2013.04.027

Doyle, J. J., Neugut, A. I., Jacobson, J. S., Grann, V. R., and Hershman, D. L. (2005). Chemotherapy and cardiotoxicity in older breast cancer patients: a population-based study. *J. Clin. Oncol.* 23, 8597–8605. doi:10.1200/JCO.2005.02.5841

Eldridge, S., Guo, L., Mussio, J., Furniss, M., Hamre, J., and Davis, M. (2014). Examining the protective role of ErbB2 modulation in human-induced pluripotent stem cell-derived cardiomyocytes. *Toxicol. Sci.* 141, 547–559. doi:10.1093/toxsci/kfu150

Fermini, B., Coyne, S. T., and Coyne, K. P. (2018). Clinical trials in a dish: a perspective on the coming revolution in drug development. *SLAS Discov.* 23, 765–776. doi:10.1177/2472555218775028

Feyen, D. A. M., McKeithan, W. L., Bruyneel, A. A. N., Spiering, S., Hörmann, L., Ulmer, B., et al. (2020). Metabolic maturation media improve physiological function of human iPSC-derived cardiomyocytes. *Cell Rep.* 32, 107925. doi:10.1016/j.celrep.2020.107925

Force, T., Krause, D. S., and Van Etten, R. A. (2007). Molecular mechanisms of cardiotoxicity of tyrosine kinase inhibition. *Nat. Rev. Cancer* 7, 332–344. doi:10.1038/nrc2106

Galindo, C. L., Ryzhov, S., and Sawyer, D. B. (2014). Neuregulin as a heart failure therapy and mediator of reverse remodeling. *Curr. Heart Fail. Rep.* 11, 40–49. doi:10.1007/s11897-013-0176-2

Giacomelli, E., Bellin, M., Sala, L., van Meer, B. J., Tertoolen, L. G., Orlova, V. V., et al. (2017). Three-dimensional cardiac microtissues composed of cardiomyocytes and endothelial cells co-differentiated from human pluripotent stem cells. *Development* 144, 1008–1017. doi:10.1242/dev.143438

Giacomelli, E., Meraviglia, V., Campostrini, G., Cochrane, A., Cao, X., van Helden, R. W. J., et al. (2020). Human-iPSC-derived cardiac stromal cells enhance maturation in 3D cardiac microtissues and reveal non-cardiomyocyte contributions to heart disease. *Cell Stem Cell* 26, 862–879.e11. doi:10.1016/j.stem.2020.05.004

Gintant, G., Burridge, P., Gepstein, L., Harding, S., Herron, T., Hong, C., et al. (2019). Use of human induced pluripotent stem cell-derived cardiomyocytes in preclinical cancer drug cardiotoxicity testing: a scientific statement from the American Heart Association. *Circ. Res.* 125, e75–e92. doi:10.1161/RES.0000000000000291

Goldfracht, I., Efraim, Y., Shinnawi, R., Kovalev, E., Huber, I., Gepstein, A., et al. (2019). Engineered heart tissue models from hiPSC-derived cardiomyocytes and cardiac ECM for disease modeling and drug testing applications. *Acta Biomater.* 92, 145–159. doi:10.1016/j.actbio.2019.05.016

Grimm, F. A., Blanchette, A., House, J. S., Ferguson, K., Hsieh, N. H., Dalaijamts, C., et al. (2018). A human population-based organotypic *in vitro* model for cardiotoxicity screening. *ALTEX* 35, 441–452. doi:10.14573/altex.1805301

Grimm, F. A., Iwata, Y., Sirenko, O., Bittner, M., and Rusyn, I. (2015). High-content assay multiplexing for toxicity screening in induced pluripotent stem cell-derived cardiomyocytes and hepatocytes. *Assay Drug Dev. Technol.* 13, 529–546. doi:10.1089/adt.2015.659

Guo, Y., and Pu, W. T. (2020). Cardiomyocyte maturation: new phase in development. *Circ. Res.* 126, 1086–1106. doi:10.1161/CIRCRESAHA.119.315862

Hansen, A., Eder, A., Bönstrup, M., Flato, M., Mewe, M., Schaaf, S., et al. (2010). Development of a drug screening platform based on engineered heart tissue. *Circ. Res.* 107, 35–44. doi:10.1161/CIRCRESAHA.109.211458

Hattori, F., Chen, H., Yamashita, H., Tohyama, S., Satoh, Y. S., Yuasa, S., et al. (2010). Nongenetic method for purifying stem cell-derived cardiomyocytes. *Nat. Methods* 7, 61–66. doi:10.1038/nmeth.1403

Hoang, P., Wang, J., Conklin, B. R., Healy, K. E., and Ma, Z. (2018). Generation of spatial-patterned early-developing cardiac organoids using human pluripotent stem cells. *Nat. Protoc.* 13, 723–737. doi:10.1038/nprot.2018.006

Holmgren, G., Synnergren, J., Bogestål, Y., Améen, C., Åkesson, K., Holmgren, S., et al. (2015). Identification of novel biomarkers for doxorubicin-induced toxicity in human cardiomyocytes derived from pluripotent stem cells. *Toxicology* 328, 102–111. doi:10.1016/j.tox.2014.12.018

Hwang, T. J., Franklin, J. M., Chen, C. T., Lauffenburger, J. C., Gyawali, B., Kesselheim, A. S., et al. (2018). Efficacy, safety, and regulatory approval of Food and Drug Administration-designated breakthrough and nonbreakthrough cancer medicines. *J. Clin. Oncol.* 36, 1805–1812. doi:10.1200/JCO.2017.77.1592

Ichikawa, Y., Ghanefar, M., Bayeva, M., Wu, R., Khechaduri, A., Naga Prasad, S. V., et al. (2014). Cardiotoxicity of doxorubicin is mediated through mitochondrial iron accumulation. *J. Clin. Invest.* 124, 617–630. doi:10.1172/JCI72931

Jacob, F., Yonis, A. Y., Cuello, F., Luther, P., Schulze, T., Eder, A., et al. (2016). Analysis of tyrosine kinase inhibitor-mediated decline in contractile force in rat engineered heart tissue. *PloS One* 11, e0145937. doi:10.1371/journal.pone.0145937

Jang, B. S., Han, W., and Kim, I. A. (2020). Tumor mutation burden, immune checkpoint crosstalk and radiosensitivity in single-cell RNA sequencing data of breast cancer. *Radiother. Oncol.* 142, 202–209. doi:10.1016/j.radonc.2019.11.003

Jirkovský, E., Jirkovská, A., Bureš, J., Chládek, J., Lenčová, O., Stariat, J., et al. (2018). Pharmacokinetics of the cardioprotective drug dexrazoxane and its active metabolite ADR-925 with focus on cardiomyocytes and the heart. *J. Pharmacol. Exp. Ther.* 364, 433–446. doi:10.1124/jpet.117.244848

Juhola, M., Joutsijoki, H., Penttinen, K., and Aalto-Setälä, K. (2018). Detection of genetic cardiac diseases by Ca2+ transient profiles using machine learning methods. *Sci. Rep.* 8, 9355. doi:10.1038/s41598-018-27695-5

Kamei, K.-I., Kato, Y., Hirai, Y., Ito, S., Satoh, J., Oka, A., et al. (2017). Integrated heart/cancer on a chip to reproduce the side effects of anti-cancer drugs *in vitro*. *RSC Adv.* 7, 36777–36786. doi:10.1039/c7ra07716e

Karbassi, E., Fenix, A., Marchiano, S., Muraoka, N., Nakamura, K., Yang, X., et al. (2020). Cardiomyocyte maturation: advances in knowledge and implications for regenerative medicine. *Nat. Rev. Cardiol.* 17, 341–359. doi:10.1038/s41569-019-0331-x

Kernik, D. C., Yang, P. C., Kurokawa, J., Wu, J. C., and Clancy, C. E. (2020). A computational model of induced pluripotent stem-cell derived cardiomyocytes for high throughput risk stratification of KCNQ1 genetic variants. *PLoS Comput. Biol.* 16, e1008109. doi:10.1371/journal.pcbi.1008109

Kim, K., Zhao, R., Doi, A., Ng, K., Unternaehrer, J., Cahan, P., et al. (2011). Donor cell type can influence the epigenome and differentiation potential of human induced pluripotent stem cells. *Nat. Biotechnol.* 29, 1117–1119. doi:10.1038/nbt.2052

Kitani, T., Ong, S. G., Lam, C. K., Rhee, J. W., Zhang, J. Z., Oikonomopoulos, A., et al. (2019). Human-induced pluripotent stem cell model of Trastuzumab-induced cardiac dysfunction in patients with breast cancer. *Circulation* 139, 2451–2465. doi:10.1161/CIRCULATIONAHA.118.037357

Knowles, D. A., Burrows, C. K., Blischak, J. D., Patterson, K. M., Serie, D. J., Norton, N., et al. (2018). Determining the genetic basis of anthracycline-cardiotoxicity by molecular response QTL mapping in induced cardiomyocytes. *Elife* 7, 1079. doi:10.7554/elife.33480

Kurokawa, Y. K., Shang, M. R., Yin, R. T., and George, S. C. (2018). Modeling trastuzumab-related cardiotoxicity *in vitro* using human stem cell-derived cardiomyocytes. *Toxicol. Lett.* 285, 74–80. doi:10.1016/j.toxlet.2018.01.001

Lebrecht, D., Setzer, B., Ketelsen, U. P., Haberstroh, J., and Walker, U. A. (2003). Time-dependent and tissue-specific accumulation of mtDNA and respiratory chain defects in chronic doxorubicin cardiomyopathy. *Circulation* 108, 2423–2429. doi:10.1161/01.CIR.0000093196.59829.DF

Lee, D. H., Chandrashekhar, S., and Fradley, M. G. (2019). Electrophysiologic complications in cancer patients. *Methodist Debakey Cardiovasc. J.* 15, 282–288. doi:10.14797/mdcj-15-4-282

Lee, K. F., Simon, H., Chen, H., Bates, B., Hung, M. C., and Hauser, C. (1995). Requirement for neuregulin receptor erbB2 in neural and cardiac development. *Nature* 378, 394–398. doi:10.1038/378394a0

Lefrak, E. A., Pitha, J., Rosenheim, S., and Gottlieb, J. A. (1973). A clinicopathologic analysis of adriamycin cardiotoxicity. *Cancer* 32, 302–314. doi:10.1002/1097-0142(197308)32:2<302::aid-cncr2820320205>3.0.co;2-2

Lemmens, K., Doggen, K., and De Keulenaer, G. W. (2007). Role of neuregulin-1/ErbB signaling in cardiovascular physiology and disease: implications for therapy of heart failure. *Circulation* 116, 954–960. doi:10.1161/CIRCULATIONAHA.107.690487

Lian, X., Hsiao, C., Wilson, G., Zhu, K., Hazeltine, L. B., Azarin, S. M., et al. (2012). Robust cardiomyocyte differentiation from human pluripotent stem cells via temporal modulation of canonical Wnt signaling. *Proc. Natl. Acad. Sci. U.S.A.* 109, E1848–E1857. doi:10.1073/pnas.1200250109

Lipshultz, S. E., Lipsitz, S. R., Sallan, S. E., Dalton, V. M., Mone, S. M., Gelber, R. D., et al. (2005). Chronic progressive cardiac dysfunction years after doxorubicin therapy for childhood acute lymphoblastic leukemia. *J. Clin. Oncol.* 23, 2629–2636. doi:10.1200/JCO.2005.12.121

Low, L. A., Mummery, C., Berridge, B. R., Austin, C. P., and Tagle, D. A. (2020). Organs-on-chips: into the next decade. *Nat. Rev. Drug Discov.* 9, 203–217. doi:10.1038/s41573-020-0079-3

Lyu, Y. L., Kerrigan, J. E., Lin, C. P., Azarova, A. M., Tsai, Y. C., Ban, Y., et al. (2007). Topoisomerase IIbeta mediated DNA double-strand breaks: implications in doxorubicin cardiotoxicity and prevention by dexrazoxane. *Cancer Res* 67, 8839–8846. doi:10.1158/0008-5472.CAN-07-1649

Mahmood, S. S., Fradley, M. G., Cohen, J. V., Nohria, A., Reynolds, K. L., Heinzerling, L. M., et al. (2018). Myocarditis in patients treated with immune checkpoint inhibitors. *J. Am. Coll. Cardiol.* 71, 1755–1764. doi:10.1016/j.jacc.2018.02.037

Maillet, A., Tan, K., Chai, X., Sadananda, S. N., Mehta, A., Ooi, J., et al. (2016). Modeling Doxorubicin-induced cardiotoxicity in human pluripotent stem cell derived-cardiomyocytes. *Sci. Rep.* 6, 25333. doi:10.1038/srep25333

Mandawat, A., Williams, A. E., and Francis, S. A. (2017). Cardio-oncology: the role of big data. *Heart Fail. Clin.* 13, 403–408. doi:10.1016/j.hfc.2016.12.010

Mannhardt, I., Eder, A., Dumotier, B., Prondzynski, M., Krämer, E., Traebert, M., et al. (2017). Blinded contractility analysis in hiPSC-cardiomyocytes in engineered heart tissue format: comparison with human atrial trabeculae. *Toxicol. Sci.* 158, 164–175. doi:10.1093/toxsci/kfx081

Menche, J., Sharma, A., Kitsak, M., Ghiassian, S. D., Vidal, M., Loscalzo, J., et al. (2015). Disease networks. Uncovering disease-disease relationships through the incomplete interactome. *Science* 347, 1257601. doi:10.1126/science.1257601

Meraviglia, V., Wen, J., Piacentini, L., Campostrini, G., Wang, C., Florio, M. C., et al. (2016). Higher cardiogenic potential of iPSCs derived from cardiac versus skin stromal cells. *Front Biosci (Landmark Ed)* 21, 719–743. doi:10.2741/4417

Miller, K. D., Nogueira, L., Mariotto, A. B., Rowland, J. H., Yabroff, K. R., Alfano, C. M., et al. (2019). Cancer treatment and survivorship statistics, 2019. *CA Cancer J. Clin.* 69, 363–385. doi:10.3322/caac.21565

Mills, R. J., Parker, B. L., Quaife-Ryan, G. A., Voges, H. K., Needham, E. J., Bornot, A., et al. (2019). Drug screening in human PSC-Cardiac organoids identifies pro-proliferative compounds acting via the mevalonate pathway. *Cell Stem Cell* 24, 895–907.e6. doi:10.1016/j.stem.2019.03.009

Morgan, R. A., Yang, J. C., Kitano, M., Dudley, M. E., Laurencot, C. M., and Rosenberg, S. A. (2010). Case report of a serious adverse event following the administration of T cells transduced with a chimeric antigen receptor recognizing ERBB2. *Mol. Ther.* 18, 843–851. doi:10.1038/mt.2010.24

Moslehi, J. J., Salem, J. E., Sosman, J. A., Lebrun-Vignes, B., and Johnson, D. B. (2018). Increased reporting of fatal immune checkpoint inhibitor-associated myocarditis. *Lancet* 391, 933. doi:10.1016/S0140-6736(18)30533-6

Mostaghim, S. R., Gagne, J. J., and Kesselheim, A. S. (2017). Safety related label changes for new drugs after approval in the US through expedited regulatory pathways: retrospective cohort study. *BMJ* 358, j3837. doi:10.1136/bmj.j3837

Necela, B. M., Axenfeld, B. C., Serie, D. J., Kachergus, J. M., Perez, E. A., Thompson, E. A., et al. (2017). The antineoplastic drug, trastuzumab, dysregulates metabolism in iPSC-derived cardiomyocytes. *Clin. Transl. Med.* 6, 5. doi:10.1186/s40169-016-0133-2

Neelapu, S. S., Tummala, S., Kebriaei, P., Wierda, W., Gutierrez, C., Locke, F. L., et al. (2018). Chimeric antigen receptor T-cell therapy - assessment and management of toxicities. *Nat. Rev. Clin. Oncol.* 15, 47–62. doi:10.1038/nrclinonc.2017.148

Nishimura, H., Okazaki, T., Tanaka, Y., Nakatani, K., Hara, M., Matsumori, A., et al. (2001). Autoimmune dilated cardiomyopathy in PD-1 receptor-deficient mice. *Science* 291, 319–322. doi:10.1126/science.291.5502.319

Nozaki, Y., Honda, Y., Watanabe, H., Saiki, S., Koyabu, K., Itoh, T., et al. (2017). CSAHi study-2: validation of multi-electrode array systems (MEA60/2100) for prediction of drug-induced proarrhythmia using human iPS cell-derived cardiomyocytes: assessment of reference compounds and comparison with non-clinical studies and clinical information. *Regul. Toxicol. Pharmacol.* 88, 238–251. doi:10.1016/j.yrtph.2017.06.006

Oleaga, C., Bernabini, C., Smith, A. S., Srinivasan, B., Jackson, M., McLamb, W., et al. (2016). Multi-Organ toxicity demonstration in a functional human *in vitro* system composed of four organs. *Sci. Rep.* 6, 20030. doi:10.1038/srep20030

Pandey, P., Hawkes, W., Hu, J., Megone, W. V., Gautrot, J., Anilkumar, N., et al. (2018). Cardiomyocytes sense matrix rigidity through a combination of muscle and non-muscle myosin contractions. *Dev. Cell* 44, 326–336.e3. doi:10.1016/j.devcel.2017.12.024

Papadopoulou, L. C., and Tsiftsoglou, A. S. (1993). Mitochondrial cytochrome c oxidase as a target site for daunomycin in K-562 cells and heart tissue. *Cancer Res.* 53, 1072–1078.

Parikh, S. S., Blackwell, D. J., Gomez-Hurtado, N., Frisk, M., Wang, L., Kim, K., et al. (2017). Thyroid and glucocorticoid hormones promote functional T-tubule development in human-induced pluripotent stem cell derived cardiomyocytes. *Circ. Res.* 121, 1323–1330. doi:10.1161/CIRCRESAHA.117.311920

Pinto, A. R., Ilinykh, A., Ivey, M. J., Kuwabara, J. T., D'Antoni, M. L., Debuque, R., et al. (2016). Revisiting cardiac cellular composition. *Circ. Res.* 118, 400–409. doi:10.1161/CIRCRESAHA.115.307778

Polonchuk, L., Chabria, M., Badi, L., Hoflack, J. C., Figtree, G., Davies, M. J., et al. (2017). Cardiac spheroids as promising *in vitro* models to study the human heart microenvironment. *Sci. Rep.* 7, 7005–7012. doi:10.1038/s41598-017-06385-8

Rhee, J. W., Yi, H., Thomas, D., Lam, C. K., Belbachir, N., Tian, L., et al. (2020). Modeling secondary iron overload cardiomyopathy with human induced pluripotent stem cell-derived cardiomyocytes. *Cell Rep.* 32, 107886. doi:10.1016/j.celrep.2020.107886

Ronaldson-Bouchard, K., Ma, S. P., Yeager, K., Chen, T., Song, L., Sirabella, D., et al. (2018). Advanced maturation of human cardiac tissue grown from pluripotent stem cells. *Nature* 556, 239–243. doi:10.1038/s41586-018-0016-3

Rouhani, F., Kumasaka, N., de Brito, M. C., Bradley, A., Vallier, L., and Gaffney, D. (2014). Genetic background drives transcriptional variation in human induced pluripotent stem cells. *PLoS Genet.* 10, e1004432. doi:10.1371/journal.pgen.1004432

Saelens, W., Cannoodt, R., Todorov, H., and Saeys, Y. (2019). A comparison of single-cell trajectory inference methods. *Nat. Biotechnol.* 37, 547–554. doi:10.1038/s41587-019-0071-9

Sanchez-Freire, V., Lee, A. S., Hu, S., Abilez, O. J., Liang, P., Lan, F., et al. (2014). Effect of human donor cell source on differentiation and function of cardiac induced pluripotent stem cells. *J. Am. Coll. Cardiol.* 64, 436–448. doi:10.1016/j.jacc.2014.04.056

Sarfati, D., Koczwara, B., and Jackson, C. (2016). The impact of comorbidity on cancer and its treatment. *CA Cancer J. Clin.* 66, 337–350. doi:10.3322/caac.21342

Sayed, N., Ameen, M., and Wu, J. C. (2019). Personalized medicine in cardio-oncology: the role of induced pluripotent stem cell. *Cardiovasc. Res.* 115, 949–959. doi:10.1093/cvr/cvz024

Sayed, N., Liu, C., Ameen, M., Himmati, F., Zhang, J. Z., Khanamiri, S., et al. (2020). Clinical trial in a dish using iPSCs shows lovastatin improves endothelial dysfunction and cellular cross-talk in LMNA cardiomyopathy. *Sci. Transl. Med.* 12, eaax9276. doi:10.1126/scitranslmed.aax9276

Sayed, N., Liu, C., and Wu, J. C. (2016). Translation of human-induced pluripotent stem cells: from clinical trial in a dish to precision medicine. *J. Am. Coll. Cardiol.* 67, 2161–2176. doi:10.1016/j.jacc.2016.01.083

Sayed, N., and Wu, J. C. (2017). Towards cardio-precision medicine. *Eur. Heart J.* 38, 1014–1016. doi:10.1093/eurheartj/ehx089

Schwach, V., Slaats, R. H., and Passier, R. (2020). Human pluripotent stem cell-derived cardiomyocytes for assessment of anticancer drug-induced cardiotoxicity. *Front Cardiovasc. Med.* 7, 50. doi:10.3389/fcvm.2020.00050

Sharma, A., Burridge, P. W., McKeithan, W. L., Serrano, R., Shukla, P., Sayed, N., et al. (2017). High-throughput screening of tyrosine kinase inhibitor cardiotoxicity with human induced pluripotent stem cells. *Sci. Transl. Med.* 9, eaaf2584. doi:10.1126/scitranslmed.aaf2584

Siegel, R. L., Miller, K. D., and Jemal, A. (2019). Cancer statistics, 2019. *CA A Cancer J. Clin.* 69, 7–34. doi:10.3322/caac.21551

Sorensen, K., Levitt, G. A., Bull, C., Dorup, I., and Sullivan, I. D. (2003). Late anthracycline cardiotoxicity after childhood cancer: a prospective longitudinal study. *Cancer* 97, 1991–1998. doi:10.1002/cncr.11274

Ståhl, P. L., Salmén, F., Vickovic, S., Lundmark, A., Navarro, J. F., Magnusson, J., et al. (2016). Visualization and analysis of gene expression in tissue sections by spatial transcriptomics. *Science* 353, 78–82. doi:10.1126/science.aaf2403

Swain, S. M., Whaley, F. S., Gerber, M. C., Weisberg, S., York, M., Spicer, D., et al. (1997). Cardioprotection with dexrazoxane for doxorubicin-containing therapy in advanced breast cancer. *J. Clin. Oncol.* 15, 1318–1332. doi:10.1200/JCO.1997.15.4.1318

Takeda, M., Miyagawa, S., Fukushima, S., Saito, A., Ito, E., Harada, A., et al. (2018). Development of *in vitro* drug-induced cardiotoxicity assay by using three-dimensional cardiac tissues derived from human induced pluripotent stem cells. *Tissue Eng Part C Methods* 24, 56–67. doi:10.1089/ten.TEC.2017.0247

Tang, F., Barbacioru, C., Wang, Y., Nordman, E., Lee, C., Xu, N., et al. (2009). mRNA-Seq whole-transcriptome analysis of a single cell. *Nat. Methods* 6, 377–382. doi:10.1038/nmeth.1315

Thomas, D., Marsico, G., Mohd Isa, I. L., Thirumaran, A., Chen, X., Lukasz, B., et al. (2020). Temporal changes guided by mesenchymal stem cells on a 3D microgel platform enhance angiogenesis *in vivo* at a low-cell dose. *Proc. Natl. Acad. Sci. U. S. A.* 117, 19033–19044. doi:10.1073/pnas.2008245117

Thomas, D., O'Brien, T., and Pandit, A. (2018). Toward customized extracellular niche engineering: progress in cell-entrapment technologies. *Adv. Mater.* 30, 1703948. doi:10.1002/adma.201703948

Tohyama, S., Fujita, J., Fujita, C., Yamaguchi, M., Kanaami, S., Ohno, R., et al. (2017). Efficient large-scale 2D culture system for human induced pluripotent stem cells and differentiated cardiomyocytes. *Stem Cell Reports* 9, 1406–1414. doi:10.1016/j.stemcr.2017.08.025

Tohyama, S., Hattori, F., Sano, M., Hishiki, T., Nagahata, Y., Matsuura, T., et al. (2013). Distinct metabolic flow enables large-scale purification of mouse and human pluripotent stem cell-derived cardiomyocytes. *Cell Stem Cell* 12, 127–137. doi:10.1016/j.stem.2012.09.013

Truitt, R., Mu, A., Corbin, E. A., Vite, A., Brandimarto, J., Ky, B., et al. (2018). Increased afterload augments sunitinib-induced cardiotoxicity in an engineered cardiac microtissue model. *JACC Basic Transl. Sci.* 3, 265–276. doi:10.1016/j.jacbts.2017.12.007

van den Berg, C. W., Okawa, S., Chuva de Sousa Lopes, S. M., van Iperen, L., Passier, R., Braam, S. R., et al. (2015). Transcriptome of human foetal heart compared with cardiomyocytes from pluripotent stem cells. *Development* 142, 3231–3238. doi:10.1242/dev.123810

van Midwoud, P. M., Janssen, J., Merema, M. T., de Graaf, I. A., Groothuis, G. M., and Verpoorte, E. (2011). On-line HPLC analysis system for metabolism and inhibition studies in precision-cut liver slices. *Anal. Chem.* 83, 84–91. doi:10.1021/ac1018638

Vejpongsa, P., and Yeh, E. T. (2014). Topoisomerase 2β: a promising molecular target for primary prevention of anthracycline-induced cardiotoxicity. *Clin. Pharmacol. Ther.* 95, 45–52. doi:10.1038/clpt.2013.201

Von Hoff, D. D., Layard, M. W., Basa, P., Davis, H. L., Von Hoff, A. L., Rozencweig, M., et al. (1979). Risk factors for doxorubicin-induced congestive heart failure. *Ann. Intern. Med.* 91, 710–717.

Wang, H., Sheehan, R. P., Palmer, A. C., Everley, R. A., Boswell, S. A., Ron-Harel, N., et al. (2019). Adaptation of human iPSC-derived cardiomyocytes to tyrosine kinase inhibitors reduces acute cardiotoxicity via metabolic reprogramming. *Cell Syst* 8, 412–426.e7. doi:10.1016/j.cels.2019.03.009

Wang, J., Xu, R., Yuan, H., Zhang, Y., and Cheng, S. (2019). Single-cell RNA sequencing reveals novel gene expression signatures of trastuzumab treatment in HER2+ breast cancer: a pilot study. *Medicine (Baltimore)* 98, e15872. doi:10.1097/MD.0000000000015872

Wang, X., Allen, W. E., Wright, M. A., Sylwestrak, E. L., Samusik, N., Vesuna, S., et al. (2018). Three-dimensional intact-tissue sequencing of single-cell transcriptional states. *Science* 361, eaat5691. doi:10.1126/science.aat5691

Wang, X., Sun, C. L., Quiñones-Lombraña, A., Singh, P., Landier, W., Hageman, L., et al. (2016). CELF4 Variant and anthracycline-related cardiomyopathy: a children's oncology group genome-wide association study. *J. Clin. Oncol.* 34, 863–870. doi:10.1200/JCO.2015.63.4550

Weng, K. C., Kurokawa, Y. K., Hajek, B. S., Paladin, J. A., Shirure, V. S., and George, S. C. (2020). Human induced pluripotent stem-cardiac-endothelial-tumor-on-a-chip to assess anticancer efficacy and cardiotoxicity. *Tissue Eng. Part C Methods* 26, 44–55. doi:10.1089/ten.TEC.2019.0248

Zhang, S., Liu, X., Bawa-Khalfe, T., Lu, L. S., Lyu, Y. L., Liu, L. F., et al. (2012). Identification of the molecular basis of doxorubicin-induced cardiotoxicity. *Nat. Med.* 18, 1639–1642. doi:10.1038/nm.2919

Zhang, Y. S., Aleman, J., Shin, S. R., Kilic, T., Kim, D., Mousavi Shaegh, S. A., et al. (2017). Multisensor-integrated organs-on-chips platform for automated and continual *in situ* monitoring of organoid behaviors. *Proc. Natl. Acad. Sci. U.S.A.* 114, E2293–E2302. doi:10.1073/pnas.1612906114

Conflict of Interest: The authors declare that the research was conducted in the absence of any commercial or financial relationships that could be construed as a potential conflict of interest.

frontiers in Pharmacology

MINI REVIEW
published: 10 March 2021
doi: 10.3389/fphar.2021.613837

Human Induced Pluripotent Stem Cells as a Screening Platform for Drug-Induced Vascular Toxicity

Chengyi Tu[1], Nathan J. Cunningham[1], Mao Zhang[1] and Joseph C. Wu[1,2,3]*

[1]Stanford Cardiovascular Institute, Stanford University, Stanford, CA, United States, [2]Department of Medicine, Stanford University, Stanford, CA, United States, [3]Department of Radiology, Stanford University, Stanford, CA, United States

Evaluation of potential vascular injury is an essential part of the safety study during pharmaceutical development. Vascular liability issues are important causes of drug termination during preclinical investigations. Currently, preclinical assessment of vascular toxicity primarily relies on the use of animal models. However, accumulating evidence indicates a significant discrepancy between animal toxicity and human toxicity, casting doubt on the clinical relevance of animal models for such safety studies. While the causes of this discrepancy are expected to be multifactorial, species differences are likely a key factor. Consequently, a human-based model is a desirable solution to this problem, which has been made possible by the advent of human induced pluripotent stem cells (iPSCs). In particular, recent advances in the field now allow the efficient generation of a variety of vascular cells (e.g., endothelial cells, smooth muscle cells, and pericytes) from iPSCs. Using these cells, different vascular models have been established, ranging from simple 2D cultures to highly sophisticated vascular organoids and microfluidic devices. Toxicity testing using these models can recapitulate key aspects of vascular pathology on molecular (e.g., secretion of proinflammatory cytokines), cellular (e.g., cell apoptosis), and in some cases, tissue (e.g., endothelium barrier dysfunction) levels. These encouraging data provide the rationale for continuing efforts in the exploration, optimization, and validation of the iPSC technology in vascular toxicology.

Keywords: vascular toxicity, IPSC disease modeling, drug testing, endothelial cells, smooth muscle cells, vascular organoids, vasculature-on-a-chip

OPEN ACCESS

Edited by:
Tamer M. A. Mohamed,
University of Louisville, United States

Reviewed by:
Wolfgang F. Graier,
Medical University of Graz, Austria
Pasquale Maffia,
University of Glasgow,
United Kingdom

****Correspondence:***
Joseph C. Wu
joewu@stanford.edu

Specialty section:
This article was submitted to Cardiovascular and Smooth Muscle Pharmacology, a section of the journal Frontiers in Pharmacology

Received: *03 October 2020*
Accepted: *22 January 2021*
Published: *10 March 2021*

Citation:
Tu C, Cunningham NJ, Zhang M and Wu JC (2021) Human Induced Pluripotent Stem Cells as a Screening Platform for Drug-Induced Vascular Toxicity. Front. Pharmacol. 12:613837. doi: 10.3389/fphar.2021.613837

INTRODUCTION

Drug-induced vascular toxicity is a multifaceted problem besetting the pharmaceutical industry, the healthcare professionals, and most importantly the patients (Qureshi et al., 2011; Herrmann, 2020). Vascular toxicity that goes unidentified during preclinical and clinical drug studies can present a serious safety hazard to the patients, often leading to drug withdrawal from the market. In fact, multiple major drug withdrawals in the past two decades are attributed to increased vascular events such as strokes and heart attacks (Qureshi et al., 2011). In addition, numerous FDA-approved life-saving chemotherapies, while effective at combating tumor growth, can also result in a wide spectrum of vascular dysfunctions, including acute vasospasm, acute thrombosis, and acceleration of atherosclerosis (Herrmann, 2020). Prevention or mitigation of these debilitating effects in patients remains a challenge for scientists and clinicians.

There is a strong need for a model that can predict drug-induced vascular toxicity, provide insights into the underlying mechanisms, and test potential therapeutics. Currently, animal models such as mice and dogs are the standard preclinical models for toxicological evaluations. Despite their indispensable role in pharmaceutical development, there is a growing recognition that existing animal models alone are inadequate for the accurate prediction of drug toxicity in humans due to differences in physiology, metabolism, and molecular functions between species (Bailey et al., 2013; Chen et al., 2013). The advent and maturation of induced pluripotent stem cell (iPSC) technology presents a valuable opportunity to solve this problem by offering a human cell model. Genetically identical to the donors, iPSCs hold the promise to recapitulate individual predisposition to various risks (Kitani et al., 2019; Lam et al., 2019). Furthermore, recent advances in iPSC differentiation strategies now enable the efficient generation of all the major cell lineages of the human cardiovascular system, including cardiomyocytes (CMs) (Lian et al., 2012; Burridge et al., 2014), endothelial cells (ECs) (Lian et al., 2014; Olmer et al., 2018; Williams and Wu, 2019; Wang et al., 2020), smooth muscle cells (SMCs) (Cheung et al., 2012; Patsch et al., 2015), and cardiac fibroblasts (CFs) (Zhang et al., 2019a). These cells functionally and structurally resemble their counterpart primary cells. Among them, human iPSC-derived cardiomyocytes (iPSC-CMs) have already shown tremendous promise in predicting chemical-induced cardiac liabilities, as exemplified by the Comprehensive *in vitro* Proarrhythmia Assay (CiPA) initiative led by the FDA (Colatsky et al., 2016; Fermini et al., 2016; Millard et al., 2018). Though similar large-scale studies have yet to be performed to validate the utility of iPSCs in vascular toxicology, emerging studies have shown encouraging results to justify further exploration of this technology as a candidate tool in preclinical and clinical investigations of drug-induced vascular toxicity. In this review, we will discuss the background of drug-induced vascular toxicity, and how iPSC technology may help us transform this field, with an emphasis on comparing the utility and drawbacks of different iPSC-based vascular models.

DRUG-INDUCED VASCULAR TOXICITY

Drug Withdrawals due to Vascular Toxicity

Unanticipated vascular toxicity is a significant cause for approved drugs to be withdrawn from the market (Qureshi et al., 2011). Using WITHDRAWN (Siramshetty et al., 2016), a publicly available database for discontinued and withdrawn drugs, we identified eight recent drug withdrawals caused by adverse vascular events. These drugs are diverse in applications, including nonsteroidal anti-inflammatory drugs (valdecoxib and rofecoxib), appetite suppressants (sibutramine, dexfenfluramine, and phenylpropanolamine), anti-diabetic drugs (benfluorex), constipation treatment (tegaserod) as well as treatment for Parkinson's diseases (pergolide). The frequently observed risks of these drugs are strokes, myocardial infarctions (MIs), and valvular heart diseases. Among these drugs, the most recently withdrawn is sibutramine, which was found to increase the risk of non-fatal MIs by 28% and non-fatal strokes by 36% in a 2010 randomized study (James et al., 2010), and it was withdrawn from the United States market in the same year. Notably, the median time on the market of these medications, from their initial approvals to the withdrawals, is 16 years, with the longest for phenylpropanolamine (42 years) and the shortest for valdecoxib (3 years). Undoubtedly, the observed delay of these necessary withdrawals puts patients at risk and creates an extra burden to the healthcare system. Furthermore, these withdrawals highlight the inadequacy of the current system to accurately detect and predict drug-induced vascular dysfunctions.

Vascular Toxicity by Chemotherapies

Chemotherapy drugs are widely known for having cardiotoxic effects (Orphanos et al., 2009; McGowan et al., 2017). However, they also cause a wide spectrum of vascular dysfunctions such as hypertension, ischemic events, and thromboembolism (Cameron et al., 2016; Nebigil and Désaubry, 2018; Herrmann, 2020). In fact, the majority of chemotherapies, both conventional ones (e.g., alkylating agents, antimetabolites, and anthracyclines) and targeted ones (e.g., tyrosine kinase inhibitors, proteasome inhibitors, and monoclonal antibodies) have varying degrees of vascular toxicity (Herrmann et al., 2016; Luu et al., 2018; Sayed et al., 2019; Herrmann, 2020; Rhee et al., 2020). However, unlike those drugs withdrawn from the market, the life-saving nature of chemotherapeutic agents generally tips the scale in the benefit-risk assessment, allowing them to be continuously used to treat cancer patients despite the observed risk to the vasculature. Detection and management of chemotherapy—induced vascular injuries is an important yet highly challenging task, with several major difficulties. First, there is a lack of specific circulating biomarkers for early vascular injuries in humans (Louden et al., 2006; Mikaelian et al., 2014). Second, vascular susceptibility to drugs is patient-specific, depending on numerous pre-existing conditions of an individual (Oren and Herrmann, 2018). Lastly, the mode of injury varies significantly from drug to drug (Herrmann, 2020). Collectively, these challenges call for a new vascular model that allows us to perform patient-specific testing and discover specific biomarkers for vascular injuries.

HUMAN IPSC-BASED VASCULAR MODEL

The ideal platform to study drug toxicity should meet several key criteria. Primarily, the platform needs to faithfully recapitulate the pathological responses of the target organ on molecular, cellular, and tissue levels. From a translational standpoint, the source materials required for testing must be easily accessible and consistent in quality. Lastly, moving into the area of precision medicine, the testing platform should provide patient-specific risk prediction and facilitate the development of personalized prevention and treatment (Sayed et al., 2016; Wu et al., 2019). Conventional animal models and primary cell lines can at best partially fulfill the first two requirements, but are unlikely to meet the growing demand for personalized medicine.

The advent of iPSC technology offers us a valuable opportunity to transform the field of toxicology. Human iPSC-derived cells are genetically identical to the donor cells and hence are expected to respond to drugs in a patient-specific manner (Burridge et al., 2016; Kitani et al., 2019). In addition, the rapid progress in iPSC technology has enabled us to efficiently generate functional ECs (Cao et al., 2013; Olmer et al., 2018; Rosa et al., 2019) and SMCs (Biel et al., 2015; Patsch et al., 2015; Granata et al., 2017), two major cell types comprising the blood vessel. Furthermore, advances in tissue engineering (Chang and Niklason, 2017; Liu et al., 2018b; Ben-Shaul et al., 2019; Crosby et al., 2019) and organ-on-chip technologies (Mori et al., 2017; Zhang et al., 2018; Wnorowski et al., 2019) have enabled us to simulate the *in vivo* vascular structure and their biophysical environment at an unprecedented pace, making it possible to model more sophisticated pathological processes on multiple scales (**Figure 1**).

The Building Blocks: iPSC-Derived ECs and SMCs

EC dysfunction plays a significant role in vascular diseases such as atherosclerosis (Davignon and Ganz, 2004), thrombosis (Yau et al., 2015), and hypertension (Brandes, 2014). The generation of iPSC-derived endothelial cells (iPSC-ECs) that resemble *in vivo* ECs is a critical step toward building an *in vitro* vascular model. In the past decade, numerous methods have been developed to produce functional ECs from iPSCs, which are well summarized in a recent review (Williams and Wu, 2019). The general principle is similar among different EC differentiation methods. Human iPSCs are usually first induced into the mesoderm by a cocktail of Activin A, BMP-4, and/or GSK3 inhibitors, and subsequently specified into ECs with VEGF, FGF2, and bFGF treatment (Lian et al., 2014; Palpant et al., 2017; Liu et al., 2018a). To further enrich ECs, the differentiated cells can be sorted for the CD31 positive population (Liu et al., 2018a). In a recent study from our lab, we demonstrated that iPSC-ECs exhibit a wide range of properties characteristic of primary ECs (Sayed et al., 2020). Specifically, iPSC-ECs showed morphological similarity to primary ECs with a cobblestone cell shape. Functionally, these cells increased nitric oxide (NO) production in response to shear stress or vasodilators such as acetylcholine and A23187. Metabolically, they can incorporate acetylated low—density lipoprotein (ac-LDL), another hallmark of primary ECs.

In addition to ECs, vascular SMCs are also essential for maintaining the homeostasis of a healthy vasculature. SMCs not only provide mechanical support for a vasculature, but also regulate blood vessel tone, inflammation, and vascular remodeling (Majesky et al., 2011; Lim and Park, 2014). SMC disorder is a major contributing factor to the development of common vascular diseases such as atherosclerosis (Bennett et al., 2016) and hypertension (Touyz et al., 2018). Early methods to generate SMCs from iPSCs relied on unguided differentiation to produce a highly heterogeneous population, followed by flow cytometry sorting for Flk1^{+}/VE-cadherin^{-} cells. These cells exhibited typical SMC morphology and expressed specific markers such as alpha-smooth muscle actin (αSMA) and calponin (CNN1) (Taura et al., 2009). Since then, SMC differentiation has evolved to be more efficient and targeted (Stephenson et al., 2020). For instance, Cheung et al. developed a set of protocols to produce lineage—specific vascular SMCs (Cheung et al., 2012; Cheung et al., 2014). These iPSC-SMCs not only express markers such as CNN1

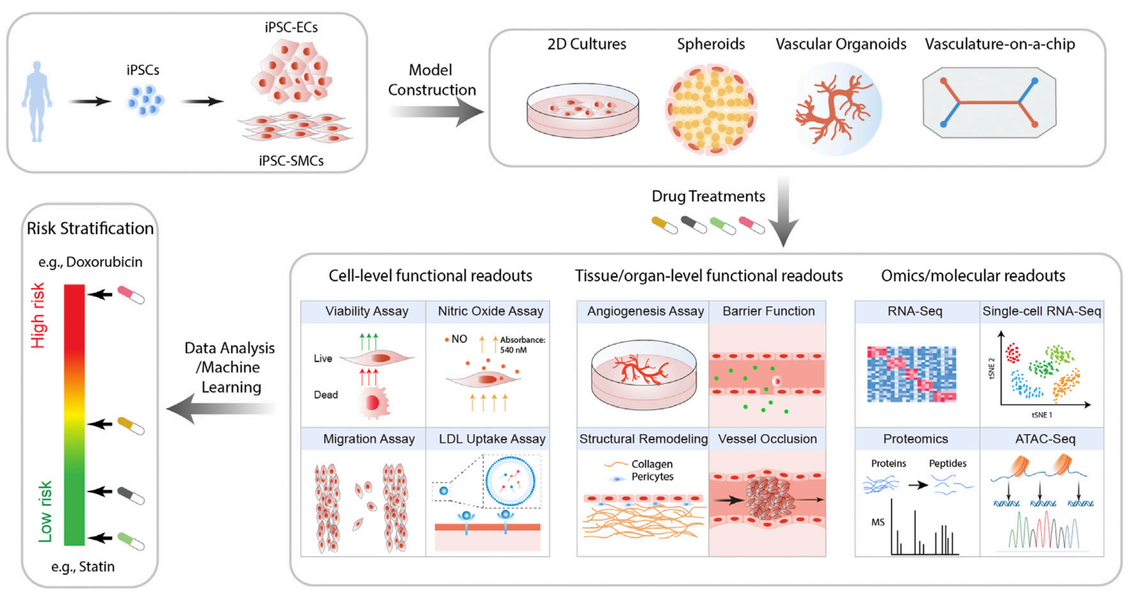

FIGURE 1 | Proposed workflow for iPSC-based models for the prediction of drug-induced vascular injuries. Vascular cells such as ECs and SMCs are generated from patient iPSCs. These cells are then employed to construct *in vitro* models of varying complexity and physiological relevance, including 2D cultures, spheroids, organoids, and vasculature-on-chips. Upon treatment with drugs of interest, a wide range of functional and molecular readouts can be obtained, with which the risk of the drug for inducing vascular disorders is then calculated.

and myosin heavy chain 11 (MYH11), but also differentially respond to cytokine stimulation depending on their lineages (Cheung et al., 2012). In addition to lineage specificity, Wanjare et al. reported that modulation of serum level and PDGF-BB could generate phenotype-specific (synthetic or contractile) SMCs from iPSCs (Wanjare et al., 2013). In this section, we will discuss the use of iPSC-ECs and iPSC-SMCs to model vascular injuries (**Table 1**).

2D Culture Model

To test the toxicity of a compound, the conventional approach is to apply it directly to a monolayer culture of target cells. Although they lack the sophisticated tissue architecture or biophysical stimulation (e.g., shear stress) present *in vivo*, numerous studies have demonstrated that iPSC-ECs or iPSC-SMCs cultured in monolayers respond to chemical or genetic stress in ways that are largely consistent with clinical observations or data from primary cells (Zhang et al., 2011; Cheung et al., 2012; Biel et al., 2015; Belair et al., 2016; Tang et al., 2017; Rieker et al., 2019; Chu et al., 2020). For instance, our lab recently found that e-cigarette liquid (e-liquid) triggered a broad array of molecular and functional disorders in iPSC-ECs, including activation of cell apoptosis, increased reactive oxygen species (ROS) production and LDL uptake, as well as reduced cell migration (Lee et al., 2019). Conditioned medium from e-liquid-treated iPSC-ECs induced macrophage polarization, suggesting a pro-inflammation effect of e-cigarettes on the cardiovascular system. Importantly, these data were corroborated by an analysis of the serum from e-cigarettes users, which revealed a similar upregulation of inflammatory cytokines (Lee et al., 2019).

A key advantage of a 2D model is the compatibility with high-throughput assays. Furthermore, the unlimited proliferative potential of iPSCs allows us to generate large quantities of cells required for large-scale screening experiments, which can be challenging when using primary cells. In fact, several studies have employed high-throughput platforms to investigate drug-induced vascular toxicity or to identify therapeutic agents using iPSC-ECs (Iwata et al., 2017; Sharma et al., 2017) or iPSC-SMCs (Zhang et al., 2019b). For instance, Iwata et al. used high-content imaging in a 384-well plate format to test a variety of compounds with or without vascular toxicity on iPSC-ECs (Iwata et al., 2017). Based on readouts including ATP content, nuclear content, cell viability, and tube formation, this platform successfully identified the toxic compounds with high reproducibility (Iwata et al., 2017). Moreover, the high-throughput format is also suitable for screening therapeutic compounds that could induce a desirable phenotype. Zhang et al. engineered a MYH11 reporter cell line in human embryonic stem cells (Zhang et al.,

TABLE 1 | Recent human iPSC-based models of vascular injuries.

Year	Model	Toxicants/Stress	Main outcome	Ref
2015	2D iPSC-SMC	TNFα	Increased CX3CL1 and MMP9 expression	Biel et al. (2015)
2016	2D sprouting assay of iPSC-EC	A panel of 38 putative vascular disrupting drugs from ToxCast library	Reduced iPSC-EC sprouting and/or reduced cell viability	Belair et al. (2016)
2017	2D lineage-specific iPSC-SMC	Genetic stress: *FBN1* mutation	Reduced vascular SMC proliferation and reduced contractile stress. Increased TGF-β signaling and matrix remodeling. Identification of P38, AGTR1 and KLF4 as therapeutic targets	Granata et al. (2017)
2017	2D high-throughput iPSC-EC and HUVEC model	Suramin, nocodazole, colchicine, histamine, concanamycin A, SU5402	Reduction in nuclear content, viability, ATP content as well as angiogenesis capacity *in vitro*	Iwata et al. (2017)
2017	3D microfluidic iPSC-SMC	Genetic stress: progerin	Increased media wall thickness, increased calcification, and increased cell apoptosis	Atchison et al. (2017)
2017	3D microfluidic iPSC-EC	Thrombin and sunitinib	Disruption of cell-cell junctions in response to thrombin. Reduction in blood vessel area by sunitinib	Kurokawa et al. (2017)
2017	2D high-throughput iPSC-EC model	TKIs	Reduced viability in a dose-responsive manner across multiple cell lines	Sharma et al. (2017)
2019	3D vascular organoids with ECs + pericytes	Hyperglycemia and cytokines	Thickening of vascular basement membrane. Increased expression of collagen type IV and other basement membrane components	Wimmer et al. (2019)
2019	3D microfluidic microvessel of blood-brain barrier	TNFα	Increased expression of ICAM-1 and VCAM-1 and leukocytes adhesion	Linville et al. (2019)
2019	2D iPSC-EC	Genetic stress: ApoE (apolipoprotein) allele epsilon 4 expression	Activation of the proinflammatory state and prothrombotic state. Increased VWF expression and increased platelets adhesion	Rieker et al. (2019)
2019	2D iPSC-EC	E-cigarettes liquid	Increased cell apoptosis, ROS level and LDL uptake. Reduced migration. Conditioned medium increased macrophage activation	Lee et al. (2019)
2019	3D microfluidic blood brain barrier	TNFα, IL-1β, and IL-8	Compromised tight junctions in the barrier and increased leaking	Vatine et al. (2019)
2020	2D iPSC-EC	Cigarette smoke	Secretion of cytokines involved in coagulation, inflammation, and fibrosis	Chu et al. (2020)
2020	2D microfluidic iPSC-SMC	Genetic stress: progerin	Upregulation of MMP13 and increased detachment of SMCs	Pitrez et al. (2020)

Abbreviations: AGTR1, angiotensin II receptor type 1; CX3CL, C-X3-C motif chemokine ligand 1; ICAM-1, intercellular adhesion molecule 1; IL-1 β, interleukin 1beta. IL-8, interleukin 8; KLF4, Kruppel like factor 4; LDL, low-density lipoproteins; MMP13, matrix metallopeptidase 13; MMP9, matrix metallopeptidase 9; P38, p38 mitogen activated protein kinase; ROS, reactive oxygen species; TGF-β, transforming growth factor beta; TKIs, tyrosine kinase inhibitors; TNFα, tumor necrosis factor alpha; VCAM-1, vascular cell adhesion protein 1; vWF, von Willebrand factor.

2019b). MYH11 expression was chosen as a surrogate for the desired contractile phenotype in SMCs. By doing so, they successfully identified RepSox, a small molecule inhibitor of TGF-β type 1 receptor, as a potent drug that could mitigate intimal hyperplasia, a condition characterized by the pathological switch of SMCs from the contractile to the synthetic phenotype.

Vascular Spheroids and Organoids

Application of 3D culture is a common strategy to improve the physiological relevance of an *in vitro* model (Duval et al., 2017). Generally speaking, cells grown as 3D constructs experience more cell-cell interactions and cell-extracellular matrix (ECM) interactions than in 2D (Duval et al., 2017). In addition, a compact 3D environment creates diffusion gradients for biochemical signals, increasing the retention of secreted factors and allowing for a localized build-up of metabolic waste, all of which are typical features of the *in vivo* environment. Thanks to these advantages, 3D vascular models have been broadly exploited to investigate tumor angiogenesis and to test anti-angiogenic compounds (Taubenberger et al., 2016; Amann et al., 2017; Chiew et al., 2017; Klimkiewicz et al., 2017).

A simple method to generate vascular spheroids is to aggregate vascular cells, either stem cell-derived or primary, directly into 3D spheres. This can be done using the hanging-drop technique (Markou et al., 2020) or using an ultra—low attachment culture substrate (Moldovan et al., 2017). Interestingly, distinct cell types mixed together to form spheroids tend to spontaneously organize themselves into a structural hierarchy reminiscent of a native vasculature. For instance, Markou et al. generated small vascular spheroids (~100 μm) from iPSC-ECs and iPSC-SMCs (Markou et al., 2020). The iPSC-ECs spontaneously formed the outer lining of these spheroids, allowing them to be in direct contact with the culture medium, whereas the iPSC-SMCs lined beneath the iPSC-ECs, forming the interior layer (Markou et al., 2020). Despite being a relatively crude model, these spheroids emulate some aspects of vascular anatomy that are not present in a 2D culture.

To create more sophisticated vascular organoids, biomaterials such as collagen, fibrin, and hyaluronic acid can be employed to initiate angiogenesis inside the organoids (Crosby et al., 2019; Crosby and Zoldan, 2019). Compared with cell—only spheroids, the introduction of biomaterials improves the control over the microenvironment, making it possible to develop high-fidelity vasculatures. This is well illustrated recently by Wimmer et al., who combined the use of fine-tuned iPSC vascular differentiation and a 3D matrix (collagen and Matrigel) to produce highly elaborate capillary vasculatures composed of ECs, pericytes, and basement membrane (Wimmer et al., 2019). These engineered microvessels have a hollow lumen and could integrate into the native vasculature upon transplantation *in vivo*, indicating the functionality of these capillaries. Upon exposure to diabetic stress consisting of hyperglycemia, tumor necrosis factor (TNF), and interleukin-6 (IL-6), these capillaries underwent massive thickening in the basement membrane as evidenced by collagen IV staining, a hallmark of diabetes-induced vasculopathy. Notably, identical treatment applied to iPSC-ECs or iPSC-SMCs in 2D cultures did not result in any increase in collagen IV accumulation, suggesting the necessity of the 3D structure to recapitulate this pathological change.

Microfluidic Vascular Chips

Microfluidic organ-on-a-chip technology is a fast-growing field arising from the convergence of engineering, material science, and human biology. Essentially, these microchips are miniaturized physiological systems engineered to emulate key features of native organ architecture and function (Atchison et al., 2017; Kurokawa et al., 2017; Gold et al., 2019). By modulating channel geometry, substrate stiffness, perfusion rate, and biochemical signals, microfluidic chips can model a wide range of vascular diseases on an organ scale. For instance, vascular chips can be engineered with inward protrusions in the middle of the channels to mimic the narrowing of arteries caused by atherosclerosis plaque (Westein et al., 2013). This special geometrical design resulted in platelet aggregation and increased vWF expression, in alignment with the increased thrombus events observed in animals and patients with atherosclerosis. Another example by Qiu et al. showed that the perfusion of microvascular chips *in vitro* using red blood cells (RBCs) harvested from sickle patients could cause vessel occlusions in the chip, similar to the vascular obstructions seen in sickle cell anemia patients (Qiu et al., 2018).

The fusion of iPSC technology and microfluidics is revealing even more exciting possibilities. Specifically, early vascular chips mainly relied on primary ECs like human umbilical vein endothelial cells (HUVECs) to generate a functional endothelium. While these HUVEC-based models are useful as a generic representation of vasculatures, they are not ideal models for organ-specific blood vessels. In fact, it is well-known that ECs in distinct organs differ in both molecular signature and function (Marcu et al., 2018; Paik et al., 2020b). By contrast, human iPSCs can be differentiated into organ-specific ECs, allowing us to manufacture more specialized and physiologically representative vasculatures. The blood-brain barrier (BBB), for instance, is one of the most specialized and clinically important vasculatures. Researchers have demonstrated that iPSC-derived brain microvascular ECs (iPSC-BMECs) can form a functional endothelium barrier in microfluidics and exhibit a large transendothelial electrical resistance (TEER) characteristic of the human BBB (Linville et al., 2019; Vatine et al., 2019). Furthermore, the engineered BBB exhibited selective permeability and remained functional while being perfused with human whole blood (Westein et al., 2013). In addition to modeling endothelium, microfluidic platforms can also be utilized to investigate vascular smooth muscle pathology in a patient-specific manner. Using microfluidics, iPSC-SMCs derived from progeroid patients were found to be more susceptible to detachment under flow-induced shear stress compared to the healthy control, and metalloprotease 13 (MMP13) was identified as a potential therapeutic target (Pitrez et al., 2020).

Considerations for Choosing the Model

Generally speaking, there are two fundamental considerations in choosing *in vitro* models for vascular toxicity studies or toxicity studies in general. The first consideration is physiological relevance, which determines whether a model can precisely recapitulate the human response to a given drug. Overall, organoids and microfluidic vascular chips are expected to be more physiologically relevant than 2D models or simple vascular spheroids (Duval et al., 2017). The second factor to consider is experimental throughput. This factor is especially important during the early stage of drug research and development, when it is often necessary to screen tens of thousands of compounds. 2D models, despite their limited physiological relevance, are most commonly used for high-throughput screenings to identify toxic vs. therapeutic compounds. Therefore, a rational strategy would be to employ 2D models for early exploratory investigations that are focused on narrowing down the list of candidates or gaining preliminary insights. Afterward, 3D organoids or microfluidic platforms can be adopted to develop a more comprehensive and accurate understanding of the drug's effects.

MOVING FORWARD-WHAT IS NEXT?

Improving the Quality of the Cells

A universal concern regarding iPSC-derived cells is that they tend to be very heterogeneous, and this is no exception for iPSC-derived vascular cells (Karakikes et al., 2015; Paik et al., 2018; Kwong et al., 2019; Volpato and Webber, 2020). Drug testing using heterogeneous cell populations may lead to an inaccurate conclusion, especially if it is based on ensemble measurements (Altschuler and Wu, 2010). To tackle this issue, a variety of strategies can be employed, such as optimization of the differentiation protocol (Wang et al., 2020), purification using genetically engineered reporter cell lines (Hu et al., 2018), or magnetic-activated cell sorting (MACS) based on the desired surface marker (Li et al., 2017).

Future iPSC-based vascular models may benefit from using tissue-specific or vessel-specific cells to improve their physiological relevance. In recent years, it is increasingly appreciated that ECs or SMCs may vary considerably in both function and molecular signature depending on their subtype (Cheung et al., 2012; Bennett et al., 2016; Williams and Wu, 2019; Jambusaria et al., 2020). Some successful efforts have been made on this front, such as the development of brain microvascular chips (Linville et al., 2019; Vatine et al., 2019; Weaver and Valentin, 2019) and drug testing using lineage-specific SMCs (Cheung et al., 2012).

Validation Studies

One representative iPSC technology at the forefront of transforming drug toxicology is the use of iPSC-derived cardiomyocytes (Gintant et al., 2019; Pang et al., 2019). In particular, large-scale efforts exemplified by the CiPA initiative have been coordinated by academia, industry, and regulatory bodies to explore and validate iPSC-CMs as a viable option for predicting cardiac liabilities in a translational setting (Colatsky et al., 2016; Blinova et al., 2017). Clearly, for iPSC-based vascular models to be accepted as a tool in preclinical or even clinical investigation, a similar pathway is inevitable. Particularly, iPSC vascular models should be rigorously tested with double-blinded experiments to quantify the specificity and sensitivity, and their performance needs to be compared with animal models.

Exploring Emerging Technologies

The past decade has witnessed a bountiful rise of exciting technologies in the biomedical field. These technologies can be exploited to empower iPSC-based drug testing. 3D bioprinting technologies using iPSC-derived cells can help us build more realistic vasculatures on a chip (Kolesky et al., 2014; Maiullari et al., 2018). Single-cell technologies such as single-cell RNA sequencing can reveal hidden pathological changes at an unprecedented resolution (Chaudhry et al., 2019; Paik et al., 2020a). CRISPR-based gene editing tools together with patient-specific iPSCs may unveil the effects of single nucleotide polymorphism (SNP) on drug response and hence determine individual predisposition to toxicity (Pang et al., 2009; Burridge et al., 2016; Seeger et al., 2017; Garg et al., 2018; Ma et al., 2018). Machine learning supported with big data has also shown promise in improving the prediction of drug toxicity (Lau et al., 2019; Vo et al., 2020). Collectively, these technologies have led us to uncharted territory for toxicology. The utility of iPSC-based platforms in predicting vascular toxicity, or any drug-induced toxicity, is likely to be significantly expanded in combination with these state-of-the-art tools.

CONCLUDING REMARKS

Prediction and understanding of drug-induced toxicity is a critical part of pharmaceutical development as well as patient care. The vascular system as the network for transporting nutrients and hormones is at a high risk of exposure to drug-induced off-target damages, as evidenced by notable major drug withdrawals caused by vascular events and frequent vascular complications observed in patients undergoing chemotherapy. However, the detection of drug-induced vascular toxicity in humans is difficult, partly because its manifestation may be slow and patient-specific (Cameron et al., 2016; Herrmann, 2020). In fact, it was suggested that surveillance of vascular health in certain cancer survivors should last several years after chemotherapy (Herrmann, 2020). Obviously, such a long time frame would be impractical in most translational and clinical settings. The use of animal models is intended to accelerate the discovery and understanding of drug toxicity. However, it is increasingly recognized that fundamental species differences on molecular, cellular, and tissue levels limit the predictive power of animal models for human toxicity

(Bailey et al., 2013; Bailey et al., 2014). The invention of iPSC technology presents a paradigm shift improvement in our ability to predict and dissect drug-induced vascular injuries. For the first time, it is possible to establish a scalable and personalized drug testing platform. To be sure, iPSC models are still very immature for the time being, and issues such as consistency and physiological relevance are yet to be comprehensively examined. Nevertheless, with the rapid and continuous improvements made by researchers from different disciplines, we are optimistic that they will be an increasingly powerful tool in the future of vascular toxicology.

AUTHOR CONTRIBUTIONS

CT wrote the manuscript. CT, NC, MZ, and JW revised the manuscript and provided critical input.

FUNDING

This work was supported by the American Heart Association 20POST35080175 (CT) and 17MERIT33610009 (JW), the National Institutes of Health R01 HL141851, R01 HL141371, R01 HL146690, UH3 TR002588, and TRDRP 27IR-0012 (JW).

REFERENCES

Altschuler, S. J., and Wu, L. F. (2010). Cellular heterogeneity: do differences make a difference?. *Cell* 141, 559–563. doi:10.1016/j.cell.2010.04.033

Amann, A., Zwierzina, M., Koeck, S., Gamerith, G., Pechriggl, E., Huber, J. M., et al. (2017). Development of a 3D angiogenesis model to study tumour-endothelial cell interactions and the effects of anti-angiogenic drugs. *Sci. Rep.* 7, 2963. doi:10.1038/s41598-017-03010-6

Atchison, L., Zhang, H., Cao, K., and Truskey, G. A. (2017). A tissue engineered blood vessel model of hutchinson-gilford progeria syndrome using human iPSC-derived smooth muscle cells. *Sci. Rep.* 7, 8168. doi:10.1038/s41598-017-08632-4

Bailey, J., Thew, M., and Balls, M. (2014). An analysis of the use of animal models in predicting human toxicology and drug safety. *Altern. Lab. Anim.* 42, 181–199. doi:10.1177/026119291404200306

Bailey, J., Thew, M., and Balls, M. (2013). An analysis of the use of dogs in predicting human toxicology and drug safety. *Altern. Lab. Anim.* 41, 335–350. doi:10.1177/026119291304100504

Belair, D. G., Schwartz, M. P., Knudsen, T., and Murphy, W. L. (2016). Human iPSC-derived endothelial cell sprouting assay in synthetic hydrogel arrays. *Acta Biomater.* 39, 12–24. doi:10.1016/j.actbio.2016.05.020

Ben-Shaul, S., Landau, S., Merdler, U., and Levenberg, S. (2019). Mature vessel networks in engineered tissue promote graft-host anastomosis and prevent graft thrombosis. *Proc. Natl. Acad. Sci. U. S. A.* 116, 2955–2960. doi:10.1073/pnas.1814238116

Bennett, M. R., Sinha, S., and Owens, G. K. (2016). Vascular smooth muscle cells in atherosclerosis. *Circ. Res.* 118, 692–702. doi:10.1161/CIRCRESAHA.115.306361

Biel, N. M., Santostefano, K. E., DiVita, B. B., El Rouby, N., Carrasquilla, S. D., Simmons, C., et al. (2015). Vascular smooth muscle cells from hypertensive patient-derived induced pluripotent stem cells to advance hypertension pharmacogenomics. *Stem Cell Transl. Med.* 4, 1380–1390. doi:10.5966/sctm.2015-0126

Blinova, K., Stohlman, J., Vicente, J., Chan, D., Johannesen, L., Hortigon-Vinagre, M. P., et al. (2017). Comprehensive translational assessment of human-induced pluripotent stem cell derived cardiomyocytes for evaluating drug-induced arrhythmias. *Toxicol. Sci.* 155, 234–247. doi:10.1093/toxsci/kfw200

Brandes, R. P. (2014). Endothelial dysfunction and hypertension. *Hypertension* 64, 924–928. doi:10.1161/HYPERTENSIONAHA.114.03575

Burridge, P. W., Li, Y. F., Matsa, E., Wu, H., Ong, S. G., Sharma, A., et al. (2016). Human induced pluripotent stem cell-derived cardiomyocytes recapitulate the predilection of breast cancer patients to doxorubicin-induced cardiotoxicity. *Nat. Med.* 22, 547–556. doi:10.1038/nm.4087

Burridge, P. W., Matsa, E., Shukla, P., Lin, Z. C., Churko, J. M., Ebert, A. D., et al. (2014). Chemically defined generation of human cardiomyocytes. *Nat. Methods* 11, 855–860. doi:10.1038/nMeth.2999

Cameron, A. C., Touyz, R. M., and Lang, N. N. (2016). Vascular complications of cancer chemotherapy. *Can. J. Cardiol.* 32, 852–862. doi:10.1016/j.cjca.2015.12.023

Cao, N., Liang, H., Huang, J., Wang, J., Chen, Y., Chen, Z., et al. (2013). Highly efficient induction and long-term maintenance of multipotent cardiovascular progenitors from human pluripotent stem cells under defined conditions. *Cell Res.* 23, 1119–1132. doi:10.1038/cr.2013.102

Chang, W. G., and Niklason, L. E. (2017). A short discourse on vascular tissue engineering. *Npj Regen. Med.* 2, 1–8. doi:10.1038/s41536-017-0011-6

Chaudhry, F., Isherwood, J., Bawa, T., Patel, D., Gurdziel, K., Lanfear, D. E., et al. (2019). Single-cell RNA sequencing of the cardiovascular system: new looks for old diseases. *Front. Cardiovasc. Med.* 6, 173. doi:10.3389/fcvm.2019.00173

Chen, J., Kang, D., Xu, J., Lake, M., Hogan, J. O., Sun, C., et al. (2013). Species differences and molecular determinant of TRPA1 cold sensitivity. *Nat. Commun.* 4, 2501–2751. doi:10.1038/ncomms3501

Cheung, C., Bernardo, A. S., Pedersen, R. A., and Sinha, S. (2014). Directed differentiation of embryonic origin-specific vascular smooth muscle subtypes from human pluripotent stem cells. *Nat. Protoc.* 9, 929–938. doi:10.1038/nprot.2014.059

Cheung, C., Bernardo, A. S., Trotter, M. W., Pedersen, R. A., and Sinha, S. (2012). Generation of human vascular smooth muscle subtypes provides insight into embryological origin-dependent disease susceptibility. *Nat. Biotechnol.* 30, 165–173. doi:10.1038/nbt.2107

Chiew, G. G. Y., Wei, N., Sultania, S., Lim, S., and Luo, K. Q. (2017). Bioengineered three-dimensional co-culture of cancer cells and endothelial cells: a model system for dual analysis of tumor growth and angiogenesis. *Biotechnol. Bioeng.* 114, 1865–1877. doi:10.1002/bit.26297

Chu, P. H., Chen, G., Kuo, D., Braisted, J., Huang, R., Wang, Y., et al. (2020). Stem cell-derived endothelial cell model that responds to tobacco smoke like primary endothelial cells. *Chem. Res. Toxicol.* 33, 751–763. doi:10.1021/acs.chemrestox.9b00363

Colatsky, T., Fermini, B., Gintant, G., Pierson, J. B., Sager, P., Sekino, Y., et al. (2016). The comprehensive *in Vitro* proarrhythmia assay (CiPA) initiative - update on progress. *J. Pharmacol. Toxicol. Methods* 81, 15–20. doi:10.1016/j.vascn.2016.06.002

Crosby, C. O., Valliappan, D., Shu, D., Kumar, S., Tu, C., Deng, W., et al. (2019). Quantifying the vasculogenic potential of induced pluripotent stem cell-derived endothelial progenitors in collagen hydrogels. *Tissue Eng. Part. A.* 25, 746–758. doi:10.1089/ten.tea.2018.0274

Crosby, C. O., and Zoldan, J. (2019). Mimicking the physical cues of the ECM in angiogenic biomaterials. *Regen. Biomater.* 6, 61–73. doi:10.1093/rb/rbz003

Davignon, J., and Ganz, P. (2004). Role of endothelial dysfunction in atherosclerosis. *Circulation* 109, III27. doi:10.1161/01.cir.0000131515.03336.f8

Duval, K., Grover, H., Han, L. H., Mou, Y., Pegoraro, A. F., Fredberg, J., et al. (2017). Modeling physiological events in 2D vs. 3D cell culture. *Physiology* 32, 266–277. doi:10.1152/physiol.00036.2016

Fermini, B., Hancox, J. C., Abi-Gerges, N., Bridgland-Taylor, M., Chaudhary, K. W., Colatsky, T., et al. (2016). A new perspective in the field of cardiac safety testing through the comprehensive *in vitro* proarrhythmia assay paradigm. *J. Biomol. Screen.* 21, 1–11. doi:10.1177/1087057115594589

Garg, P., Oikonomopoulos, A., Chen, H., Li, Y., Lam, C. K., Sallam, K., et al. (2018). Genome editing of induced pluripotent stem cells to decipher cardiac channelopathy variant. *J. Am. Coll. Cardiol.* 72, 62–75. doi:10.1016/j.jacc.2018.04.041

Gintant, G., Burridge, P., Gepstein, L., Harding, S., Herron, T., Hong, C., et al. (2019). Use of human induced pluripotent stem cell-derived cardiomyocytes in preclinical cancer drug cardiotoxicity testing: a scientific statement from the American Heart Association. *Circ. Res.* 125, e75–e92. doi:10.1161/RES.0000000000000291

Gold, K., Gaharwar, A. K., and Jain, A. (2019). Emerging trends in multiscale modeling of vascular pathophysiology: organ-on-a-chip and 3D printing. *Biomaterials* 196, 2–17. doi:10.1016/j.biomaterials.2018.07.029

Granata, A., Serrano, F., Bernard, W. G., McNamara, M., Low, L., Sastry, P., et al. (2017). An iPSC-derived vascular model of Marfan syndrome identifies key mediators of smooth muscle cell death. *Nat. Genet.* 49, 97–109. doi:10.1038/ng.3723

Herrmann, J. (2020). Vascular toxic effects of cancer therapies. *Nat. Rev. Cardiol.* 17, 503–522. doi:10.1038/s41569-020-0347-2

Herrmann, J., Yang, E. H., Iliescu, C. A., Cilingiroglu, M., Charitakis, K., Hakeem, A., et al. (2016). Vascular toxicities of cancer therapies: the old and the new--an evolving avenue. *Circulation* 133, 1272–1289. doi:10.1161/CIRCULATIONAHA.115.018347

Hu, Z., Wu, Y., Zhou, M., Wang, X., Pang, J., Li, Z., et al. (2018). Generation of reporter hESCs by targeting *EGFP* at the CD144 locus to facilitate the endothelial differentiation. *Dev. Growth Differ.* 60, 205–215. doi:10.1111/dgd.12433

Iwata, Y., Klaren, W. D., Lebakken, C. S., Grimm, F. A., and Rusyn, I. (2017). High-content assay multiplexing for vascular toxicity screening in induced pluripotent stem cell-derived endothelial cells and human umbilical vein endothelial cells. *Assay Drug Dev. Technol.* 15, 267–279. doi:10.1089/adt.2017.786

Jambusaria, A., Hong, Z., Zhang, L., Srivastava, S., Jana, A., Toth, P. T., et al. (2020). Endothelial heterogeneity across distinct vascular beds during homeostasis and inflammation. *Elife* 9, e51413. doi:10.7554/eLife.51413

James, W. P., Caterson, I. D., Coutinho, W., Finer, N., Van Gaal, L. F., Maggioni, A. P., et al. (2010). Effect of sibutramine on cardiovascular outcomes in overweight and obese subjects. *N. Engl. J. Med.* 363, 905–917. doi:10.1056/NEJMoa1003114

Karakikes, I., Ameen, M., Termglinchan, V., and Wu, J. C. (2015). Human induced pluripotent stem cell-derived cardiomyocytes: insights into molecular, cellular, and functional phenotypes. *Circ. Res.* 117, 80–88. doi:10.1161/CIRCRESAHA.117.305365

Kitani, T., Ong, S. G., Lam, C. K., Rhee, J. W., Zhang, J. Z., Oikonomopoulos, A., et al. (2019). Human-induced pluripotent stem cell model of trastuzumab-induced cardiac dysfunction in patients with breast cancer. *Circulation* 139, 2451–2465. doi:10.1161/CIRCULATIONAHA.118.037357

Klimkiewicz, K., Weglarczyk, K., Collet, G., Paprocka, M., Guichard, A., Sarna, M., et al. (2017). A 3D model of tumour angiogenic microenvironment to monitor hypoxia effects on cell interactions and cancer stem cell selection. *Cancer Lett.* 396, 10–20. doi:10.1016/j.canlet.2017.03.006

Kolesky, D. B., Truby, R. L., Gladman, A. S., Busbee, T. A., Homan, K. A., and Lewis, J. A. (2014). 3D bioprinting of vascularized, heterogeneous cell-laden tissue constructs. *Adv. Mater. Weinheim* 26, 3124–3130. doi:10.1002/adma.201305506

Kurokawa, Y. K., Yin, R. T., Shang, M. R., Shirure, V. S., Moya, M. L., and George, S. C. (2017). Human induced pluripotent stem cell-derived endothelial cells for three-dimensional microphysiological systems. *Tissue Eng. Part. C Methods* 23, 474–484. doi:10.1089/ten.tec.2017.0133

Kwong, G., Marquez, H. A., Yang, C., Wong, J. Y., and Kotton, D. N. (2019). Generation of a purified iPSC-derived smooth muscle-like population for cell sheet engineering. *Stem Cell Rep.* 13, 499–514. doi:10.1016/j.stemcr.2019.07.014

Lam, C. K., Tian, L., Belbachir, N., Wnorowski, A., Shrestha, R., Ma, N., et al. (2019). Identifying the transcriptome signatures of calcium channel blockers in human induced pluripotent stem cell-derived cardiomyocytes. *Circ. Res.* 125, 212–222. doi:10.1161/CIRCRESAHA.118.314202

Lau, E., Paik, D. T., and Wu, J. C. (2019). Systems-wide approaches in induced pluripotent stem cell models. *Annu. Rev. Pathol.* 14, 395–419. doi:10.1146/annurev-pathmechdis-012418-013046

Lee, W. H., Ong, S. G., Zhou, Y., Tian, L., Bae, H. R., Baker, N., et al. (2019). Modeling cardiovascular risks of E-cigarettes with human-induced pluripotent stem cell-derived endothelial cells. *J. Am. Coll. Cardiol.* 73, 2722–2737. doi:10.1016/j.jacc.2019.03.476

Li, Y., Green, M., Wen, Y., Wei, Y., Wani, P., Wang, Z., et al. (2017). Efficacy and safety of immuno-magnetically sorted smooth muscle progenitor cells derived from human-induced pluripotent stem cells for restoring urethral sphincter function. *Stem Cell Transl. Med.* 6, 1158–1167. doi:10.1002/sctm.16-0160

Lian, X., Bao, X., Al-Ahmad, A., Liu, J., Wu, Y., Dong, W., et al. (2014). Efficient differentiation of human pluripotent stem cells to endothelial progenitors via small-molecule activation of WNT signaling. *Stem Cell Rep.* 3, 804–816. doi:10.1016/j.stemcr.2014.09.005

Lian, X., Hsiao, C., Wilson, G., Zhu, K., Hazeltine, L. B., Azarin, S. M., et al. (2012). Robust cardiomyocyte differentiation from human pluripotent stem cells via temporal modulation of canonical Wnt signaling. *Proc. Natl. Acad. Sci. U.S.A.* 109, E1848–E1857. doi:10.1073/pnas.1200250109

Lim, S., and Park, S. (2014). Role of vascular smooth muscle cell in the inflammation of atherosclerosis. *BMB Rep.* 47, 1–7. doi:10.5483/BMBRep.2014.47.1.285

Linville, R. M., DeStefano, J. G., Sklar, M. B., Xu, Z., Farrell, A. M., Bogorad, M. I., et al. (2019). Human iPSC-derived blood-brain barrier microvessels: validation of barrier function and endothelial cell behavior. *Biomaterials* 190-191, 24–37. doi:10.1016/j.biomaterials.2018.10.023

Liu, C., Cheng, L., Chen, C., and Sayed, N. (2018a). Generation of endothelial cells from human induced pluripotent stem cells. *Bio-Protocol* 8, 1–9. doi:10.21769/bioprotoc.3086

Liu, C., Oikonomopoulos, A., Sayed, N., and Wu, J. C. (2018b). Modeling human diseases with induced pluripotent stem cells: from 2D to 3D and beyond. *Development* 145, dev156166. doi:10.1242/dev.156166

Louden, C., Brott, D., Katein, A., Kelly, T., Gould, S., Jones, H., et al. (2006). Biomarkers and mechanisms of drug-induced vascular injury in non-rodents. *Toxicol. Pathol.* 34, 19–26. doi:10.1080/01926230500512076

Luu, A. Z., Chowdhury, B., Al-Omran, M., Teoh, H., Hess, D. A., and Verma, S. (2018). Role of endothelium in doxorubicin-induced cardiomyopathy. *JACC Basic Transl. Sci.* 3, 861–870. doi:10.1016/j.jacbts.2018.06.005

Ma, N., Zhang, J. Z., Itzhaki, I., Zhang, S. L., Chen, H., Haddad, F., et al. (2018). Determining the pathogenicity of a genomic variant of uncertain significance using CRISPR/Cas9 and human-induced pluripotent stem cells. *Circulation* 138, 2666–2681. doi:10.1161/CIRCULATIONAHA.117.032273

Maiullari, F., Costantini, M., Milan, M., Pace, V., Chirivì, M., Maiullari, S., et al. (2018). A multi-cellular 3D bioprinting approach for vascularized heart tissue engineering based on HUVECs and iPSC-derived cardiomyocytes. *Sci. Rep.* 8, 13532–13615. doi:10.1038/s41598-018-31848-x

Majesky, M. W., Dong, X. R., Regan, J. N., and Hoglund, V. J. (2011). Vascular smooth muscle progenitor cells: building and repairing blood vessels. *Circ. Res.* 108, 365–377. doi:10.1161/CIRCRESAHA.110.223800

Marcu, R., Choi, Y. J., Xue, J., Fortin, C. L., Wang, Y., Nagao, R. J., et al. (2018). Human organ-specific endothelial cell heterogeneity. *iScience* 4, 20–35. doi:10.1016/j.isci.2018.05.003

Markou, M., Kouroupis, D., Badounas, F., Katsouras, A., Kyrkou, A., Fotsis, T., et al. (2020). Tissue engineering using vascular organoids from human pluripotent stem cell derived mural cell phenotypes. *Front. Bioeng. Biotechnol.* 8, 278. doi:10.3389/fbioe.2020.00278

McGowan, J. V., Chung, R., Maulik, A., Piotrowska, I., Walker, J. M., and Yellon, D. M. (2017). Anthracycline chemotherapy and cardiotoxicity. *Cardiovasc. Drugs Ther.* 31, 63–75. doi:10.1007/s10557-016-6711-0

Mikaelian, I., Cameron, M., Dalmas, D. A., Enerson, B. E., Gonzalez, R. J., Guionaud, S., et al. (2014). Nonclinical safety biomarkers of drug-induced vascular injury: current status and blueprint for the future. *Toxicol. Pathol.* 42, 635–657. doi:10.1177/0192623314525686

Millard, D., Dang, Q., Shi, H., Zhang, X., Strock, C., Kraushaar, U., et al. (2018). Cross-site reliability of human induced pluripotent stem cell-derived cardiomyocyte based safety assays using microelectrode arrays: results from a blinded CiPA pilot study. *Toxicol. Sci.* 164, 550–562. doi:10.1093/toxsci/kfy110

Moldovan, L., Barnard, A., Gil, C. H., Lin, Y., Grant, M. B., Yoder, M. C., et al. (2017). iPSC-derived vascular cell spheroids as building blocks for scaffold-free biofabrication. *Biotechnol. J.* 12. doi:10.1002/biot.201700444

Mori, N., Morimoto, Y., and Takeuchi, S. (2017). Skin integrated with perfusable vascular channels on a chip. *Biomaterials* 116, 48–56. doi:10.1016/j.biomaterials.2016.11.031

Nebigil, C. G., and Désaubry, L. (2018). Updates in anthracycline-mediated cardiotoxicity. *Front. Pharmacol.* 9, 1262. doi:10.3389/fphar.2018.01262

Olmer, R., Engels, L., Usman, A., Menke, S., Malik, M. N. H., Pessler, F., et al. (2018). Differentiation of human pluripotent stem cells into functional endothelial cells in scalable suspension culture. *Stem Cell Rep.* 10, 1657–1672. doi:10.1016/j.stemcr.2018.03.017

Oren, O., and Herrmann, J. (2018). Arterial events in cancer patients-the case of acute coronary thrombosis. *J. Thorac. Dis.* 10, S4367–S4385. doi:10.21037/jtd.2018.12.79

Orphanos, G. S., Ioannidis, G. N., and Ardavanis, A. G. (2009). Cardiotoxicity induced by tyrosine kinase inhibitors. *Acta Oncol.* 48, 964–970. doi:10.1080/02841860903229124

Paik, D. T., Cho, S., Tian, L., Chang, H. Y., and Wu, J. C. (2020a). Single-cell RNA sequencing in cardiovascular development, disease and medicine. *Nat. Rev. Cardiol.* 17, 457–473. doi:10.1038/s41569-020-0359-y

Paik, D. T., Tian, L., Williams, I. M., Rhee, S., Zhang, H., Liu, C., et al. (2020b). Single-cell RNA sequencing unveils unique transcriptomic signatures of organ-specific endothelial cells. *Circulation* 142, 1848. doi:10.1161/CIRCULATIONAHA.119.041433

Paik, D. T., Tian, L., Lee, J., Sayed, N., Chen, I. Y., Rhee, S., et al. (2018). Large-scale single-cell RNA-seq reveals molecular signatures of heterogeneous populations of human induced pluripotent stem cell-derived endothelial cells. *Circ. Res.* 123, 443–450. doi:10.1161/CIRCRESAHA.118.312913

Palpant, N. J., Pabon, L., Friedman, C. E., Roberts, M., Hadland, B., Zaunbrecher, R. J., et al. (2017). Generating high-purity cardiac and endothelial derivatives from patterned mesoderm using human pluripotent stem cells. *Nat. Protoc.* 12, 15–31. doi:10.1038/nprot.2016.153

Pang, G. S., Wang, J., Wang, Z., and Lee, C. G. (2009). Predicting potentially functional SNPs in drug-response genes. *Pharmacogenomics* 10, 639–653. doi:10.2217/pgs.09.12

Pang, L., Sager, P., Yang, X., Shi, H., Sannajust, F., Brock, M., et al. (2019). Workshop report: FDA workshop on improving cardiotoxicity assessment with human-relevant platforms. *Circ. Res.* 125, 855–867. doi:10.1161/CIRCRESAHA.119.315378

Patsch, C., Challet-Meylan, L., Thoma, E. C., Urich, E., Heckel, T., O'Sullivan, J. F., et al. (2015). Generation of vascular endothelial and smooth muscle cells from human pluripotent stem cells. *Nat. Cell Biol.* 17, 994–1003. doi:10.1038/ncb3205

Pitrez, P. R., Estronca, L., Monteiro, L. M., Colell, G., Vazão, H., Santinha, D., et al. (2020). Vulnerability of progeroid smooth muscle cells to biomechanical forces is mediated by MMP13. *Nat. Commun.* 11, 4110–4116. doi:10.1038/s41467-020-17901-2

Qiu, Y., Ahn, B., Sakurai, Y., Hansen, C. E., Tran, R., Mimche, P. N., et al. (2018). Microvasculature-on-a-chip for the long-term study of endothelial barrier dysfunction and microvascular obstruction in disease. *Nat. Biomed. Eng.* 2, 453–463. doi:10.1038/s41551-018-0224-z

Qureshi, Z. P., Seoane-Vazquez, E., Rodriguez-Monguio, R., Stevenson, K. B., and Szeinbach, S. L. (2011). Market withdrawal of new molecular entities approved in the United States from 1980 to 2009. *Pharmacoepidemiol. Drug Saf.* 20, 772–777. doi:10.1002/pds.2155

Rhee, J. W., Ky, B., Armenian, S. H., Yancy, C. W., and Wu, J. C. (2020). Primer on biomarker discovery in cardio-oncology: application of omics technologies. *JACC CardioOncol.* 2, 379–384. doi:10.1016/j.jaccao.2020.07.006

Rieker, C., Migliavacca, E., Vaucher, A., Baud, G., Marquis, J., Charpagne, A., et al. (2019). Apolipoprotein E4 expression causes gain of toxic function in isogenic human induced pluripotent stem cell-derived endothelial cells. *Arterioscler. Thromb. Vasc. Biol.* 39, e195–e207. doi:10.1161/ATVBAHA.118.312261

Rosa, S., Praça, C., Pitrez, P. R., Gouveia, P. J., Aranguren, X. L., Ricotti, L., et al. (2019). Functional characterization of iPSC-derived arterial- and venous-like endothelial cells. *Sci. Rep.* 9, 3826–3915. doi:10.1038/s41598-019-40417-9

Sayed, N., Ameen, M., and Wu, J. C. (2019). Personalized medicine in cardio-oncology: the role of induced pluripotent stem cell. *Cardiovasc. Res.* 115, 949–959. doi:10.1093/cvr/cvz024

Sayed, N., Liu, C., and Wu, J. C. (2016). Translation of human-induced pluripotent stem cells: from clinical trial in a dish to precision medicine. *J. Am. Coll. Cardiol.* 67, 2161–2176. doi:10.1016/j.jacc.2016.01.083

Sayed, N., Liu, C., Ameen, M., Himmati, F., Zhang, J. Z., Khanamiri, S., et al. (2020). Clinical trial in a dish using iPSCs shows lovastatin improves endothelial dysfunction and cellular cross-talk in LMNA cardiomyopathy. *Sci. Transl. Med.* 12, eaax9276. doi:10.1126/scitranslmed.aax9276

Seeger, T., Porteus, M., and Wu, J. C. (2017). Genome editing in cardiovascular biology. *Circ. Res.* 120, 778–780. doi:10.1161/CIRCRESAHA.116.310197

Sharma, A., Burridge, P. W., McKeithan, W. L., Serrano, R., Shukla, P., Sayed, N., et al. (2017). High-throughput screening of tyrosine kinase inhibitor cardiotoxicity with human induced pluripotent stem cells. *Sci. Transl. Med.* 9, eaaf2584. doi:10.1126/scitranslmed.aaf2584

Siramshetty, V. B., Nickel, J., Omieczynski, C., Gohlke, B. O., Drwal, M. N., and Preissner, R. (2016). WITHDRAWN--a resource for withdrawn and discontinued drugs. *Nucleic Acids Res.* 44, D1080–D1086. doi:10.1093/nar/gkv1192

Stephenson, M., Reich, D. H., and Boheler, K. R. (2020). Induced pluripotent stem cell-derived vascular smooth muscle cells. *Vasc. Biol.* 2, R1–R15. doi:10.1530/vb-19-0028

Tang, L., Su, J., and Liang, P. (2017). Modeling cadmium-induced endothelial toxicity using human pluripotent stem cell-derived endothelial cells. *Sci. Rep.* 7, 14811–14812. doi:10.1038/s41598-017-13694-5

Taubenberger, A. V., Bray, L. J., Haller, B., Shaposhnykov, A., Binner, M., Freudenberg, U., et al. (2016). 3D extracellular matrix interactions modulate tumour cell growth, invasion and angiogenesis in engineered tumour microenvironments. *Acta Biomater.* 36, 73–85. doi:10.1016/j.actbio.2016.03.017

Taura, D., Sone, M., Homma, K., Oyamada, N., Takahashi, K., Tamura, N., et al. (2009). Induction and isolation of vascular cells from human induced pluripotent stem cells--brief report. *Arterioscler. Thromb. Vasc. Biol.* 29, 1100–1103. doi:10.1161/ATVBAHA.108.182162

Touyz, R. M., Alves-Lopes, R., Rios, F. J., Camargo, L. L., Anagnostopoulou, A., Arner, A., et al. (2018). Vascular smooth muscle contraction in hypertension. *Cardiovasc. Res.* 114, 529–539. doi:10.1093/cvr/cvy023

Vatine, G. D., Barrile, R., Workman, M. J., Sances, S., Barriga, B. K., Rahnama, M., et al. (2019). Human iPSC-derived blood-brain barrier chips enable disease modeling and personalized medicine applications. *Cell Stem Cell* 24, 995. doi:10.1016/j.stem.2019.05.011

Vo, A. H., Van Vleet, T. R., Gupta, R. R., Liguori, M. J., and Rao, M. S. (2020). An overview of machine learning and big data for drug toxicity evaluation. *Chem. Res. Toxicol.* 33, 20–37. doi:10.1021/acs.chemrestox.9b00227

Volpato, V., and Webber, C. (2020). Addressing variability in iPSC-derived models of human disease: guidelines to promote reproducibility. *Dis. Model. Mech.* 13, dmm042317. doi:10.1242/dmm.042317

Wang, K., Lin, R.-Z., Hong, X., Ng, A. H., Lee, C. N., Neumeyer, J., et al. (2020). Robust differentiation of human pluripotent stem cells into endothelial cells via temporal modulation of ETV2 with modified mRNA. *Sci. Adv.* 6, eaba7606. doi:10.1126/sciadv.aba7606

Wanjare, M., Kuo, F., and Gerecht, S. (2013). Derivation and maturation of synthetic and contractile vascular smooth muscle cells from human pluripotent stem cells. *Cardiovasc. Res.* 97, 321–330. doi:10.1093/cvr/cvs315

Weaver, R. J., and Valentin, J. P. (2019). Today's challenges to de-risk and predict drug safety in human "Mind-the-Gap". *Toxicol. Sci.* 167, 307–321. doi:10.1093/toxsci/kfy270

Westein, E., Van Der Meer, A. D., Kuijpers, M. J., Frimat, J. P., Van Den Berg, A., and Heemskerk, J. W. (2013). Atherosclerotic geometries exacerbate pathological thrombus formation poststenosis in a von Willebrand factor-dependent manner. *Proc. Natl. Acad. Sci. U.S.A.* 110, 1357–1362. doi:10.1073/pnas.1209905110

Williams, I. M., and Wu, J. C. (2019). Generation of endothelial cells from human pluripotent stem cells. *Atvb* 39, 1317–1329. doi:10.1161/ATVBAHA.119.312265

Wimmer, R. A., Leopoldi, A., Aichinger, M., Wick, N., Hantusch, B., Novatchkova, M., et al. (2019). Human blood vessel organoids as a model of diabetic vasculopathy. *Nature* 565, 505–510. doi:10.1038/s41586-018-0858-8

Wnorowski, A., Yang, H., and Wu, J. C. (2019). Progress, obstacles, and limitations in the use of stem cells in organ-on-a-chip models. *Adv. Drug Deliv. Rev.* 140, 3–11. doi:10.1016/j.addr.2018.06.001

Wu, J. C., Garg, P., Yoshida, Y., Yamanaka, S., Gepstein, L., Hulot, J. S., et al. (2019). Towards precision medicine with human iPSCs for cardiac channelopathies. *Circ. Res.* 125, 653–658. doi:10.1161/CIRCRESAHA.119.315209

Yau, J. W., Teoh, H., and Verma, S. (2015). Endothelial cell control of thrombosis. *BMC Cardiovasc. Disord.* 15, 130. doi:10.1186/s12872-015-0124-z

Zhang, B., Lai, B. F. L., Xie, R., Davenport Huyer, L., Montgomery, M., and Radisic, M. (2018). Microfabrication of angiochip, a biodegradable polymer scaffold with microfluidic vasculature. *Nat. Protoc.* 13, 1793–1813. doi:10.1038/s41596-018-0015-8

Zhang, H., Tian, L., Shen, M., Tu, C., Wu, H., Gu, M., et al. (2019a). Generation of quiescent cardiac fibroblasts from human induced pluripotent stem cells for *in vitro* modeling of cardiac fibrosis. *Circ. Res.* 125, 552–566. doi:10.1161/CIRCRESAHA.119.315491

Zhang, J., McIntosh, B. E., Wang, B., Brown, M. E., Probasco, M. D., Webster, S., et al. (2019b). A human pluripotent stem cell-based screen for smooth muscle cell differentiation and maturation identifies inhibitors of intimal hyperplasia. *Stem Cell Rep.* 12, 1269–1281. doi:10.1016/j.stemcr.2019.04.013

Zhang, J., Lian, Q., Zhu, G., Zhou, F., Sui, L., Tan, C., et al. (2011). A human iPSC model of Hutchinson Gilford progeria reveals vascular smooth muscle and mesenchymal stem cell defects. *Cell Stem Cell* 8, 31–45. doi:10.1016/j.stem.2010.12.002

Conflict of Interest: JW is a cofounder of Khloris Biosciences but has no competing interests, as the work presented here is completely independent.

The remaining authors declare that the research was conducted in the absence of any commercial or financial relationships that could be construed as a potential conflict of interest.

frontiers in Pharmacology

ORIGINAL RESEARCH
published: 15 March 2021
doi: 10.3389/fphar.2021.604713

Comparison of the Simulated Response of Three *in Silico* Human Stem Cell-Derived Cardiomyocytes Models and *in Vitro* Data Under 15 Drug Actions

Michelangelo Paci [1]*, ***Jussi T. Koivumäki*** [1], ***Hua Rong Lu*** [2], ***David J. Gallacher*** [2], ***Elisa Passini*** [3] ***and Blanca Rodriguez*** [3]

[1]BioMediTech, Faculty of Medicine and Health Technology, Tampere University, Tampere, Finland, [2]Global Safety Pharmacology, Discovery Sciences, Janssen Research and Development, Janssen Pharmaceutica NV, Beerse, Belgium, [3]Department of Computer Science, University of Oxford, Oxford, United Kingdom

OPEN ACCESS

Edited by:
Jonathan Satin,
University of Kentucky, United States

Reviewed by:
Cees Korstanje,
Consultant, Nieuw-Vennep, Netherlands
Veronica Milesi,
National University of La Plata, Argentina

****Correspondence:***
Michelangelo Paci
michelangelo.paci@tuni.fi

Specialty section:
This article was submitted to Cardiovascular and Smooth Muscle Pharmacology, a section of the journal Frontiers in Pharmacology

Received: *10 September 2020*
Accepted: *15 January 2021*
Published: *15 March 2021*

Citation:
Paci M, Koivumäki JT, Lu HR, Gallacher DJ, Passini E and Rodriguez B (2021) Comparison of the Simulated Response of Three in Silico *Human Stem Cell-Derived Cardiomyocytes Models and* in Vitro *Data Under 15 Drug Actions. Front. Pharmacol. 12:604713. doi: 10.3389/fphar.2021.604713*

Objectives: Improvements in human stem cell-derived cardiomyocyte (hSC-CM) technology have promoted their use for drug testing and disease investigations. Several *in silico* hSC-CM models have been proposed to augment interpretation of experimental findings through simulations. This work aims to assess the response of three hSC-CM *in silico* models (Koivumäki2018, Kernik2019, and Paci2020) to simulated drug action, and compare simulation results against *in vitro* data for 15 drugs.

Methods: First, simulations were conducted considering 15 drugs, using a simple pore-block model and experimental data for seven ion channels. Similarities and differences were analyzed in the *in silico* responses of the three models to drugs, in terms of Ca^{2+} transient duration (CTD_{90}) and occurrence of arrhythmic events. Then, the sensitivity of each model to different degrees of blockage of Na^{+} (I_{Na}), L-type Ca^{2+} (I_{CaL}), and rapid delayed rectifying K^{+} (I_{Kr}) currents was quantified. Finally, we compared the drug-induced effects on CTD_{90} against the corresponding *in vitro* experiments.

Results: The observed CTD_{90} changes were overall consistent among the *in silico* models, all three showing changes of smaller magnitudes compared to the ones measured *in vitro*. For example, sparfloxacin 10 μM induced +42% CTD_{90} prolongation *in vitro*, and +17% (Koivumäki2018), +6% (Kernik2019), and +9% (Paci2020) *in silico*. Different arrhythmic events were observed following drug application, mainly for drugs affecting I_{Kr}. Paci2020 and Kernik2019 showed only repolarization failure, while Koivumäki2018 also displayed early and delayed afterdepolarizations. The spontaneous activity was suppressed by Na^{+} blockers and by drugs with similar effects on I_{CaL} and I_{Kr} in Koivumäki2018 and Paci2020, while only by strong I_{CaL} blockers, e.g. nisoldipine, in Kernik2019. These results were confirmed by the sensitivity analysis.

Conclusion: To conclude, The CTD_{90} changes observed *in silico* are qualitatively consistent with our *in vitro* data, although our simulations show differences in drug responses across the hSC-CM models, which could stem from variability in the experimental data used in their construction.

Keywords: human stem cell-derived cardiomyocyte, action potential, calcium transient, *in silico* modeling, drug test, sensitivity analysis

INTRODUCTION

Human stem cell-derived cardiomyocytes (hSC-CMs) have emerged as a promising tool for translational research, cardiac repair and drug development (Bezzerides et al., 2017; Miyagawa and Sawa, 2018; de Korte et al., 2020). After the initial hype, it has, however, become widely acknowledged that with current methods and technology hSC-CMs have a fundamental limitation: the cells cannot be fully matured into human ventricular cardiomyocytes (hV-CMs). Instead, hSC-CMs have a distinct phenotype of their own that shares features with partially differentiated developing cells (Khan et al., 2013). Furthermore, hSC-CMs show less robustness and greater tendency for arrhythmic events than native hV-CMs; a phenomenon that appears to be linked to a weaker repolarization reserve (Paci et al., 2015; Koivumäki et al., 2018; Lemoine et al., 2018; Treat et al., 2019). Thus, although hSC-CMs do resolve the problem of species-dependent differences related to use of animal models, the translation of data obtained from hSC-CMs to humans is not straightforward.

Computational modeling and simulation offer tools to augment experimental investigations by aiding their interpretation, and identifying possible sources and modulators of hSC-CM electrophysiology. For example, *in silico* approaches have already been successfully employed to investigate the translatability of drug responses from immature hSC-CMs to mature hV-CMs (Gong and Sobie, 2018; Tveito et al., 2018), creating a math-based and mechanistic virtual link to the phenotype of hV-CMs. *In silico* hSC-CM models also helped to gain insight on specific features of hSC-CMs, e.g. automaticity and its causes (Koivumäki et al., 2018; Paci et al., 2020), and to tackle the huge electrophysiological variability observed in action potentials (AP) and Ca^{2+} transients (CaT) recorded *in vitro* (Paci et al., 2017; Kernik et al., 2019), e.g. showing potential combination of ion currents that could make cardiac cells more prone to develop arrhythmic behaviors in response to drugs or in presence of disease phenotypes (Paci et al., 2017; Paci et al., 2018a; Kernik et al., 2020). Currently, there are three pedigrees of hSC-CM *in silico* models, all parametrized on hSC-CM data, developed and published by 1) Paci et al., 2) Koivumäki et al., and 2) Kernik et al. (Koivumäki et al., 2018; Kernik et al., 2019; Paci et al., 2020).

The goal of this work is to investigate differences and similarities in the response of the three latest hSC-CM models to 15 different drugs, and their comparison against an *in vitro* hSC-CM experimental dataset. We expect the insights from our study will enable other researchers to select the most appropriate model for their specific investigations.

METHODS

Model Components and Structures

Table 1 shows the number of compartments and the ion currents, pumps and exchangers included in the three considered computational (*in silico*) cellular models: Kernik2019 (Kernik et al., 2019), Koivumäki2018 (Koivumäki et al., 2018), and Paci2020 (Paci et al., 2019; Paci et al., 2020). They are all single cell models, with a similar formulation for certain ionic currents, as they are all based on the original hSC-CM model from Paci et al. (Paci et al., 2013). The following currents/fluxes are modeled using the Hodgkin-Huxley paradigm, even if with different formulations: fast Na^+ current (I_{Na}), funny current (I_f), L-type Ca^{2+} current (I_{CaL}), rapid and slow delayed rectifier K^+ currents (I_{Kr} and I_{Ks}), inward rectifying K^+ current (I_{K1}), transient outward K^+ current (I_{to}). Of note, I_{CaL} driving force

TABLE 1 | Summary of the compartments and the ion currents and fluxes included in the three models.

	Paci2020	Koivumäki2018	Kernik2019
Compartments	2	61	2
I_{Na}	HH	HH	HH
I_{NaL}	HH	—	—
I_f	HH	HH	HH
I_{CaL} Ca^{2+}	HH, GHK	HH	HH, GHK
I_{CaL} Na^+	—	—	HH, GHK
I_{CaL} K^+	—	—	HH, GHK
I_{CaT}	—	—	HH
I_{Kr}	HH	HH	HH
I_{Ks}	HH	HH	HH
I_{K1}	HH	HH	HH
I_{to}	HH	HH	HH
I_{NCX}	TT	TT	TT
I_{NaK}	TT	TT	TT
I_{pCa}	TT	TT	TT
I_{bNa}	HH, R	HH, R	HH, R
I_{bCa}	HH, R	HH, R	HH, R
J_{RyR}	HH, R	M[2]	M[1]
J_{SERCA}	TT	TT	TT
J_{leak}	HH, R	HH, R	HH, R
J_{IP3}	—	M[3]	—

We reported the modeling paradigm for each ion current/flux: Hodgkin and Huxley (HH), Hodgkin and Huxley as resistive current/flux (HH,R), Hodgkin and Huxley gates with Goldman-Hodgkin-Katz driving force (HH,GHK), Markov (M), based on the TenTusscher2004 model (ten Tusscher et al., 2004) (TT).
[1]*(Shannon et al., 2004),*
[2]*(Keizer and Levine, 1996),*
[3]*(Sneyd and Dufour, 2002).*

is formulated according to the Goldman-Hodgkin-Katz flux equation in Paci2020 and Kernik2019. Na^+ and Ca^{2+} background currents were represented as resistive fluxes. The Na^+/K^+ pump (I_{NaK}), the Na^+/Ca^{2+} exchanger (I_{NCX}) and the Ca^{2+} sarcolemmal pump (I_{pCa}) follow the formulation used in (ten Tusscher et al., 2004). Kernik2019 and Koivumäki2018 use two different Markov formulations for the Ca^{2+} release from the sarcoplasmic reticulum (SR) (Shannon et al., 2004) and (Keizer and Levine, 1996), respectively. Conversely, Paci2020 uses a Hodgkin-Huxley formulation. The Kernik2019 model is the only one including the T-type Ca^{2+} current (I_{CaT}), as well as the Na^+ and K^+ fluxes via I_{CaL} channels. Paci2020 is the only model including the late Na^+ (I_{NaL}) current (Ma et al., 2013). Koivumäki2018 is the only model including the inositol 1,4,5 triphosphate (IP3) receptor-mediated Ca^{2+} release (J_{IP3}).

The three models show differences in their compartmental structure and description of Ca^{2+} dynamics. Paci2020 and Kernik2019 share the same cylindrical structure and compartmentalization: one compartment for cytosol and one for SR. Koivumäki2018 includes an additional Ca^{2+} outward flux from the SR, transmitted by IP3, and formulated as a Markov model. Moreover, Koivumäki2018 has a more complex layered "onion-like" compartmentalization for Ca^{2+}. In order to describe the Ca^{2+} spatial distribution and diffusion, the CM is approximated as a sphere whose radius from SR towards the sarcolemma is divided in 61 sub-compartments. This enables a more refined description of the cytosolic Ca^{2+} dynamics, with no need for partial differential equations, at the price of longer computing time, as shown in the Results section.

In vitro Drug Data

A total of 15 drugs were tested *in vitro* at multiple concentrations: antiarrhythmic drugs (bepridil, dofetilide, flecainide, lidocaine, mexiletine, procainamide and verapamil), an antiepileptic drug (phenytoin), antibiotics (moxifloxacin and sparfloxacin), hypertension drugs (nimodipine and nisoldipine), anticonvulsants (primidone), antianginals (ranolazine) and Ba^{2+} salts ($BaCl_2$). Data were the same used in (Passini et al., 2017).

Briefly, CaT recordings from hSC-CMs (Cor.4U) were acquired at 37°C and 5% CO_2 on pre-plated preparations from Axiogenesis (Cologne, Germany). Cells were seeded in fibronectin-coated 96-well plates at a density suited to form a monolayer and maintained in culture in a stage incubator. The tested 15 drugs were dissolved in DMSO to obtain a stock solution of 1,000x the highest test concentration. Further dilutions were made with DMSO to obtain concentrations of 1,000x intended concentration. On the experiment day these solutions were diluted with Tyrode (Sigma), supplemented with 10 mM HEPES to solutions containing twice the intended concentration (compound plate: 2x intended concentration). Final DMSO concentration in test solutions and vehicle control was 0.1%. Full method details are reported earlier in (Lu et al., 2019) and (Kopljar et al., 2018). Ca^{2+} transients (CaT) recorded as the calcium dye-fluorescence signal integrated over the whole well. CaT duration at 90% of the initial base value (CTD_{90}) was quantified, as it is known to be correlated with APD (Gauthier et al., 2012; Spencer et al., 2014), similarly to other studies (Lu et al., 2015; Zeng et al., 2016). The CTD_{90} values used in this study were measured from 24 to 28 min after compound addition. Therefore, an excessive increment of CTD_{90}, as well as an anomalous CaT time-course, can be considered as markers of APD or QT prolongation and pro-arrhythmic risk - early afterdepolarization (EAD) or torsades de pointes (TdP).

In silico Drug Trials

All the drugs and concentrations tested *in vitro* were simulated *in silico* using the three hSC-CM models. Drug effects on seven ion currents (I_{Na}, I_{Kr}, I_{CaL}, I_{NaL}, I_{Ks}, I_{to} and I_{K1}) were simulated using the single pore block model (Brennan et al., 2009; Paci et al., 2015; Williams and Mirams, 2015), formulated as

$$I_i([D]) = \frac{I_i'}{1 + ([D]/IC_{50})^{n_H}},$$

where I_i is the ion current corresponding to the drug concentration [D], I_i' the ion current in control conditions, IC_{50} is the half-maximal dose response and n_H is the Hill coefficient. The used IC_{50} and Hill coefficients are reported in **Supplementary Table S1** (Passini et al., 2017). For seven drugs, multiple (IC_{50}, Hill coefficient) pairs were considered, as in (Passini et al., 2017). Each model was run for 800 s to reach the steady state. For each drug, concentration and model, simulations were run for 200 s starting from steady state, and then CTD_{90} was computed on the last eight spontaneous CaTs, and the occurrence of proarrhythmic events was assessed. No external pacing was applied to the three models. Since each of the models was tuned and validated on a specific working point, we used the baseline models as originally published by the authors.

Arrhythmic Event Classification

Abnormal rhythms *in vitro* were visually assessed from CaT traces. *In silico*, they were defined based on the AP time-course, as in (Paci et al., 2020). Five types of arrhythmic events were considered. Early after-depolarizations (EADs) were defined as aberrant and transient reversals of the membrane potential repolarization (during phase two or three of the AP) or of the CaT decay. Delayed afterdepolarizations (DADs, observed only *in silico*) were defined as transient depolarizations of the membrane potential or increments of the cytosolic Ca^{2+} from its basal value during their diastolic phases. EADs and DADs were visually assessed. Repolarization failure (RF), i.e. when the membrane potential or the cytosolic Ca^{2+} do not return to their diastolic values for several seconds, was identified when a stable (maximum upstroke velocity smaller than 0.2 V/s) membrane potential >−40 mV was observed during the last 15 s of simulation. Irregular rhythm (IRR) was identified if the difference in cycle length between two consecutive APs or CaTs was greater than 150%. Spontaneous rate greater than 2 Hz was labeled as ventricular tachycardia-like rhythm (VT, observed only *in vitro*).

We also identified two patterns related to the cessation of the spontaneous electrical activity of hSC-CMs, that we did not considered pro-arrhythmic: quiescence (Q) and residual

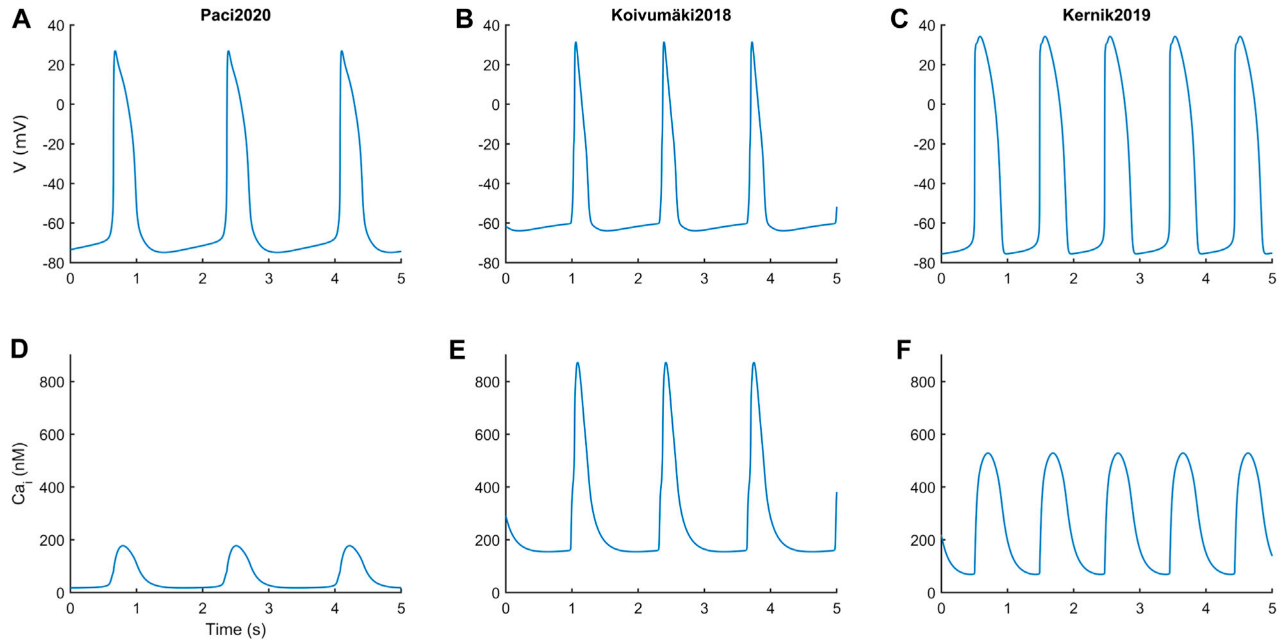

FIGURE 1 | Action potentials **(A and B, C)** and Ca^{2+} transients **(D and E, F)** in steady state for the three *in silico* hSC-CM models.

TABLE 2 | Morphological features from spontaneous action potentials (APs) and Ca^{2+} transients (CaTs).

Morphological feature	Paci2020	Kernik2019	Koivumäki2018
APA (mV)	102	110	95
MDP (mV)	−75	−76	−64
APD_{90} (ms)	390	414	247
AP_Tri (-)	2.8	2.6	1.7
Rate (bpm)	35	61	45
Diastolic Cai (nM)	18	68	154
Systolic Cai (nM)	177	529	873
CTD_{90} (ms)	550	601	407

APA: AP amplitude. MDP: maximum diastolic potential. APD_{90}: AP duration at 90% of repolarization. AP_Tri: AP triangulation ratio, defined as (APD_{40}-APD_{30})/(APD_{80}-APD_{70}). Rate: rate of the spontaneous APs/CaTs. CTD_{90}: CaT duration at 90% decay.

activity (RESAC). If the membrane potential showed small peaks, greater than −40 mV but smaller than 0 mV, not developing APs, the model was labeled as RESAC. Conversely, we considered the model quiescent (Q), i.e. not producing spontaneous AP and CaTs, if during the last 15 s the average membrane potential was smaller than −40 mV or the residual activity's peak potentials were all the smaller than −40 mV.

Sensitivity to Simultaneous Current Blocks

A systematic sensitivity analysis was also conducted by considering simultaneous blocks of I_{Kr} vs I_{CaL} and I_{Na} vs I_{CaL} by blocking (0, 20, 40, 60, 80, 100)% of each current (thirty six tests for each couple of currents). For each test we assessed if the model 1) produced spontaneous APs, 2) triggered repolarization abnormalities or irregular rhythms, 3) showed quiescence or residual activity without or 4) with irregular rhythm after drug administration. Simulations with Paci2020 and Kernik2019 models were run for 500 s, while simulations with Koivumäki2018 were run for 200 s only, due to the long computing time required by this model (only the tests showing irregular rhythm were extended until 500 s to check if it persisted or turned into quiescence or residual activity).

RESULTS

Simulations With the Three Models Yield Different Action Potentials and Ca^{2+} Transients Shapes

Figure 1 reports the spontaneous APs and CaTs produced by the three models in steady state, and **Table 2** summarizes the main AP and CaT morphological features. The AP and CaT traces are quite different, reflecting the fact that hSC-CMs can exhibit remarkable differences, *in silico* as well as *in vitro*, e.g. different AP morphologies (Paci et al., 2017; Kernik et al., 2019). In terms of APs, Koivumäki2018 shows the most triangular ones, with depolarized maximum diastolic potential (MDP) and the shortest AP duration at 90% (APD_{90}). Paci2020 and Kernik2019 show quite similar AP features, in agreement with (Ma et al., 2011), except for the rate of the spontaneous APs, which is almost double in the latter.

In terms of CaT, Paci2020 shows the lowest diastolic and systolic cytosolic Ca^{2+} levels, and CaT amplitude is in agreement with the measurements by Rast et al. (Rast et al., 2015). The Kernik2019 CaT was calibrated on the data from Garg et al. (Garg et al., 2018), after their conversion from fluorescence level to actual concentrations.

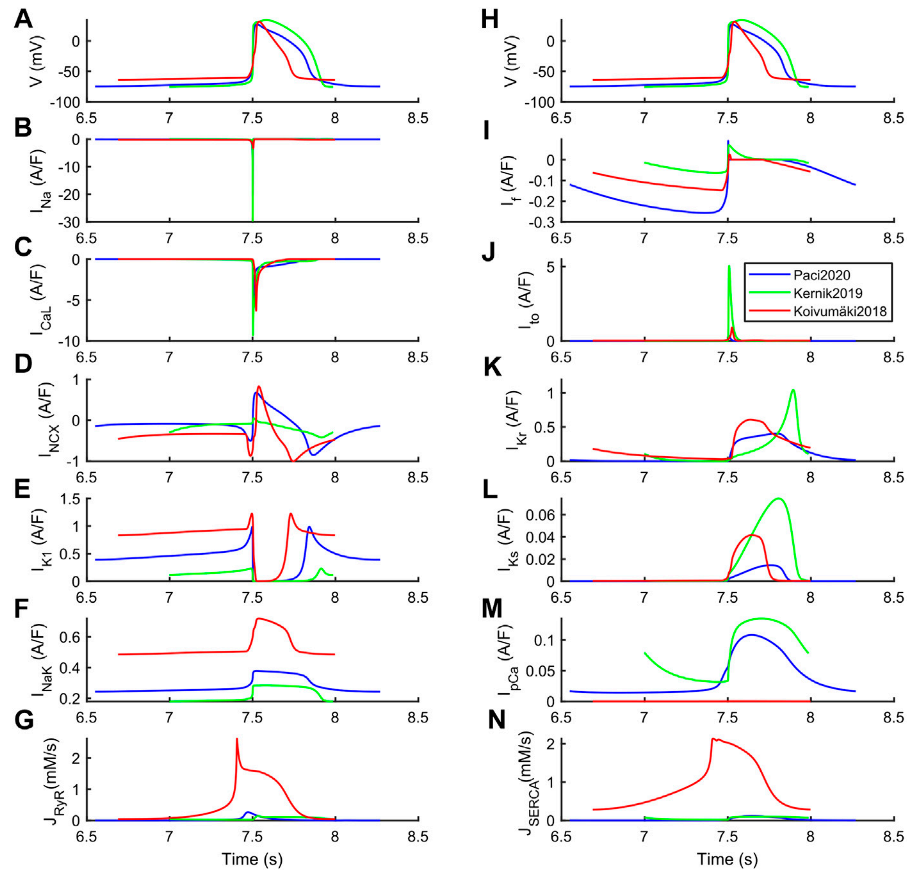

FIGURE 2 | Ion currents underlying the steady-state action potentials in the Paci2020 (blue), Kernik2019 (green) and Koivumäki2018 (red) models. **(A and H)** Membrane potential. **(B)** Fast Na^+ current (I_{Na}). **(C)** L-type Ca^{2+} current (I_{CaL}). **(D)** Na^+-Ca^{2+} exchanger (I_{NCX}). **(E)** Inward rectifying K^+ current (I_{K1}). **(F)** Na^+-K^+ pump (I_{NaK}). **(G)** Ca^{2+} release from sarcoplasmic reticulum (J_{RyR}). **(I)** Funny current (I_f). **(J)** Transient outward K^+ current (I_{to}). **(K)** Rapid delayed rectifying K^+ current (I_{Kr}). **(L)** Slow delayed rectifying K^+ current (I_{Ks}). **(M)** Sarcolemma Ca^{2+} pump (I_{pCa}). **(N)** SERCA pump (J_{SERCA}).

The differences among the three models can be explained based on their steady state ion currents and fluxes, reported in **Figure 2** and further expanded in **Supplementary Figures S1–S3**. Kernik2019 has the greatest I_{Na}, I_{CaL}, I_{to}, I_{Kr} and I_{Ks}. Conversely, it has the smallest I_{K1}, and the highest rate of spontaneous APs (a 20% I_{K1} increment would reduce the spontaneous rate to 38 bpm, similar to the other two models). Paci2020 and Koivumäki2018 show a very similar I_{NCX} shape, coming from the fact that in both models the automaticity is sustained by the pre-upstroke inward component of I_{NCX} (only partly for Paci2020). This pre-upstroke I_{NCX} inward component is missing in Kernik2019. Paci2020 and Koivumäki2018 also have a similar I_{CaL} peak current, and Koivumäki2018 shows the smallest I_{Na} across the three models.

These differences are particularly relevant to understand the different responses to some of the drugs, reported in the next section. The structural differences in the three models are also reflected in their running time. Being characterized by simpler structure and compartmentalization, Paci2020 and Kernik2019 are faster (210 s simulations take 22 s). Conversely, due to its higher complexity, Koivumäki2018 is more than 100 times slower (210 s simulations take 2,331 s). These benchmark simulations were run in Matlab 2017b on a laptop computer (i7 @2.80 GHz and 32 GB memory).

In silico drug tests: characterization of diverse responses in the three models

Before proceeding with an *in vitro–in silico* comparison, we aim to show in detail how the three models react to a specific set of three drugs, namely dofetilide (**Figure 3**), flecainide (**Figure 4**) and nisoldipine (**Figure 5**), each one highlighting a specific mechanism of action.

Dofetilide (**Figure 3**) is a well-known hERG blocker that triggers AP prolongation and repolarization abnormalities, such as EAD and RF. The rationale behind this test is to show how these phenomena are recapitulated by the three models in response to a strong hERG block. These phenomena are recapitulated, as shown in **Figure 3A**, when considering dofetilide I IC_{50} as in **Supplementary Table S1**. For the two lowest doses, 0.001 and 0.01 µM, dofetilide prolongs the APs and CaTs in all three models. However, at the highest concentration (0.1 µM, corresponding to an I_{Kr} 96% block), dofetilide triggers three different behaviors. It prolongs the AP and CaT durations

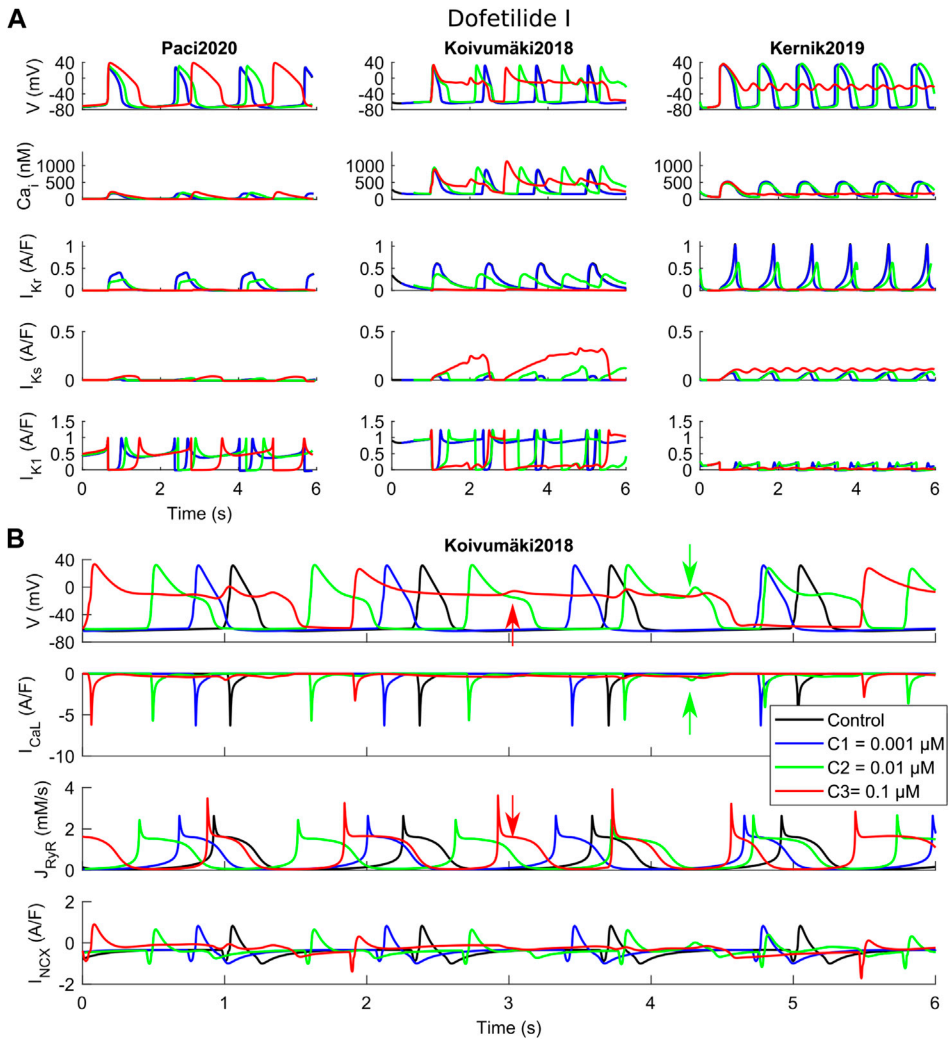

FIGURE 3 | Effects of dofetilide I on the three in silico models for the three tested concentrations (C1, C2 and C3). **(A)** Comparison of action potentials, Ca^{2+} transients and the main K^+ currents. **(B)** Detail of the Koivumäki2018 traces, showing the development of EADs following reactivation of I_{CaL} (green arrows) and spontaneous Ca^{2+} releases from the sarcoplasmic reticulum (red arrows).

in Paci2020, but it does not trigger any repolarization abnormality. In this model, I_{Ks} and the strong I_{K1} can support the late repolarization phase, despite the strong AP prolongation. Conversely, Kernik2019 has a small I_{K1} compared to Paci2020 and Koivumäki2018, which makes it more difficult to stabilize the membrane potential to its diastolic value. In fact, at the highest dofetilide concentration, Kernik2019 fails to repolarize in the late repolarization phase and it sets around −20 mV. Particular attention is paid to Koivumäki2018, which triggers EADs at both intermediate and high concentrations, showing two different mechanisms. At the intermediate concentration, I_{CaL} reactivation occurs, due to the prolonged AP (**Figure 3B**, green arrows). This influx of positive charges depolarizes the membrane potential and generates the EAD. In this example, all the Ca^{2+} releases from the SR are synchronized with the AP upstrokes. At the highest concentration, spontaneous releases of Ca^{2+} from the SR occur (**Figure 3B**, red arrows). They are not synchronized with the AP upstrokes, and instead they happen during the prolonged repolarization phase. Such releases induce an increment in the cytosolic Ca^{2+} concentration, which enhances the inward I_{NCX} component, and then triggers the EAD.

Flecainide blocks primarily I_{Kr} and I_{Na}, but also I_{CaL} to a minor extent, as shown in **Supplementary Table S1**. **Figure 4** shows APs and CaTs when considering flecainide I (as defined in **Supplementary Table S1**). The lowest concentration (1 μM) blocks I_{Na}, I_{Kr} and I_{CaL} by 30%, 40% and 4%, while the intermediate concentration (10 μM) blocks the same currents by 69%, 81% and 28%, respectively. The results illustrate how flecainide stops spontaneous electrical activity, or allows only a residual activity, in Paci2020 and Koivumäki2018, whereas with the Kernik2019 model, beating still occurs spontaneously, showing stronger automaticity. Indeed, in agreement with our *in vitro* data (**Supplementary Figure S7**), both Paci2020 and Kernik2019 show AP/CaT prolongation at low dose. However,

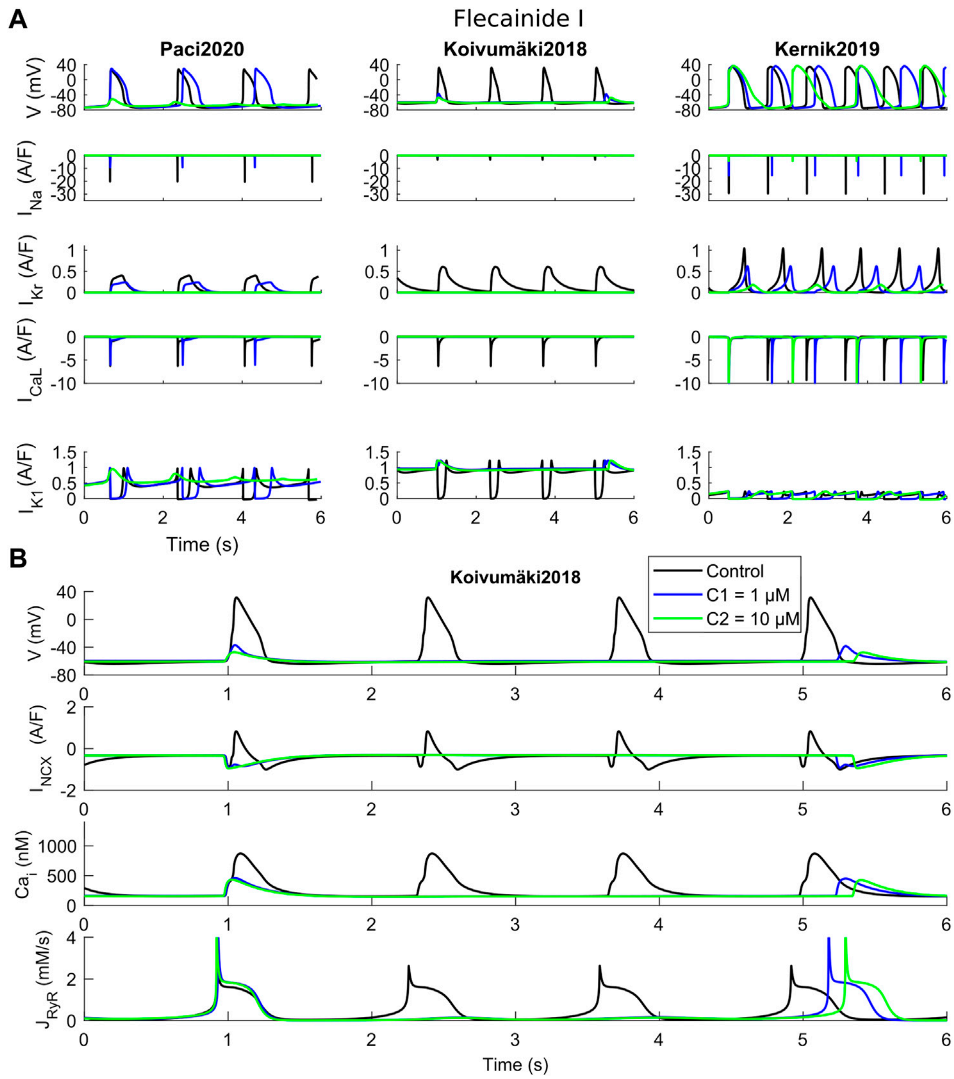

FIGURE 4 | Effects of flecainide I on the three in silico models for the two tested concentrations (C1 and C2). **(A)** Comparison of action potentials, Ca^{2+} transients and ion currents. **(B)** Detail of the Koivumäki2018 traces, showing a residual activity due to spontaneous Ca^{2+} releases from the sarcoplasmic reticulum that activate the inward component of I_{NCX}.

with Paci2020 spontaneous activity stops, not sustained anymore by I_{Na} which is blocked by 69%, while Kernik2019 still produces APs. This phenomenon is even clearer in Koivumäki2018, where I_{Na} is extremely small also in control conditions. Already at the low concentration, APs do not develop anymore, but there is a residual activity, only due to spontaneous Ca^{2+} releases from SR (about every 4 s). These releases trigger the inward I_{NCX} component that slightly depolarizes the membrane potential. Conversely, Kernik2019 maintains its automaticity, despite the strong I_{Na} block: indeed, the authors of the Kernik2019 model reported that the model spontaneously beats also in case of full I_{Na} block. However, flecainide at the intermediate concentration does induce a prolongation of APs and CaTs in the Kernik2019 model.

Nisoldipine is a powerful I_{CaL} blocker, with minor effects also on I_{Na}, I_{NaL}, I_{Kr} and I_{Ks}. The three concentrations considered here, 0.1, 1 and 10 μM, induced I_{CaL} blocks of 85%, 97% and 99%. The rationale behind this test is showing how a strong I_{CaL} blocker can affect the automaticity in the three models. Few seconds after drug administration, Paci2020 and Koivumäki2018 show complete quiescence and a residual activity, respectively, at all three nisoldipine concentrations. The importance of I_{CaL} in the first two models is related to the role of Ca^{2+} handling and I_{NCX} in sustaining the automaticity. As reported in (Koivumäki et al., 2018; Paci et al., 2020), one mechanism sustaining the automaticity is a small inward component of I_{NCX} inducing the depolarization of the membrane potential until it reaches the activation threshold for I_{Na}. After I_{CaL} block, less Ca^{2+} enters the cytosol and is available for the Ca^{2+}-induced Ca^{2+} release, and the Ca^{2+} transient pre-upstroke component becomes smaller and smaller and this reduces the activity of I_{NCX} that cannot support anymore proper automaticity. This phenomenon is particularly

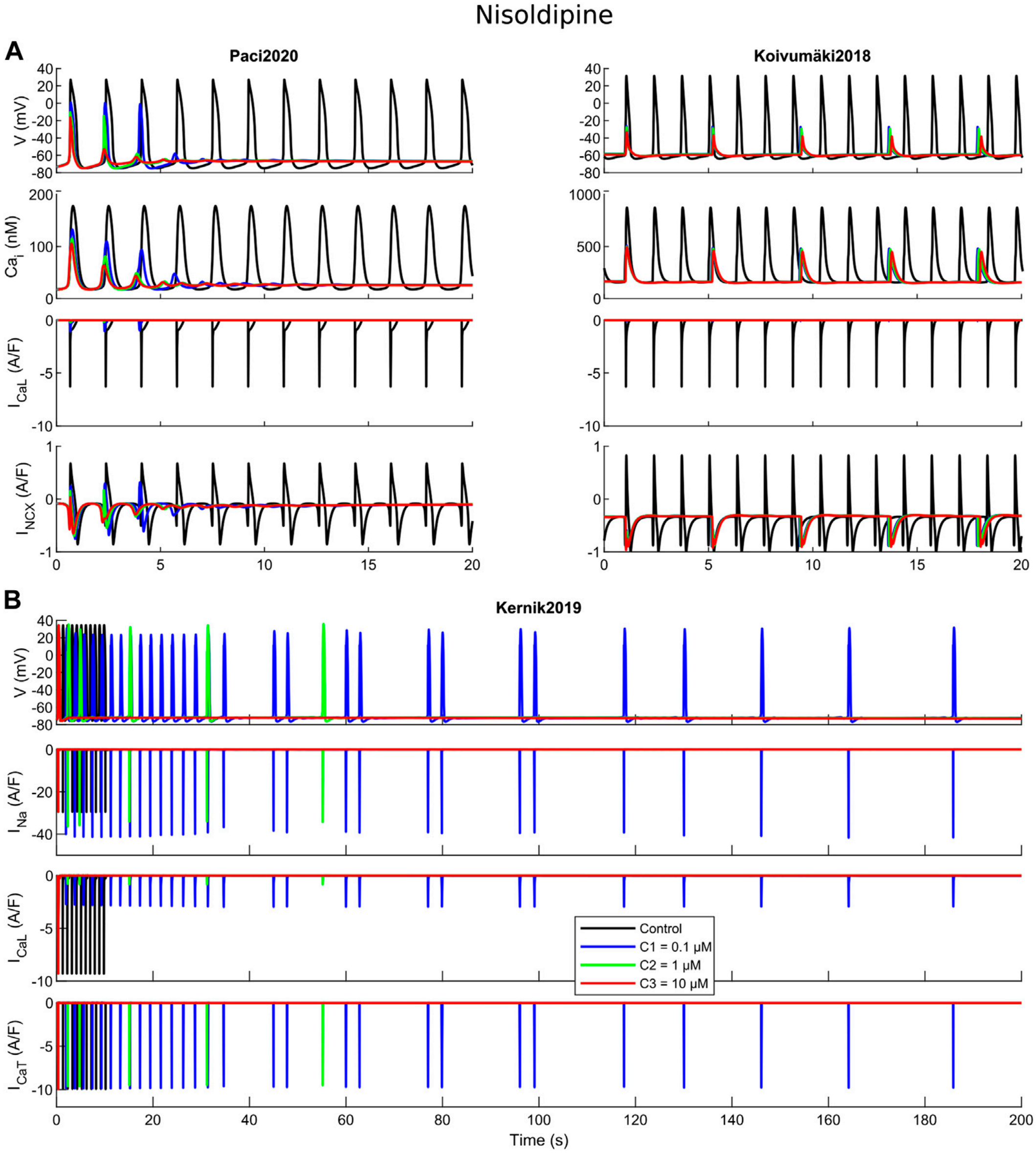

FIGURE 5 | Cessation of the spontaneous electrical activity upon administration of nisoldipine. For all the three tested concentrations (C1, C2 and C3), Paci2020 becomes quiescent and Koivumäki2018 maintains a residual electrical activity not sufficient to trigger action potentials. For concentrations one and two, Kernik2019 shows an irregular rhythm before quiescence, while concentration three terminates immediately the automaticity.

clear in the Paci2020 model (**Figure 5A**). Koivumäki2018 shows a residual activity since it has a greater spontaneous Ca^{2+} release from SR (**Figure 2**) that can still trigger the membrane potential depolarization via I_{NCX} up to about -40 or -30 mV, but not enough to trigger a full AP. I_{CaL} is also fundamental in Kernik2019. Actually, spontaneous APs in Kernik2019 rely more on I_{CaL} than I_{Na}, even in their upstroke phase. This model continues to beat spontaneously with I_{Na} full block (tested up to 1,000 s, not shown): I_{CaL} can compensate the lack of I_{Na} and sustain the upstroke. On the other hand, when I_{CaL} is blocked (e.g. by concentration one), the spontaneous activity slows down and becomes irregular, until it stops. Kernik2019 can also count on an additional depolarizing current, not present in the other two models: I_{CaT}. Combining nisoldpine at concentration two with the full I_{CaT} block, the automaticity terminates upon *in silico* drug administration.

In order to generalize the results obtained for dofetilide, flecainide and nisoldipine, we ran a sensitivity analysis by testing the simultaneous current blocks showed in **Figure 6**: I_{Kr} vs I_{CaL} (**Figures 6A–C**) and I_{Na} vs I_{CaL} (**Figures 6D–F**). Firstly, the Paci2020 model does not develop repolarization abnormalities in response to I_{Kr} block, Kernik2019 responds to high I_{Kr} block only with repolarization failures, while Koivumäki2018 develops multiple repolarization abnormalities

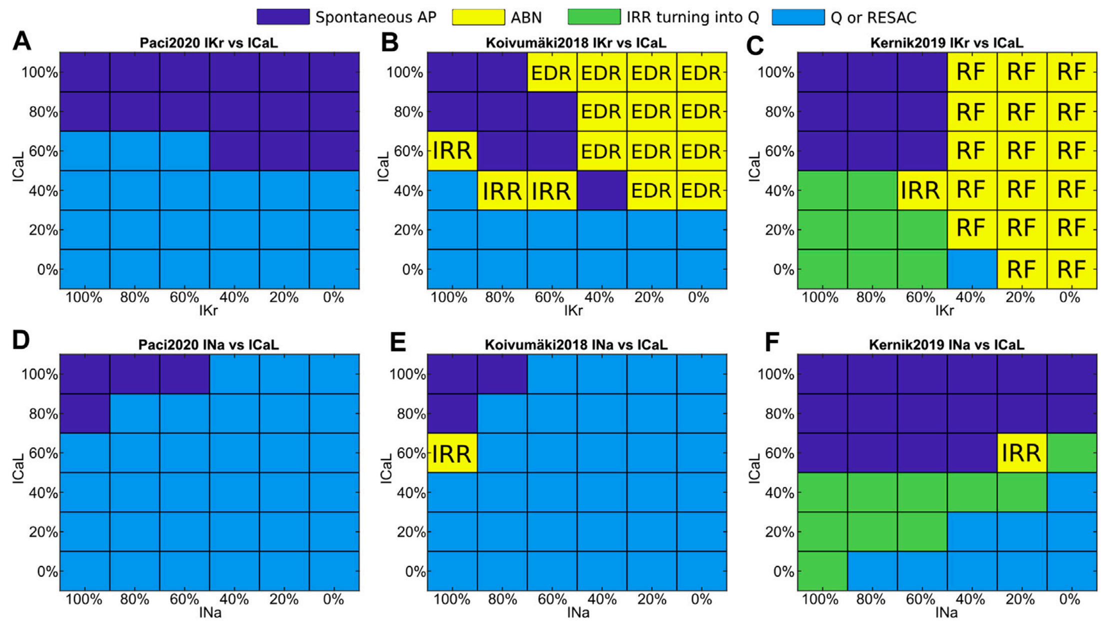

FIGURE 6 | Sensitivity maps to simultaneous I_{Kr} and I_{CaL} blocks **(A and B, C)** or I_{Na} and I_{CaL} blocks **(D and E, F)**. Color code: Spontaneous APs, blue; quiescence or residual activity, cyan; transient irregular rhythm turning into quiescence, green; arrhythmic events, yellow. The yellow squares include also the event type: irregular rhythm (IRR), repolarization failure (RF), and simultaneous occurrence of EAD, DAD and repolarization failure (EDR).

(EADs, DADs and RF). Secondly, Koivumäki2018 and Paci2020 are more sensitive to I_{Na} block than Kernik2019 (**Figures 6D–F**). They show much smaller I_{Na} peaks (**Figure 2**), and this I_{Na} cannot sustain the upstroke in case of ~50% block for Paci2020 and ~30% block for Koivumäki2018. This is clear in case of blockade of Na^+ currents (e.g., mexiletine I, II, III at concentration three and lidocaine II at concentration two), which impairs automaticity in all models but Kernik2019 (that shows spontaneous APs also with I_{Na} fully blocked) (**Figure 6F**). Thirdly, Koivumäki2018 and Paci2020 are the most sensitive to I_{CaL} block. Finally, Kernik2019 has the strongest automaticity. This has been confirmed also by additional tests (not shown), e.g. Kernik2019 spontaneous activity lasts about 400 s in conditions of 90% I_f block, and a 90% I_{NCX} block does not stop the spontaneous APs and CaTs as observed in Paci2020 and Koivumäki2018. For some of the drugs blocking at the same time I_{CaL} and I_{Kr} (e.g. moxifloxacin I, II at concentration two or bepridil I, II, III at concentration two), this enables Kernik2019 to trigger repolarization abnormalities typical of I_{Kr} block, when the other models show residual or cessation of spontaneous activity.

In silico Drug Tests: Comparison With the *in vitro* Results

A detailed *in vitro–in silico* comparison is presented in **Figure 7**, **Supplementary Figures S5–S7** and **Supplementary Table S2**. **Figure 7** and **Supplementary Table S2** report the *in silico* drug trial results and the comparison with the *in vitro* experiments in terms of CTD_{90} percent variations, occurrence of arrhythmic events, and cessation of automaticity, also for the alternative drug formulations not shown in **Supplementary Figures S5–S7**. In these three supplementary figures, we graphically report the percent *in vitro* and *in silico* CTD_{90} variations, arrhythmic events or the cessation of the spontaneous activity, and the main mechanisms of action, for the 15 drugs in the panel. If an *in vitro* or *in silico* CTD_{90} data is missing, it means that the spontaneous activity stopped, or an arrhythmic event prevented measuring CTD_{90}. *In vitro*, most of the drugs induced prolongation of CTD_{90}, except nimodipine, nisoldipine and verapamil. Bepridil, flecainide, lidocaine, mexiletine, phenytoin and ranolazine did not induce arrhythmic events, despite all but ranolazine stopping the spontaneous activity at the highest doses in at least a few cells.

The *in silico* results with the three models are in agreement (all showing consistent CTD_{90} prolongation or shortening). In absence of arrhythmic events, all the three models showed smaller CTD_{90} changes than *in vitro* experiments, e.g. sparfloxacin at concentration two prolonged by 42% *in vitro* CaTs, while *in silico* sparfloxacin I induced 17% prolongation in Koivumäki2018 and less than 10% prolongation in Paci2020 and Kernik2019. The extreme prolongations for Koivumäki2018 for dofetilide, flecainide II and III (concentration one), and moxifloxacin III (concentration one) are due to computing CTD_{90} manually on EADs. We did not compute the CTD_{90} for $BaCl_2$ concentrations two and three for Kernik2019. In fact, I_{K1} block slightly depolarizes the maximum diastolic potential in Kernik2019 but not to the extent to trigger a repolarization failure (**Supplementary Figure S4**). However, the membrane potential and cytosolic Ca^{2+} start oscillating at a high rate and these oscillations do not have the morphology of CaTs.

Illustrative arrhythmic events and abnormal rhythms are presented in **Figure 8**. Paci2020 did not show arrhythmic events for any drug but for the maximum concentration of

Drug	Conc. (μM)	In vitro $\Delta CTD_{90}\%$	In vitro ARR, AC	Paci2020 $\Delta CTD_{90}\%$, ARR, AC			Koivumäki2018 $\Delta CTD_{90}\%$, ARR, AC			Kernik2019 $\Delta CTD_{90}\%$, ARR, AC		
BaCl2	1	5	X	4			6			-3		
	10	20	OTH 1/6	29			83* ER			**		
	100	47	VT 1/6; OTH 2/6	RF			RF			**		
Bepridil	1	65	X	Q	Q	25	RESAC	RESAC	RESAC	RF	RF	RF
	10	151	Q 5/6	Q	Q	Q	RESAC	RESAC	RESAC	Q	Q	Q
Dofetilide	0.001	29	X	1	1	17	1	0	881* EDR	0	0	12
	0.01	75	EAD 2/6	14	7	35	277* EDR	8	523* EDR	8	4	RF
	0.1	645	EAD 4/6; VT 4/6	65	35	62	503* EAD; RF	610* EDR	641* EDR	RF	RF	RF
Flecainide	1	45	X	16	14	20	RESAC	219* EDR	599* EDR	7	8	RF
	10	78	Q 2/6	Q	Q	Q	RESAC	RESAC	RESAC	19	RF	RF
Lidocaine II	10	50	X	2			5			1		
	100	81	X	Q			RESAC			4		
Mexiletine II	10	26	Q 3/6	0			7			2		
	100	130	Q 4/6	Q			RESAC			12		
Moxifloxacin	30	32	X	3	3	12	9	9	141* EDR	4	4	8
	300	179	EAD 1/6	Q	Q	30	RESAC	RESAC	RF	RF	RF	RF
Nimodipine	0.1	7	Q2/6	Q			IRR			-7		
	1	-14	VT 1/6; Q 2/6	Q			RESAC			IRR		
Nisoldipine	0.1	31	X	Q			RESAC			IRR; Q		
	1	32	VT 4/6; Q 2/6	Q			RESAC			IRR; Q		
	10	-32	X	Q			RESAC			Q		
Phenytoin	3	24	X	-5			0			-1		
	30	15	Q 1/6	Q			RESAC			-8		
Primidone	1	31	OTH 1/6	0			1			0		
	10	6	OTH 1/6	0			0			0		
Procainamide	10	36	X	-1			1			0		
	100	89	EAD 1/6	-3			9			2		
Ranolazine	1	34	X	2	6		3	7		1	3	
	10	48	X	14	20		RESAC	591* EDR		8	RF	
Sparfloxacin	1	38	X	1	1		2	2		1	1	
	10	42	X	9	8		17	13		6	5	
	100	86	EAD 2/6; Q 1/6; OTH 2/6	Q	Q		386* EDR	324* EDR		RF	RF	
Verapamil	0.01	25	X	-2	-9	-1	1	-1	0	0	-1	0
	0.1	-20	VT 2/6; Q 2/6	Q	Q	Q	8	IRR	2	1	-7	-2

-100% 0% +100%

FIGURE 7 | Qualitative and quantitative comparison of *in silico* drug tests in the three hSC-CM models against our *in vitro* data, for the 15 reference compounds. For each drug we report i) the tested concentrations, ii) the percent CaT duration variation with respect to baseline ($\Delta CTD_{90}\%$), arrhythmic events (ARR) and automaticity cessation (AC) recorded *in vitro* and *in silico*. Arrhythmic events: early and delayed after-depolarization (EAD, DAD), repolarization failure (RF), irregular rhythm (IRR), ventricular tachycardia-like rhythm (VT) and other arrhythmic events (OTH). Automaticity cessation (AC): quiescence (Q) and residual activity (RESAC). Q and RESAC are not considered pro-arrhythmic. For Koivumäki2018, the $\Delta CTD_{90}\%$ marked with a star were computed on EADs and the model showed arrhythmic patterns including the combination of EADs, DADs and RF (shortened as EDR) or EADs and RF (shortened as ER). For Kernik2019, two stars in $BaCl_2$ mean high rate $Ca2^+$ oscillations and depolarized maximum diastolic potential, but no RF. When multiple combinations of IC_{50} and Hill coefficient were tested in simulation for the same compound, the corresponding *in silico* results consist of multiple sub-columns. In case of no *in vitro* arrhythmic events, the corresponding cell contains an X. An expanded version of this table is presented in the Supplementary material as **Supplementary Table S2**.

$BaCl_2$ where it failed to repolarize (**Figure 8A**). It also showed the greatest CTD_{90} prolongations with no EADs among the three models (e.g. dofetilide III +62%). Furthermore, it simulated well the cessation of the spontaneous activity (Q) for drugs mainly blocking Na^+ currents (e.g., mexiletine and lidocaine), I_{CaL} (e.g., nimodipine, nisoldipine and phenytoin), or a mixed combination of IC_{50} (e.g. bepridil, flecainide and sparfloxacin) (**Figure 8D**).

Conversely, Koivumäki2018 was the most sensitive one, triggering arrhythmic events, e.g. EAD and RF, for most of the drugs affecting the K^+ currents ($BaCl_2$, dofetilide and sparfloxacin) (**Figure 8B**). It never showed a complete stop of the spontaneous activity, but responded with a residual activity (RESAC), i.e. small depolarization of the membrane potential with peaks reaching about −30 mV, that cannot be considered APs (**Figure 8E**). This happened consistently with the quiescence of Paci2020 and the *in vitro* data, in case of drugs affecting mainly I_{Na} or I_{CaL}.

Kernik2019 never produced EADs, but it responded with RF in most of the cases when the Koivumäki2018 model showed arrhythmogenic events (**Figure 8C**). Kernik2019 maintained also its automaticity in all the cases the Paci2020 and the Koivumäki2018

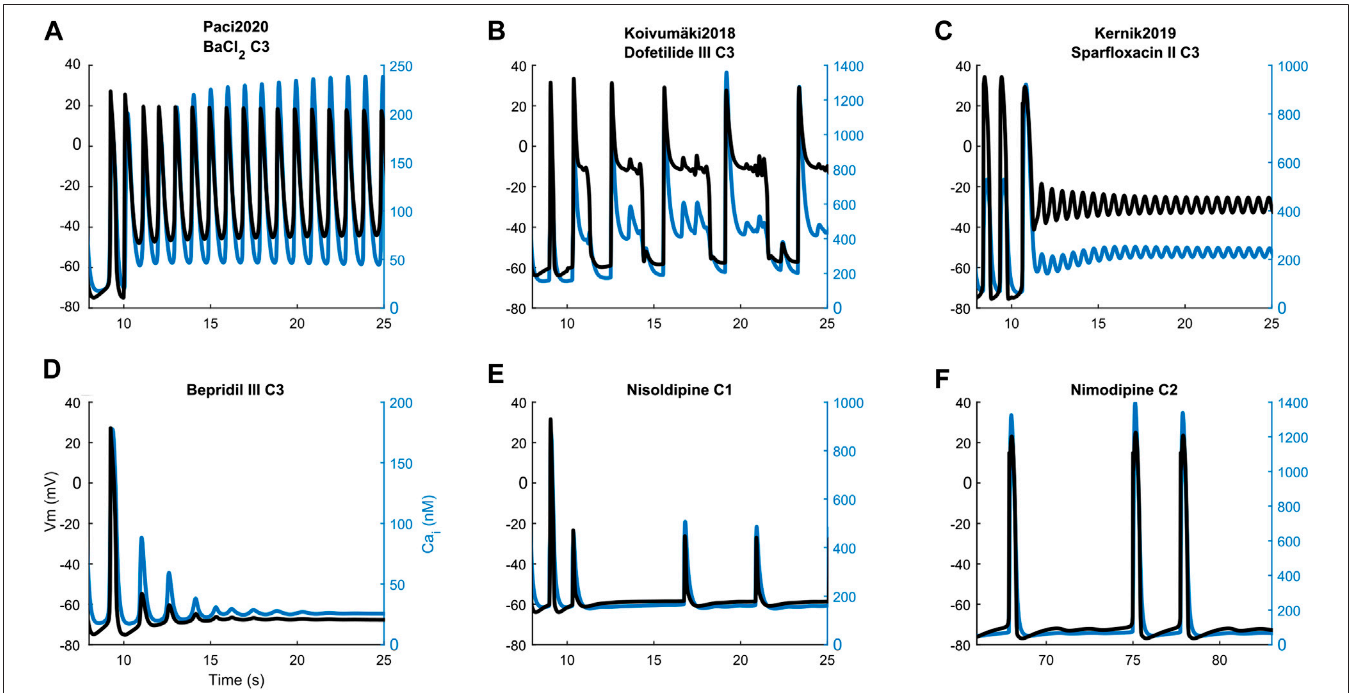

FIGURE 8 | Illustrative action potential (black) and Ca^{2+} transient (blue) arrhythmic rhythms, abnormalities and the cessation of spontaneous activity produced by the three models. Paci2020: repolarization failure **(A)**, quiescence **(D)**. Koivumäki2018: early after-depolarizations **(B)** and residual activity **(E)**. Kernik2019: repolarization failure **(C)** and irregular rhythm **(F)**. The drug concentrations are reported as C1, C2 and C3, consistently with **Supplementary Table S2**.

models showed quiescence or residual activity, except for nimodipine (**Figure 8F**) and nisoldipine, where it also showed cases of irregular rhythm (IRR). Nonetheless, these irregular rhythms lasted only 320 s (nimodipine concentration one) and 250 s (nisoldipine concentration one), then the automaticity stopped consistently with the other two models. None of the models showed ventricular tachycardia-like events that were on the contrary observed *in vitro*.

In silico Drug Tests: Influence of Different IC_{50} and Ion Channel Characterizations

The same drug can have different effects in the same model (**Figure 7**), according to the drug characterization in terms of IC_{50} magnitude and how many ion channels were considered in the specific characterization. In fact, we used multiple characterizations for seven drugs, as in (Passini et al., 2017). For example, moxifloxacin I and II show consistent results in each of the three models. On the contrary, moxifloxacin III triggers different responses in Paci2020 (concentration two does not stop automaticity as it happens for moxifloxacin I and II) and Koivumäki2018 (concentration one triggers EADs and DADs instead of CTD_{90} prolongation and concentration two fails the repolarization). This is explained by the fact that characterizations moxifloxacin I and II show very similar IC_{50} and act on the same ion currents (I_{Na}, I_{Kr} and I_{CaL}), while moxifloxacin III does not block I_{Na} and I_{CaL} (that the sensitivity analysis demonstrated fundamental to keep the automaticity in Paci 2019 and Koivumäki2018), acting only on I_{Kr}, I_{Ks} and I_{NaL} (which is present only in Paci2020 as individual ion current). Therefore, the results for moxifloxacin I and II are typical of an I_{Na} and/or I_{CaL} blocker, while moxifloxacin III behaves mainly as K^+ current blocker. The same considerations can be also done for ranolazine I and II, which have different effects at concentration two in Koivumäki2018 (residual activity vs EADs and DADs).

DISCUSSION

In this work, we analyze and compare the simulated response of three recent *in silico* models of hSC-CM in control and under 15 drugs action, in terms of CaT duration, pro-arrhythmic behavior and automaticity. A comparison is also conducted between simulations with the three models and corresponding *in vitro* experiments on hSC-CMs. The generated insights provide a characterization and comparison of the three models that could inform selecting the model best suited for specific applications. The main contributions of our work are:

- The three models show qualitatively consistent *in silico* results in terms of CTD_{90} prolongation and shortening for specific drugs.
- The three models show different susceptibility to drug-induced pro-arrhythmic events. Paci2020 is the least prone to develop them, whereas Kernik2019 produces repolarization failures and Koivumäki2018 exhibits the

highest variety of events (including EADs and DADs) and triggering mechanisms (I_{CaL} reactivation and spontaneous Ca^{2+} releases from SR).

- The strength of the automaticity is different across the three models. Kernik2019 shows the strongest spontaneous activity, supported by a combination of inward currents where I_{CaL} plays a fundamental role. Paci2020 and Koivumäki2018 are more sensitive to drug-induced impairment of automaticity, being mainly supported by Ca^{2+} handling and I_{NCX}.
- The three models simulate CTD_{90} percent variations qualitatively in agreement, even though smaller, than the specific *in vitro* data considered here.
- For compounds with multiple experimental ion channel data, the sets of ion channels taken into account (e.g. I_{Na}, I_{Kr}, I_{CaL} vs I_{Kr} only) and the variations in IC_{50} and Hill values can lead to divergent simulation results, e.g. the AP/CaT prolongation and the occurrence of pro-arrhythmic events (typical of K^+ current blockers), or the depolarization impairment and suppression of hSC-CM automaticity (typical of Na^+ and Ca^{2+} blockers). The input ion channel data are therefore essential in determining the results of *in silico* drug tests.

Origins and Basic Features of the Three Human Stem Cell-Derived Cardiomyocyte Models

Since the proposal of the Comprehensive *in vitro* Proarrhythmia Assay (CiPA) initiative (Colatsky et al., 2016; Strauss et al., 2019), the acceptance of hSC-CMs and *in silico* models in the field of pharmacology and drug safety has increased steadily. As a consequence, the number of hSC-CM *in silico* models available has also increased. At the time of the publication of the first *in silico* hSC-CM model (Paci et al., 2013), a limited amount of *in vitro* data was available in spite of the seminal work by Ma et al. (Ma et al., 2011), that represented the most complete characterization of ion currents and APs from control hSC-CMs. Due to the growing interest in the hSC-CM technology and its applications, additional experimental data were published, enabling the development of more sophisticated hSC-CM models (Paci et al., 2018b; Paci et al., 2020; Koivumäki et al., 2018; Kernik et al., 2019).

The first Paci model, Paci 2013 (Paci et al., 2013), was developed entirely based on the Ma et al. (Ma et al., 2011) dataset (Ma 2011) and additional *in vitro* data from cardiomyocytes derived from human embryonic stem cells for the ion currents missing in the Ma et al. dataset. Its structure closely resembles the structure of the TenTusscher hV-CM model (ten Tusscher et al., 2004). Over the years, many new Paci models were released (Paci et al., 2015; Paci et al., 2017; Paci et al., 2018b; Paci et al., 2020), integrating more mechanisms based on new *in vitro* data, e.g. I_{NaL} (Ma et al., 2013) or a more accurate Ca^{2+} handling calibrated on in-house measurements, described in (Paci et al., 2018b). The Paci2020 model used in this paper is the latest one and, in addition to being able simulate all the mechanisms successfully reproduced by its predecessors, it also encapsulates a more physiological description of the mechanisms underlying the hSC-CM automaticity, i.e. the joint role of I_f and I_{NCX} in sustaining the hSC-CM spontaneous electrical activity.

The Koivumäki2018 model was mainly based as well on the Ma2011 dataset, but it included also new in-house measurements of I_{CaL} (Koivumäki et al., 2018). Many currents (e.g. I_{to}, I_{Kr}, I_{Ks}, I_{K1}) in Koivumäki2018 shared the same structure (with conveniently tuned parameters) observed in the Paci models. A core difference with respect to the Paci models, is a more detailed description of the cell topology. Without need of partial differential equations, Koivumäki2018 can accurately simulate the spatial diffusion of Ca^{2+} in the cytosol, showing good agreement with the *in vitro* data. The formulation was inherited from a previous model of cardiomyocyte derived from mouse embryonic stem cells (Korhonen et al., 2008). However, such refined description of Ca^{2+} diffusion comes at the cost of 100 times longer simulation time.

The Kernik2019 model (Kernik et al., 2019) adopts the same "simple" structure of the Paci models, while integrating a plethora of additional new *in vitro* data (Bellin et al., 2013; Cordeiro et al., 2013; Ma et al., 2015; Es-Salah-Lamoureux et al., 2016; Herron et al., 2016; Veerman et al., 2016; Li et al., 2017; Garg et al., 2018), in addition to the well-known Ma2011 dataset; see **Table 1** in the original Kernik et al. publication. However, the authors reformulated seven key ion currents (I_{Na}, I_{CaL}, I_{Kr}, I_{Ks}, I_{K1}, I_{to} and I_f). Their motivation was to compensate the lack of time constant information in several published datasets of hSC-CM voltage-clamp data: remarkably, they fit the normalized current recordings to single exponential functions in order to estimate activation/inactivation time constants, to be used then to optimize model parameters. The remaining ion currents followed canonical formulations from literature, e.g. (Shannon et al., 2004; ten Tusscher et al., 2004). Given the shared model structure, Kernik2019 and Paci2020 have similar computing time.

At the time of this paper, two more hSC-like CM models were published, based on reparameterization of hV-CMs models: Zhang et al. (Zhang et al., 2012) and Lemoine et al. (Lemoine et al., 2018). However, their inclusion was out of the scope of this study.

Drug Responses *in vitro* and *in silico*

The three models simulated consistently drug-induced changes in CTD_{90}, all showing CaT prolongation or shortening for the same drug. Although qualitatively in agreement with the *in vitro* experiments, all three models showed smaller percentage variations.

The models demonstrated different susceptibility to generating repolarization abnormalities, summarized in **Figure 7**, **Supplementary Figures S5–S7** and **Supplementary Table S2**. Paci2020 showed the lowest number of arrhythmic events: the repolarization failure only for the highest concentration of I_{K1} blocker $BaCl_2$. In case of drugs blocking I_{Kr}, this model consistently prolonged the duration of the CaT, but no EAD or DAD appeared. Kernik2019 failed to repolarize in response to six drugs (for at least one formulation in case of multiple drug formulations) blocking prevalently I_{Kr}, although it never developed EADs or DADs. Finally, Koivumäki2018 showed the highest variety of arrhythmic events, including EADs, DADs, repolarization failure and irregular rhythm for nine drugs. The drugs that triggered arrhythmic events in Koivumäki2018 and Kernik2019 were all classified as "Known Risk of TdP" by CredibleMeds (Woosley et al., 2020), except for Ranolazine

("Conditional Risk of TdP"), $BaCl_2$ and Nimodipine (not reviewed) and Verapamil (not classified).

Automaticity is one key-feature of hSC-CMs, being a macromarker of the successful differentiation into CMs, but also a sign of hSC-CM immaturity when compared to adult cardiac cells. Automaticity in Paci2020 and Koivumäki2018 stopped (or produced minor residual electrical activity) for the drugs strongly blocking I_{Na} and/or I_{CaL} (e.g. bepridil, ranolazine I, flecainide, lidocaine, mexiletine, nimodipine, nisoldipine and phenytoin). Conversely, only bepridil and nisoldipine, Ca^{2+} current blockers, terminated the spontaneous electrical activity in Kernik2019: this model exhibited the stronger automaticity, as we report in our sensitivity analysis (**Figure 6**).

It must be noted that the *in vitro* data included observations of six recordings, and only a few of them showed arrhythmic events or quiescence following drug administration, thus highlighting variability in the *in vitro* responses. This is not different from the behavior of the three *in silico* models.

Since *in silico* drug tests are based on simulations, not only the biophysical accuracy of the models, but also the precision of the characterization of drugs is critical (in terms of what ion channels are affected and to what extent). Our tests showed that the effect of a certain drug concentration can be very different depending on the *in vitro* characterization, e.g. moxifloxacin I and II vs moxifloxacin III. Recently, Zhou et al. (Zhou et al., 2020) demonstrated how reducing the amount of ion currents considered in drug characterizations (e.g. I_{Na}, I_{Kr} and I_{CaL} vs I_{Kr} only) reduces the specificity of the *in silico* predictions, marking safe drugs as at risk. The same authors examined also how moderate changes in IC_{50} and variable Hill coefficients (representing the steepness of the drug dose-response curves) lead to divergent predictions using the same population of hV-CM models, e.g. for sotalol and verapamil.

Accounting for Variability

High phenotypical and electrophysiological variability is one key feature of hSC-CMs and one of the reason of skepticism (together with their structural immaturity (Knollmann, 2013; Koivumäki et al., 2018)) when using them in real-world applications, where results should be then translated to the human. However, it is important to acknowledge that, despite the limitations, *in vitro* drug tests on hSC-CMs showed already their capability to meet and surpass traditional preclinical tests on animal models, considering as metric the CaT prolongation (Pfeiffer et al., 2016).

A recent work by Biendarra-Tiegs et al. (Biendarra-Tiegs et al., 2019) identifies many potential sources of variability in producing induced pluripotent stem cells (abnormalities at genetic/epigenetic level, differences among donors, endogenous signaling and extrinsic factors such as culture conditions, media, substrate, pH) and differentiating them into cardiomyocytes (differentiation methods, maturation protocols and level of maturation of hSC-CMs when *in vitro* measurements are done). By deep-diving in the eleven *in vitro* datasets used to build the three *in silico* models here studied, we observe already many potential sources of variability:

- Four datasets used only iCell pluripotent stem cells (including the Ma2011 dataset, used for all the three models), six datasets used only in-house cells from donors, in most cases healthy, but e.g. Bellin et al. report fibroblasts from a LQT2 patient (hSC-CMs were corrected later) (Bellin et al., 2013). For the dataset from (Ma et al., 2015), the authors used both iCell hSCs (for control) and in-house hSC-CMs produced from a LQT1 patient.
- Combinations of different reprogramming factors were used to induce the pluripotency in the in-house cells from donors, e.g. combinations from (Takahashi et al., 2007; Yu et al., 2007).
- Different methods were used to differentiate hSCs into CMs: embryoid bodies (e.g. (Garg et al., 2018)), coculturing with mouse visceral endodermal-like cells (END-2) (e.g. in-house cells for the Paci2020 model), modulation of the WNT signaling (e.g. in-house cells for I_{CaL} measures for the Koivumäki2018 model and (Ma et al., 2015)).

There is clear need for standardization for *in vitro* hSC-CM drug assays. For example, Blinova et al. (Blinova et al., 2018) demonstrated that, despite hSC-CM variability, good consensus can be achieved across multiple laboratories on drug test results, by means of a scrupulously planned multi-site study. In addition to the differences in the equations and structures of the Paci2020, Koivumäki2018 and Kernik2019 models, the aforementioned sources of variability identified in the *in vitro* datasets could play a role in the differences in the APs and CaTs simulated by the three *in silico* models, also in basal conditions.

Nevertheless, it is not common considering sources of variability such as differences among donors or maturation level when modeling the electrophysiology of hSC-CMs. What has been already done with the three *in silico* models we considered is to account for the *in vitro* variability observed in AP features, responses to drugs, and sensitivity to channelopathies by developing *in silico* hSC-CM populations, following different approaches. In (Paci et al., 2020), Paci et al. randomly sampled 22 models parameters (maximum conductances and dynamic parameters, covering all the main ion currents/exchangers/pumps in the model) using the Latin Hypercube sampling, thus obtaining a random population. The random population was then experimentally calibrated using AP and CaT features. Kernik et al. followed a different approach, sampling the model parameters (five dynamic parameters and maximum conductance for five ion currents) from independent distributions, each one centered on the baseline value of each of the chosen parameters. Also, Koivumäki2018 was used as baseline for a population where seven maximum conductances/currents were sampled according to literature data, but only two AP features (maximum diastolic potential and AP peak) were used as exclusion criteria.

CONCLUSION

In this paper, we investigate the simulated response of three hSC-CM models to drug action in order to 1) highlight the differences in their principal functional features, and 2) compare their drug responses, based on a panel of *in vitro* data. We extract the following recommendations.

- In order to assess the potential arrhythmogenic activity of a compound on a single simulation, Koivumäki2018 might be the best option because of its high sensitivity to I_{Na}, I_{CaL} and I_{Kr} blocks. However, Koivumäki2018 could predict an excess of false positives. Also, for a population-based study, the Koivumäki2018 model requires an excessively long running time.
- To account for hSC-CM variability (in terms of responses to drugs and sensitivity to channelopathies), the Paci2020 and Kernik2019 models are more suitable to be baselines for populations of *in silico* models. Furthermore, because of the very similar structure and running time of Paci2020 and Kernik2019, variability could also be simulated in population-based studies not only by sampling parameters (according to the techniques presented in this section), but also by using both models as baselines for a hybrid population.

Our simulation study shows differences in the drug responses across the different hSC-CM models, which could reflect the variability in the *in vitro* data used to design them and, more generally, of the results of *in vitro* drug tests done on hSC-CMs.

DATA AVAILABILITY STATEMENT

The raw data supporting the conclusions of this article will be made available on request by contacting the authors, without undue reservation.

AUTHOR CONTRIBUTIONS

MP, EP and BR conceived and designed the study. HRL and DJG performed the experimental drug assays. MP and EP performed the *in silico* drug assays. MP and JTK analyzed the *in silico* data and prepared the figures. MP, JTK, EP and BR drafted the manuscript. All the authors interpreted the results and revised the manuscript.

FUNDING

MP was supported by the Academy of Finland (decision number 307967) and by the Finnish Cultural Foundation (Central Fund, grant number 00160735). JTK was supported by the Academy of Finland Center of Excellence in Body-on-Chip Research and the Pirkanmaa regional fund of the Finnish Cultural Foundation (grant numbers 50171514 and 50201322). EP and BR were supported by an NC3Rs Infrastructure for Impact Award (NC/P001076/1), a Wellcome Trust Senior Research Fellowship in Basic Biomedical Sciences (214290/Z/18/Z), the CompBioMed project (European Commission grant agreement No. 823712), the Oxford BHF Center of Research Excellence (RE/13/1/30181), and the TransQST project (Innovative Medicines Initiative 2 Joint Undertaking under grant agreement No. 116030, receiving support from the European Union's Horizon 2020 research and innovation program and EFPIA).

SUPPLEMENTARY MATERIAL

The Supplementary Material for this article can be found online at: https://www.frontiersin.org/articles/10.3389/fphar.2021.604713/full#supplementary-material.

REFERENCES

Bellin, M., Casini, S., Davis, R. P., D'Aniello, C., Haas, J., Ward-van Oostwaard, D., et al. (2013). Isogenic human pluripotent stem cell pairs reveal the role of a KCNH2 mutation in long-QT syndrome. *EMBO J.* 32, 3161–3175. doi:10.1038/emboj.2013.240

Bezzerides, V. J., Zhang, D., and Pu, W. T. (2017). Modeling inherited arrhythmia disorders using induced pluripotent stem cell-derived cardiomyocytes. *Circ. J.* 81, 12–21. doi:10.1253/circj.CJ-16-1113

Biendarra-Tiegs, S. M., Secreto, F. J., and Nelson, T. J. (2019). Addressing variability and heterogeneity of induced pluripotent stem cell-derived cardiomyocytes. *Adv. Exp. Med. Biol.* 6, 1–29. doi:10.1007/5584_2019_350

Blinova, K., Dang, Q., Millard, D., Smith, G., Pierson, J., Guo, L., et al. (2018). International multisite study of human-induced pluripotent stem cell-derived cardiomyocytes for drug proarrhythmic potential assessment. *Cell Rep.* 24, 3582–3592. doi:10.1016/j.celrep.2018.08.079

Brennan, T., Fink, M., and Rodriguez, B. (2009). Multiscale modelling of drug-induced effects on cardiac electrophysiological activity. *Eur. J. Pharm. Sci.* 36, 62–77. doi:10.1016/j.ejps.2008.09.013

Colatsky, T., Fermini, B., Gintant, G., Pierson, J. B., Sager, P., Sekino, Y., et al. (2016). The comprehensive *in Vitro* Proarrhythmia assay (CiPA) initiative — update on progress. *J. Pharmacol. Toxicol. Methods* 81, 15–20. doi:10.1016/j.vascn.2016.06.002

Cordeiro, J. M., Nesterenko, V. V., Sicouri, S., Goodrow, R. J., Treat, J. A., Desai, M., et al. (2013). Identification and characterization of a transient outward K+ current in human induced pluripotent stem cell-derived cardiomyocytes. *J. Mol. Cell. Cardiol.* 60, 36–46. doi:10.1016/j.yjmcc.2013.03.014

de Korte, T., Katili, P. A., Mohd Yusof, N. A. N., van Meer, B. J., Saleem, U., Burton, F. L., et al. (2020). Unlocking personalized biomedicine and drug discovery with human induced pluripotent stem cell–derived cardiomyocytes: fit for purpose or forever elusive?. *Annu. Rev. Pharmacol. Toxicol.* 60, 529–551. doi:10.1146/annurev-pharmtox-010919-023309

Es-Salah-Lamoureux, Z., Jouni, M., Malak, O. A., Belbachir, N., Al Sayed, Z. R., Gandon-Renard, M., et al. (2016). HIV-Tat induces a decrease in I Kr and I Ks via reduction in phosphatidylinositol-(4,5)-bisphosphate availability. *J. Mol. Cell. Cardiol.* 99, 1–13. doi:10.1016/j.yjmcc.2016.08.022

Garg, P., Oikonomopoulos, A., Chen, H., Li, Y., Lam, C. K., Sallam, K., et al. (2018). Genome editing of induced pluripotent stem cells to decipher cardiac channelopathy variant. *J. Am. Coll. Cardiol.* 72, 62–75. doi:10.1016/j.jacc.2018.04.041

Gauthier, L. D., Greenstein, J. L., and Winslow, R. L. (2012). Toward an integrative computational model of the Guinea pig cardiac myocyte. *Front. Physiol.* 3, 1–19. doi:10.3389/fphys.2012.00244

Gong, J. Q. X., and Sobie, E. A. (2018). Population-based mechanistic modeling allows for quantitative predictions of drug responses across cell types. *Npj Syst. Biol. Appl.* 4, 11. doi:10.1038/s41540-018-0047-2

Herron, T. J., Rocha, A. M. Da., Campbell, K. F., Ponce-Balbuena, D., Willis, B. C., Guerrero-Serna, G., et al. (2016). Extracellular matrix–mediated maturation of human pluripotent stem cell–derived cardiac monolayer structure and electrophysiological function. *Circ. Arrhythmia Electrophysiol.* 9, 139–148. doi:10.1161/CIRCEP.113.003638

Keizer, J., and Levine, L. (1996). Ryanodine receptor adaptation and Ca2+-Induced Ca2+ release- dependent Ca2+ oscillations. *Biophys. J.* 71, 3477–3487. doi:10.1016/S0006-3495(96)79543-7

Kernik, D. C., Morotti, S., Wu, H., Garg, P., Duff, H. J., Kurokawa, J., et al. (2019). A computational model of induced pluripotent stem-cell derived cardiomyocytes incorporating experimental variability from multiple data sources. *J. Physiol.* 597, 4533–4564. doi:10.1113/jp277724

Kernik, D. C., Yang, P.-C., Kurokawa, J., Wu, J. C., and Clancy, C. E. (2020). A computational model of induced pluripotent stem-cell derived cardiomyocytes for high throughput risk stratification of KCNQ1 genetic variants. *PLoS Comput. Biol.* 16, e1008109. doi:10.1371/journal.pcbi.1008109

Khan, J. M., Lyon, A. R., and Harding, S. E. (2013). The case for induced pluripotent stem cell-derived cardiomyocytes in pharmacological screening. *Br. J. Pharmacol.* 169, 304–317. doi:10.1111/j.1476-5381.2012.02118.x

Knollmann, B. C. (2013). Induced pluripotent stem cell-derived cardiomyocytes: boutique science or valuable arrhythmia model?. *Circ. Res.* 112, 969–976. doi:10.1161/CIRCRESAHA.112.300567

Koivumäki, J. T., Naumenko, N., Tuomainen, T., Takalo, J., Oksanen, M., Puttonen, K. A., et al. (2018). Structural immaturity of human iPSC-derived cardiomyocytes: in silico investigation of effects on function and disease modeling. *Front. Physiol.* 9, 1–17. doi:10.3389/fphys.2018.00080

Kopljar, I., Lu, H. R., Van Ammel, K., Otava, M., Tekle, F., Teisman, A., et al. (2018). Development of a human iPSC cardiomyocyte-based scoring system for cardiac hazard identification in early drug safety de-risking. *Stem Cell Rep.* 11, 1365–1377. doi:10.1016/j.stemcr.2018.11.007

Korhonen, T., Rapila, R., and Tavi, P. (2008). Mathematical model of mouse embryonic cardiomyocyte excitation-contraction coupling. *J. Gen. Physiol.* 132, 407–419. doi:10.1085/jgp.200809961

Lemoine, M. D., Krause, T., Koivumäki, J. T., Prondzynski, M., Schulze, M. L., Girdauskas, E., et al. (2018). Human induced pluripotent stem cell–derived engineered heart tissue as a sensitive test system for QT prolongation and arrhythmic triggers. *Circ. Arrhythmia Electrophysiol.* 11, e006035. doi:10.1161/CIRCEP.117.006035

Li, M., Kanda, Y., Ashihara, T., Sasano, T., Nakai, Y., Kodama, M., et al. (2017). Overexpression of KCNJ2 in induced pluripotent stem cell-derived cardiomyocytes for the assessment of QT-prolonging drugs. *J. Pharmacol. Sci.* 134, 75–85. doi:10.1016/j.jphs.2017.05.004

Lu, H. R., Whittaker, R., Price, J. H., Vega, R., Pfeiffer, E. R., Cerignoli, F., et al. (2015). High throughput measurement of Ca++dynamics in human stem cell-derived cardiomyocytes by kinetic image cytometery: a cardiac risk assessment characterization using a large panel of cardioactive and inactive compounds. *Toxicol. Sci.* 148, 503–516. doi:10.1093/toxsci/kfv201

Lu, H. R., Zeng, H., Kettenhofen, R., Guo, L., Kopljar, I., van Ammel, K., et al. (2019). Assessing drug-induced long QT and proarrhythmic risk using human stem-cell-derived cardiomyocytes in a Ca2+ imaging assay: evaluation of 28 CiPA compounds at three test sites. *Toxicol. Sci.* 170, 345–356. doi:10.1093/toxsci/kfz102

Ma, D., Wei, H., Lu, J., Huang, D., Liu, Z., Loh, L. J., et al. (2015). Characterization of a novel KCNQ1 mutation for type 1 long QT syndrome and assessment of the therapeutic potential of a novel IKs activator using patient-specific induced pluripotent stem cell-derived cardiomyocytes. *Stem Cell Res. Ther.* 6, 39. doi:10.1186/s13287-015-0027-z

Ma, D., Wei, H., Zhao, Y., Lu, J., Li, G., Binte, N., et al. (2013). Modeling type 3 long QT syndrome with cardiomyocytes derived from patient-specific induced pluripotent stem cells. *Int. J. Cardiol.* 168, 5277–5286. doi:10.1016/j.ijcard.2013.08.015

Ma, J., Guo, L., Fiene, S. J., Anson, B. D., Thomson, J. A., Kamp, T. J., et al. (2011). High purity human-induced pluripotent stem cell-derived cardiomyocytes: electrophysiological properties of action potentials and ionic currents. *AJP - Hear. Circ. Physiol.* 301, H2006–H2017. doi:10.1152/ajpheart.00694.2011

Miyagawa, S., and Sawa, Y. (2018). Building a new strategy for treating heart failure using induced pluripotent stem cells. *J. Cardiol.* 72, 445–448. doi:10.1016/j.jjcc.2018.05.002

Paci, M., Casini, S., Bellin, M., Hyttinen, J., and Severi, S. (2018a). Large-scale simulation of the phenotypical variability induced by loss-of-function long QT mutations in human induced pluripotent stem cell cardiomyocytes. *Int. J. Mol. Sci.* 19, 3583. doi:10.3390/ijms19113583

Paci, M., Hyttinen, J., Aalto-Setälä, K., and Severi, S. (2013). Computational models of ventricular- and atrial-like human induced pluripotent stem cell derived cardiomyocytes. *Ann. Biomed. Eng.* 41, 2334–2348. doi:10.1007/s10439-013-0833-3

Paci, M., Hyttinen, J., Rodriguez, B., and Severi, S. (2015). Human induced pluripotent stem cell-derived versus adult cardiomyocytes: an in silico electrophysiological study on effects of ionic current block. *Br. J. Pharmacol.* 172, 5147–5160. doi:10.1111/bph.13282

Paci, M., Passini, E., Klimas, A., Severi, S., Hyttinen, J., Rodriguez, B., et al. (2020). All-optical electrophysiology refines populations of in silico human iPSC-CMs for drug evaluation. *Biophys. J.* 58, 7250–7257. doi:10.1016/j.bpj.2020.03.018

Paci, M., Passini, E., Severi, S., Hyttinen, J., and Rodriguez, B. (2017). Phenotypic variability in LQT3 human induced pluripotent stem cell-derived cardiomyocytes and their response to antiarrhythmic pharmacologic therapy: an in silico approach. *Hear. Rhythm.* 14, 1704–1712. doi:10.1016/j.hrthm.2017.07.026

Paci, M., Pölönen, R.-P., Cori, D., Penttinen, K., Aalto-Setälä, K., Severi, S., et al. (2018b). Automatic optimization of an in silico model of human iPSC derived cardiomyocytes recapitulating calcium handling abnormalities. *Front. Physiol.* 9, 709. doi:10.3389/FPHYS.2018.00709

Paci, M., Severi, S., and Hyttinen, J. (2019). "Automaticity in cardiomyocytes derived from human induced pluripotent stem cells as result of different mechanisms," in Proceedings of the Computing in Cardiology Conference, Singapore, September 8–11, 2019. doi:10.22489/CinC.2019.101

Passini, E., Britton, O. J., Lu, H. R., Rohrbacher, J., Hermans, A. N., Gallacher, D. J., et al. (2017). Human in silico drug trials demonstrate higher accuracy than animal models in predicting clinical pro-arrhythmic cardiotoxicity. *Front. Physiol.* 8, 1–15. doi:10.3389/fphys.2017.00668

Pfeiffer, E. R., Vega, R., McDonough, P. M., Price, J. H., and Whittaker, R. (2016). Specific prediction of clinical QT prolongation by kinetic image cytometry in human stem cell derived cardiomyocytes. *J. Pharmacol. Toxicol. Methods* 81, 263–273. doi:10.1016/j.vascn.2016.04.007

Rast, G., Weber, J., Disch, C., Schuck, E., Ittrich, C., and Guth, B. D. (2015). An integrated platform for simultaneous multi-well field potential recording and Fura-2-based calcium transient ratiometry in human induced pluripotent stem cell (hiPSC)-derived cardiomyocytes. *J. Pharmacol. Toxicol. Methods* 75, 91–100. doi:10.1016/j.vascn.2015.04.005

Shannon, T., Wang, F., Puglisi, J., Weber, C., and Bers, D. M. (2004). A mathematical treatment of integrated Ca dynamics within the ventricular myocyte. *Biophys. J.* 87, 3351–3371. doi:10.1529/biophysj.104.047449

Sneyd, J., and Dufour, J.-F. (2002). A dynamic model of the type-2 inositol trisphosphate receptor. *Proc. Natl. Acad. Sci. U S A.* 99, 2398–2403.doi:10.1073/pnas.032281999

Spencer, C. I., Baba, S., Nakamura, K., Hua, E. A., Sears, M. A. F., Fu, C., et al. (2014). Calcium transients closely reflect prolonged action potentials in iPSC models of inherited cardiac arrhythmia. *Stem Cell Rep.* 3, 269–281. doi:10.1016/j.stemcr.2014.06.003

Strauss, D. G., Gintant, G., Li, Z., Wu, W., Blinova, K., Vicente, J., et al. (2019). Comprehensive in vitro Proarrhythmia assay (CiPA) update from a cardiac safety research consortium/health and environmental Sciences institute/FDA meeting. *Ther. Innov. Regul. Sci.* 53, 519–525. doi:10.1177/2168479018795117

Takahashi, K., Tanabe, K., Ohnuki, M., Narita, M., Ichisaka, T., Tomoda, K., et al. (2007). Induction of pluripotent stem cells from adult human fibroblasts by defined factors. *Cell* 131, 861–872. doi:10.1016/j.cell.2007.11.019

ten Tusscher, K. H. W. J., Noble, D., Noble, P. J., and Panfilov, A. V. (2004). A model for human ventricular tissue. *Am. J. Physiol. Hear. Circ. Physiol.* 286, H1573–H1589. doi:10.1152/ajpheart.00794.2003

Treat, J. A., Goodrow, R. J., Bot, C. T., Haedo, R. J., and Cordeiro, J. M. (2019). Pharmacological enhancement of repolarization reserve in human induced pluripotent stem cells derived cardiomyocytes. *Biochem. Pharmacol.* 169, 113608. doi:10.1016/j.bcp.2019.08.010

Tveito, A., Jæger, K. H., Huebsch, N., Charrez, B., Edwards, A. G., Wall, S., et al. (2018). Inversion and computational maturation of drug response using human stem cell derived cardiomyocytes in microphysiological systems. *Sci. Rep.* 8, 17626. doi:10.1038/s41598-018-35858-7

Veerman, C. C., Mengarelli, I., Guan, K., Stauske, M., Barc, J., Tan, H. L., et al. (2016). hiPSC-derived cardiomyocytes from Brugada Syndrome patients without identified mutations do not exhibit clear cellular electrophysiological abnormalities. *Sci. Rep.* 6, 30967. doi:10.1038/srep30967

Williams, G., and Mirams, G. R. (2015). A web portal for in-silico action potential predictions. *J. Pharmacol. Toxicol. Methods* 75, 10–16. doi:10.1016/j.vascn.2015.05.002

Woosley, R., Heise, C., and Romero, K. (2020). QTdrugs list www.CredibleMeds.org. Available at: https://crediblemeds.org/ (Accessed August 31, 2020).

Yu, J., Vodyanik, M. A., Smuga-Otto, K., Antosiewicz-Bourget, J., Frane, J. L., Tian, S., et al. (2007). Induced pluripotent stem cell lines derived from human somatic cells. *Science* 318, 1917–1920. doi:10.1126/science.1151526

Zeng, H., Roman, M. I., Lis, E., Lagrutta, A., and Sannajust, F. (2016). Use of FDSS/μCell imaging platform for preclinical cardiac electrophysiology safety screening of compounds in human induced pluripotent stem cell-derived cardiomyocytes. *J. Pharmacol. Toxicol. Methods* 81, 217–222. doi:10.1016/j.vascn.2016.05.009

Zhang, H., Zou, B., Yu, H., Moretti, A., Wang, X., Yan, W., et al. (2012). Modulation of hERG potassium channel gating normalizes action potential duration prolonged by dysfunctional KCNQ1 potassium channel. *Proc. Natl. Acad. Sci. U S A.* 109, 11866–11871. doi:10.1073/pnas.1205266109

Zhou, X., Qu, Y., Passini, E., Bueno-Orovio, A., Liu, Y., Vargas, H. M., et al. (2020). Blinded *in silico* drug trial reveals the minimum set of ion channels for torsades de Pointes risk assessment. *Front. Pharmacol.* 10, 1–17. doi:10.3389/fphar.2019.01643

Conflict of Interest: MP and Tampere University collaborated with InSilicoTrials Technologies SRL for developing a software for predicting drug cardiac safety risk based on an in silico model of human induced pluripotent stem cell-derived cardiomyocyte. HRL, and DJG are employees of Janssen Pharmaceutica NV.

The remaining authors declare that the research was conducted in the absence of any commercial or financial relationships that could be construed as a potential conflict of interest.

frontiers in Pharmacology

MINI REVIEW
published: 29 March 2021
doi: 10.3389/fphar.2021.603016

New Modalities of 3D Pluripotent Stem Cell-Based Assays in Cardiovascular Toxicity

Barbara Orsolits[1], *Zsófia Kovács*[1], *János Kriston-Vizi*[2], *Béla Merkely*[1] *and Gábor Földes*[1,3]*

[1]Heart and Vascular Center, Semmelweis University Budapest, Budapest, Hungary, [2]Bioinformatics Image Core (BIONIC), MRC Laboratory for Molecular Cell Biology, University College London, London, United Kingdom, [3]National Heart and Lung Institute, Imperial Centre for Experimental and Translational Medicine, Imperial College London, London, United Kingdom

The substantial progress of the human induced pluripotent stem cell (hiPSC) technologies over the last decade has provided us with new opportunities for cardiovascular drug discovery, regenerative medicine, and disease modeling. The combination of hiPSC with 3D culture techniques offers numerous advantages for generating and studying physiological and pathophysiological cardiac models. Cells grown in 3D can overcome many limitations of 2D cell cultures and animal models. Furthermore, it enables the investigation in an architecturally appropriate, complex cellular environment *in vitro*. Yet, generation and study of cardiac organoids—which may contain versatile cardiovascular cell types differentiated from hiPSC—remain a challenge. The large-scale and high-throughput applications require accurate and standardised models with highly automated processes in culturing, imaging and data collection. Besides the compound spatial structure of organoids, their biological processes also possess different temporal dynamics which require other methods and technologies to detect them. In this review, we summarise the possibilities and challenges of acquiring relevant information from 3D cardiovascular models. We focus on the opportunities during different time-scale processes in dynamic pharmacological experiments and discuss the putative steps toward one-size-fits-all assays.

Keywords: human induced pluripotent stem cells, cardiovascular, 3D models, assay, toxicology

OPEN ACCESS

Edited by:
Jonathan Satin,
University of Kentucky, United States

Reviewed by:
Bradley Berron,
University of Kentucky, United States
Oren Caspi,
Rambam Health Care Campus, Israel

Correspondence:
Gábor Földes
g.foldes@imperial.ac.uk

Specialty section:
This article was submitted to Cardiovascular and Smooth Muscle Pharmacology, a section of the journal Frontiers in Pharmacology

Received: *04 September 2020*
Accepted: *04 February 2021*
Published: *29 March 2021*

Citation:
Orsolits B, Kovács Z, Kriston-Vizi J, Merkely B and Földes G (2021) New Modalities of 3D Pluripotent Stem Cell-Based Assays in Cardiovascular Toxicity. Front. Pharmacol. 12:603016. doi: 10.3389/fphar.2021.603016

PRESERVING OR REBUILDING CARDIOVASCULAR STRUCTURES FOR MODELLING

The human heart is a complex organ with multiple cell types, including cardiomyocytes, fibroblasts, endothelial cells and perivascular cells, scaffolded by extracellular matrix (ECM) (Pinto et al., 2016). Functional and structural changes occur during cardiovascular disease development, presented with different spatial and temporal dynamics. Thus, there is an unmet need for complex 3D models with realistic architecture which can mimic physiological and pathophysiological conditions. Compared with conventional 2D cell cultures, the construction of organ-like cardiac 3D models may provide a higher fidelity system to investigate cell function and viability. Novel 2D and 3D cell and tissue culture techniques are being developed for disease modeling, drug discovery and toxicity testing. The first 3D cardiovascular models appeared about 100 years ago. Yet, the importance of these technologies has increased only for the last decade. The advancement and the increasing number in publications of these cardiac models are shown in **Figure 1**.

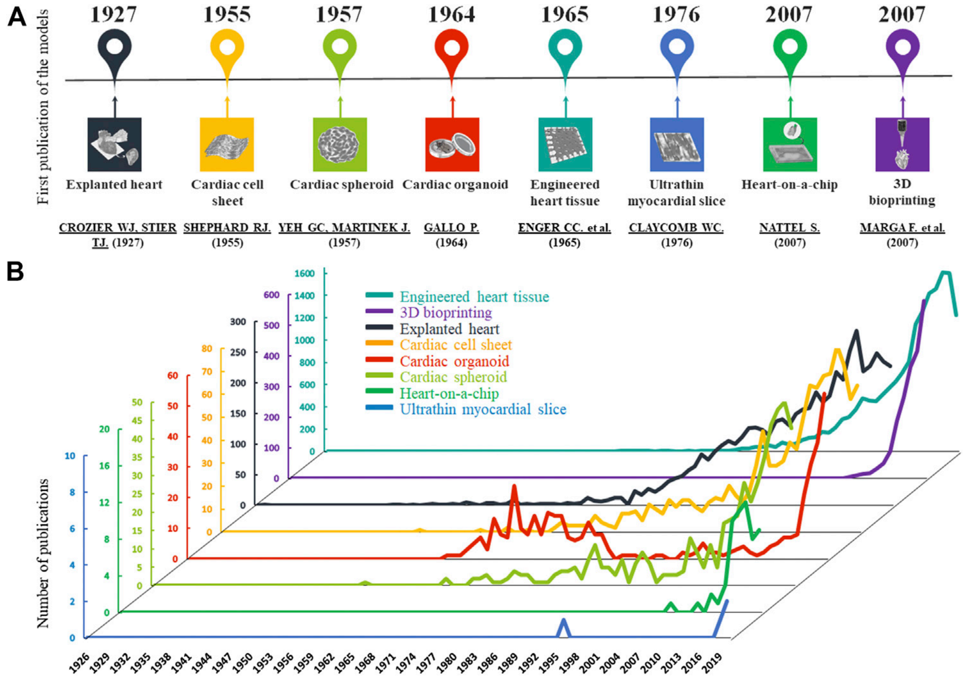

FIGURE 1 | Development of cardiac models. **(A)**: The graphs show the number of published articles of the different models on a timeline based on PubMed data. In the last 20 years, the number of publications has increased in all cases. **(B)**: The timescale presents the first publications of the cardiac models based on PubMed.

One of the first approaches is the use of myocardium of the explanted hearts from animals or patients which preserve the original architecture. One can also gather samples during interventions such as coronary artery bypass surgery, valve replacement, closure of ventricular or atrial septal defects and cardiomyotomy (Lal et al., 2015). These serve as excellent sources of ethically-sourced myocardial samples of end-stage failing hearts. Their particular advantage is that the donor's medical history, the clinical presentation of the disease, and the genetic background are usually available. Examination of explanted heart samples represents a platform for identifying and optimising heart disease treatment strategies and developing better diagnostic tools (Song et al., 2014). However, this approach is not suitable to handle a large number of samples (Tudorache et al., 2013) or for long-term experiments (Harding et al., 1992). These limitations explain why explanted hearts may be inadequate for routine toxicological testing. The advantages and disadvantages of this and other cardiac models below are summarised in **Table 1**.

Ultrathin Myocardial Slices

Myocardial slices are ~100–400 μm slices of living adult heart and can also be used as a model for the native myocardium. These ultrathin slices preserve native cardiac contractility, physiology and its complex multicellular structure. Protocols are being optimised for prolonged survival of these tissue slices in their native form (Watson et al., 2019). The most challenging issue is how to prepare these slices while preserving the native tissue architecture. Manual slicing has been replaced by vibratomes over the decades, making it easier to produce them and be suitable for drug and toxicology testing (Pitoulis et al., 2020). Slices can be obtained from animals and human biopsies. The main advantage is that the preparation is scalable: one can get multiple slices from each heart, allowing one to simultaneously carry out several tests. Various assays have been created to provide high-resolution real-time monitoring of changes in the function and architecture of the slices. Based on laser diffraction, the length of the sarcomeres can be detected as a functional surrogate for contractility and Ca^{2+} signaling. These myocardial slices can be used for *in vitro* drug testing as they still show reproducible pharmacodynamics even beyond 24 h after preparation (Bussek et al., 2012). Cardiotoxic compounds like doxorubicin and allylamine were tested on rat myocardial slices, which reduced protein synthesis and ATP content and increased lipid peroxidation (Parrish et al., 1994).

In addition to human myocardium, with the discovery of human induced pluripotent (hiPSC) technologies, there may be a new source of authentic human cells at hand to find accurate and specific answers in cardiovascular pharmacology. The reprogramming human somatic cells into hiPSC, and their subsequent differentiation to any cell types, allows the production of personalised, well-characterised cardiomyocytes and other cardiovascular cell derivatives, in expandable and long-term cultures. Furthermore, with the use of hiPSC, we can

TABLE 1 | Advantages and disadvantages of technologies in cardiovascular modeling.

Technologies	Advantages	Disadvantages	References
Explanted heats	Preserve the original architecture of the organ.	Ethical concerns, time limitation for measurements.	Song et al., (2014) Hartung and Corsini (2013)
Ultrathin myocardial slices	Several slices can be prepared from each organ, preserves tissue structure, appropriate model for acute pharmacological testing and in vitro safety screening, ensures oxygen diffusion.	Requires a novel protocol for culturing myocardial slices in their naative state, with preserved structure and function.	Pitoulis et al., (2020) Watson et al., (2019)
Engineered heart tissues	Sarcomeric alignment of CMS, improved contractile function, electromechanical cellular coupling.	Requires optimization, lack of vasculature, challenges with cells or materials, issues with tissue maturation, hurdles of imaging.	Eder and Herrling (2016) Eng et al., (2013) Zimmermann et al., (2004)
Spheroids	Co-culture ability, high reproducibility, inexpensive and less labor intensive than animal models, adaptable for medium-to-high throughput applications.	Size variability and non uniformity of spheroids, limited diffusion, limitation of complexity, small seeding number of cell is challenging.	Mehta et al., (2012)
Cell sheets	Possibility to make various tissue reconstructions such as cardiac patches.	Poor nutrition, hypoxia, necrosis can occur in the middle of multilayered cell sheets.	Chen et al., (2015) Yamato and Okano (2004)
Organoids	Biomimetic microenvironment, ability for long term culture, models for translational medicine.	Non-efficient testing platform, must be optimized, imaging challenges, shape of organoids changes constantly.	Richards et al., (2020) Nugraha et al., (2018) Hynds and Adam (2014)
Organ-on-a-chip	Constant nutrition, oxygen supply and waste removal, in vitro drug screening, mimics dynamic physical vascular microenvironment, tissue-tissue interfaces, vascular perfusion, high throughput screening, long-term co-culture.	Variation and inconsistency between different manufacturing batches, laminar flow causes poor mixing, requires integration of measuring systems.	Ingber (2018) Ribas et al., (2016)
3D bioprinting	Fully automated method, ability to bioprint 3D structure of heart.	No functional performance or histological data, immature and improper mirocirculation due to inadeuate perfusion.	Birla and Williams (2020)

overcome some of the ethical concerns that have plagued human embryonic stem cell and animal models (King and Jacob, 2014; Volarevic et al., 2018). We can also eliminate the species differences and perform conventional higher fidelity human-specific *in vitro* assays. Finally, by combining iPSC and gene editing technologies (i.e. CRISPR/Cas9) one can create cells with a well-defined genetic background (Boretto et al., 2019; Gopal et al., 2020; Sacchetto et al., 2020). Human iPSC cultures can remain genetically and phenotypically stable for long periods, permitting us to monitor time-dependent processes during the maintenance (Liu et al., 2020). Human iPSC allow investigations of heart disease-associated models *in vitro*. Seeding hiPSC-CM (hiPSC-derived cardiomyocytes) onto thin decellularised thin myocardial slices created tissue-like constructs that exhibit a robust response to cardiac drugs for a wide range of concentrations and pacing rates. These recellularised slices recapitulated structural, functional and electrophysiological features of native myocardium and proved sensitive in drug screening assays (Blazeski et al., 2019). Despite the advantages, ultrathin myocardial slices are not yet suitable for chronic experiments, this limits their use in hiPSC-related drug discovery and complex toxicology studies.

Cell Sheet Engineering

Cell sheet technology is a scaffold-free method where thermosensitive substrates produce single cells and complete layers of cells for tissue regeneration. This cardiac tissue engineering approach may provide better heart models in the long-term (Sekine et al., 2016; Kobayashi et al., 2019; Zurina et al., 2020). The technique generally uses specific culture dishes, coated with temperature-sensitive polymers such as poly(N-isopropylacrylamide). It allows the cells to adhere, spread and proliferate at 37°C. However, at 32°C, the polymer dissolves in water, and the cells spontaneously detach from the culture. This method's advantage is that adherent cells can be harvested without using any proteolytic enzymes, severely damaging the cultured cells (Yang et al., 2005). This way, the cell adhesion molecules of the cultured cells and the cell-cell junction proteins can be preserved, and the extracellular matrix remains deposited in the cell sheets without degradation. This technology is readily usable, and live cell sheets can be generated. For hiPSC-CM models, the "Cardiac *In Vitro* Proarrhythmia Assessment initiative" may be the first attempt for drug proarrhythmic potential assessment on cell sheets (Gintant et al., 2019).

Spheroids

The ample literature of 3D spheroid cell culturing spans decades (**Figure 1**). Spheroids are adherent cell populations which organise in a spherical shape. They can be formed by various scaffold-free methods like spinner flasks, hanging drops, or non-adhesive surfaces. There is a continuous agitation in spinner flasks that prevents the sedimentation of the cells to the bottom of the flask and promotes cell-cell adhesion to form spheroids in suspension. This method allows for long-term cell culturing with sufficient nutrient supply (Mehta et al., 2012). This technique's initial disadvantages had been the non-uniformly created spheroids, and the undesirable shear stress generated during the continuous agitation (Lin and Chang, 2008). Indeed, these methods mostly produced spheroids which are variable in size, complexity and morphology. Spheroids could only reach a few hundred micrometres in size due to the limited oxygen and nutrient distribution. Thus, for *in vitro* testing, particularly for drug screening, we needed to improve the quality and increase the predictive power of these 3D cultures (Fennema et al., 2013).

3D spheroids were studied in a low-throughput fashion so far. Seemingly trivial components of an image acquisition pipeline, such as identifying the 3D spatial location of a spheroid in an ECM volume, the localisation challenge, becomes prohibitively complex as soon as human expertise is needed to be replaced with robotic automation. The first label-free, standardised, 96-well plate-based systems that enable the pharmacological responses of 3D hiPSC-CM spheroids are now available (Burnham et al., 2020). The high-content analysis of hiPSC-CM serves another example where the individual heart muscle cell locations were identified using image analysis followed by 3D re-imaging with a high magnification lens (Földes et al., 2014). Most commercially available 3D high-content imaging systems are primarily designed to acquire adherent monolayer cell images in specified field-of-view locations in wells. However, a 3D spheroid cultured inside ECM can be located randomly in its volume (Debnath et al., 2003). The spatial localisation challenge of 3D cardiovascular spheroid imaging can be addressed using a non-adhesive, ultra-low attachment surface combined with round bottom well geometry to ensure the spheroid's central positioning gravitational force. The use of the same multiwell plate for both culturing and imaging of the spheroids simplifies the workflow, eases the spheroid maintenance and reproducibility (Bresciani et al., 2019) as increases the throughput and at the same time decreases the spheroid size and shape variability. The stiff plastic can affect cell physiology, and the long culturing time increases the chance of edge effects. Live imaging of spheroids allows viability assessment (LaBarbera et al., 2012). Treatment can be performed directly, adding medium into the wells, and the central location of spheroids allows more straightforward image acquisition (Bresciani et al., 2019). Depending on the feature of interest, we can choose widefield or confocal imaging. In confocal microscopy, Z-stack or single slice imaging can be performed with ~100 μm maximal penetration depth. The image data size of a 3D time-lapse can easily reach terabyte-scale (Hoffman et al., 2017). However, 3D culturing is not always coupled with Z-stack imaging. As an example, necessary information for spheroid stress gradient studies (metabolic, hypoxic) can be obtained by single optical slice confocal imaging, that intersects the tested spheroid region. We should always minimise the amount of acquired image data using single optical slice confocal imaging as long as it addresses the given question. That principle applies to high-content analysis. Volumetric, surface, or 3D distance feature extraction needs 3D high-throughput image analysis (Boutin et al., 2018) using software equipped with a 26-neighbour connected component analysis algorithm (Hoffman et al., 2017). Otherwise, various image analysis Z-projection methods (maximum, sum, average intensity), can be applied to a 3D Z-stack to reduce the dimensionality and use a wide range of 2D image analysis algorithms.

Engineered Heart Tissue

Tissue engineering is a relatively new field which combines cells with efficient regenerative capacity, synthetic or native scaffolds, and growth factors to improve the regeneration of injured tissues. Human iPSC-CM can be combined with a hydrogel-based scaffold to recapitulate human myocardium. Characterisation of these engineered heart tissues (EHT) reveals an anisotropic muscle structure, with embedded hiPSC-CM showing more mature structural and contractile properties than those cells in 2D cultures (Eschenhagen et al., 1997). In contrast to 2D cultures, EHT provides a suitable platform to measure contractile properties such as beating rate, contractile kinetics, and force (Eder and Herrling, 2016). Recent advancements in the EHT method have been significant with cell constructions, scaffold modification, in silico analysis or electrical stimulation (Hirt et al., 2012; Eder et al., 2014). However, the dynamic imaging of EHTs remains a hurdle to overcome. With confocal laser scanning microscopy after a tissue clearing, the organisation and orientation of hiPSC-CM can be imaged with sufficient resolution (Nakane et al., 2020). However, a faster confocal imaging system could further improve larger tissue samples imaging in a time- and cost-efficient way.

Organoids

Cardiac organoids are built from multiple, cardiovascular cell types which can self-organise into an authentic structure with added or self-generated matrices. They show realistic cardiac microanatomy, cell-to-cell and cell-to-matrix interactions, and tissue-specific architecture. Therefore, the creation of patient-specific organoids from hiPSC may be the most advanced 3D technology to date. The first models with primary cell populations that have been gradually replaced by hiPSC-derivatives as cell sources (Hynds and Adam, 2013). Human iPSC-derived cardiac organoids can model ischemic conditions and drug-induced cardiotoxicity (Richards et al., 2020). Like primary cardiac cells, cardiac organoids show measurable action potential activity, spontaneous beating, and abundant expression of cardiac-specific receptors like ryanodine receptor, L-type calcium channels and proteins such as troponin I, ventricular myosin light chain and atrial myosin light chain (Richards et al., 2017). Self-organising organoids contain a major cell type (usually cardiomyocytes). For higher fidelity use and prevascularisation, they can be co-cultured with heterotypic cell types (hiPSC-derived endothelial cells, smooth muscle cells or pericytes) to model cell-cell interactions and cell states (proliferating, quiescent and apoptotic) of myocardial tissue (reviewed elsewhere, see Nugraha et al., 2018; Gomez et al., 2018; Talman and Kivelä, 2018; Nugraha et al., 2019; Madeddu and Foldes, 2019). In multicellular organoids, cell-type-specific post-translational modifications regulate critical biological processes and are frequently dysregulated in disease. Similar to other 3D models, low-dimensional fluorescent imaging cannot capture the complexity of these signaling network nodes. A promising method to comprehensively analyze cell-type-specific changes utilises thiol-reactive organoid barcoding *in situ*. Integrating single-cell post-translational modifications analysis with multiplexed organoid-barcoding enables high-throughput comparison of signaling networks between hiPSC-based heterocellular organoid cultures (Qin et al., 2020). Therefore, hiPSC-derived cardiovascular organoids are an excellent choice for patient-specific toxicity studies; yet, the lack of standardised organoids production results in variable responsiveness to particular treatments (Takebe et al., 2013).

Heart-on-A-Chip

The organ-on-a-chip is a miniature organotypic cell culture on a chip equipped with a complete microfluidic system. Due to the regulation of microfluidic parameters, we can manipulate the cellular microenvironment and control mini-organ behavior. This complex platform provides constant nutrition and oxygen supply and simultaneous waste removal by its multi-microchannels (which mimics the vascular system). Many single and multiorgan organ-on-chips have been presented (Lee and Sung, 2017; Wu et al., 2020). With fast engineering and biomaterial technology progression, we may even achieve complete human-on-chip technology soon (Marx et al., 2020). Heart-on-chip is an excellent implementation in toxicology by incorporating beating hiPSC-CM (Abulaiti et al., 2020). By high-speed impedance detection on heart-on-chip, we can detect the drug responsiveness on the cardiac tissue (Zhang et al., 2016). Upon drug-related stimuli such as doxorubicin or isoproterenol, the contractile function of the 3D cardiac construct can be detected by the piezoelectric sensing system. At the same time, image processing can provide *in situ* multi-site detections. The amplitude of the voltage output decreases in both treatments, while the contraction frequency is increased by isoproterenol and decreased by doxorubicin. These two measurements can provide us with mutual information of the fabricated heart construct's contractile behavior on a chip (Sakamiya et al., 2020). For localised real-time monitoring of cellular activities and physicochemical changes in an organ-on-chip, electrical sensors were first integrated with macroporous 3D scaffolds a decade ago (Tian et al., 2012). Functionalised synthetic 3D biomaterials allow for studies of cell/tissue development in the presence of biochemical stimuli and monitoring the pharmacological responses of cells within synthetic tissues may provide a more robust link to *in vivo* disease treatment compared with 2D cell cultures. Seamless integration of 3D (silicon nanowire field effect transistor-based) nanoelectronic scaffolds into tissue materials can serve as lab-on-a-chip pharmacological platforms and records both extracellular and intracellular signals of contracting cardiomyocytes and other cells with subcellular and sub-millisecond time resolution. As an initial example of a drug screening assay, recordings from the nanowire of a 3D cardiomyocyte mesh construct showed increased beating rate in response to adrenergic norepinephrine. Functional tubular structures of vascular nanoelectronics with human aortic smooth muscle cells also showed contractile activity (Marsano et al., 2016).

3D Bioprinting

Printing biocompatible materials and supporting components with the desired cells offers us the ability to create precisely designed structures of different cardiac tissue constructs. 3D bioprinting shows extraordinary versatility to build living cardiac tissues in a point-by-point and/or layer-by-layer manner. To date, several constructs have been made available for vascular (Norotte et al., 2009; Duan et al., 2013; Cui et al., 2019), or cardiac use (Cui et al., 2018; Noor et al., 2019). Human iPSC-derived cardiac patches with contractile function have successfully been printed (Lee et al., 2019). High throughput 3D printing of prevascularised hiPSC-CM structures could be personalised for drug discovery and toxicology (Arai et al., 2020). One may envisage that the generation of a subpopulation of chamber-specific cardiomyocytes or arterial/venous endothelial cells would further reduce variability and cellular heterogeneity of the printed constructs.

CATCHING FAST-CHANGING PROCESSES

Changes of cellular and extracellular processes in primary and hiPSC-derived cardiovascular cell constructs are highly dynamic and show variable kinetic profiles (**Figure 2**). This improved technology with physiologically relevant cellular function data can generate adequate information on pharmacokinetics and pharmacodynamics during drug screening. It may mimic dosing regimens used *in vivo* (similar to insulin regimen in diabetes, natriuretic peptide release in heart failure, as well as endocrinology-related disorders) (Kriston-Vizi et al., 2017). Until recently, the high-throughput imaging methods and reconstruction of images were too slow in many dynamic live-hPSC-derived cell applications, such as the measurements of mitochondrial calcium uptake, sarcomeric addition and myofibrillar remodeling of hiPSC-CM and endothelial cells, lipid droplet formation in metabolic disorders, and internalisation for drug delivery. The recent introduction of commercially available HCS systems (e.g. Hamamatsu Photonics, Molecular Devices) can address fast-response assays, such as calcium flux or cardiomyocyte beating, using imaging frame rates as fast as 100 frames per second (e.g. PerkinElmer). The high temporal resolution allows us to study rapid intracellular processes that happen on a millisecond timescale. Providing multiple endpoints is an excellent advantage of novel high-content imaging-based assays. However, parallel assessment of complex changes in hiPSC-derived cardiovascular cells, such as 3D rearrangements of sarcomere structure and dynamic translocation of natriuretic peptides, transcription factors and other second messengers, requires 3D imaging, high-performance computing and storage. These improved assays can readily predict molecular targets and off-target effects of test compounds, such as cytotoxicity or cardiovascular cell morphology changes. We can better investigate these predominantly short-term manifestations of cardiac pathologies in hiPSC-CM, including assays on depressed cell contraction, changes in electrophysiology, metabolism and intracellular $Cafn^{++}$ levels.

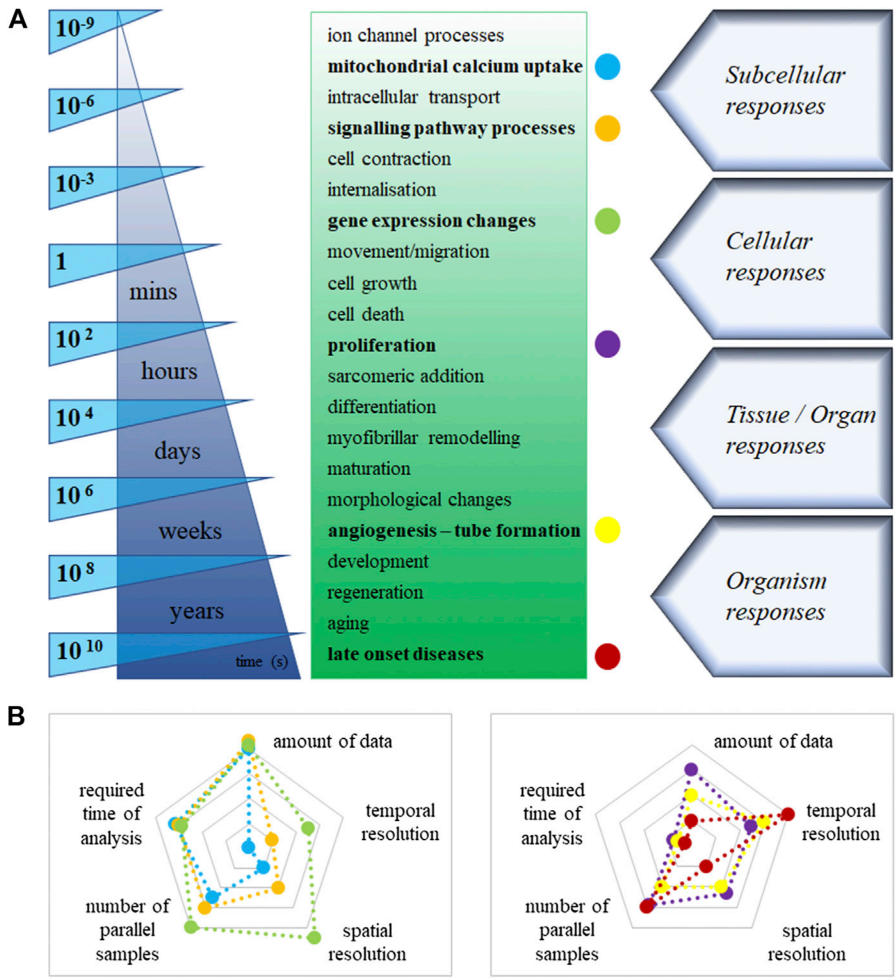

FIGURE 2 | (A): Estimated timeline of the main cellular processes in cardiovascular cells. **(B)**: Labeled cellular processes [colored dots in Panel. **(A)**], displayed on two-dimensional spider charts. The logarithmic scales demonstrate the values of different technical necessities, increasingly from the centre to the edges in the graph.

LONG-TERM PROCESSES IN THE CARDIOVASCULAR SYSTEM

Underlying cellular pathways in cardiovascular cell growth, proliferation, survival, and death are controlled by the steady-state level of regulatory proteins and enzymes (**Figure 2**). Multiple endpoints from high-content assays would provide users with a great advantage to better understand these complex processes. Improved assays can readily predict molecular targets and off-target effects of test compounds, such as cell morphology and viability changes. Indeed, longer-term assays focus on abnormal morphology, hypertrophy and increased susceptibility to cell death. Cell-based assays performed using an automated fluorescence imaging platform, and high-content analysis is valuable in characterising hypertrophic states induced in hiPSC-CM upon exposure to cardiotoxic compounds. We can assess the detailed 3D hypertrophic profiles of cardiomyocytes based on information captured at cellular and subcellular levels. Therefore, the assays can easily predict molecular targets and off-target effects of test compounds, such as cytotoxicity in cardiovascular cell morphology changes. Human iPSC-derived cardiomyocytes and endothelial cells retain their proliferative activity in culture. Compared to conventional static immunohistochemistry, time-lapse imaging, e.g. Premo Fucci system can reveal comprehensive data and could visualise real-time cell cycle transitions (Yano and Hoffman, 2018). Another notable example is the endothelial-mesenchymal transition, a particular version of the vascular system's epithelial-mesenchymal transition. It is extensively investigated in physiologic cardiac development and pathologic fibrosis. It is accompanied by cell morphology and identity changes in various diseases and one-way drift from one cell type to another with intermediate phases. Similarly, image processing is not currently possible in live assays monitoring tube formation as markers of disease (i.e. angiogenesis for anti-cancer indications). Understanding chronic treatment regimens (rather just one-off curative, like advanced therapies) leveraging *in vitro* platforms may require long-term cultured cells and follow-up, and long-term recording (Habeler et al., 2009).

TOWARDS MAPPING ORGANOIDS WITH HIGH SPATIOTEMPORAL RESOLUTIONS

Understanding the development, function and pathology of heterogeneous cell-cell interaction within organoids requires system-level mapping of the cell-based activities with high resolutions in space and time across the 3D volumes over a particular time window. Indeed, current workflows rely on fixed cells and can only assess only one time point, not continuous periods. Tissue-wide electrophysiology with single-cell/subcellular spatial and millisecond temporal resolution is critical for high-fidelity and long-term cardiovascular studies. However, it is an issue to invasively implant and localise sensors without destroying the well-connected cellular networks within the complex and matured organoids. Human cardiac cyborg organoids via organogenetic 2D–3D reconfiguration may overcome this hurdle and generate electrophysiological patterns during organogenesis. The platform is also scalable for integrating a larger number of sensors and stimulators fabricated into a stretchable nanoelectric mesh structure. The connection between electronics and cells enables long-term recording of electric dynamics in human cardiac organoids. It may be applicable for hiPSC-based modeling of cardiac diseases and therapeutics (Lancaster and Knoblich, 2014; Li et al., 2019). An alternative approach leverages radio frequency identification (RFID) technology, which is used to trace and track individual objects in multiple contexts by wirelessly providing digital signals; hiPSC-derived organoids integrating RFID microchips inside can be used for phenotypic screens and deliver readouts in real-time via a coiled antenna. Following an aggregation via a self-assembling cavitation process, chips integrate well into the organoids without impairing structure or functions. One proof-of-principle example to prove this was to test fat accumulation using fluorescence imaging based on a phenotyping assay coupled with the RFID-integrated organoids in an inherited hepatic lipid-storage disease model (Kimura et al., 2018). It is again a scalable technology which may become accessible to study genotype-phenotype relations in human cardiovascular pathologies.

FUTURE PROSPECTS

Drug development and toxicological testing are time-consuming and costly processes and require many parallel samples. To collect more and more information from many parallel samples and complex architectures of our modeling system massively increases the data acquired. Furthermore, the large amount of data increases the complexity of the analysis and the interpretation's difficulty. Additionally, the high similarity to native organs causes an increase of the initially high financial inputs. Fluorescence microscopy with automated, physiologically relevant cell-based 3D assays and image analysis; immediate identification and recording of cell-based activity; ability to identify novel complex cellular processes by multiple pathways; high-performance computing, storage, analysis and data management; establishment of standardised, high-fidelity *in vitro* models and the large-scale automation in several processes are the key to the new generation of high-throughput toxicological testing with hiPSC derivatives.

There is a hope that these 3D humanised cell platforms will improve predictive capabilities since cardiotoxicity is one of the most common causes for attrition of both cardiac and non-cardiac drugs. Recent advances in generating high-fidelity, *in vivo*-like cellular settings with hiPSC derivatives can provide us with consistent performance while permitting continuous and quantitative imaging. There is a need for better and more affordable medicines, with the burden of disease rising faster than GDP due to an ageing population and increasing chronic disease prevalence. Of importance, cardiovascular disease is the leading cause of mortality and morbidity. Today, less than 30% of all the work in personalised medicine targets the various non-oncological targets. The survey/study like that of the BioIndustry Association confirms the need for competitive improvements in screening technology and processes for humanised stem cell models of drug discovery to enable better predictability in clinical trials. Adaptation of these next-generation technologies could support disease prevention and proactive management of health and chronic conditions. It provides earlier and better detection and diagnosis of disease, leading to better patient outcomes, and finally leads to tailored treatments that either change the underlying disease or offer potential cures. According to the latest report published by FMI, the global organoids market is expected to reach ~ US$ 134 Mn by the forecast year 2029. The report further projects that the organoids market will grow at a CAGR of ~15% during 2019–2029 (Valley Cottage, 2019).

AUTHOR CONTRIBUTIONS

All authors listed have made a substantial, direct, and intellectual contribution to the work and approved it for publication.

FUNDING

The research was funded by the Higher Education Institutional Excellence Programme of the Ministry of Human Capacities in Hungary, within the framework of the Therapeutic Development thematic programme of the Semmelweis University, the Hungarian National Research, Development and Innovation Fund (NKFIA; NVKP-16-1-2016-0017, “National Heart Program” and 128444), and by the Medical Research Council (MR/R025002/1). This work was also supported by Medical Research Council core funding to the MRC-UCL University Unit Grant Ref MC_U12266B (JKV). This project was also supported by grants from the NIHR Imperial Biomedical Research Centre.

SUPPLEMENTARY MATERIAL

The Supplementary Material for this article can be found online at: https://www.frontiersin.org/articles/10.3389/fphar.2021.603016/full#supplementary-material.

REFERENCES

Abulaiti, M., Yalikun, Y., Murata, K., Sato, A., Sami, M. M., Sasaki, Y., et al. (2020). Establishment of a heart-on-a-chip microdevice based on human IPS cells for the evaluation of human heart tissue function. *Sci. Rep.* 10 (1), 19201. doi:10.1038/s41598-020-76062-w

Arai, K., Murata, D., Takao, S., Nakamura, A., Itoh, M., Kitsuka, T., et al. (2020). Drug response analysis for scaffold-free cardiac constructs fabricated using bio-3D printer. *Sci. Rep.* 10 (1). doi:10.1038/s41598-020-65681-y

Birla, R. K., and Williams, S. K. (2020). 3D bioprinting and its potential impact on cardiac failure treatment: an industry perspective. *APL. Bioeng.* 4 (1), 010903. doi:10.1063/1.5128371

Blazeski, A., Lowenthal, J., Zhu, R., Ewoldt, J., Boheler, K. R., and Tung, L. (2019). Functional properties of engineered heart slices incorporating human induced pluripotent stem cell-derived cardiomyocytes. *Stem. Cel. Rep.* 12 (5), 982–995. doi:10.1016/j.stemcr.2019.04.002

Boretto, M., Maenhoudt, N., Luo, X., Hennes, A., Boeckx, B., Bui, B., et al. (2019). Patient-derived organoids from endometrial disease capture clinical heterogeneity and are amenable to drug screening. *Nat. Cel. Biol.* 21 (8), 1041–1051. doi:10.1038/s41556-019-0360-z

Boutin, M. E., Voss, T. C., Titus, S. A., Cruz-Gutierrez, K., Micheal, S., and Ferrer, M. (2018). A high-throughput imaging and nuclear segmentation analysis protocol for cleared 3D culture models. *Sci. Rep.* 8 (1), 11135. doi:10.1038/s41598-018-29169-0

Bresciani, G., Hofland, L. J., Dogan, F., Giamas, G., Gagliano, T., and Zatelli, M. C. (2019). Evaluation of spheroid 3D culture methods to study a pancreatic neuroendocrine neoplasm cell line. *Front. Endocrinol. (Lausanne)* 10, 682. doi:10.3389/fendo.2019.00682

Burnham, M. P., Harvey, R., Sargeant, R., Fertig, N., and Haddrick, M. (2020). A scalable approach reveals functional responses of IPSC cardiomyocyte 3D spheroids. *Slas. Discov.* 26, 352–363. doi:10.1177/2472555220975332

Bussek, A., Schmidt, M., Bauriedl, J., Ravens, U., Wettwer, E., and Lohmann, H. (2012). Cardiac tissue slices with prolonged survival for *in Vitro* drug safety screening. *J. Pharmacol. Toxicol. Methods* 66 (2), 145–151. doi:10.1016/j.vascn.2011.12.002

Chen, J, Ma, D., and Ren, L. (2015). Development of cell sheet engineering technology in engineering vascularized tissue. *Zhongguo Xiu Fu Chong Jian Wai Ke Za Zhi* 29 (3), 368–371.

Claycomb, W. C. (1976). Biochemical aspects of cardiac muscle differentiation. Possible control of deoxyribonucleic acid synthesis and cell differentiation by adrenergic innervation and cyclic adenosine 3′:5′-monophosphate. *J. Biol. Chem.* 251 (19), 6082–6089. doi:10.1016/s0021-9258(17)33062-4

Crozier, W. J., and Stier, T. J. B. (1927). Temperature and frequency of cardiac contractions in embryos of limulus. *J. Gen. Physiol.* 10 (4), 501–518. doi:10.1085/jgp.10.4.501

Cui, H, Miao, S., Esworthy, T., Zhou, X., Lee, S., Liu, C., et al. (2018). 3D bioprinting for cardiovascular regeneration and Pharmacology. *Adv. Drug Deliv. Rev.* 132, 252–269. doi:10.1016/j.addr.2018.07.014

Cui, H., Zhu, W., Huang, Y., Liu, C., Yu, Z.-X., Nowicki, M., et al. (2019). *In vitro* and *in vivo* evaluation of 3D bioprinted small-diameter vasculature with smooth muscle and endothelium. *Biofabrication* 12 (1), 015004. doi:10.1088/1758-5090/ab402c

Debnath, J., Muthuswamy, S. K., and Brugge, J. S. (2003). Morphogenesis and oncogenesis of MCF-10A mammary epithelial Acini grown in three-dimensional basement membrane cultures. *Methods* 30, 256–268. doi:10.1016/S1046-2023(03)00032-X

Duan, B., Hockaday, L. A., Kang, K. H., and Butcher, J. T. (2013). 3D bioprinting of heterogeneous aortic valve conduits with alginate/gelatin hydrogels. *J. Biomed. Mater. Res.* 101 (5), 1255–1264. doi:10.1002/jbm.a.34420

Eder, A., Hansen, A., Uebeler, J., Schulze, T., Neuber, C., Schaaf, S., et al. (2014). Effects of proarrhythmic drugs on relaxation time and beating pattern in rat engineered heart tissue. *Basic Res. Cardiol.* 109 (6), 436. doi:10.1007/s00395-014-0436-7

Eder, J, and Herrling, P. L. (2016). Trends in modern drug discovery, *Handb Exp. Pharmacol.* 232, 3–22. doi:10.1007/164_2015_20

Eng, G., Radisic, M., and Vunjak-Novakovic, G. (2013). "Cardiac tissue engineering," in *Principles of tissue engineering*. 4th Edn, 771–792. Elsevier. doi:10.1016/B978-0-12-398358-9.00038-0

Enger, C. C., Kennedy, J. H., and Michel, A. G. (1965). A subminiature implantable self-powered cardiac pacemaker. *Trans. Am. Soc. Artif. Intern. Organs* 11 (1), 148–151. doi:10.1097/00002480-196504000-00029

Eschenhagen, T., Fink, C., Remmers, U., Scholz, H., Wattchow, J., Weil, J., et al. (1997). Three-dimensional reconstitution of embryonic cardiomyocytes in a collagen matrix: a new heart muscle model system. *FASEB J.* 11 (8), 683–694. doi:10.1096/fasebj.11.8.9240969

Dohmen, E., Rivron, N., Rouwkema, J., Van Blitterswijk, C., and De Boer, J. (2013). Spheroid culture as a tool for creating 3D complex tissues. *Trends Biotechnol.*, 31, 108–115. doi:10.1016/j.tibtech.2012.12.003

Földes, G., Matsa, E., Kriston-Vizi, J., Leja, T., Amiste, S., Kolker, L., et al. (2014). Aberrant α-adrenergic hypertrophic response in cardiomyocytes from human induced pluripotent cells. *Stem. Cell Reports* 3 (5), 905–914. doi:10.1016/j.stemcr.2014.09.002

Dolatshad, P. (1964). The decrease in volume of the sarcosomes during myocardial contraction and its biochemical significance. *Cardiologia* 45 (1), 1–15. doi:10.1159/000168148

Gintant, G., Burridge, P., Gepstein, L., Harding, S., Herron, T., Hong, C., et al. (2019). Use of human induced pluripotent stem cell-derived cardiomyocytes in preclinical cancer drug cardiotoxicity testing: a scientific statement from the American heart association. *Circ. Res.* 125, e75–e92. doi:10.1161/RES.0000000000000291

Gomez, I., Duval, V., and Silvestre, J. S. (2018). Cardiomyocytes and macrophages discourse on the method to govern cardiac repair. *Front Cardiovasc. Med.* 5, 134. doi:10.3389/fcvm.2018.00134

Gopal, S., André, L. R., Jonathan, S, and Dordick, J. S. (2020). Exploiting CRISPR Cas9 in three-dimensional stem cell cultures to model disease. *Front Bioeng. Biotechnol.* 8, 692. doi:10.3389/fbioe.2020.00692

Habeler, W., Pouillot, S., Plancheron, P., Pucéat, M., Peschanski, M., and Monville, C. (2009). An *in Vitro* beating heart model for long-term assessment of experimental therapeutics. *Cardiovasc. Res.* 81 (2), 253–259. doi:10.1093/cvr/cvn299

Harding, S., Mary Jones, S., Peter, O, FedericaVescovo, G., Philip, A., et al. (1992). Isolated ventricular myocytes from failing and non-failing human heart; the relation of age and clinical status of patients to isoproterenol response. *J. Mol. Cell Cardiol.* 24 (5), 549–564. doi:10.1016/0022-2828(92)91843-T

Hartung, T., and Corsini, E. (2013). Immunotoxicology: challenges in the 21st century and *in vitro* opportunities. *ALTEX* 30 (4), 411–426. doi:10.14573/altex.2013.4.411

Hirt, M. N., Sörensen, N. A., Bartholdt, L. M., Boeddinghaus, J., Schaaf, S., Eder, A., et al. (2012). Increased afterload induces pathological cardiac hypertrophy: a new *in Vitro* model. *Basic. Res. Cardiol.* 107 (6), 307. doi:10.1007/s00395-012-0307-z

Hoffman, A. F., Simpson, K. J., Horvath, P., Lovitt, C., Silver, S., Easton, E., et al. (2017). SBI2 HCS/HCA 3D imaging: best practices and unmet needs colloquium. *Assay Drug Dev. Technol.* 15 (1), 1–7. doi:10.1089/adt.2016.29054.afh

Hynds, R. E., and Adam, G. (2013). Concise review: the relevance of human stem cell-derived organoid models for epithelial translational medicine. *Stem Cells* 31, 417–422. doi:10.1002/stem.1290

Ingber, D (2018). Developmentally inspired human "organs on chips". *Development* 145, dev156125. doi:10.1242/dev.156125

Kimura, M., Azuma, M., Zhang, R. R., Thompson, W., Mayhew, C. N., and Takebe, T. (2018). Digitalized human organoid for wireless phenotyping. *iScience* 4, 294–301. doi:10.1016/j.isci.2018.05.007

King, N., and Jacob, P. (2014). Ethical issues in stem cell research and therapy. *Stem Cell Res. Ther.* 5, 85. doi:10.1186/scrt474

Kobayashi, J., Kikuchi, A., Takao, A., and Okano, T. (2019). Cell sheet tissue engineering: cell sheet preparation, harvesting/manipulation, and transplantation. *J Biomed Mater Res A.* 107, 955–967. doi:10.1002/jbm.a.36627

Kriston-Vizi, J., Harding, S, S. E., and Földes, G. (2017). Structural toxicity: hypertrophy models of human pluripotent stem cell-derived cardiomyocytes, 271–291. doi:10.1007/978-1-4939-6661-5_14

LaBarbera, D. V., Reid, B. G., and Yoo, B. H. (2012). The multicellular tumor spheroid model for high-throughput cancer drug discovery. *Expert Opin. Drug Discov.* 7, 819–830. doi:10.1517/17460441.2012.708334

Lal, S, Li, A., Allen, D., Allen, P. D., Bannon, P, Cartmill, T., et al. (2015) Best practice BioBanking of human heart tissue, *Biophys. Rev.* 7, 399–406. doi:10.1007/s12551-015-0182-6

Lancaster, M. A., and Knoblich, J. A. (2014). Organogenesis in a dish: modeling development and disease using organoid technologies. *Science*, 345, 1247125. doi:10.1126/science.1247125

Lee, A., Hudson, A. R., Shiwarski, D. J., Tashman, J. W., Hinton, T. J., Yerneni, S., et al. (2019). 3D bioprinting of collagen to rebuild components of the human heart. *Science* 365 (6452), 482–487. doi:10.1126/science.aav9051

Lee, S. H., and Sung, J. H. (2017). Microtechnology-based multi-organ models. *Bioengineering*, 4, 46. doi:10.3390/bioengineering4020046

Li, Q., Nan, K., Le Floch, P., Lin, Z., Sheng, H., and Liu, J. (2019). Cyborg organoids: implantation of nanoelectronics via organogenesis for tissue-wide electrophysiology. *Nano. Lett.* 19, 5871–5789. doi:10.1021/acs.nanolett.9b02512

Lin, R., and Chang, H. U. (2008). Recent advances in three-dimensional multicellular spheroid culture for biomedical research. *Biotechnol. J.* 3, 1172–1184. doi:10.1002/biot.200700228

Liu, G., David, B. T., Trawczynski, M., and Fessler, R. (2020). Advances in pluripotent stem cells: history, mechanisms, technologies, and applications. *Stem Cell Rev. Rep.* 16 (1), 3–32. doi:10.1007/s12015-019-09935-x

Madeddu, P., and Foldes, G. (2019). Editorial: multicellularity in the cardiovascular system. *Front Cardiovasc. Med.* 6, 2. doi:10.3389/fcvm.2019.00002

Marga, F., Neagu, A., Kosztin, I., and Forgacs, G. (2007). Developmental biology and tissue engineering. *Birth Defects Res. C Embryo Today* 81 (4), 320–328. doi:10.1002/bdrc.20109

Marsano, A., Conficconi, C., Lemme, M., Occhetta, P., Gaudiello, E., Votta, E., et al. (2016). Beating heart on a chip: a novel microfluidic platform to generate functional 3D cardiac microtissues. *Lab. Chip* 16 (3), 599–610. doi:10.1039/c5lc01356a

Marx, U., Akabane, T., Andersson, T., Baker, E., Beilmann, M., Beken, S., et al. (2020). Biology-inspired microphysiological systems to advance medicines for patient benefit and animal welfare. *ALTEX* 37 (3), 364–394. doi:10.14573/altex.2001241

Mehta, G., Hsiao, A. Y., Ingram, M., Luker, G. D., and Takayama, S. (2012). Opportunities and challenges for use of tumor spheroids as models to test drug delivery and efficacy. *J. Control. Release* 164 (2), 192–204. doi:10.1016/j.jconrel.2012.04.045

Nakane, T., Abulaiti, M., Sasaki, Y., Kowalski, W. J., Keller, B. B., and Masumoto, H. (2020). Preparation of mesh-shaped engineered cardiac tissues derived from human ips cells for *in Vivo* myocardial repair. *J. Vis. Exp.* 160, e61246. doi:10.3791/61246

Nattel, S (2007). The heart on a chip: the role of realistic mathematical models of cardiac electrical activity in understanding and treating cardiac arrhythmias. *Heart Rhythm* 4 (6), 779–780. doi:10.1016/j.hrthm.2007.03.038

Noor, N., Shapira, A., Edri, R., Gal, I., Wertheim, L., and Dvir, T. (2019). 3D printing of personalized thick and perfusable cardiac patches and hearts. *Adv. Sci.* 6 (11), 1900344. doi:10.1002/advs.201900344

Norotte, C., Marga, F. S., Niklason, L. E., and Forgacs, G. (2009). Scaffold-free vascular tissue engineering using bioprinting. *Biomaterials* 30 (30), 5910–5917. doi:10.1016/j.biomaterials.2009.06.034

Nugraha, B., Buono, M. F., Boehmer, L., Hoerstrup, S. P., and Emmert, M. Y. (2019). Human cardiac organoids for disease modeling. *Clin. Pharmacol. Ther.* 105 (1), 79–85. doi:10.1002/cpt.1286

Nugraha, B., Buono, M. F., and Emmert, M. Y. (2018). Modelling human cardiac diseases with 3D organoid. *Eur. Heart J.* 39 (48), 4234–4237. doi:10.1093/eurheartj/ehy765

Parrish, A. R., Dorr, R. T., Gandolfi, A. J., and Brendel, K. (1994). Adult rat myocardial slices: a tool for studies of comparative cardiotoxicity. *Toxicol. In Vitro.* 8 (6), 1233–1237. doi:10.1016/0887-2333(94)90114-7

Pinto, A. R., Ilinykh, A., Ivey, M. J., KuwabaraIvey, J. T., D'Antoni, M. L., Debuque, R., et al. (2016). Revisiting cardiac cellular composition. *Circ. Res.* 118 (3), 400–409. doi:10.1161/CIRCRESAHA.115.307778

Pitoulis, F. G., Watson, S. A., Perbellini, F., and Terracciano, C. M. (2020). Myocardial slices come to age: an intermediate complexity *in Vitro* cardiac model for translational research. *Cardiovasc. Res.* 116 (7), 1275–1287. doi:10.1093/cvr/cvz341

Qin, X., Sufi, J., Vlckova, P., Kyriakidou, P., Acton, S. E., Li, V. S. W., et al. (2020). Cell-type-specific signaling networks in heterocellular organoids. *Nat. Methods* 17 (3), 335–342. doi:10.1038/s41592-020-0737-8

Ribas, J., Sadeghi, H., Manbachi, A., Leijten, J., Brinegar, K., Zhang, Y. S., et al. (2016). Cardiovascular organ-on-a-chip platforms for drug discovery and development. *Appl. Vitro Toxicol.* 2 (2), 82–96. doi:10.1089/aivt.2016.0002

Richards, D. J., Coyle, R. C., Tan, Y., Jia, J., Wong, K., Toomer, K., et al. (2017). Inspiration from heart development: biomimetic development of functional human cardiac organoids. *Biomaterials* 142, 112–123. doi:10.1016/j.biomaterials.2017.07.021

Richards, D. J., Li, Y., Kerr, C. M., Yao, J., Beeson, G. C., et al. (2020). Human cardiac organoids for the modelling of myocardial infarction and drug cardiotoxicity. *Nat. Biomed. Eng.* 4 (4), 446–462. doi:10.1038/s41551-020-0539-4

Chen, C., Vitiello, L., De Windt, L. J., Rampazzo, A., Calore, M., and Calore, M. (2020). Modeling cardiovascular diseases with hipsc-derived cardiomyocytes in 2D and 3D cultures. *Int. J. Mol. Sci.* 21, 3404. doi:10.3390/ijms21093404

Sakamiya, M., Fang, Y., Mo, X., Shen, J., and Zhang, T. (2020). A heart-on-a-chip platform for online monitoring of contractile behavior via digital image processing and piezoelectric sensing technique. *Med. Eng. Phys.* 75, 36–44. doi:10.1016/j.medengphy.2019.10.001

Sekine, H., Shimizu, T., and Okano, T. (2016). "Cell sheet tissue engineering for heart failure," in *Etiology and morphogenesis of congenital heart disease: from gene function and cellular interaction to morphology*. Tokyo, Japan: Springer Japan, 19–24. doi:10.1007/978-4-431-54628-3_3

Shephard, R. J. (1955). The carbon dioxide balance-sheets of the body: their determination in normal subjects and in cases of congenital heart disease. *J. Physiol.* 129 (1), 142–158. doi:10.1113/jphysiol.1955.sp005343

Song, J, Xing, Y., Chen, X., Song, Z., Teng, X, Wang, M., et al. (2014). Processing of the explanted heart. *N. Am. J. Med. Sci.* 6 (12), 613–617. doi:10.4103/1947-2714.147975

Takebe, T., Sekine, K., Enomura, M., Koike, H., Kimura, M., Ogaeri, T., et al. (2013). Vascularized and functional human liver from an IPSC-derived organ bud transplant. *Nature* 499 (7459), 481–484. doi:10.1038/nature12271

Talman, V, and Kivelä, R. (2018). Cardiomyocyte—endothelial cell interactions in cardiac remodeling and regeneration. *Front Cardiovasc Med.* 26, 101. doi:10.3389/fcvm.2018.00101

Tian, B., Liu, J., Dvir, T., Jin, L., Tsui, J. H., Qing, Q., et al. 2012. Macroporous nanowire nanoelectronic scaffolds for synthetic tissues. *Nat. Mater* 11 (11), 986–994. doi:10.1038/nmat3404

Tudorache, I., Calistru, A., Baraki, H., Meyer, T., Höffler, K., Sarikouch, S., et al. (2013). Orthotopic replacement of aortic heart valves with tissue-engineered grafts. *Tissue Eng. Part A.* 19 (15–16): 1686–1694. doi:10.1089/ten.tea.2012.0074

Valley Cottage N. Y. (2019). Organoids market is projected to grow at a significant CAGR of ~15% during 2019 to 2029—future market insights. Available at: https://www.globenewswire.com/news-release/2019/09/11/1914110/0/en/Organoids-Market-is-projected-to-grow-at-a-Significant-CAGR-of-15-during-2019-to-2029-Future-Market-Insights.html. (Accessed August 17, 2020).

Görler, V., Bojana, S. M., Markovic, B.S., Gazdic, M., Volarevic, A., Jovicic, N., et al. (2018). Ethical and safety issues of stem cell-based therapy. *Int. J. Med. Sci.* 15, 36–45. doi:10.7150/ijms.21666

Watson, S. A., Terracciano, C. M., and Perbellini, F. (2019). Myocardial slices: an intermediate complexity platform for translational cardiovascular research. *Cardiovasc. Drugs Ther.* 33 (2), 239–244. doi:10.1007/s10557-019-06853-5

Wu, Q., Liu, J., Wang, X., Feng, L., Wu, J., Zhu, X., et al. (2020). Organ-on-a-Chip: recent breakthroughs and future prospects, *Biomed. Eng. Online*, 19, 9. doi:10.1186/s12938-020-0752-0

Yamato, M., and Okano, T. (2004). Cell sheet engineering. *Mater. Today* 7 (5), 42–47. doi:10.1016/S1369-7021(04)00234-2

Yang, J., Yamato, M., Kohno, C., Nishimoto, A., Sekine, H., Fukai, F., et al. (2005). Cell sheet engineering: recreating tissues without biodegradable scaffolds. *Biomaterials* 26 (33), 6415–6422. doi:10.1016/j.biomaterials.2005.04.061

Yano, S., and Hoffman, R. (2018). Real-time determination of the cell-cycle position of individual cells within live tumors using FUCCI cell-cycle imaging. *Cells* 7 (10), 168. doi:10.3390/cells7100168

Yeh, G. C. K., and Martinek, J. (1957). The potential of a general dipole in a homogeneous conducting prolate spheroid. *Ann. N. Y. Acad. Sci.* 65 (6), 1003–1006. doi:10.1111/j.1749-6632.1957.tb36700.x

Zhang, X., Wang, T., Wang, P., and Hu, N. (2016). High-throughput assessment of drug cardiac safety using a high-speed impedance detection technology-based heart-on-a-chip. *Micromachines (Basel).* 7 (7), 122. doi:10.3390/mi7070122

Zimmermann, W.-H., Melnychenko, I., and Eschenhagen, T. (2004). Engineered heart tissue for regeneration of diseased hearts. *Biomaterials* 25 (9), 1639–1647. doi:10.1016/S0142-9612(03)00521-0

Zurina, I. M., Presniakova, V. S., Butnaru, D. V., Svistunov, A. A, Timashev, P. S, and Rochev, Y. A (2020). Tissue engineering using a combined cell sheet technology and scaffolding approach. *Acta. Biomater.*, 113, 63–83. doi:10.1016/j.actbio.2020.06.016

Conflict of Interest: The authors declare that the research was conducted in the absence of any commercial or financial relationships that could be construed as a potential conflict of interest.

frontiers in Pharmacology

ORIGINAL RESEARCH
published: 12 April 2021
doi: 10.3389/fphar.2021.649414

Patch-Clamp Recordings of Action Potentials From Human Atrial Myocytes: Optimization Through Dynamic Clamp

Arie O. Verkerk[1,2*†], Gerard A. Marchal[2†], Jan G. Zegers[1], Makiri Kawasaki[2], Antoine H. G. Driessen[3], Carol Ann Remme[2], Joris R. de Groot[4] and Ronald Wilders[1]

[1]Department of Medical Biology, Amsterdam UMC, University of Amsterdam, Amsterdam, Netherlands, [2]Department of Experimental Cardiology, Amsterdam UMC, University of Amsterdam, Amsterdam, Netherlands, [3]Department of Cardiothoracic Surgery, Amsterdam UMC, University of Amsterdam, Amsterdam, Netherlands, [4]Department of Cardiology, Amsterdam UMC, University of Amsterdam, Amsterdam, Netherlands

OPEN ACCESS

Edited by:
Tamer M. A. Mohamed,
University of Louisville, United States

Reviewed by:
Oscar Casis,
Universidad del País Vasco UPV/EHU, Spain
Felix Wiedmann,
Heidelberg University Hospital, Germany
Andrew F. James,
University of Bristol, United Kingdom

***Correspondence:**
Arie O. Verkerk
a.o.verkerk@amsterdamumc.nl

†These authors have contributed equally to this work

Specialty section:
This article was submitted to Cardiovascular and Smooth Muscle Pharmacology, a section of the journal Frontiers in Pharmacology

Received: 04 January 2021
Accepted: 18 February 2021
Published: 12 April 2021

Citation:
Verkerk AO, Marchal GA, Zegers JG, Kawasaki M, Driessen AHG, Remme CA, de Groot JR and Wilders R (2021) Patch-Clamp Recordings of Action Potentials From Human Atrial Myocytes: Optimization Through Dynamic Clamp. Front. Pharmacol. 12:649414. doi: 10.3389/fphar.2021.649414

Introduction: Atrial fibrillation (AF) is the most common cardiac arrhythmia. Consequently, novel therapies are being developed. Ultimately, the impact of compounds on the action potential (AP) needs to be tested in freshly isolated human atrial myocytes. However, the frequent depolarized state of these cells upon isolation seriously hampers reliable AP recordings.

Purpose: We assessed whether AP recordings from single human atrial myocytes could be improved by providing these cells with a proper inward rectifier K^+ current (I_{K1}), and consequently with a regular, non-depolarized resting membrane potential (RMP), through "dynamic clamp".

Methods: Single myocytes were enzymatically isolated from left atrial appendage tissue obtained from patients with paroxysmal AF undergoing minimally invasive surgical ablation. APs were elicited at 1 Hz and measured using perforated patch-clamp methodology, injecting a synthetic I_{K1} to generate a regular RMP. The injected I_{K1} had strong or moderate rectification. For comparison, a regular RMP was forced through injection of a constant outward current. A wide variety of ion channel blockers was tested to assess their modulatory effects on AP characteristics.

Results: Without any current injection, RMPs ranged from −9.6 to −86.2 mV in 58 cells. In depolarized cells (RMP positive to −60 mV), RMP could be set at −80 mV using I_{K1} or constant current injection and APs could be evoked upon stimulation. AP duration differed significantly between current injection methods ($p < 0.05$) and was shortest with constant current injection and longest with injection of I_{K1} with strong rectification. With moderate rectification, AP duration at 90% repolarization (APD_{90}) was similar to myocytes with regular non-depolarized RMP, suggesting that a synthetic I_{K1} with moderate rectification is the most appropriate for human atrial myocytes. Importantly, APs evoked using each injection method were still sensitive to all drugs tested (lidocaine, nifedipine, E-4031, low dose 4-aminopyridine, barium, and apamin), suggesting that the major ionic currents of the atrial cells remained functional. However, certain drug effects were quantitatively dependent on the current injection approach used.

Conclusion: Injection of a synthetic I_{K1} with moderate rectification facilitates detailed AP measurements in human atrial myocytes. Therefore, dynamic clamp represents a promising tool for testing novel antiarrhythmic drugs.

Keywords: drug testing, patch clamp, human, cardiac myocytes, left atrial appendage, action potential, dynamic clamp, inward rectifier potassium current

INTRODUCTION

Atrial fibrillation (AF) is the most common type of sustained cardiac arrhythmia in the elderly, with a substantially increasing prevalence anticipated over the next decades (Wakili et al., 2011; Milnes et al., 2012; Colilla et al., 2013; Krijthe et al., 2013). Data from the Framingham Heart Study revealed that AF is independently associated with a 50–90% increase in the risk of death (Benjamin et al., 1998). Clinical AF therapy focuses on prevention of severe complications secondary to AF, in addition to restoration of normal atrial rhythm (Milnes et al., 2012; Kirchhof et al., 2016; January et al., 2019). However, currently available drugs are associated with significant side effects as most of these compounds also affect ventricular function (Milnes et al., 2012). Consequently, current research focuses on atrial-specific pharmacological targeting of ion channels, such as $K_V1.5$, Kir3.1/3.4, small conductance Ca^{2+}-activated K^+ (SK) channels, and $Na_V1.5$, in order to generate new therapeutic strategies for AF (Antzelevitch and Burashnikov, 2010; Dobrev and Nattel, 2010; Wakili et al., 2011; Dobrev et al., 2012; Milnes et al., 2012; Peyronnet and Ravens, 2019).

Various *in vitro* (Papke and Smith-Maxwell, 2009; Ebert et al., 2012; Devalla et al., 2015; Hu et al., 2018) and *in vivo* animal models (Olgin and Verheule, 2002; Finet et al., 2009; Nishida et al., 2010), including AF models, are available for atrial drug testing, all with their individual strengths and limitations. While these models provide an excellent starting point for atrial and AF-related drug studies, assessments of action potentials (APs) of native human atrial cardiomyocytes remain essential due to distinct inter-species differences in ion channel expression profiles (Varró et al., 2021), and because drugs frequently act through AP shortening or prolonging effects, which may be frequency dependent (Peyronnet and Ravens, 2019). Samples of human left or right atrial appendage can be readily obtained during cardiac surgery (Hatem et al., 2010; Voigt et al., 2015), and studies employing such samples have provided detailed knowledge of human atrial electrophysiology in healthy and diseased states, as reviewed elsewhere (Nattel et al., 2007; Schotten et al., 2011; Dobrev et al., 2012; Heijman et al., 2014). So far, a variety of methods have been used for the electrophysiological analysis of human atrial tissue and cells, including sharp electrode measurements (Trautwein et al., 1962; Ten Eick and Singer, 1979), patch clamp methodology (Van Wagoner et al., 1997; Hoppe and Beuckelmann, 1998), multi-electrode arrays (MEAs) (Kanagaratnam et al., 2006), and voltage-sensitive fluorescence (Krul et al., 2015). In particular, the patch clamp technique, which is considered the gold standard in electrophysiology due to the ability to measure both membrane currents and APs in single cells (Kornreich, 2007), has demonstrated the functional presence of various types of ion channels in human atrial cells. However, AP measurements from isolated human atrial myocytes using patch clamp methodology are limited by the frequent depolarized state of the resting membrane potential (RMP) of these myocytes (Hoppe and Beuckelmann, 1998; Colman et al., 2018). Upon isolation, generally only a fraction of cells, approximately 5–20%, have an RMP sufficiently negative to elicit APs (Amos et al., 1996; Schreieck et al., 2000), and even within this fraction highly depolarized myocytes are frequently excluded from analysis (Loose et al., 2014).

Various patch clamp studies on human atrial myocytes have addressed this major problem of depolarized state by injection of a hyperpolarizing current of constant amplitude, resulting in an RMP near −80 mV (Wang et al., 1993; Le Grand et al., 1994; Bénardeau et al., 1996; Workman et al., 2001; Pau et al., 2003; Workman et al., 2003; Lagrutta et al., 2006; Limberg et al., 2011; Workman et al., 2012; Skibsbye et al., 2014; Schmidt et al., 2015). However, this hyperpolarizing current of constant amplitude also affects the AP repolarization phase to a considerable extent, thereby potentially hampering the assessment of the impact of drugs on AP duration (APD).

Human induced pluripotent stem cell-derived cardiomyocytes (hiPSC-CMs) frequently display similar depolarized membrane potentials due to their relative immaturity (Veerman et al., 2015). In these cells, however, the dynamic clamp methodology (Wilders, 2006; Berecki et al., 2014; Ortega et al., 2018; Verkerk and Wilders, 2021) has been successfully applied to overcome the depolarized state by injection of an *in silico* inward rectifier K^+ current (I_{K1}) (Bett et al., 2013; Meijer van Putten et al., 2015; Verkerk et al., 2017), which is the main current responsible for setting the RMP close to the potassium equilibrium potential (E_K) of approximately −85 mV. Consequently, hiPSC-CMs could be stimulated at fixed rates with fast sodium current (I_{Na}) driven upstrokes. Furthermore, this dynamic clamp reduced the variability of various AP parameters (Verkerk et al., 2017), thus allowing easier detection of small changes in these parameters.

We here tested whether the injection of a synthetic I_{K1}, which is computed in real time based on the acquired membrane potential and then injected into the cell through the patch pipette, can also improve AP measurements in human left atrial appendage (LAA) myocytes. We used two different I_{K1}

TABLE 1 | Patient characteristics.

Number of patients, *n*	8
Gender, M/F	6/2
Age (years)	53.3 ± 3.4
Heart rate (beats min^{-1})[a]	58.4 ± 4.0
PR interval (ms)[a]	179.5 ± 10.2
QRS interval (ms)[a]	102.0 ± 9.4
QTc interval (ms)[a]	431.0 ± 9.2
Hypertension, *n*	5
Pulmonary hypertension, *n*	1
Diabetes, *n*	N/A
ACE inhibitors, *n*	6
Ca^{2+} antagonists, *n*	1
Class IC blockers, *n*	4
Class II blockers, *n*	2
Class III blockers, *n*	5
Lipid-lowering drugs, *n*	4

[a]*In sinus rhythm. ACE, angiotensin-converting enzyme.*

current-voltage relationships, i.e., one with large and one with moderate rectification, and compared the results to those obtained with the injection of a repolarizing current of constant amplitude. In addition, we tested a broad range of ion channel blockers to see if drugs are still able to modify AP characteristics under these conditions and to test if drug effects are dependent on the current injection approach used.

MATERIALS AND METHODS

Human Cell Preparation

Human Myocardial Tissue

Written informed consent was obtained from all patients, and the study was approved by the local ethics committee and conducted in accordance with the Declaration of Helsinki. LAAs were obtained from eight patients with paroxysmal AF undergoing minimally invasive surgical ablation (mini-maze procedure). **Table 1** shows the patient characteristics. Immediately after surgical removal of the specimens, the LAA tissue was placed in chilled (0°C) Ca^{2+}-free MOPS solution, and carried to the laboratory within 30 min. The Ca^{2+}-free MOPS solution was composed of (in mM): 100 NaCl, 10 KCl, 5 glucose, 5 $MgSO_4$, 50 taurine, 11 creatine, 5 MOPS; pH 7.0 (NaOH).

Isolated Human Atrial Myocytes

Single cells were obtained by an enzymatic isolation method modified from Dobrev et al. (2000). In short, fatty tissue and endocardial connective tissue were removed and the remaining tissue was cut into small cubic pieces (≈1 mm^3), and washed three times for 10 min in Ca^{2+}-free MOPS solution (37°C). Then, the LAA tissue pieces were incubated for 60 min in Ca^{2+}-free MOPS solution (37°C) to which collagenase A (250 U/ml; Roche) and proteinase XXIV (3.5–7.0 U/ml; Sigma) were added. In these 60 min, the Ca^{2+} concentration was gradually increased to 0.15 mM by adding Ca^{2+} three times (i.e., at 15, 40, and 50 min). Subsequently, the tissue pieces were placed in 0.1 mM Ca^{2+} MOPS solution (37°C) with collagenase A (310 U/ml; Roche). During this last incubation period, the tissue pieces were gently stirred and at regular intervals of 15 min the solution was microscopically examined for the presence of dissociated rod-shaped myocytes. Once single, rod-shaped myocytes were observed (usually after 75 min), cells were removed, and this was repeated every 10 min for 80 min, resulting in several batches of isolated cells. The isolated cells were transferred into Ca^{2+}-free MOPS solution (37°C) containing 1% BSA. Isolated cells were stored for at least 45 min at room temperature in a modified Tyrode's solution containing (in mM): 145 NaCl, 5.4 KCl, 0.9 $CaCl_2$, 0.5 $MgCl_2$, 5.5 glucose and 5.0 HEPES; pH 7.4 (NaOH).

Electrophysiological Experiments

Recording Procedures and Data Acquisition

The myocytes were placed in a cell chamber mounted on the stage of an inverted microscope (Nikon Diaphot), and allowed to settle for 5 min before they were superfused with Tyrode's solution containing 1.8 mM $CaCl_2$ and 1 mM $MgCl_2$. Single myocytes having smooth surfaces with cross striations were selected for electrophysiological measurements. APs were recorded using an Axopatch 200B amplifier (Molecular Devices, Sunnyvale, CA, United States). Data acquisition, voltage control, and analysis were accomplished using custom software. All potentials were corrected for the estimated liquid junction potential (Barry and Lynch, 1991). Pipettes (resistance 2–3 MΩ) were pulled from borosilicate glass capillaries (Harvard Apparatus, United Kingdom) using a custom-made vertical microelectrode puller. Cell membrane capacitance (C_m) was estimated by dividing the time constant of the decay of the capacitive transient in response to 5 mV hyperpolarizing voltage clamp steps from −40 mV by the series resistance. Average C_m was 114 ± 9 pF (n = 58; mean ± SEM). Signals were low-pass filtered with a cut-off frequency of 5 kHz and digitized at 40 kHz.

Action Potentials

APs were measured at 36 ± 0.2°C using the amphotericin-perforated patch-clamp method. These were mostly obtained from the 5–8th isolation batch of myocytes, because the myocytes of the first batches had relatively "weak" membranes and frequently displayed loss of seal, unwanted ruptured patch, and/or large "leak currents". Pipette solution contained (in mM): 125 K-gluc, 20 KCl, 5 NaCl, 0.44 amphotericin-B, 10 HEPES (pH 7.2; KOH). APs were continuously elicited at 1 Hz with square 3-ms, ≈1.2× threshold current pulses through the patch pipette. APs were measured at steady-state baseline conditions and at 5 min after drug application. We analyzed RMP, maximum AP upstroke velocity (dV/dt_{max}), AP amplitude (APA), AP plateau amplitude (PlatA; measured 20 ms after initiation of the AP upstroke), and APD at 20, 50, and 90% repolarization (APD_{20}, APD_{50}, and APD_{90}, respectively). Parameters from 10 consecutive APs were averaged.

Constant Current Injection and Dynamic Clamp

In the present study, we used constant and dynamic clamp current injections to set the RMP of single atrial myocytes at

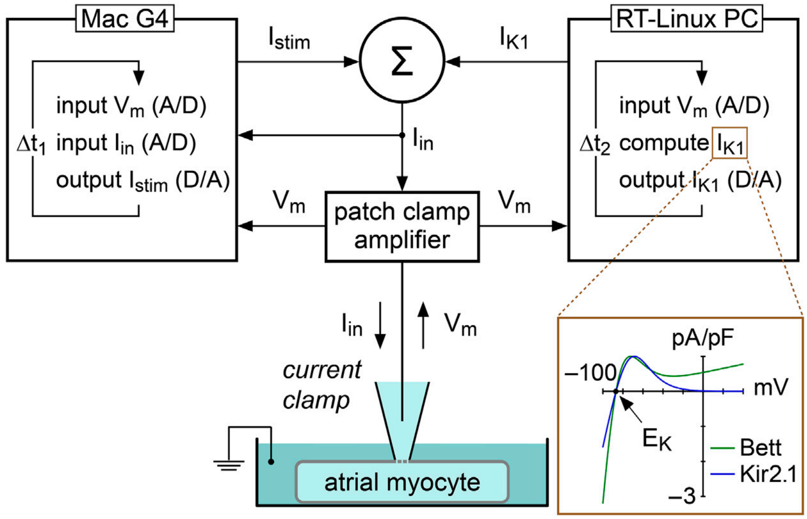

FIGURE 1 | Experimental approach to supply a patched atrial myocyte with a synthetic inward rectifier K^+ current (I_{K1}). A Real-Time Linux (RT-Linux) based PC computes the synthetic I_{K1} according to the membrane potential (V_m) that is read into the PC. After addition of any stimulus current (I_{stim}), this I_{K1} is sent to the patch clamp amplifier, which operates in current clamp mode and injects the net current (I_{in}) into the patched myocyte. This process is updated with a time step Δt_2 of 40 µs. I_{stim} is sent out by the Apple Macintosh (Mac) G4 computer that is used to control the experiment and record both V_m and I_{in} at a rate of 40 kHz, corresponding with a time step Δt_1 of 25 µs. Inset: current–voltage relationship of the synthetic I_{K1} with moderate rectification ("Bett" current; Bett et al., 2013) and the synthetic I_{K1} with strong rectification ("Kir2.1" current; Meijer van Putten et al., 2015). E_K denotes the potassium equilibrium potential.

−80 mV, i.e., close to the RMP in atrial tissue from patients with AF (Christ et al., 2008). Constant current was injected with our standard patch clamp software and the amount of injected current was adapted in every myocyte to set its RMP at −80 mV. A custom dynamic clamp setup was used to inject an *in silico* I_{K1}, as illustrated in **Figure 1**, and previously described in detail (Meijer van Putten et al., 2015). In short, we extended our standard patch clamp setup with a separate Real-Time Linux (RT-Linux) based PC that continuously reads in the membrane potential (V_m) of the atrial myocyte and computes the V_m-dependent synthetic I_{K1}. Within the time step Δt_2 of 40 µs, a command potential is generated that, combined with a command potential for any stimulus current, is sent to the patch clamp amplifier to inject this current into the human atrial myocyte. For our synthetic I_{K1}, we used two different I_{K1} current-voltage relationships.

One I_{K1} had a current-voltage relationship based on a fit to data from Kir2.1 channels expressed in HEK-293 cells by Dhamoon et al. (2004), defined "Kir2.1" in the remainder of the study. The Kir2.1 current has a strong rectification, as illustrated in **Figure 1** (inset), resulting in absence of a substantial current positive to −20 mV (Dhamoon et al., 2004; Meijer van Putten et al., 2015), and is computed according to:

$$I_{K1} = A \times 0.12979 \times \left\{ \frac{V_m - E_K}{1.0 + e^{[0.093633 \times (V_m + 72)]}} \right\},$$

in which V_m and E_K denote the membrane potential and potassium equilibrium potential (in mV), respectively, and E_K amounts to −86.9 mV. "A" denotes a scaling factor which is adapted in every experiment to set the RMP at −80 mV. If A is set to 1, the peak outward current density of I_{K1} amounts to 1 pA/pF.

The other I_{K1} had a current-voltage relationship showing moderate rectification, defined "Bett" in the rest of the study, referring to the I_{K1} used in the dynamic clamp study by Bett et al. (2013). Their I_{K1} has a substantial current at positive potentials, as illustrated in **Figure 1** (inset), consistent with I_{K1} currents observed in human atrial myocytes (Koumi et al., 1995), and is computed according to:

$$I_{K1} = A \times \left[0.307 \times \left(\frac{V_m - E_K}{1 + e^{(0.0896 (V_m - E_K))}} \right) + 0.00614 \times (V_m - E_K) \right],$$

in which V_m and E_K denote the membrane potential and potassium equilibrium potential (in mV), respectively, and E_K amounts to −86.9 mV. "A" denotes a scaling factor which is adapted in every experiment to set the RMP at −80 mV. If A is set to 1, the peak outward current density of I_{K1} equals 1 pA/pF.

Drugs

Various general ion channel blockers with well-known effects on human atrial tissue and/or cells were used to test their ability to modify AP characteristics when applying current injection and to validate if potential drug effects depend on the I_{K1} or constant current injection approach used. Each drug was tested in myocytes isolated from two patients. 4-Aminopyridine (4-AP; Merck) was freshly prepared as 10 mM stock solution in Tyrode's solution and pH was readjusted to 7.4 (HCl). Nifedipine (Sigma) was prepared as 5 mM stock solution in ethanol, and stored in the

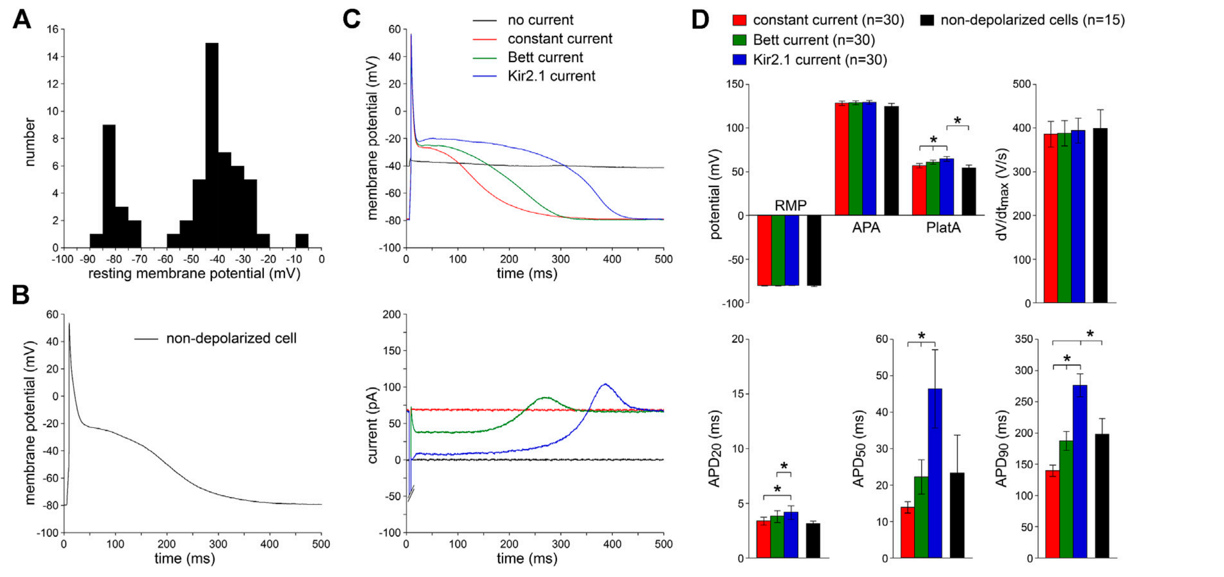

FIGURE 2 | Effects of injection of constant repolarizing current or synthetic I_{K1} (with moderate or strong rectification, supplied through dynamic clamp) on action potentials of enzymatically isolated human atrial myocytes. **(A)** Resting membrane potential (RMP) of 58 human atrial myocytes in absence of repolarizing current injection. Note the group of 15 non-depolarized myocytes (leftmost group of bars) with an RMP of −70 mV or more negative. **(B)** Typical action potential (AP), elicited at 1 Hz, of a non-depolarized myocyte in absence of any repolarizing current injection. **(C) Top:** typical APs elicited at 1 Hz in presence of injected constant or I_{K1} current within one originally depolarized cell (with an original RMP near −40 mV). **Bottom:** associated injected currents. Synthetic I_{K1} supplied as detailed in **Figure 1**. **(D)** Average AP parameters of 30 originally depolarized myocytes during constant current and I_{K1} injections with dynamic clamp. Non-depolarized cells are the 15 cells of panel A with an RMP of −70 mV or more negative in absence of any repolarizing current injection. APA, AP amplitude; PlatA, amplitude of the AP plateau; dV/dt_{max}, maximum AP upstroke velocity; APD_{20}, APD_{50}, and APD_{90}, AP duration at 20, 50, and 90% repolarization, respectively. $^{*}p < 0.05$.

dark. E-4031 (Tocris), apamin (Sigma), and $BaCl_2$ (Sigma) were prepared as 5, 0.1, and 1000 mM stock solutions, respectively, in distilled water. All stock solutions and lidocaine (10 mg/ml; Braun) were diluted appropriately before use.

Statistics

All data are presented as mean ± SEM. Potential differences in membrane capacitance between non-depolarized and depolarized myocytes were assessed with an unpaired Student's *t*-test. Drug effects were tested with a paired Student's *t*-test. Differences between three or more groups were assessed using one-way RM ANOVA followed by pairwise comparison using the Student-Newman-Keuls test. $p < 0.05$ was considered statistically significant.

RESULTS

Basic Action Potential Characterization of Isolated Human Atrial Myocytes

We patched 58 single human atrial myocytes enzymatically isolated from LAAs that were obtained from eight patients with paroxysmal AF (**Table 1**). **Figure 2A** shows the distribution of the RMP of these cells. In only 15 (26%) of these cells, we were able to obtain an RMP sufficiently negative (−70 mV or more negative; **Figure 2A**, leftmost group of bars) to elicit APs. A typical AP of an intrinsically non-depolarized myocyte is shown in **Figure 2B**. C_m did not differ significantly between non-depolarized and depolarized myocytes (112 ± 13 vs. 115 ± 12 pF, respectively) and the AP parameters of the 15 intrinsically non-depolarized cells appear in **Figure 2D** as black bars. The remaining 43 (74%) of these cells were too depolarized to evoke APs with an I_{Na} driven upstroke (Gelband et al., 1972; Berecki et al., 2010). Typically, the RMP of these cells was positive to −60 mV (**Figure 2A**, rightmost group of bars).

Effects of I_{K1} and Constant Current Injection on Action Potentials

Next, we studied the effects of the two types of dynamic clamp-injected synthetic I_{K1} currents (**Figure 1**, inset) as well as constant current injection on the AP morphology of 30 depolarized myocytes. To compare potential differences of these three approaches, all types of current injection were tested in every cell measured. **Figure 2C**, top panel, shows representative recordings of the membrane potential. The associated traces in **Figure 2C**, bottom panel, show the injected currents. In the absence of I_{K1} or constant current injection, the membrane potential was around −40 mV and no APs could be evoked (black lines). Upon switching on the dynamic clamp system with the synthetic "Kir2.1" I_{K1} [i.e., the I_{K1} with strong rectification (**Figure 1**, inset)], the RMP hyperpolarized consistent with the generated outward current (blue lines). We chose an I_{K1} amplitude that set the RMP at −80 mV, which is close to the RMP in human AF cells previously reported by Christ et al. (2008) and to the RMP that we observed in the 15 intrinsically non-depolarized cells (**Figure 2D**). At this potential, the synthetic I_{K1} was still substantial [0.71 ± 0.08 pA/pF (n = 30), consistent with the current-voltage relationship of Kir2.1]. When the synthetic I_{K1} was added, APs could be elicited, and average AP characteristics with the Kir2.1 injection are summarized **Figure 2D** (blue bars). The APs had fast upstroke velocities of ≈400 V/s, indicating that they were importantly driven by I_{Na} (Berecki et al., 2010). The phase 1 repolarization was fast, resulting in a relatively short APD_{20} and a plateau potential of around −20 mV, typical for human atrial myocytes with the co-called "Type A" (Bénardeau et al., 1996) and "Type 3" (Dawodu et al., 1996; Workman et al., 2001) AP shape. Thus, the dynamic clamp-injected Kir2.1 I_{K1} enabled the generation of APs in originally depolarized human atrial myocytes.

We followed the same approach for the injection of the "Bett" I_{K1}, i.e., the I_{K1} with moderate rectification (**Figure 1**, inset). The results are shown in **Figure 2C,D**, as green lines and bars, respectively. Again, the RMP was successfully hyperpolarized to −80 mV [with an I_{K1} amplitude of 0.73 ± 0.08 pA/pF (n = 30) at this potential], and APs could be evoked. However, the APD was significantly shorter at all repolarization phases and the AP plateau amplitude was significantly lower compared to the APs with Kir2.1 I_{K1} injection (**Figure 2C,D**). As expected from the I_{K1} current-voltage relationships (**Figure 1**, inset), this was due to the lower amount of rectification resulting in a larger injected outward current during phase 1 and phase 2 of the AP (**Figure 2C**, bottom). In each of the cells, we also applied the constant current injection (**Figure 2C,D**, red lines and bars). Again, the RMP was successfully hyperpolarized to −80 mV [with an outward current amplitude of 0.71 ± 0.09 pA/pF (n = 30)]. However, this approach was accompanied by a severe AP shortening compared to APs measured with Kir2.1 I_{K1} injection (**Figure 2C,D**), due to the large injected outward current over the complete course of the AP (**Figure 2C**, bottom).

While all three types of injected current resulted in successful RMP hyperpolarization to −80 mV, and consequently allowed the elicitation of I_{Na} driven APs, the APD and AP plateau amplitude differed significantly between the methods used. On average, APD_{20}, APD_{50}, and APD_{90} were longest using the Kir2.1 current and shortest with the constant current injection (**Figure 2D**). Neither the APA nor the dV/dt_{max} differed between the three different current types, but AP plateau amplitude was lowest with constant current injection and highest with injection of Kir2.1 (**Figure 2D**). To test which approach most closely resembled the physiological conditions, we compared the AP parameters measured with each of the three types of current injection with those of the non-depolarized cells. As shown in **Figure 2D**, the average AP parameters of the 15 non-depolarized cells (black bars) matched closely with the AP parameters measured with the current injection methods, except that APD_{90} significantly differed from the Kir2.1 and constant current injection approaches. In addition, the AP plateau amplitude was significantly different between the non-depolarized cells and the cells injected with Kir2.1 I_{K1}.

In summary, both I_{K1} formulations as well as the constant current injection appeared sufficient to obtain a stable RMP near −80 mV, enabling the generation of I_{Na} driven APs. Especially APs obtained with the Bett I_{K1} were highly similar to those of non-depolarized cells.

Effects of Drugs

Next, we tested a wide range of ion channel blockers to find out whether these still exert their effects when applying current injection to obtain an RMP near −80 mV and whether the effects on AP morphology depend on the injection approach used. We anticipated that drug effects, especially those related to APD, may differ between approaches consequent to the observed APD differences among the latter (**Figure 2D**).

Lidocaine

First, we tested the effects of 20 μM lidocaine, an antiarrhythmic agent that specifically blocks I_{Na} (Bean et al., 1983). **Figure 3**, shows typical examples (**Figure 3A**) and the average effects (**Figure 3B**) of the partial block of I_{Na} at this concentration of lidocaine, respectively. Lidocaine significantly reduced dV/dt_{max} by ≈ 10%, as also illustrated in **Figure 3A**, inset, and significantly shortened APD at all repolarization phases. AP plateau amplitude was significantly decreased, but RMP and APA were unaltered. The effects of lidocaine did not differ significantly between the I_{K1} and constant current injections.

Nifedipine

Second, 0.1 μM nifedipine was used to specifically block the L-type Ca^{2+} current ($I_{Ca,L}$) by ≈ 50% (Eroglu et al., 2020). **Figure 3C,D**, show representative examples and summarizes the average effects on AP parameters, respectively. Nifedipine did not affect RMP, APA, or dV/dt_{max}, but significantly reduced APD at all repolarization phases as well as AP plateau amplitude. The nifedipine-induced AP shortening was most prominent with injection of Kir2.1 I_{K1} (**Figure 3C,D**), i.e., the approach with the longest baseline APs. In case of APD_{90}, the effects of nifedipine differed significantly between the Kir2.1 I_{K1} and constant current injection approaches (**Figure 3D**).

4-Aminopyridine

Third, we assessed the effects of 50 μM 4-AP, which is known to reduce the ultra-rapid component of the delayed rectifier K^+ current (I_{Kur}) by ≈50% without affecting the transient outward K^+ current (I_{to1}) (Wang et al., 1993). **Figure 4A,B**, show typical examples of APs and the average effects of the low dose 4-AP, respectively. 4-AP affected all AP parameters except RMP and dV/dt_{max}. The 4-AP-induced blockade of I_{Kur} did not only result in a significant increase in APA and AP plateau amplitude, but also in a significant AP prolongation at most repolarization phases. At 50% repolarization, the increase in APD was significantly larger with the Kir2.1 I_{K1} compared to the constant current injection method, and at 90% repolarization the increase in APD was significantly larger with the Kir2.1 I_{K1} compared to both the Bett I_{K1} and constant current injection methods.

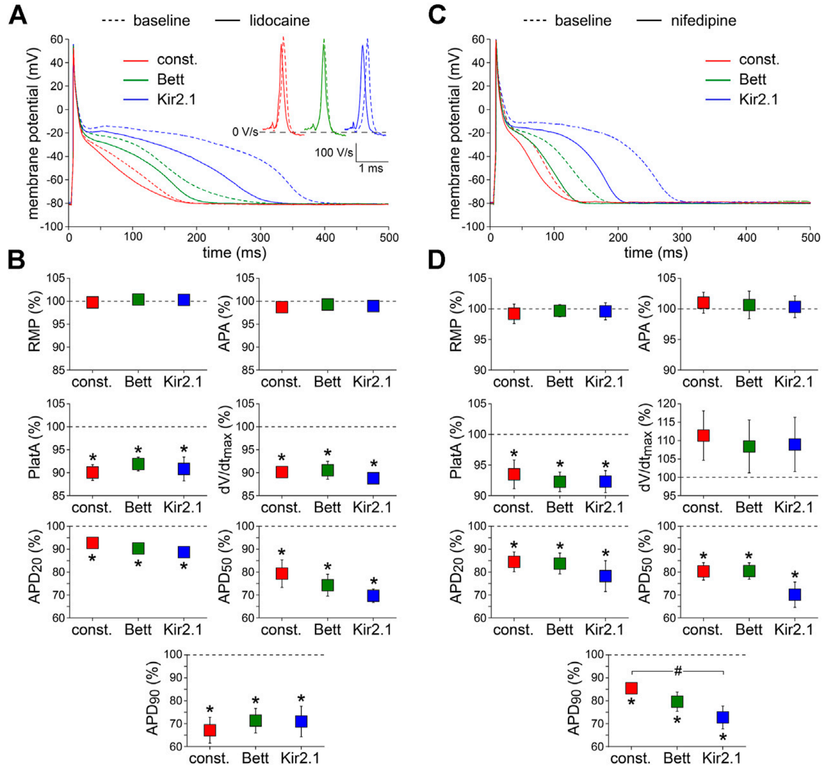

FIGURE 3 | Effects of inward current blockade on APs measured with constant and I_{K1} current injection. **(A)** Typical APs of one atrial myocyte in absence (baseline) and presence of lidocaine to block the fast Na^+ current. Inset: first derivatives of the AP upstrokes, reflecting the amplitude of the fast Na^+ current. **(B)** Average AP parameters measured in five cells in presence of lidocaine. AP parameters are normalized to the AP parameters measured under baseline conditions in the same cell. **(C)** Typical APs of one atrial myocyte in absence (baseline) and presence of nifedipine to block the L-type Ca^{2+} current. **(D)** Average AP parameters measured in six cells in presence of nifedipine. AP parameters are normalized to the AP parameters measured under baseline conditions in the same cell. $^*p < 0.05$, drug vs. baseline (paired *t*-test); $^{\#}p < 0.05$, drug effects observed with constant current, Bett current, and Kir2.1 current (ANOVA with follow-up test).

E-4031

Fourth, we measured the effects of specific and complete blockade of the rapid component of the delayed rectifier K^+ current (I_{Kr}), which was induced by 5 µM E-4031 (Sanguinetti and Jurkiewicz, 1990). **Figure 4C,D** show typical examples and the average effects of E-4031, respectively. E-4031 resulted in a significant increase in both APD_{50} and APD_{90}, without affecting other AP parameters. The effects of E-4031 on APD_{50} were most prominent with the Kir2.1 I_{K1} approach, resulting in a significantly larger increase as compared to the Bett I_{K1} and constant current injection methods.

Apamin

Fifth, the effects of the bee venom neurotoxin apamin (Banks et al., 1979), which is a highly potent and specific blocker of small conductance Ca^{2+}-activated K^+ channels (SK channels) (Xu et al., 2003; Yu et al., 2014), was tested at a concentration of 50 pM. Typical examples and the average effects of SK channel blockade on APs are shown in **Figure 5A,B**, respectively. Apamin significantly depolarized the RMP, significantly decreased APA and dV/dt_{max}, and significantly increased APD_{90} with all three types of current injection. The effects of apamin did not differ significantly between the I_{K1} and constant current injection approaches.

Barium

Finally, we tested the effects of 1 mM Ba^{2+}, which completely blocks inward rectifier channels (Schram et al., 2003), to find out whether I_{K1} is still functional in the initially depolarized cells. **Figure 5C** shows typical AP recordings before and after the addition of Ba^{2+} to the extracellular solution; **Figure 5D** summarizes the average AP changes. As illustrated, Ba^{2+} significantly depolarized the RMP, significantly decreased APA and dV/dt_{max}, and induced significant prolongation of the APD_{90}. The effects were similar with all three types of current injection.

DISCUSSION

Overview

In accordance with previous studies, we here observed a wide range of RMP values in single human LAA myocytes following isolation. In the depolarized cells (RMP positive to −60 mV), RMP could be set at −80 mV using I_{K1} or constant current injection, and consequently APs could be evoked upon stimulation. The AP morphology of cells with current

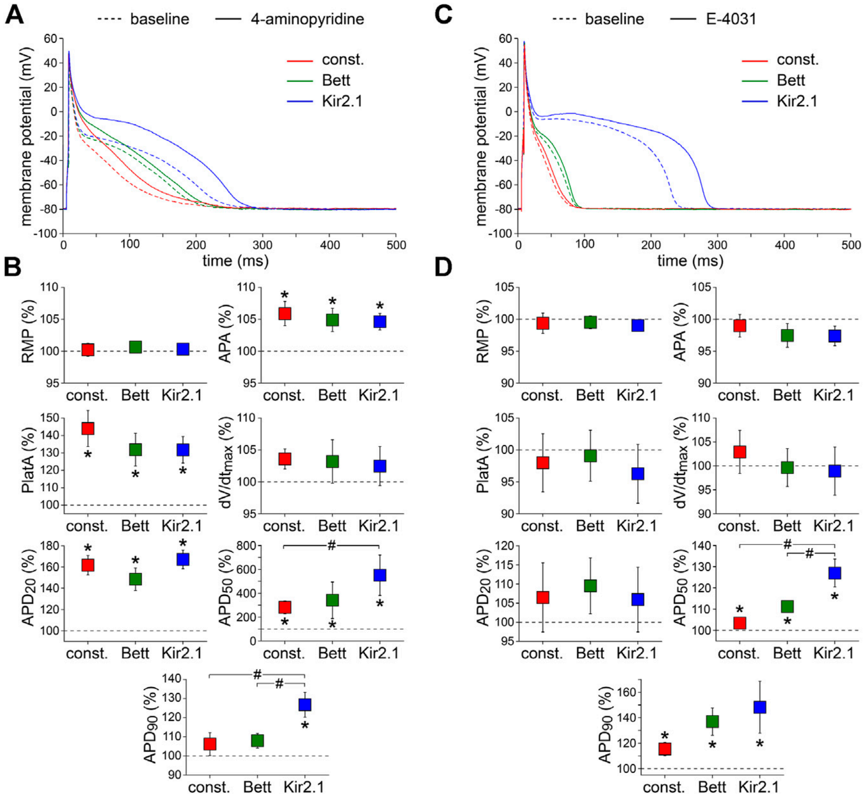

FIGURE 4 | Effects of delayed rectifier K^+ current blockade on APs measured with constant and I_{K1} current injection. **(A)** Typical APs of one atrial myocyte in absence (baseline) and presence of low dose 4-aminopyridine (4-AP) to block the ultra-rapid delayed rectifier K^+ current. **(B)** Average AP parameters measured in five cells in presence of 4-AP. AP parameters are normalized to the AP parameters measured under baseline conditions in the same cell. **(C)** Typical APs of one atrial myocyte in absence (baseline) and presence of E-4031 to block the rapid delayed rectifier K^+ current. **(D)** Average AP parameters measured in five cells in presence of E-4031. AP parameters are normalized to the AP parameters measured under baseline conditions in the same cell. *$p < 0.05$, drug vs. baseline (paired *t*-test); #$p < 0.05$, drug effects observed with constant current, Bett current, and Kir2.1 current (ANOVA with follow-up test).

injection was quite similar to that of regular non-depolarized cells, especially when using I_{K1} with "Bett" characteristics, i.e., with moderate rectification. APs evoked using constant current or I_{K1} injection were still sensitive to all tested drugs (lidocaine, nifedipine, low dose of 4-AP, E-4031, apamin and barium), suggesting that the major ionic currents of the atrial cells were still functional in the initially depolarized myocytes. However, drug effects, especially those related to APD, were in some cases dependent on the current injection approach used.

Current Injection Facilitates Action Potential Recordings From Human Atrial Myocytes

In ≈75% of the freshly isolated human atrial myocytes, we found an RMP positive to −60 mV (**Figure 2A**). While this is generally observed with patch clamp methodology in this cell type (Amos et al., 1996; Schreieck et al., 2000; Loose et al., 2014), the exact reason for the depolarized state of the RMP still remains to be resolved. It may be intrinsic to human LAA myocytes (Mary-Rabine et al., 1980; Escande et al., 1986), for example due to the presence of the hyperpolarization-activated inward current (I_f) (Thuringer et al., 1992; Hoppe and Beuckelmann, 1998; Stillitano et al., 2013), the lower density of I_{K1} compared to ventricular myocytes (Varró et al., 1993), or the presence of an as yet unknown "native" depolarizing conductance. In addition, it may be introduced by the diseased state of the myocytes (Nattel et al., 2007), since the tissue in the present study is obtained from patients suffering from AF. However, depolarized cells are also frequently found in myocytes isolated from tissue obtained from patients undergoing aortocoronary bypass surgery and from donor hearts (Amos et al., 1996; Schreieck et al., 2000), suggesting that the diseased state is a less plausible explanation. In fact, I_{K1} is upregulated in response to AF (Van Wagoner et al., 1997; Bosch et al., 1999; Workman et al., 2001; Dobrev et al., 2005), suggesting a limited number of depolarized cells, which, however, was not the case, as shown in **Figure 2A**. It might also result from technical issues related to the patch clamp technique with imperfect seals resulting in "leak currents" that depolarize the RMP (Verkerk and Wilders, 2021). RMP depolarizations would be more pronounced in smaller cells, but in the present study non-depolarized and depolarized myocytes had a similar C_m. Finally, effects from cell isolation procedures cannot be

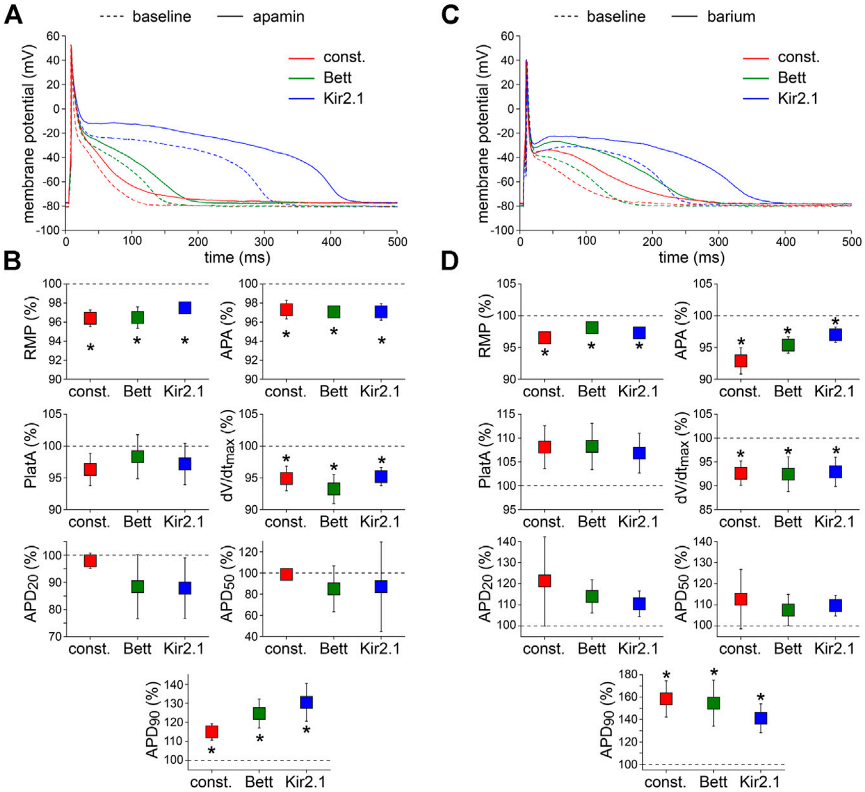

FIGURE 5 | Effects of apamin and barium on APs measured with constant and I_{K1} current injection. **(A)** Typical APs of one atrial myocyte in absence (baseline) and presence of apamin to block the Ca^{2+}-dependent K^+ current. **(B)** Average AP parameters measured in five cells in presence of apamin. AP parameters are normalized to the AP parameters measured under baseline conditions in the same cell. **(C)** Typical APs of one atrial myocyte in absence (baseline) and presence of barium to block the native I_{K1}. **(D)** Average AP parameters measured in four cells in presence of barium. AP parameters are normalized to the AP parameters measured under baseline conditions in the same cell. $^*p$ < 0.05, drug vs. baseline (paired *t*-test).

excluded (Varró et al., 2021). We here isolated myocytes enzymatically by the chunk method, and this method results in smaller I_{K1} densities compared to myocytes isolated using Langendorff perfusion (Hoshino et al., 2012).

The issue of the depolarized state of freshly isolated native human atrial myocytes is similar to that of hiPSC-CMs (Veerman et al., 2015), a relatively new and very promising model to test drugs (Magdy et al., 2018) and genetic disorders (Hoekstra et al., 2012; Brandão et al., 2017) in a human background. Recently, we and others have developed a dynamic clamp method to overcome the depolarized state of hiPSC-CMs [for reviews, see Ortega et al. (2018) and Verkerk and Wilders (2021)]. In the present study, we have extended the applicability of dynamic clamp to native human LAA myocytes of AF patients (**Figure 2**). We found that a stable RMP of −80 mV in our myocytes was achieved with ≈0.7 pA/pF repolarizing current. This amount of current is largely similar to the 0.3–1.2 pA/pF mentioned in, or calculated from, other studies (Bénardeau et al., 1996; Workman et al., 2001; Limberg et al., 2011; Workman et al., 2012) in human right atrial appendage myocytes. Using I_{K1} or constant current injection, APs could be evoked upon stimulation. The AP upstroke velocity, dV/dt_{max}, was high, demonstrating that the AP upstroke is due to activation of I_{Na} (Berecki et al., 2010). The AP morphology was largely comparable to the so-called "Type A" and "Type 3" APs, as defined by Bénardeau et al. (1996) and Dawodu et al. (1996), respectively. Thus, the APs had a fast phase 1 repolarization, without a dome, and a plateau at around −20 mV. Other AP types were not observed, consistent with studies of Workman and colleagues (Workman et al., 2001; Workman et al., 2012). The exact reason for the notable finding of Type A/Type 3 APs is unknown. We exclude the dynamic clamp, or the use of the originally depolarized cells, as mechanism because it was also found when injecting Kir2.1 current, which lacks a repolarizing current at positive potentials, as well as in non-depolarized cells, without injection of any repolarizing current. It also may be related to experimental techniques. Here, we have used the perforated patch clamp technique for the AP measurements, while many studies employed the ruptured patch technique, where the pipette solution frequently contains EGTA to buffer intracellular Ca^{2+}. Consequently, Ca^{2+} modulation of various ion channels and exchangers may be overlooked using the latter approach (Hume and Leblanc, 1988; Koivumäki et al., 2011). This may be of particular relevance for SK channels, the expression of which is increased during the early stages of AF (Ozgen et al., 2007; Qi et al., 2014). Moreover, effects of regional differences and heterogeneity in AP morphology in human atria (Gelband et al., 1972; Gong et al., 2008) may also contribute substantially to our primary finding of Type A/Type 3 APs. Finally, chronic treatment of AF patients with Ca^{2+} antagonists is known to depress $I_{Ca,L}$, resulting in shorter APs with suppressed plateau amplitudes (Le Grand et al., 1991), but in our study just one out of 8 patients was treated with Ca^{2+} antagonists (**Table 1**).

In the present study, we used two different I_{K1} equations as well as a constant current to set the RMP at a non-depolarized level, which made AP elicitation possible. We found that the APD and AP plateau potential were dependent on the approach of current injection. In the case of the Kir2.1 I_{K1}, which exhibits strong rectification (**Figure 1**, inset), the outward current at the AP plateau level is negligible (**Figure 2C**, blue lines). With the Bett I_{K1}, which has a moderate rectification consistent with a more atrial-like I_{K1} (Bett et al., 2013), the outward current at the plateau level is no longer negligible (**Figure 2C**, green lines) and consequently shortens the AP and lowers the AP plateau potential substantially (**Figure 2D**). The constant current injection results in an even larger outward current at the plateau level (**Figure 2C**, red lines), causing a substantial lowering of the plateau level and most pronounced APD shortening (**Figure 2D**). These findings indicate the importance of the amount of rectification and agree with previous findings in hiPSC-CMs and computer simulations using mathematical models of hiPSC-CMs and human atrial cells (Dhamoon et al., 2004; Meijer van Putten et al., 2015; Verkerk et al., 2017). With the Bett I_{K1}, AP plateau potential and APD match closely with those of non-depolarized cells (**Figure 2D**), suggesting that this approach of dynamic clamp current injection is most suitable to overcome the depolarized state of freshly isolated human atrial myocytes.

Drug-Induced Action Potential Changes and Comparison With Previous Studies

We have additionally tested various drugs to find out whether their modulatory effects could still be detected in the APs measured with constant and dynamic clamp injected currents. We have focused on well-established drugs with well-known effects on human atrial tissue and/or cells.

Lidocaine

We found a lidocaine-induced reduction in dV/dt_{max} in human atrial myocytes, consistent with findings using sharp microelectrode measurements in human atrial fibers (Lauribe et al., 1989) and in agreement with the blockade of peak I_{Na} by lidocaine in human atria (Jia et al., 1993). We also observed a decrease of APD in response to lidocaine, which confirms previous findings in human atrial fibers (Lauribe et al., 1989). The AP shortening is likely due to blockade of the slowly inactivating component of I_{Na}, in combination with a decrease in I_{Na} window current caused by a hyperpolarizing shift in I_{Na} voltage dependency (Jia et al., 1993). A lidocaine-induced AP shortening is also found in dog (Burashnikov et al., 2007), but is in contrast with findings in guinea pig, rabbit, and rat, where no effect (Betancourt and Dresel, 1979; Shirayama et al., 1991; Goineau et al., 2012) or even an increase in APD (Goldberg and Roberts, 1981) was observed. These contradictory findings in various species clearly highlight the need to validate drugs in a human myocyte setting.

While the effect on dV/dt_{max} was relatively mild, the severe APD decrease observed upon lidocaine treatment might be explained by the voltage dependency of lidocaine-induced I_{Na} blockade, with a preference of blockade at more positive potentials (Bean et al., 1983; Jia et al., 1993). In our experiments, we did not find a significant difference in lidocaine effects using the various current injections. Previously it was found that the effect of lidocaine on dV/dt_{max} is more pronounced in the setting of longer APs (Burashnikov et al., 2015), but apparently the APD differences due to the various current injections (**Figure 2D**) were too small to obtain a detectable effect in upstroke velocities of APs stimulated at 1 Hz.

Nifedipine

In our patch clamp studies, nifedipine shortened the APD, which is in agreement with previous findings in human atrial myocytes (Li and Nattel, 1997; Van Wagoner et al., 1999; Workman et al., 2001). The shortening was smaller compared to these previous studies, but that is likely related to the used concentrations. We used 0.1 μM nifedipine, which is close to the IC_{50} (Eroglu et al., 2020), while a concentration with almost complete $I_{Ca,L}$ blockade was used in the previous studies. One should note that a nifedipine-induced decrease in $I_{Ca,L}$ may also influence intracellular Ca^{2+} dynamics and consequently the sodium-calcium exchange current (I_{NCX}), which has a relatively high impact on atrial APs due to its high expression level and the rather negative plateau of the atrial AP (Bénardeau et al., 1996; Carmeliet, 2004). Thus the AP shortening in response to nifedipine is likely not only attributable to reduced $I_{Ca,L}$, but also due to a reduction in I_{NCX} (Bénardeau et al., 1996).

The effect of nifedipine on APD was more pronounced using the dynamic clamp-injected Kir2.1 I_{K1} compared to the Bett and constant current injections. We speculate that this relates to the distinct AP morphologies induced by the different current injection strategies, with a significantly longer APD obtained with Kir2.1 I_{K1} injection (**Figure 2D**). Previous studies revealed that drugs modulating APD have an augmented effect in cells with longer APs (Wu et al., 2008; Bárándi et al., 2010; Matsa et al., 2011). This can be explained by the lower net repolarizing current in longer APs, making such APs more sensitive to any change in repolarizing and depolarizing current (Gaur et al., 2020). Indeed, our experiments demonstrate that depending on the current injection approach used, drug effects can be more or less pronounced.

4-Aminopyridine

A low dose of the selective I_{Kur} blocker 4-AP (Wang et al., 1993) significantly prolonged APD_{20}, consistent with previous findings in isolated human atrial myocytes of patients undergoing coronary artery bypass surgery (Wang et al., 1993; Li et al., 2008) and in human right atrial trabeculae from patients in sinus rhythm and chronic AF (Wettwer et al., 2004). We also found a significant APD_{50} prolongation, consistent with the study of Li and colleagues (Li et al., 2008), and this prolongation was even more pronounced with the Kir2.1 I_{K1} injection. In our experiments, I_{Kur} blockade by 4-AP also resulted in a significant APD_{90} prolongation when the Kir2.1 I_{K1} injection was used, but not when the Bett or constant current injection was applied. Variable 4-AP effects on APD_{90} are also reported by others. Li et al. (2008) found no significant change in APD_{90}, but Wang et al. (1993) found a 66% prolongation and Wettwer et al. (2004) reported a 7% increase in tissue of AF patients. In tissue of patients in sinus rhythm, however, the APD_{90} was shortened in response to 4-AP (Wettwer et al., 2004). Underlying disease with a consequent more positive AP plateau potential in AF tissue is thought to be responsible for these variable findings (Wettwer et al., 2004). Differences in AP plateau potential may also be an explanation for our distinct APD_{90} findings, with a prolongation only found with Kir2.1 I_{K1} injection, which typically has the largest AP plateau potential amplitude, PlatA (**Figure 2D**).

E-4031

In our experiments, we found that E-4031 prolonged the APD_{50} and APD_{90}. This contrasts with previous findings in human atrial myocytes from patients in sinus rhythm (Wettwer et al., 2004; Skibsbye et al., 2014), although Wettwer and colleagues did mention a tendency to AP prolongation. The reason underlying this apparent discrepancy is unclear, but may be consequent to the diseased state of our cells and/or the use of initially depolarized AF cells in the present study. In addition, it might be related to differences in AP morphology because I_{Kr} channel activation during relatively short atrial APs with negative plateau phase will be far from complete (Carmeliet, 2004). Indeed, we found that the AP prolonging effect of E-4031 at 50% repolarization was more pronounced using the Kir2.1 I_{K1}, likely because there is more time for channel activation in the setting of the relatively long APD_{50} associated with the Kir2.1 I_{K1} (**Figure 2D**). This, in combination with the lower net current at the plateau of the Kir2.1 I_{K1} APs, likely makes the effects of drugs that modulate the plateau current more easily detectable.

Apamin

Apamin did not affect APD_{50}, but prolonged APD_{90} consistent with previously observed SK blockade effects in human single atrial myocytes and tissue (Xu et al., 2003; Skibsbye et al., 2014). In addition, we found that apamin depolarized the RMP, and decreased APA and dV/dt_{max} in agreement with NS8593-induced SK current reduction measured with microelectrodes in human atrial tissue (Skibsbye et al., 2014). Since the used apamin concentration does not block I_{Na} (Yu et al., 2014), the decreased dV/dt_{max} observed by us is likely the consequence of the RMP depolarization resulting in more inactivated I_{Na} channels (Berecki et al., 2010). The latter could also explain the observed decrease in APA. Apamin-induced AP prolongation has also been observed in mice (Xu et al., 2003), but not in dog and rat (Nagy et al., 2009), further emphasizing the need for experiments on human cells and tissue. In the present study, we have used cells from paroxysmal AF patients and there is growing evidence that SK channels may contribute to AF-induced APD abbreviation. Some laboratories report upregulation of SK channel expression in chronic AF, but this is not a consistent finding [Peyronnet and Ravens (2019) and Shamsaldeen et al. (2019), and primary references cited therein]. Therefore, we cannot exclude that the apamin-induced effects we observed are influenced by the diseased state of the tissue used.

Barium

We here demonstrate a small, but significant RMP depolarization upon application of Ba^{2+}, which is consistent with previous findings in human right atrial appendage (Escande et al., 1986). This indicates that the native I_{K1} was still functionally present in the initially depolarized cells and that the injected current does not obscure changes in I_{K1} completely. However, spontaneous activity was not observed in the measured cells, as occurred in a computer model of a guinea pig ventricular myocyte upon an 81% decrease in I_{K1} (Silva and Rudy, 2003). On the other hand, the application of 0.05–5 mM Ba^{2+} usually did not induce automatic activity in single ventricular myocytes obtained from adult guinea pig hearts (Imoto et al., 1987). Anyhow, one should keep in mind that drug effects on the native I_{K1} will be masked by the *in silico* injection of I_{K1} to a certain extent, simply because the *in silico* I_{K1} is not affected by the drug. The observed RMP depolarization may also lead to inactivation of I_{Na} channels and thus underlie the observed decrease in APA and dV/dt_{max} (Berecki et al., 2010). Additionally, we here observed a substantial Ba^{2+}-induced increase in APD_{90} (**Figure 5C,D**), consistent with previous findings in human right atrial appendage and papillary muscle (Escande et al., 1986; Jost et al., 2013). The effects of I_{K1} blockade on the APs were independent of the used current injections.

Limitations

We demonstrated that the APs of initially depolarized atrial myocytes, with three different types of current injection to arrive at a stable RMP near −80 mV, were sensitive to all drugs tested. This indicates that the major ionic currents were still functional in the initially depolarized cells. Drugs were not tested on intrinsically non-depolarized cells because of the limited number of such cells. Therefore, we cannot exclude that drug effects differ between initially depolarized myocytes on the one hand and intrinsically non-depolarized cells on the other hand. Frequency dependence was not tested in initially depolarized myocytes due to the already lengthy experimental protocol of the three current injection approaches in combination with the drug effect evaluations. Further studies are required to test whether the frequency dependencies of the initially depolarized myocytes and the non-depolarized ones are similar.

In our patch clamp experiments, we injected an *in silico* I_{K1} or constant current of ≈0.7 pA/pF to obtain a stable RMP near −80 mV in LAA myocytes of AF patients. It has been consistently demonstrated, in both animal models and humans, that I_{K1} is upregulated during AF (Van Wagoner et al., 1997; Bosch et al., 1999; Workman et al., 2001; Dobrev et al., 2005), resulting in a 4–6 mV RMP hyperpolarization in AF tissue. Thus, if myocytes of patients in sinus rhythm would be included, the I_{K1} density must likely be adapted with also consequent effects on the AP repolarization. Nevertheless, this limitation could also be considered as strength of the dynamic clamp to systematically study the effects of remodeled I_{K1} in human AF, but further studies are needed to address this issue in detail.

CONCLUSION

Patch-clamp recordings of APs from human atrial myocytes can be optimized through dynamic clamp in order to provide these cells with a substantial I_{K1} resulting in a close-to-physiological RMP. The APs measured using moderate I_{K1} rectification ("Bett" I_{K1}) matched closely those of non-depolarized cells, but effects of AP prolonging or shortening drugs are more pronounced using the dynamic clamp-injected I_{K1} with strong I_{K1} rectification ("Kir2.1" I_{K1}) for drugs blocking $I_{Ca,L}$, I_{Kur}, or I_{Kr}. Dynamic clamp therefore constitutes an appropriate tool for studying AP properties of human atrial myocytes, especially for the purpose of testing novel antiarrhythmic drugs.

DATA AVAILABILITY STATEMENT

The raw data supporting the conclusions of this article will be made available by the authors, without undue reservation.

ETHICS STATEMENT

The studies involving human participants were reviewed and approved by the Ethics Committee of the Amsterdam University Medical Centers, University of Amsterdam. The patients/participants provided their written informed consent to participate in this study.

AUTHOR CONTRIBUTIONS

AV and RW conceived, designed, and performed the experiments, and analyzed the data. AV, RW, CR, and GM wrote the paper. GM and MK isolated the human atrial myocytes and performed the patient administration. JZ installed the RT-Linux system and wrote the dynamic clamp software, AD coordinated and performed the surgeries, and JG contributed to scientific discussions.

FUNDING

This work was supported by two Innovational Research Incentives Scheme Vidi grants from the Netherlands Organisation for Health Research and Development (ZonMw 91714371 to CR and ZonMw 016.146.310 to JG).

REFERENCES

Amos, G. J., Wettwer, E., Metzger, F., Li, Q., Himmel, H. M., and Ravens, U. (1996). Differences between outward currents of human atrial and subepicardial ventricular myocytes. *J. Physiol.* 491, 31–50. doi:10.1113/jphysiol.1996.sp021194

Antzelevitch, C., and Burashnikov, A. (2010). Atrial-selective sodium channel block as a novel strategy for the management of atrial fibrillation. *Ann. N. Y. Acad. Sci.* 1188, 78–86. doi:10.1111/j.1749-6632.2009.05086.x

Bárándi, L., Virág, L., Jost, N., Horváth, Z., Koncz, I., Papp, R., et al. (2010). Reverse rate-dependent changes are determined by baseline action potential duration in mammalian and human ventricular preparations. *Basic Res. Cardiol.* 105, 315–323. doi:10.1007/s00395-009-0082-7

Banks, B. E., Brown, C., Burgess, G. M., Burnstock, G., Claret, M., Cocks, T. M., et al. (1979). Apamin blocks certain neurotransmitter-induced increases in potassium permeability. *Nature* 282, 415–417. doi:10.1038/282415a0

Barry, P. H., and Lynch, J. W. (1991). Liquid junction potentials and small cell effects in patch-clamp analysis. *J. Membr. Biol.* 121, 101–117. doi:10.1007/BF01870526

Bean, B. P., Cohen, C. J., and Tsien, R. W. (1983). Lidocaine block of cardiac sodium channels. *J. Gen. Physiol.* 81, 613–642. doi:10.1085/jgp.81.5.613

Bénardeau, A., Hatem, S. N., Rücker-Martin, C., Le Grand, B., Macé, L., Dervanian, P., et al. (1996). Contribution of Na^+/Ca^{2+} exchange to action potential of human atrial myocytes. *Am. J. Physiol.* 271, H1151–H1161. doi:10.1152/ajpheart.1996.271.3.H1151

Benjamin, E. J., Wolf, P. A., D'Agostino, R. B., Silbershatz, H., Kannel, W. B., and Levy, D. (1998). Impact of atrial fibrillation on the risk of death: the Framingham Heart Study. *Circulation* 98, 946–952. doi:10.1161/01.cir.98.10.946

Berecki, G., Wilders, R., De Jonge, B., Van Ginneken, A. C. G., and Verkerk, A. O. (2010). Re-evaluation of the action potential upstroke velocity as a measure of the Na^+ current in cardiac myocytes at physiological conditions. *PLoS One* 5, e15772. doi:10.1371/journal.pone.0015772

Berecki, G., Verkerk, A. O., Van Ginneken, A. C. G., and Wilders, R. (2014). Dynamic clamp as a tool to study the functional effects of individual membrane currents. *Methods Mol. Biol.* 1183, 309–326. doi:10.1007/978-1-4939-1096-0_20

Betancourt, O. J., and Dresel, P. E. (1979). Interaction of lidocaine and calcium on the electrical characteristics of rabbit atria. *J. Pharmacol. Exp. Ther.* 210, 64–69.

Bett, G. C. L., Kaplan, A. D., Lis, A., Cimato, T. R., Tzanakakis, E. S., Zhou, Q., et al. (2013). Electronic "expression" of the inward rectifier in cardiocytes derived from human-induced pluripotent stem cells. *Heart Rhythm* 10, 1903–1910. doi:10.1016/j.hrthm.2013.09.061

Bosch, R. F., Zeng, X., Grammer, J. B., Popovic, K., Mewis, C., and Kühlkamp, V. (1999). Ionic mechanisms of electrical remodeling in human atrial fibrillation. *Cardiovasc. Res.* 44, 121–131. doi:10.1016/s0008-6363(99)00178-9

Brandão, K. O., Tabel, V. A., Atsma, D. E., Mummery, C. L., and Davis, R. P. (2017). Human pluripotent stem cell models of cardiac disease: from mechanisms to therapies. *Dis. Model. Mech.* 10, 1039–1059. doi:10.1242/dmm.030320

Burashnikov, A., Belardinelli, L., and Antzelevitch, C. (2015). Inhibition of I_{Kr} potentiates development of atrial-selective I_{Na} block leading to effective suppression of atrial fibrillation. *Heart Rhythm* 12, 836–844. doi:10.1016/j.hrthm.2014.12.033

Burashnikov, A., Di Diego, J. M., Zygmunt, A. C., Belardinelli, L., and Antzelevitch, C. (2007). Atrium-selective sodium channel block as a strategy for suppression of atrial fibrillation: differences in sodium channel inactivation between atria and ventricles and the role of ranolazine. *Circulation* 116, 1449–1457. doi:10.1161/CIRCULATIONAHA.107.704890

Carmeliet, E. (2004). Intracellular Ca^{2+} concentration and rate adaptation of the cardiac action potential. *Cell Calcium* 35, 557–573. doi:10.1016/j.ceca.2004.01.010

Christ, T., Wettwer, E., Voigt, N., Hála, O., Radicke, S., Matschke, K., et al. (2008). Pathology-specific effects of the I_{Kur}/I_{to}/$I_{K,ACh}$ blocker AVE0118 on ion channels in human chronic atrial fibrillation. *Br. J. Pharmacol.* 154, 1619–1630. doi:10.1038/bjp.2008.209

Colilla, S., Crow, A., Petkun, W., Singer, D. E., Simon, T., and Liu, X. (2013). Estimates of current and future incidence and prevalence of atrial fibrillation in the U.S. adult population. *Am. J. Cardiol.* 112, 1142–1147. doi:10.1016/j.amjcard.2013.05.063

Colman, M. A., Saxena, P., Kettlewell, S., and Workman, A. J. (2018). Description of the human atrial action potential derived from a single, congruent data source: novel computational models for integrated experimental-numerical study of atrial arrhythmia mechanisms. *Front. Physiol.* 9, 1211. doi:10.3389/fphys.2018.01211

Dawodu, A. A., Monti, F., Iwashiro, K., Schiariti, M., Chiavarelli, R., and Puddu, P. E. (1996). The shape of human atrial action potential accounts for different frequency-related changes in vitro. *Int. J. Cardiol.* 54, 237–249. doi:10.1016/0167-5273(96)02605-8

Devalla, H. D., Schwach, V., Ford, J. W., Milnes, J. T., El-Haou, S., Jackson, C., et al. (2015). Atrial-like cardiomyocytes from human pluripotent stem cells are a robust preclinical model for assessing atrial-selective pharmacology. *EMBO Mol. Med.* 7, 394–410. doi:10.15252/emmm.201404757

Dhamoon, A. S., Pandit, S. V., Sarmast, F., Parisian, K. R., Guha, P., Li, Y., et al. (2004). Unique Kir2.x properties determine regional and species differences in the cardiac inward rectifier K^+ current. *Circ. Res.* 94, 1332–1339. doi:10.1161/01.RES.0000128408.66946.67

Dobrev, D., Carlsson, L., and Nattel, S. (2012). Novel molecular targets for atrial fibrillation therapy. *Nat. Rev. Drug Discov.* 11, 275–291. doi:10.1038/nrd3682

Dobrev, D., Friedrich, A., Voigt, N., Jost, N., Wettwer, E., Christ, T., et al. (2005). The G protein-gated potassium current $I_{K,ACh}$ is constitutively active in patients with chronic atrial fibrillation. *Circulation* 112, 3697–3706. doi:10.1161/CIRCULATIONAHA.105.575332

Dobrev, D., and Nattel, S. (2010). New antiarrhythmic drugs for treatment of atrial fibrillation. *Lancet* 375, 1212–1223. doi:10.1016/S0140-6736(10)60096-7

Dobrev, D., Wettwer, E., Himmel, H. M., Kortner, A., Kuhlisch, E., Schüler, S., et al. (2000). G-Protein β_3-subunit 825T allele is associated with enhanced human atrial inward rectifier potassium currents. *Circulation* 102, 692–697. doi:10.1161/01.cir.102.6.692

Ebert, A. D., Liang, P., and Wu, J. C. (2012). Induced pluripotent stem cells as a disease modeling and drug screening platform. *J. Cardiovasc. Pharmacol.* 60, 408–416. doi:10.1097/FJC.0b013e318247f642

Eroglu, T. E., Mohr, G. H., Blom, M. T., Verkerk, A. O., Souverein, P. C., Torp-Pedersen, C., et al. (2020). Differential effects on out-of-hospital cardiac arrest of dihydropyridines: real-world data from population-based cohorts across two European countries. *Eur. Heart J. Cardiovasc. Pharmacother.* 6, 347–355. doi:10.1093/ehjcvp/pvz038

Escande, D., Coraboeuf, E., Planché, C., and Lacour-Gayet, F. (1986). Effects of potassium conductance inhibitors on spontaneous diastolic depolarization and abnormal automaticity in human atrial fibers. *Basic Res. Cardiol.* 81, 244–257. doi:10.1007/BF01907407

Finet, J. E., Rosenbaum, D. S., and Donahue, J. K. (2009). Information learned from animal models of atrial fibrillation. *Cardiol. Clin.* 27, 45–54. doi:10.1016/j.ccl.2008.09.005

Gaur, N., Ortega, F., Verkerk, A. O., Mengarelli, I., Krogh-Madsen, T., Christini, D. J., et al. (2020). Validation of quantitative measure of repolarization reserve as a novel marker of drug induced proarrhythmia. *J. Mol. Cell Cardiol.* 145, 122–132. doi:10.1016/j.yjmcc.2020.04.019

Gelband, H., Bush, H. L., Rosen, M. R., Myerburg, R. J., and Hoffman, B. F. (1972). Electrophysiologic properties of isolated preparations of human atrial myocardium. *Circ. Res.* 30, 293–300. doi:10.1161/01.res.30.3.293

Goineau, S., Castagné, V., Guillaume, P., and Froget, G. (2012). The comparative sensitivity of three *in vitro* safety pharmacology models for the detection of lidocaine-induced cardiac effects. *J. Pharmacol. Toxicol. Methods* 66, 52–58. doi:10.1016/j.vascn.2012.06.001

Goldberg, P. B., and Roberts, J. (1981). Age-related changes in rat atrial sensitivity to lidocaine. *J. Gerontol.* 36, 520–528. doi:10.1093/geronj/36.5.520

Gong, D., Zhang, Y., Cai, B., Meng, Q., Jiang, S., Li, X., et al. (2008). Characterization and comparison of Na^+, K^+ and Ca^{2+} currents between myocytes from human atrial right appendage and atrial septum. *Cell. Physiol. Biochem.* 21, 385–394. doi:10.1159/000129631

Hatem, S. N., Coulombe, A., and Balse, E. (2010). Specificities of atrial electrophysiology: clues to a better understanding of cardiac function and the mechanisms of arrhythmias. *J. Mol. Cel. Cardiol.* 48, 90–95. doi:10.1016/j.yjmcc.2009.08.029

Heijman, J., Voigt, N., Nattel, S., and Dobrev, D. (2014). Cellular and molecular electrophysiology of atrial fibrillation initiation, maintenance, and progression. *Circ. Res.* 114, 1483–1499. doi:10.1161/CIRCRESAHA.114.302226

Hoekstra, M., Mummery, C. L., Wilde, A. A. M., Bezzina, C. R., and Verkerk, A. O. (2012). Induced pluripotent stem cell derived cardiomyocytes as models for cardiac arrhythmias. *Front. Physiol.* 3, 346. doi:10.3389/fphys.2012.00346

Hoppe, U. C., and Beuckelmann, D. J. (1998). Characterization of the hyperpolarization-activated inward current in isolated human atrial myocytes. *Cardiovasc. Res.* 38, 788–801. doi:10.1016/s0008-6363(98)00047-9

Hoshino, S., Omatsu-Kanbe, M., Nakagawa, M., and Matsuura, H. (2012). Postnatal developmental decline in I_{k1} in mouse ventricular myocytes isolated by the Langendorff perfusion method: comparison with the chunk method. *Pflugers Arch.* 463, 649–668. doi:10.1007/s00424-012-1084-0

Hu, J., Han, J., Li, H., Zhang, X., Liu, L. L., Chen, F., et al. (2018). Human embryonic kidney 293 cells: a vehicle for biopharmaceutical manufacturing, structural biology, and electrophysiology. *Cells Tissues Organs.* 205, 1–8. doi:10.1159/000485501

Hume, J. R., and Leblanc, R. N. (1988). A whole-cell patch clamp technique which minimizes cell dialysis. *Mol. Cel. Biochem.* 80, 49–57. doi:10.1007/BF00231003

Imoto, Y., Ehara, T., and Matsuura, H. (1987). Voltage- and time-dependent block of i_{k1} underlying Ba^{2+}-induced ventricular automaticity. *Am. J. Physiol.* 252, H325–H333. doi:10.1152/ajpheart.1987.252.2.H325

January, C. T., Wann, L. S., Calkins, H., Chen, L. Y., Cigarroa, J. E., Cleveland, J. C., et al. (2019). 2019 AHA/ACC/HRS focused update of the 2014 AHA/ACC/HRS guideline for the management of patients with atrial fibrillation: a report of the American College of Cardiology/American Heart Association task force on clinical practice guidelines and the Heart Rhythm Society. *J. Am. Coll. Cardiol.* 74, 104–132. doi:10.1016/j.jacc.2019.01.011

Jia, H., Furukawa, T., Singer, D. H., Sakakibara, Y., Eager, S., Backer, C., et al. (1993). Characteristics of lidocaine block of sodium channels in single human atrial cells. *J. Pharmacol. Exp. Ther.* 264, 1275–1284.

Jost, N., Virág, L., Comtois, P., Ordög, B., Szuts, V., Seprényi, G., et al. (2013). Ionic mechanisms limiting cardiac repolarization reserve in humans compared to dogs. *J. Physiol.* 591, 4189–4206. doi:10.1113/jphysiol.2013.261198

Kanagaratnam, P., Dupont, E., Rothery, S., Coppen, S., Severs, N. J., and Peters, N. S. (2006). Human atrial conduction and arrhythmogenesis correlates with conformational exposure of specific epitopes on the connexin40 carboxyl tail. *J. Mol. Cel. Cardiol.* 40, 675–687. doi:10.1016/j.yjmcc.2006.01.002

Kirchhof, P., Benussi, S., Kotecha, D., Ahlsson, A., Atar, D., Casadei, B., et al. (2016). 2016 ESC guidelines for the management of atrial fibrillation developed in collaboration with EACTS. *Eur. Heart J.* 37, 2893–2962. doi:10.1093/eurheartj/ehw210

Koivumäki, J. T., Korhonen, T., and Tavi, P. (2011). Impact of sarcoplasmic reticulum calcium release on calcium dynamics and action potential morphology in human atrial myocytes: a computational study. *PLoS Comput. Biol.* 7, e1001067. doi:10.1371/journal.pcbi.1001067

Kornreich, B. G. (2007). The patch clamp technique: principles and technical considerations. *J. Vet. Cardiol.* 9, 25–37. doi:10.1016/j.jvc.2007.02.001

Koumi, S., Backer, C. L., and Arentzen, C. E. (1995). Characterization of inwardly rectifying K^+ channel in human cardiac myocytes. Alterations in channel behavior in myocytes isolated from patients with idiopathic dilated cardiomyopathy. *Circulation* 92, 164–174. doi:10.1161/01.cir.92.2.164

Krijthe, B. P., Kunst, A., Benjamin, E. J., Lip, G. Y., Franco, O. H., Hofman, A., et al. (2013). Projections on the number of individuals with atrial fibrillation in the European Union, from 2000 to 2060. *Eur. Heart J.* 34, 2746–2751. doi:10.1093/eurheartj/eht280

Krul, S. P. J., Berger, W. R., Veldkamp, M. W., Driessen, A. H. G., Wilde, A. A. M., Deneke, T., et al. (2015). Treatment of atrial and ventricular arrhythmias through autonomic modulation. *JACC Clin. Electrophysiol.* 1, 496–508. doi:10.1016/j.jacep.2015.09.013

Lagrutta, A., Wang, J., Fermini, B., and Salata, J. J. (2006). Novel, potent inhibitors of human Kv1.5 K^+ channels and ultrarapidly activating delayed rectifier potassium current. *J. Pharmacol. Exp. Ther.* 317, 1054–1063. doi:10.1124/jpet.106.101162

Lauribe, P., Escande, D., Nottin, R., and Coraboeuf, E. (1989). Electrical activity of human atrial fibres at frequencies corresponding to atrial flutter. *Cardiovasc. Res.* 23, 159–168. doi:10.1093/cvr/23.2.159

Le Grand, B., Hatem, S., Deroubaix, E., Couetil, J. P., and Coraboeuf, E. (1991). Calcium current depression in isolated human atrial myocytes after cessation of chronic treatment with calcium antagonists. *Circ. Res.* 69, 292–300. doi:10.1161/01.res.69.2.292

Le Grand, B., Hatem, S., Deroubaix, E., Couétil, J. P., and Coraboeuf, E. (1994). Depressed transient outward and calcium currents in dilated human atria. *Cardiovasc. Res.* 28, 548–556. doi:10.1093/cvr/28.4.548

Li, G. R., and Nattel, S. (1997). Properties of human atrial I_{Ca} at physiological temperatures and relevance to action potential. *Am. J. Physiol.* 272, H227–H235. doi:10.1152/ajpheart.1997.272.1.H227

Li, G. R., Wang, H. B., Qin, G. W., Jin, M. W., Tang, Q., Sun, H. Y., et al. (2008). Acacetin, a natural flavone, selectively inhibits human atrial repolarization potassium currents and prevents atrial fibrillation in dogs. *Circulation* 117, 2449–2457. doi:10.1161/CIRCULATIONAHA.108.769554

Limberg, S. H., Netter, M. F., Rolfes, C., Rinné, S., Schlichthörl, G., Zuzarte, M., et al. (2011). TASK-1 channels may modulate action potential duration of human atrial cardiomyocytes. *Cel. Physiol. Biochem.* 28, 613–624. doi:10.1159/000335757

Loose, S., Mueller, J., Wettwer, E., Knaut, M., Ford, J., Milnes, J., et al. (2014). Effects of I_{Kur} blocker MK-0448 on human right atrial action potentials from patients in sinus rhythm and in permanent atrial fibrillation. *Front. Pharmacol.* 5, 26. doi:10.3389/fphar.2014.00026

Magdy, T., Schuldt, A. J. T., Wu, J. C., Bernstein, D., and Burridge, P. W. (2018). Human induced pluripotent stem cell (hiPSC)-derived cells to assess drug cardiotoxicity: opportunities and problems. *Annu. Rev. Pharmacol. Toxicol.* 58, 83–103. doi:10.1146/annurev-pharmtox-010617-053110

Mary-Rabine, L., Hordof, A. J., Danilo, P., Malm, J. R., and Rosen, M. R. (1980). Mechanisms for impulse initiation in isolated human atrial fibers. *Circ. Res.* 47, 267–277. doi:10.1161/01.res.47.2.267

Matsa, E., Rajamohan, D., Dick, E., Young, L., Mellor, I., Staniforth, A., et al. (2011). Drug evaluation in cardiomyocytes derived from human induced pluripotent stem cells carrying a long QT syndrome type 2 mutation. *Eur. Heart J.* 32, 952–962. doi:10.1093/eurheartj/ehr073

Meijer van Putten, R. M., Mengarelli, I., Guan, K., Zegers, J. G., Van Ginneken, A. C. G., Verkerk, A. O., et al. (2015). Ion channelopathies in human induced pluripotent stem cell derived cardiomyocytes: a dynamic clamp study with virtual I_{k1}. *Front. Physiol.* 6, 7. doi:10.3389/fphys.2015.00007

Milnes, J. T., Madge, D. J., and Ford, J. W. (2012). New pharmacological approaches to atrial fibrillation. *Drug Discov. Today* 17, 654–659. doi:10.1016/j.drudis.2012.02.007

Nagy, N., Szuts, V., Horváth, Z., Seprényi, G., Farkas, A. S., Acsai, K., et al. (2009). Does small-conductance calcium-activated potassium channel contribute to cardiac repolarization? *J. Mol. Cel. Cardiol.* 47, 656–663. doi:10.1016/j.yjmcc.2009.07.019

Nattel, S., Maguy, A., Le Bouter, S., and Yeh, Y. H. (2007). Arrhythmogenic ion-channel remodeling in the heart: heart failure, myocardial infarction, and atrial fibrillation. *Physiol. Rev.* 87, 425–456. doi:10.1152/physrev.00014.2006

Nishida, K., Michael, G., Dobrev, D., and Nattel, S. (2010). Animal models for atrial fibrillation: clinical insights and scientific opportunities. *Europace* 12, 160–172. doi:10.1093/europace/eup328

Olgin, J. E., and Verheule, S. (2002). Transgenic and knockout mouse models of atrial arrhythmias. *Cardiovasc. Res.* 54, 280–286. doi:10.1016/s0008-6363(02)00225-0

Ortega, F. A., Grandi, E., Krogh-Madsen, T., and Christini, D. J. (2017). Applications of dynamic clamp to cardiac arrhythmia research: role in drug target discovery and safety pharmacology testing. *Front. Physiol.* 8, 1099. doi:10.3389/fphys.2017.01099

Ozgen, N., Dun, W., Sosunov, E. A., Anyukhovsky, E. P., Hirose, M., Duffy, H. S., et al. (2007). Early electrical remodeling in rabbit pulmonary vein results from trafficking of intracellular SK2 channels to membrane sites. *Cardiovasc. Res.* 75, 758–769. doi:10.1016/j.cardiores.2007.05.008

Papke, R. L., and Smith-Maxwell, C. (2009). High throughput electrophysiology with *Xenopus* oocytes. *Comb. Chem. High Throughput Screen.* 12, 38–50. doi:10.2174/138620709787047975

Pau, D., Workman, A. J., Kane, K. A., and Rankin, A. C. (2003). Electrophysiological effects of 5-hydroxytryptamine on isolated human atrial myocytes, and the influence of chronic β-adrenoceptor blockade. *Br. J. Pharmacol.* 140, 1434–1441. doi:10.1038/sj.bjp.0705553

Peyronnet, R., and Ravens, U. (2019). Atria-selective antiarrhythmic drugs in need of alliance partners. *Pharmacol. Res.* 145, 104262. doi:10.1016/j.phrs.2019.104262

Qi, X. Y., Diness, J. G., Brundel, B. J., Zhou, X. B., Naud, P., Wu, C. T., et al. (2014). Role of small-conductance calcium-activated potassium channels in atrial electrophysiology and fibrillation in the dog. *Circulation* 129, 430–440. doi:10.1161/CIRCULATIONAHA.113.003019

Sanguinetti, M. C., and Jurkiewicz, N. K. (1990). Two components of cardiac delayed rectifier K^+ current. Differential sensitivity to block by class III antiarrhythmic agents. *J. Gen. Physiol.* 96, 195–215. doi:10.1085/jgp.96.1.195

Schmidt, C., Wiedmann, F., Voigt, N., Zhou, X. B., Heijman, J., Lang, S., et al. (2015). Upregulation of $K_{2P}3.1$ K^+ current causes action potential shortening in patients with chronic atrial fibrillation. *Circulation* 132, 82–92. doi:10.1161/CIRCULATIONAHA.114.012657

Schotten, U., Verheule, S., Kirchhof, P., and Goette, A. (2011). Pathophysiological mechanisms of atrial fibrillation: a translational appraisal. *Physiol. Rev.* 91, 265–325. doi:10.1152/physrev.00031.2009

Schram, G., Pourrier, M., Wang, Z., White, M., and Nattel, S. (2003). Barium block of Kir2 and human cardiac inward rectifier currents: evidence for subunit-heteromeric contribution to native currents. *Cardiovasc. Res.* 59, 328–338. doi:10.1016/S0008-6363(03)00366-3

Schreieck, J., Wang, Y., Overbeck, M., Schömig, A., and Schmitt, C. (2000). Altered transient outward current in human atrial myocytes of patients with reduced left ventricular function. *J. Cardiovasc. Electrophysiol.* 11, 180–192. doi:10.1111/j.1540-8167.2000.tb00318.x

Shamsaldeen, Y. A., Culliford, L., Clout, M., James, A. F., Ascione, R., Hancox, J. C., et al. (2019). Role of SK channel activation in determining the action potential configuration in freshly isolated human atrial myocytes from the SKArF study. *Biochem. Biophys. Res. Commun.* 512, 684–690. doi:10.1016/j.bbrc.2019.03.074

Shirayama, T., Inoue, D., Inoue, M., Tatsumi, T., Yamahara, Y., Asayama, J., et al. (1991). Electrophysiological effects of sodium channel blockers on guinea pig left atrium. *J. Pharmacol. Exp. Ther.* 259, 884–893.

Silva, J., and Rudy, Y. (2003). Mechanism of pacemaking in I_{K1}-downregulated myocytes. *Circ. Res.* 92, 261–263. doi:10.1161/01.res.0000057996.20414.c6

Skibsbye, L., Poulet, C., Diness, J. G., Bentzen, B. H., Yuan, L., Kappert, U., et al. (2014). Small-conductance calcium-activated potassium (SK) channels contribute to action potential repolarization in human atria. *Cardiovasc. Res.* 103, 156–167. doi:10.1093/cvr/cvu121

Stillitano, F., Lonardo, G., Giunti, G., Del Lungo, M., Coppini, R., Spinelli, V., et al. (2013). Chronic atrial fibrillation alters the functional properties of I_f in the human atrium. *J. Cardiovasc. Electrophysiol.* 24, 1391–1400. doi:10.1111/jce.12212

Ten Eick, R. E., and Singer, D. H. (1979). Electrophysiological properties of diseased human atrium. I. Low diastolic potential and altered cellular response to potassium. *Circ. Res.* 44, 545–557. doi:10.1161/01.res.44.4.545

Thuringer, D., Lauribe, P., and Escande, D. (1992). A hyperpolarization-activated inward current in human myocardial cells. *J. Mol. Cel. Cardiol.* 24, 451–455. doi:10.1016/0022-2828(92)91833-q

Trautwein, W., Kassebaum, D. G., Nelson, R. M., and Hechthh, H. H. (1962). Electrophysiological study of human heart muscle. *Circ. Res.* 10, 306–312. doi:10.1161/01.res.10.3.306

Van Wagoner, D. R., Pond, A. L., Lamorgese, M., Rossie, S. S., McCarthy, P. M., and Nerbonne, J. M. (1999). Atrial L-type Ca^{2+} currents and human atrial fibrillation. *Circ. Res.* 85, 428–436. doi:10.1161/01.res.85.5.428

Van Wagoner, D. R., Pond, A. L., McCarthy, P. M., Trimmer, J. S., and Nerbonne, J. M. (1997). Outward K^+ current densities and Kv1.5 expression are reduced in chronic human atrial fibrillation. *Circ. Res.* 80, 772–781. doi:10.1161/01.res.80.6.772

Varró, A., Nánási, P. P., and Lathrop, D. A. (1993). Potassium currents in isolated human atrial and ventricular cardiocytes. *Acta Physiol. Scand.* 149, 133–142. doi:10.1111/j.1748-1716.1993.tb09605.x

Varró, A., Tomek, J., Nagy, N., Virag, L., Passini, E., Rodriguez, B., et al. (2021). Cardiac transmembrane ion channels and action potentials: cellular physiology and arrhythmogenic behavior *Physiol. Rev.* In press. doi:10.1152/physrev.00024.2019

Veerman, C. C., Kosmidis, G., Mummery, C. L., Casini, S., Verkerk, A. O., and Bellin, M. (2015). Immaturity of human stem-cell-derived cardiomyocytes in culture: fatal flaw or soluble problem? *Stem Cell Dev.* 24, 1035–1052. doi:10.1089/scd.2014.0533

Verkerk, A., Veerman, C., Zegers, J., Mengarelli, I., Bezzina, C., and Wilders, R. (2017). Patch-clamp recording from human induced pluripotent stem cell-derived cardiomyocytes: improving action potential characteristics through dynamic clamp. *Int. J. Mol. Sci.* 18, 1873. doi:10.3390/ijms18091873

Verkerk, A. O., and Wilders, R. (2020). Dynamic clamp in electrophysiological studies on stem cell-derived cardiomyocytes—why and how? *J. Cardiovasc. Pharmacol.* 77, 267-279. doi:10.1097/FJC.0000000000000955

Voigt, N., Pearman, C. M., Dobrev, D., and Dibb, K. M. (2015). Methods for isolating atrial cells from large mammals and humans. *J. Mol. Cel. Cardiol.* 86, 187–198. doi:10.1016/j.yjmcc.2015.07.006

Wakili, R., Voigt, N., Kääb, S., Dobrev, D., and Nattel, S. (2011). Recent advances in the molecular pathophysiology of atrial fibrillation. *J. Clin. Invest.* 121, 2955–2968. doi:10.1172/JCI46315

Wang, Z., Fermini, B., and Nattel, S. (1993). Sustained depolarization-induced outward current in human atrial myocytes. Evidence for a novel delayed rectifier K^+ current similar to Kv1.5 cloned channel currents. *Circ. Res.* 73, 1061–1076. doi:10.1161/01.res.73.6.1061

Wettwer, E., Hála, O., Christ, T., Heubach, J. F., Dobrev, D., Knaut, M., et al. (2004). Role of I_{Kur} in controlling action potential shape and contractility in the human atrium: influence of chronic atrial fibrillation. *Circulation* 110, 2299–2306. doi:10.1161/01.CIR.0000145155.60288.71

Wilders, R. (2006). Dynamic clamp: a powerful tool in cardiac electrophysiology. *J. Physiol. (Lond)* 576, 349–359. doi:10.1113/jphysiol.2006.115840

Workman, A. J., Kane, K. A., and Rankin, A. C. (2001). The contribution of ionic currents to changes in refractoriness of human atrial myocytes associated with chronic atrial fibrillation. *Cardiovasc. Res.* 52, 226–235. doi:10.1016/s0008-6363(01)00380-7

Workman, A. J., Kane, K. A., and Rankin, A. C. (2003). Characterisation of the Na, K pump current in atrial cells from patients with and without chronic atrial fibrillation. *Cardiovasc. Res.* 59, 593–602. doi:10.1016/s0008-6363(03)00466-8

Workman, A. J., Marshall, G. E., Rankin, A. C., Smith, G. L., and Dempster, J. (2012). Transient outward K^+ current reduction prolongs action potentials and promotes afterdepolarisations: a dynamic-clamp study in human and rabbit cardiac atrial myocytes. *J. Physiol.* 590, 4289–4305. doi:10.1113/jphysiol.2012.235986

Wu, L., Guo, D., Li, H., Hackett, J., Yan, G. X., Jiao, Z., et al. (2008). Role of late sodium current in modulating the proarrhythmic and antiarrhythmic effects of quinidine. *Heart Rhythm* 5, 1726–1734. doi:10.1016/j.hrthm.2008.09.008

Xu, Y., Tuteja, D., Zhang, Z., Xu, D., Zhang, Y., Rodriguez, J., et al. (2003). Molecular identification and functional roles of a Ca^{2+}-activated K^+ channel in human and mouse hearts. *J. Biol. Chem.* 278, 49085–49094. doi:10.1074/jbc.M307508200

Yu, C.-C., Ai, T., Weiss, J. N., and Chen, P.-S. (2014). Apamin does not inhibit human cardiac Na^+ current, L-type Ca^{2+} current or other major K^+ currents. *PLoS One* 9, e96691. doi:10.1371/journal.pone.0096691

Conflict of Interest: The authors declare that the research was conducted in the absence of any commercial or financial relationships that could be construed as a potential conflict of interest.

GLOSSARY

4-AP 4-aminopyridine

ACE angiotensin-converting enzyme

AF atrial fibrillation

AP action potential

APA action potential amplitude

APD action potential duration

APD_{20} action potential duration at 20% repolarization

APD_{50} action potential duration at 50% repolarization

APD_{90} action potential duration at 90% repolarization

C_m cell membrane capacitance

dV/dt_{max} maximum action potential upstroke velocity

E_K potassium equilibrium potential

hiPSC-CMs human induced pluripotent stem cell-derived cardiomyocytes

IC_{50} half-maximal inhibitory concentration

$I_{Ca,L}$ L-type Ca^{2+} current

I_f hyperpolarization-activated inward current

I_{in} injected current

I_{K1} inward rectifier K^+ current

I_{Kr} rapid component of the delayed rectifier K^+ current

I_{Kur} ultra-rapid component of the delayed rectifier K^+ current

I_{Na} fast sodium current

I_{NCX} sodium-calcium exchange current

I_{stim} stimulus current

I_{to1} transient outward K^+ current

LAA left atrial appendage

MEA multi-electrode array

PlatA amplitude of the action potential plateau

RMP resting membrane potential

RT-Linux Real-Time Linux

SK channels small conductance Ca^{2+}-activated K^+ channels

V_m membrane potential

frontiers in Pharmacology

MINI REVIEW
published: 19 April 2021
doi: 10.3389/fphar.2021.650039

Human Pluripotent Stem Cells for Modeling of Anticancer Therapy-Induced Cardiotoxicity and Cardioprotective Drug Discovery

Wendy Keung[1]* *and Yiu-Fai Cheung*[1,2]

[1]*Dr. Li Dak-Sum Research Centre, The University of Hong Kong, Pokfulam, Hong Kong,* [2]*Department of Paediatrics and Adolescent Medicine, Li Ka Shing Faculty of Medicine, The University of Hong Kong, Pokfulam, Hong Kong*

Anticancer chemotherapies have been shown to produce severe side effects, with cardiotoxicity from anthracycline being the most notable. Identifying risk factors for anticancer therapy-induced cardiotoxicity in cancer patients as well as understanding its underlying mechanism is essential to improving clinical outcomes of chemotherapy treatment regimens. Moreover, cardioprotective agents against anticancer therapy-induced cardiotoxicity are scarce. Human induced pluripotent stem cell technology offers an attractive platform for validation of potential single nucleotide polymorphism with increased risk for cardiotoxicity. Successful validation of risk factors and mechanism of cardiotoxicity would aid the development of such platform for novel drug discovery and facilitate the practice of personalized medicine.

Keywords: anticancer therapy, cardiotoxicity, human induced pluripotent cells, cardiomyocytes, pharmacogenomics

Edited by:
Tamer M. A. Mohamed, University of Louisville, United States

Reviewed by:
Alexandre Ribeiro, United States Food and Drug Administration, United States
Mohammad Ali Mandegar, Tenaya Therapeutics, United States

***Correspondence:**
Wendy Keung
wkeung@hku.hk

Specialty section:
This article was submitted to Cardiovascular and Smooth Muscle Pharmacology, a section of the journal Frontiers in Pharmacology

Received: *06 January 2021*
Accepted: *01 April 2021*
Published: *19 April 2021*

Citation:
Keung W and Cheung Y-F (2021) Human Pluripotent Stem Cells for Modeling of Anticancer Therapy-Induced Cardiotoxicity and Cardioprotective Drug Discovery. Front. Pharmacol. 12:650039. doi: 10.3389/fphar.2021.650039

INTRODUCTION

Cancer is one of the leading causes of morbidity and mortality worldwide. Advances in diagnosis and management have reduced death rate of cancer patients significantly over the past decade (Jemal et al., 2010; Silverman et al., 2010). However, a significant number of patients experience severe and debilitating side-effects from anticancer therapies. As survival rate in cancer patients continue to increase, the burden of side effects is also on the rise and remains a grave concern.

Cardiovascular toxicities are amongst the most debilitating side effects of anticancer therapies. Both traditional chemotherapies as well as newer targeted chemotherapies appear to cause different degrees of cardiotoxicities via various mechanisms. Traditional anticancer chemotherapies include anthracycline treatment with doxorubicin as the most commonly used agent (Krischer et al., 1997; van Dalen et al., 2006). Although effective (Jemal et al., 2010; Silverman et al., 2010), doxorubicin has been shown to produce severe side effects with cardiotoxicity being the most notable (Oeffinger et al., 2006; Mulrooney et al., 2009; Lipshultz and Adams, 2010; Tukenova et al., 2010). Novel targeted anticancer therapies may offer a lower incidence of cardiotoxicity, which is also often reversible. Cardiotoxicity of anticancer therapies is highly patient-specific. Several factors need to be taken into consideration when choosing anticancer therapy, including the pharmacodynamics and pharmacokinetics of the drug, as well as pharmacogenomics of the patient. In this review, we shall discuss the use of human pluripotent stem cell technology to study the mechanism of anticancer drug-induced cardiotoxicity, and development of a preclinical human cell-based

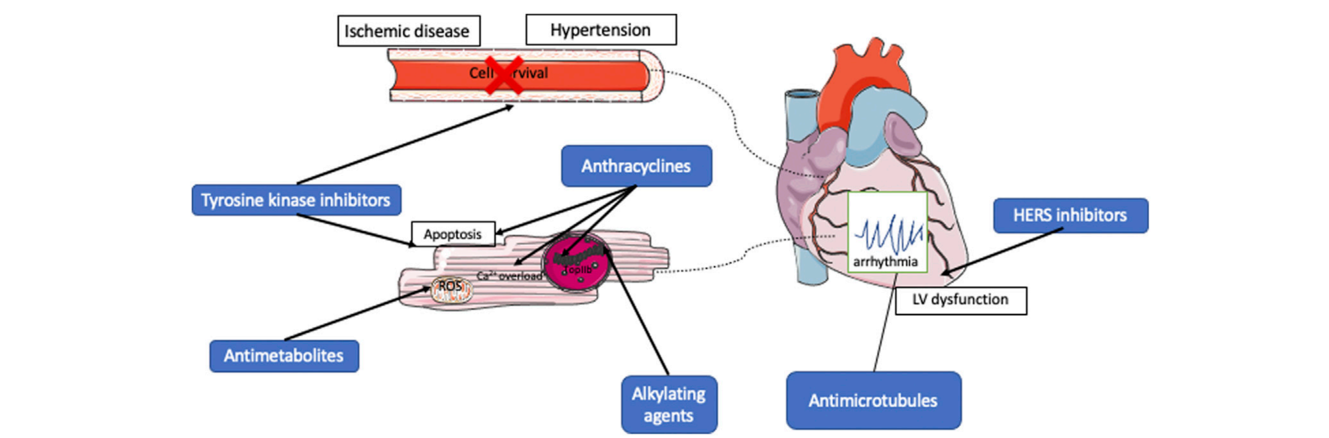

FIGURE 1 | Mechanisms of cardiotoxic effects of anticancer therapies. Anthracyclines may induce cardiotoxicity by increasing ROS production, inhibiting topoisomerase II-ß or by inducing calcium overload in cardiomyocytes. Alkylating agents cause DNA damages in cardiomyocytes. Antimetabolites increase ROS production causing apoptosis in cardiomyocytes while antimicrotubules inhibit cell division and causes arrhythmia. HER2 inhibitors cause myocardial dysfunction by rendering cardiomyocytes incapable of repairing against myocardial stress. Small molecule tyrosine kinase inhibitors cause hypertension and ischemic heart disease by inhibiting nitric oxide production and signaling in blood vessels of the heart and causing mitochondrial damage in cardiomyocytes.

model of personalized medicine for prediction of adverse effects of anticancer therapies and discovery of novel cardioprotective agents.

MECHANISM OF ANTICANCER DRUG INDUCED CARDIOTOXICITY

Understanding the fundamental mechanisms underlying anticancer therapy-induced cardiotoxicity is essential to the development of novel approaches to monitor, treat, and prevent these adverse side effects. Both traditional anthracyclines and novel targeted anticancer therapies have been shown to cause varying degrees of cardiotoxicities (**Figure 1**). However, their mechanisms of pathophysiology are different.

Anthracyclines

Anthracyclines, including doxorubicin and daunorubicin, have been used to treat a wide range of cancers, including hematological malignancies, solid tumors including neuroblastoma, nephroblastoma, osteosarcoma and Ewing's sarcoma, in both children and adults with success. Since the introduction of anthracycline to clinical practice in the early 1960s, the overall 5-years survival rates for all childhood cancers have risen from 58 to 83% in 2011 (Miller et al., 2016). Though this class of drug has been in use for over 5 decades, the mechanism of anthracycline-induced cardiotoxicity (AIC) remains understudied. Nonetheless, several hypotheses have been proposed to explain the pathophysiology. One theory is that anthracycline exposure induces the generation of reactive oxygen species (ROS), leading to DNA, protein and lipid damage and subsequent membrane damage and cell death (Deavall et al., 2012). This increase in ROS production, including superoxide and hydrogen peroxide, has been shown to involve iron, which forms an iron-anthracycline complex that catalyzes the conversion of hydrogen peroxide to hydroxyl radical (Minotti et al., 1999; Xu et al., 2005). A second hypothesis involves the inhibition of topoisomerase II-β (TOP2B) and topoisomerase I mitochondrial (TOP1MT) in cardiomyocytes. Different from topoisomerase II-α, which is responsible for the anti-tumor effect of anthracyclines, these two enzymes regulate transcriptional modulation of nuclear and mitochondrial genes and DNA-damage-induced apoptosis (Zhang et al., 2012) by preventing the religation of DNA, leading to the formation of DNA double-strand breaks. TOP2B has been associated with a reduction in mitochondrial biogenesis that is mediated by peroxisome proliferator-activated receptor gamma (PPARG) coactivator 1-α and (PPARGC1A) and PPARG coactivator 1-β (PPARGC1B) (Zhang et al., 2012). In addition, the mitochondrial dysfunction and cell death caused by TOP2B has also been shown to be due to the activation of p53 MAP kinase triggered by double-stranded DNA breaks (Nebigil and Desaubry, 2018). A third hypothesis proposes that doxorubicin and its metabolite doxorubicinol can induce Ca^{2+} release from the sarcoplasmic reticulum (Arai et al., 2000), thereby causing Ca^{2+} overload that leads to sarcomeric disarray and myofibril deterioration (Hanna et al., 2014) and arrhythmia.

Alkylating Agents

Alkylating agents including cyclophosphamide and cisplatin are amongst the oldest class of anticancer agents. Clinically, they are often used in combination with anthracycline to treat various cancers including lymphoma, multiple myeloma, breast cancer and lung cancer. They act by binding to negatively charged DNA sites, causing DNA strand breakage and cross-linking (Espinosa et al., 2003). These compounds are known to have cardiotoxic effects due to its DNA damaging effect, which can result in apoptosis of not only tumor cells but also normal tissues.

Antimetabolites and Antimicrotubules

Taxanes, including paclitaxel and docetaxel, are a group of chemotherapeutic agents isolated from natural sources. They

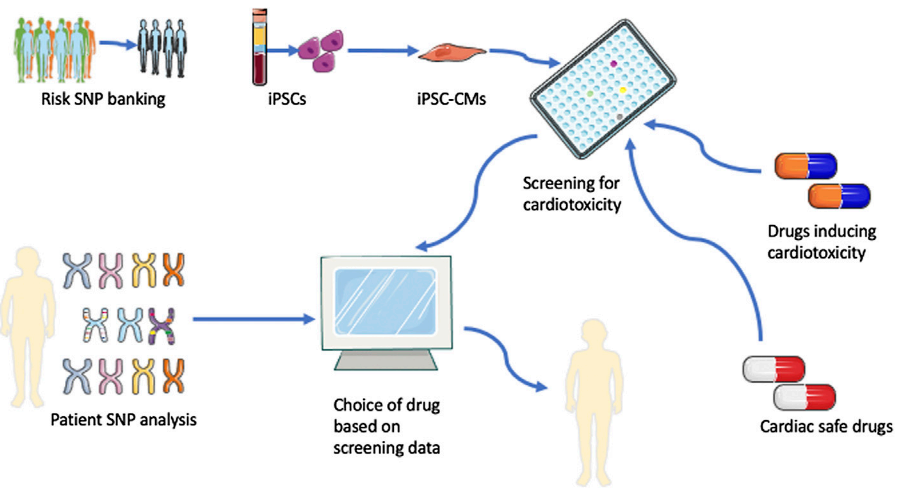

FIGURE 2 | Personalized medicine for anticancer therapy-induced cardiotoxicity. SNP that are high risks for anticancer therapy-induced cardiotoxicity are identified and a biobank of hiPSCs is established. hiPSC from individuals with these high risk SNP can help establish a risk score against each chemotherapeutic agent by screening of these drugs using the hiPSC model. Once assessed, each drug can be assigned a 'cardiac safety index/score' unique to each risk SNP. The results can help clinician make informed decision on the choice of anticancer drug with minimal side-effects for better outcome for the patient.

are commonly used to treat gynecological and breast cancers as well as lymphoma. They act by binding to microtubules, leading to their polymerization and inactivation, thereby inhibiting cell division. Cardiac arrhythmias and ischemia are the most common cardiotoxic side effects observed in patients receiving paclitaxel. The arrhythmias are related to the effect of paclitaxel on accelerated release of calcium (Zhang et al., 2010). Paclitaxel treatment causes bradycardia in up to 30% of patients and cardiac ischemia in 5% of patients (Rowinsky et al., 1991; Arbuck et al., 1993; Zhang et al., 2010), whereas docetaxel also caused myocardial ischemia albeit at a lower incidence rate of 1.7%. The antimetabolite 5-fluorouracil (5-FU) can induce apoptosis and autophagy through production of oxidative stress in cardiomyocytes and endothelial cells (Freeman and Costanza, 1988; Eskandari et al., 2015).

Novel Anticancer Therapies

Besides traditional anticancer therapies, novel targeted therapies are in increasing use to treat various types of cancers. Similar to traditional anticancer therapies, patient-specific targeted anticancer therapies also cause on-target or off target cardiotoxicities varying from hypertension, rhythm disturbances, QTc prolongation to ventricular dysfunction. Compared to traditional anticancer therapies, however, these side effects caused by novel anticancer therapies are rarely life-threatening, have no dose-dependent effect and are often reversible upon cessation of treatment (Chen and Ai, 2016).

HER2 Inhibition

A portion of breast cancers are HER2-positive. Overexpression of HER2 promotes tumorigenesis (Slamon et al., 1987). In these patients, HER2 inhibition prevents cell repair and significantly limits proliferation of metastatic HER2-positive breast cancers. Trastuzumab is a humanized anti-HER2 monoclonal antibody that targets the extracellular domain of the receptor. It is effective in treating both primary as well as metastastic breast cancers and is the first therapeutic antibody targeting molecular markers in cancer approved by the Food and Drug Administration (FDA). It is used as a first-line therapy either alone or together with other traditional chemotherapies including paclitaxel (Jelovac and Emens, 2013). Trastuzumab blocks the HER2/ErbB2 signaling in cardiomyocytes, rendering them incapable of utilizing the repair mechanism for protection against myocardial stress (Monsuez et al., 2010). In addition, trastuzumab has been shown to cause more pronounced cardiotoxicity when in the presence of anthracyclines (Bartsch et al., 2007; Hahn et al., 2014).

Small Molecule Tyrosine Kinase Inhibitor (TKI)

Small molecule TKIs have been developed against a number of targets including vascular endothelial growth factor receptors (VEGFR), platelet-derived growth factor receptors (PDGFR), epidermal growth factor receptor (EGFR) and other kinases. Imatinib is the first FDA-approved TKI for treatment of chronic myelogenous leukemia and gastrointestinal stromal tumors (Druker et al., 2001; Demetri et al., 2002). TKIs that inhibit VEGFRs have been shown to cause various degrees of congestive heart failure. Imatinib, which is a small molecule inhibitor against Abelson family of nonreceptor tyrosine kinases (ABL) with other known targets that include proto-oncogene receptor tyrosine kinase (KIT) and PDGFR, is mainly used to treat chronic myeloid leukemia, has been found to cause congestive heart failure symptoms in 1.7% of patients (Atallah et al., 2007). Imatinib has been demonstrated to cause dilated sarcoplasmic reticulum with membrane whorls, and abnormal mitochondria with effaced cristae by inhibition of ABL tyrosine kinase (Kerkela et al., 2009). Another multiple TKI sunitinib, which targets VEGFR receptors, is overall well-tolerated but may cause adverse cardiovascular effects including congestive heart failure with an incidence ranging from 1.5 to 14% (Richards et al., 2011; Hall et al., 2013) and hypertension with an incidence of 17–43% (Chu et al., 2007). A common mechanism of cardiac dysfunction between VEGFR inhibitors is the activation of hypoxia induced factor-1-alpha (HIF-1α) in response to VEGF induced decrease in capillary density (Ky et al., 2013). The common adverse effect of hypertension is thought to be due to a decreased nitric oxide signaling and increased endothelin-1 production. Sunitinib may have off-target mechanisms, inhibiting AMP-activating protein kinase which normally activates and stimulate ATP production through catabolic pathways (Kerkela et al., 2009). Additionally, PDGFR is also a target of sunitinib and may affect cardiac function in response to mechanical stress. Sunitinib, pazopanib, and vandetanib also prolong the QT interval and therefore increase the risk of Torsades de pointes (TdP).

PHARMACOGENOMICS AND GENE POLYMORPHISM OF ANTICANCER THERAPIES

An individual patient's responses to various chemotherapeutic agents are dependent on the pharmacodynamics and pharmacokinetics of the drug. In turn, polymorphism in target proteins of anticancer drugs may influence the pharmacodynamics of the drugs, while polymorphism in enzymes and transporters involved in metabolizing drugs can alter their expression and activity and affect the drug's pharmacokinetics (Evans and McLeod, 2003). Thus, identifying polymorphism related to targets in anticancer therapies in patient population may help to predict cardiotoxicities in patients. In addition, identifying risk factors for anticancer drug-induced cardiotoxicity in cancer patients as well as understanding its underlying mechanism is essential to novel drug discovery as well as improving clinical outcome of chemotherapy treatment regimens. This allows clinicians to screen patients for susceptibility variants prior to treatment and select an alternative treatment or co-administer protective adjuvant therapy or development modified chemotherapeutics that bypass off-target pathways. Candidate gene association studies (CGAS) in which frequencies of genetic variants, mainly single nucleotide polymorphisms (SNPs) are compared between cases and controls, and genome-wide association studies (GWAS), in which genetic variations across the whole genome are analyzed, are 2 widely used methods to identify variants that may contribute to drug-specific risk factors (Pinheiro et al., 2020). However, while these studies help identify numerous genetic variants, they need further validations in order to determine the causal relationship between genetic variants and occurrence of cardiotoxicities, which is essential for further development of protective therapy (Knowles et al., 2018).

Anthracycline

Four variant SNPs, CELF4 rs1786814, RARG rs2229774, SLC28A3 rs7853758 and UGT1A6 rs17863783 currently have the strongest and the most consistent evidence for association with AIC (Aminkeng et al., 2016; Wang et al., 2016; Scott et al., 2018). RARG, which codes for retinoic acid receptor gamma, normally acts to repress the expression of TOP2B in the heart, which anthracycline binds to cause double stranded DNA breaks. The rs2229774 variant could lead to reduced repression of TOP2B and thus increased anthracycline toxicity (Aminkeng et al., 2015). CELF4 is an RNA binding protein involved in tissue specific, developmentally regulated pre-mRNA splicing. Splice variants of cardiac troponin T bearing an alternative exon 5 are predominately expressed in the embryonic heart and significantly downregulated during development into the adult heart. CELF4 is known to mediate the alternative splicing of the gene TNNT2. CELF4 variants with reduced activity to target TNNT2 pre-mRNA enable the continued expression of embryonic cardiac troponin T in the adult heart. This results in a dual capacity for thin myofilaments to handle increasing calcium concentrations and potentially compromises their contractility and ultimately left ventricular ejection fraction (Tripaydonis et al., 2019). SLC28A3 belongs to a class of solute transporter proteins that have been shown to transport anthracyclines in cancer cells. It is also expressed in the myocardium. The presence of the SLC28A3 RS7853758 is thought to be protective as it reduces the exposure of cardiomyocytes to anthracyclines (Scott et al., 2018). Rs17863783 is a tag marker of the UGT1A6*4 haplotype, which has been reported to cause a 30–100% reduction in enzyme activity (Krishnaswamy et al., 2005a; Krishnaswamy et al., 2005b; Visscher et al., 2013). Reduced UGT1A6-mediated glucuronidation of anthracycline metabolites may lead to accumulation of toxic metabolites resulting in the observed increased risk of AIC. However, UGT1A6 is not expressed in the heart, which suggests that their contribution to cardiotoxicity is not related to direct effects in cardiac tissue.

Other variants including CYP3A5 rs4646450, ABCC2 rs3740066, NQO1 rs1043470, and SLC22A6 rs6591722 variants have also been reported to be associated with anthracycline-induced cardiotoxicity in children (Sagi et al., 2018). These association studies, however, were unable to establish causality of gene-disease relationship. Although several studies have evaluated the influence of patient genetics on anthracycline-induced cardiomyopathy, no SNPs have been validated by functional studies to be clinically useful predictors of cardiotoxicity risk. Reported results about genetic variants' associations with AIC are conflicting and often could not be replicated in all studies.

Alkylating Agents

Studies on the influence of genetic variations on the toxicity of alkylating agents are limited. However, polymorphisms in genes related to metabolism and transport of alkylating agents exist. CYP2B6 and CYP2C19 have been shown to influence cyclophosphamide pharmacokinetics in adult patients (Helsby et al., 2010). Patients carrying CYP2B6*6 have been shown to significantly lower cyclophosphamide clearance. However, whether this polymorphism affects the degree of cardiotoxicity remains to be determined (Veal et al., 2016).

Antimetabolites and Antimicrotubules

Functional polymorphisms of the ABCB1 gene of the ABC membrane transporter, which is involved in the transport of taxanes have been shown to significantly increase toxicity. However, knowledge on the functional significance of these genetic variants of the ABC transporter is still lacking and further investigation is warranted in order to evaluate the significance of these polymorphism in taxane-induced cardiotoxicity (Jabir et al., 2012).

Novel Anticancer Therapies

Despite the fact that TKI treatment has been proven to cause cardiotoxicity, few candidate biomarkers or risk SNPs for cardiotoxicity have been identified. Nonetheless, a few candidate biomarkers have been suggested based on CGAS. For example, in one study, patients with heterozygous and homozygous variant in the VEGF gene (rs699947, rs833061, rs1570360, rs2101963, rs3025039) had a 1.56 times higher risk of developing bevacizumab-induced hypertension (Leong et al., 2019). In HER2-positive breast cancer patients, there is a significant association for heterozygotes of rs1136201 with increased risk of developing cardiotoxicity (Beauclair et al., 2007). In another study of HER2-positive breast cancers patients, an association for heterozygous and homozygous variant genotypes of rs1136201 has also been found (Roca et al., 2013), although data pooled from multiple studies failed to show increased risk of developing heart failure (Leong et al., 2019). By contrast, in the same study, pooled analysis showed that the presence of rs1058808 SNP was potentially cardioprotective, and reduced the risk of developing heart failure by 31% (Arbuck et al., 1993).

HUMAN INDUCED PLURIPOTENT STEM CELLS AS MODEL FOR NOVEL DRUG DISCOVERY

Whereas animal models may fail to reflect the fundamental biology and therefore the cardiotoxic responses of cancer therapies in human, preclinical validation studies aiming at investigating the mechanism of cardiotoxicity of anticancer therapies traditionally has to rely on methodologies using myocardial biopsies. These novel human-tissue based assay models such as human ventricular slices have proven to be superior over animal models, as being of human origin and composed of a heterogenous mixture of cell types means a more sophisticated model without the disadvantage of species difference which can faithfully recapitulate human cardiac physiology at organ level. However, assays using myocardial tissues are both invasive and has a limited source. As such, current preclinical screening assays to detect cardiotoxicity remain suboptimal, without the capability of testing repeated and chronic dosing regimens on patient-derived cardiomyocytes.

Human induced pluripotent stem cell (hiPSCs) technology, on the other hand, has made it possible to experimentally validate the SNPs that have been identified in CGAS and GWAS studies (Knowles et al., 2018). The hiPSCs is a valuable tool for testing hypotheses of mechanisms of anthracycline-induced cardiotoxicity involving multiple cell types as they can be specified into more than one cell or tissue type. Moreover, with the advent of genome engineering such as the clustered regularly interspaced short palindromic repeat (CRISPR) technology, researchers have been able to correct these variants in a dish to further validate the importance of these genetic variants in disease progression. When validated, the data is useful for identifying novel markers and pathways for drug discovery for cardioprotection. Human iPSC-based drug testing models can also provide a reliable platform for identification of novel drugs that are free of cardiac side effects (Magdy et al., 2016). In addition, drug screening in hiPSC-CMs is now required in the Comprehensive *In Vitro* Proarrhythmia Assay (CiPA) guidelines for cardiac drug development owing to a large number of arrhythmic events identified in approved drugs in the post marketing phase (Gintant et al., 2017). The faithful recapitulation of the disease/SNP phenotype also makes hiPSC a tool for personalized medicine to avoid cardiotoxicity. While the application of hiPSC-CMs for personalized predictions of cardiotoxicity is in its infancy, the strength of their use and the promise shown in preclinical cancer drug cardiotoxicity testing has been recognized and recently been discussed in a scientific statement from the American Heart Association (Gintant et al., 2019).

hiPSC Based Models for Studying Cardiotoxicity

The earliest hiPSC based drug testing models involve cells cultured in 2D. While patient-specific hiPSC-derived cardiomyocytes have been shown to faithfully model clinical phenotypes of genetic cardiac diseases (Liang et al., 2013), culturing these hiPSC-derived cells in 2D affords limited control in tissue architecture, often resulting in sub-physiological or immature properties, including poor electrophysiology and calcium-handling, leading to poor contractile functions, and a predominantly glycolytic metabolic signature. Some of these immature properties have been proven to be difficult to overcome, such as the development of t-tubules and abolition of immature spontaneous membrane potential oscillation (Lundy et al., 2013; Keung et al., 2014; Karakikes et al., 2015). Despite the existence of these immature traits, we and others have utilized hiPSC/hESC derived cardiomyocytes to study the effects of doxorubicin and were able to demonstrate its cardiotoxic effects *in vitro* (Sirenko et al., 2013; Holmgren et al., 2015; Burridge et al., 2016; Cheung et al., 2020) as well as assess and predict cardiotoxicity in patients (Cheung et al., 2020) by measuring a number of parameters that can directly or indirectly assess the functionality and viability of hiPSC-CMs, including cell viability, contractility, single cell electrophysiology and calcium transients, as well as the detection of biomarkers such as cardiac troponins, micro-RNAs (Cheung et al., 2020; Mehrotra et al., 2020), creatine kinase (Shin et al., 2016) etc, often in high content fashion and longitudinal measurements. Burridge et al. demonstrated that patient-specific hiPSC-CMs can recapitulate predilection of breast cancer patients to AIC at the single cell level

(Burridge et al., 2016). This study, however, focused only on patient outcome as the phenotype rather than on the validation of specific SNPs. Their findings nonetheless provide promising data on the application of the hiPCS-CM platform for the validation of genetics variants identified in previous candidate gene and genome-wide association studies and discovery of novel cardioprotective agents. In addition to AIC, 2D cultured hiPSC-CMs have also been shown to successfully demonstrate the cardiotoxic effects of TKIs in a high throughput manner (Sharma et al., 2017).

Three-dimensional tissues of hiPSC-CMs have gained increasing use in modeling drug-induced cardiotoxicity. These tissues offer better control and mimicry of the *in vivo* physiological environment for maturation of cells (Li et al., 2018). Two types of 3D tissues have been used as a model to study anticancer therapies. The simpler form is cardiac organoid, which involves self-aggregation of hiPSC-CMs and or other cell types into spherical organoids in 3D with cellular organization comparable to native heart tissue and which can assess parameters such as cell viability and cytotoxicity (Polonchuk et al., 2017). A more sophisticated type of 3D tissue is engineered cardiac tissue which involves tight control of cellular organization with specific scaffold materials and cell density (Mannhardt et al., 2017a; Keung et al., 2019). The improved alignment of these engineered tissue constructs yields more mature cells and more physiologically relevant functional assessment capabilities that can be adapted to high throughput and high content assays, including true twitch forces, pressure-volume relationships, stroke work and macroelectrophysiological parameters (Mannhardt et al., 2017b; Li et al., 2018; Keung et al., 2019). For example, in a recent study using a form of 3D microtissue to model cardiotoxicity, the authors were able to demonstrate an increase in afterload on cardiomyocytes with increased sunitinib-induced cardiotoxicity, highlighting the superiority of 3D models to assess more complex physiological parameters which are not feasible with 2D culture models (Truitt et al., 2018).

Given the mechanisms of cardiotoxicity induced by different anticancer chemotherapies involve cardiomyocytes, blood vessels, in particular endothelial cells, as well as hepatocytes, an ideal model for validating risk factors and drug discovery should include all relevant cell types (McAleer et al., 2019). Microfluidic systems have been used to connect different cell types derived from hiPSC cultured in 2D to allow for interaction between the different cell types. Such organ-on-a-chip system was able to demonstrate a drug's effect on multiple cell types including hiPSC-CMs and endothelial cells, hepatocytes and neurons, mimicking the effects of the circulation system, metabolism and/or detoxification of drugs as well as sympathetic control respectively (Oleaga et al., 2016; Weng et al., 2020). Other more sophisticated multiple organ-on-chip devices with organ-level functionality have also been designed, where each 'organ' is connected to each other with vascularized, endothelium-lined channels, mimicking blood circulation and recapitulating tissue-tissue interfaces, thus modeling organ crosstalk and metabolism of compounds in a single system. Such multi-cell type assay system could also facilitate drug screening by fulfilling the requirement for *in vitro* physicochemical as well as absorption, distribution, metabolism and excretion (ADME) measurements and help predict pharmacokinetic parameters of drugs, which were previously difficult to measure or model *in vitro*, by introducing cell types including liver and kidney, which can mimic processes including metabolism and excretion respectively (McAleer et al., 2019). An assay system combining multiple cell types and 3D tissue engineering technology would further enhance the organ functionality and interaction. However, such sophisticated system may compromise the throughput of the assay. In the future, a tiered assay system that can accommodate both high throughput and high functionality may be employed in order to more accurately test the increasing amount of new anticancer therapies for cardiotoxic effects (Keung et al., 2019).

Toward Personalized Medicine: Patient-Specific hiPSC Based Model for Drug Discovery and Testing

Various hiPSC based models have been used for testing of the safety and efficacy of anticancer drugs in a quantitative manner. In one study, a high throughput screening of TKIs has been performed using a 2D hiPSC based model, where different aspects of cell toxicity including cell viability, contractility, calcium handling and electrophysiology were measured to determine a 'cardiac safety index' for each TKIs used (Sharma et al., 2017). In addition, the effect of insulin and IGF-1 as protective agents against TKI induced toxicity has also been evaluated. The use of a quantifiable parameter to assess drug toxicity may further facilitate decision making by clinician when evaluating the cardiotoxicity risk of anticancer therapies for patients. Interestingly, only hiPSCs from healthy subjects have been used in this study, the effect of different TKIs on hiPSCs from different genetic background remains to be determined.

It is conceivable that the hiPSC model could allow a personalized assessment by screening a patient's cardiomyocytes with different chemotherapeutic agents for prediction of cardiotoxicity. Once assessed, each drug can be assigned a 'cardiac safety index/score' unique to the patient in order for the oncologist to make informed decision about the choice of chemotherapy. However, as aforementioned, there are limitations that need to be overcome to enhance the practicality of this approach. One limitation is the time required for the establishment of patient specific hiPSC and their adaptation for drug screening assays. At the current state, this time-consuming process precludes the use of hiPSC for personalized pre-screening of drugs before the choice of chemotherapy has to be made. Alternatively, identifying and validating high risk SNP and establishing biobank of hiPSCs from individuals with these high risk SNP can help establish a risk score for each individual against each chemotherapeutic agent (Sayed et al., 2019), and help clinician to make informed decision on the choice of anticancer drug with minimal side-effects for better outcome for the patient (**Figure 2**).

CONCLUSION

Cardiotoxicity remains to be an important side effect of anticancer chemotherapies. The hiPSC platform offers promise to advance personalized medicine for chemotherapy. With further improvement in maturation of cardiomyocytes and reproducibility of the hiPSC platform, functional validation of pharmacogenomic studies where polymorphisms in genes associated with anticancer drug-induced cardiotoxicity can be achieved. This may provide an invaluable tool to individualize patient-specific chemotherapies and to maximize their benefits and minimal side-effects, thus improving treatment outcome based on the practice of personalized medicine.

AUTHOR CONTRIBUTIONS

WK and Y-FC wrote, revised and approved the final version of the manuscript.

REFERENCES

Aminkeng, F., Bhavsar, A. P., Bhavsar, A. P., Visscher, H., Rassekh, S. R., Li, Y., et al. (2015). A Coding Variant in RARG Confers Susceptibility to Anthracycline-Induced Cardiotoxicity in Childhood Cancer. *Nat. Genet.* 47, 1079–1084. doi:10.1038/ng.3374

Aminkeng, F., Ross, C. J. D., Rassekh, S. R., Hwang, S., Rieder, M. J., Bhavsar, A. P., et al. (2016). Recommendations for Genetic Testing to Reduce the Incidence of Anthracycline-induced Cardiotoxicity. *Br. J. Clin. Pharmacol.* 82, 683–695. doi:10.1111/bcp.13008

Arai, M., Yoguchi, A., Takizawa, T., Yokoyama, T., Kanda, T., Kurabayashi, M., et al. (2000). Mechanism of Doxorubicin-Induced Inhibition of Sarcoplasmic Reticulum Ca 2+ -ATPase Gene Transcription. *Circ. Res.* 86, 8–14. doi:10.1161/01.res.86.1.8

Arbuck, S. G., Strauss, H., Rowinsky, E., Christian, M., Suffness, M., Adams, J., et al. (1993). A Reassessment of Cardiac Toxicity Associated with Taxol. *J. Natl. Cancer Inst. Monogr.*, 117–130.

Atallah, E., Durand, J.-B., Kantarjian, H., and Cortes, J. (2007). Congestive Heart Failure is a Rare Event in Patients Receiving Imatinib Therapy. *Blood* 110, 1233–1237. doi:10.1182/blood-2007-01-070144

Bartsch, R., Wenzel, C., and Steger, G. G. (2007). Trastuzumab in the Management of Early and Advanced Stage Breast Cancer. *Biologics* 1, 19–31.

Beauclair, S., Formento, P., Fischel, J. L., Lescaut, W., Largillier, R., Chamorey, E., et al. (2007). Role of the HER2 [Ile655Val] Genetic Polymorphism in Tumorogenesis and in the Risk of Trastuzumab-Related Cardiotoxicity. *Ann. Oncol.* 18, 1335–1341. doi:10.1093/annonc/mdm181

Burridge, P. W., Li, Y. F., Matsa, E., Wu, H., Ong, S.-G., Sharma, A., et al. (2016). Human Induced Pluripotent Stem Cell-Derived Cardiomyocytes Recapitulate the Predilection of Breast Cancer Patients to Doxorubicin-Induced Cardiotoxicity. *Nat. Med.* 22, 547–556. doi:10.1038/nm.4087

Chen, Z., and Ai, D. (2016). Cardiotoxicity Associated with Targeted Cancer Therapies. *Mol. Clin. Oncol.* 4, 675–681. doi:10.3892/mco.2016.800

Cheung, Y. F., Li, V. W., Lai, C. T., Shin, V. Y., Keung, W., Cheuk, D. K., et al. (2020). Circulating High-Sensitivity Troponin T and microRNAs as Markers of Myocardial Damage during Childhood Leukaemia Treatment. *Pediatr. Res.* doi:10.1038/s41390-020-1049-5

Chu, T. F., Rupnick, M. A., Kerkela, R., Dallabrida, S. M., Zurakowski, D., Nguyen, L., et al. (2007). Cardiotoxicity Associated with Tyrosine Kinase Inhibitor Sunitinib. *Lancet* 370, 2011–2019. doi:10.1016/s0140-6736(07)61865-0

Deavall, D. G., Martin, E. A., Horner, J. M., and Roberts, R. (2012). Drug-Induced Oxidative Stress and Toxicity. *J. Toxicol.* 2012, 645460. doi:10.1155/2012/645460

Demetri, G. D., von Mehren, M., Blanke, C. D., Van den Abbeele, A. D., Eisenberg, B., Roberts, P. J., et al. (2002). Efficacy and Safety of Imatinib Mesylate in Advanced Gastrointestinal Stromal Tumors. *N. Engl. J. Med.* 347, 472–480. doi:10.1056/nejmoa020461

Druker, B. J., Talpaz, M., Resta, D. J., Peng, B., Buchdunger, E., Ford, J. M., et al. (2001). Efficacy and Safety of a Specific Inhibitor of the BCR-ABL Tyrosine Kinase in Chronic Myeloid Leukemia. *N. Engl. J. Med.* 344, 1031–1037. doi:10.1056/nejm200104053441401

Eskandari, M. R., Moghaddam, F., Shahraki, J., and Pourahmad, J. (2015). A Comparison of Cardiomyocyte Cytotoxic Mechanisms for 5-fluorouracil and its Pro-drug Capecitabine. *Xenobiotica* 45, 79–87. doi:10.3109/00498254.2014.942809

Espinosa, E., Zamora, P., Feliu, J., and González Barón, M. (2003). Classification of Anticancer drugs-a New System Based on Therapeutic Targets. *Cancer Treat. Rev.* 29, 515–523. doi:10.1016/s0305-7372(03)00116-6

Evans, W. E., and McLeod, H. L. (2003). Pharmacogenomics - Drug Disposition, Drug Targets, and Side Effects. *N. Engl. J. Med.* 348, 538–549. doi:10.1056/nejmra020526

Freeman, N. J., and Costanza, M. E. (1988). 5-Fluorouracil-associated Cardiotoxicity. *Cancer* 61, 36–45. doi:10.1002/1097-0142(19880101)61:1<36::aid-cncr2820610108>3.0.co;2-6

Gintant, G., Burridge, P., Gepstein, L., Harding, S., Herron, T., Hong, C., et al. (2019). Use of Human Induced Pluripotent Stem Cell-Derived Cardiomyocytes in Preclinical Cancer Drug Cardiotoxicity Testing: A Scientific Statement from the American Heart Association. *Circ. Res.* 125, e75–e92. doi:10.1161/res.0000000000000291

Gintant, G., Fermini, B., Stockbridge, N., and Strauss, D. (2017). The Evolving Roles of Human iPSC-Derived Cardiomyocytes in Drug Safety and Discovery. *Cell Stem Cell* 21, 14–17. doi:10.1016/j.stem.2017.06.005

Hahn, V. S., Lenihan, D. J., and Ky, B. (2014). Cancer Therapy-Induced Cardiotoxicity: Basic Mechanisms and Potential Cardioprotective Therapies. *J. Am. Heart Assoc.* 3, e000665. doi:10.1161/jaha.113.000665

Hall, P. S., Harshman, L. C., Srinivas, S., and Witteles, R. M. (2013). The Frequency and Severity of Cardiovascular Toxicity from Targeted Therapy in Advanced Renal Cell Carcinoma Patients. *JACC: Heart Fail.* 1, 72–78. doi:10.1016/j.jchf.2012.09.001

Hanna, A. D., Lam, A., Tham, S., Dulhunty, A. F., and Beard, N. A. (2014). Adverse Effects of Doxorubicin and its Metabolic Product on Cardiac RyR2 and SERCA2A. *Mol. Pharmacol.* 86, 438–449. doi:10.1124/mol.114.093849

Helsby, N. A., Hui, C.-Y., Goldthorpe, M. A., Coller, J. K., Soh, M. C., Gow, P. J., et al. (2010). The Combined Impact of CYP2C19 and CYP2B6 Pharmacogenetics on Cyclophosphamide Bioactivation. *Br. J. Clin. Pharmacol.* 70, 844–853. doi:10.1111/j.1365-2125.2010.03789.x

Holmgren, G., Synnergren, J., Bogestål, Y., Améen, C., Åkesson, K., Holmgren, S., et al. (2015). Identification of Novel Biomarkers for Doxorubicin-Induced Toxicity in Human Cardiomyocytes Derived from Pluripotent Stem Cells. *Toxicology* 328, 102–111. doi:10.1016/j.tox.2014.12.018

Jabir, R. S., Naidu, R., Annuar, M. A. B. A., Ho, G. F., Munisamy, M., and Stanslas, J. (2012). Pharmacogenetics of Taxanes: Impact of Gene Polymorphisms of Drug Transporters on Pharmacokinetics and Toxicity. *Pharmacogenomics* 13, 1979–1988. doi:10.2217/pgs.12.165

Jelovac, D., and Emens, L. A. (2013). HER2-directed Therapy for Metastatic Breast Cancer. *Oncology* 27, 166–175.

Jemal, A., Siegel, R., Xu, J., and Ward, E. (2010). Cancer Statistics, 2010. *CA: A Cancer J. Clin.* 60, 277–300. doi:10.3322/caac.20073

Karakikes, I., Ameen, M., Termglinchan, V., and Wu, J. C. (2015). Human Induced Pluripotent Stem Cell-Derived Cardiomyocytes: Insights into Molecular, Cellular, and Functional Phenotypes. *Circ. Res.* 117, 80–88. doi:10.1161/circresaha.117.305365

Kerkela, R., Woulfe, K. C., Durand, J.-B., Vagnozzi, R., Kramer, D., Chu, T. F., et al. (2009). Sunitinib-Induced Cardiotoxicity is Mediated by Off-Target Inhibition of AMP-Activated Protein Kinase. *Clin. Transl Sci.* 2, 15–25. doi:10.1111/j.1752-8062.2008.00090.x

Keung, W., Boheler, K. R., and Li, R. A. (2014). Developmental Cues for the Maturation of Metabolic, Electrophysiological and Calcium Handling Properties of Human Pluripotent Stem Cell-Derived Cardiomyocytes. *Stem Cel Res. Ther.* 5, 17. doi:10.1186/scrt406

Keung, W., Chan, P. K. W., Backeris, P. C., Lee, E. K., Wong, N., Wong, A. O. T., et al. (2019). Human Cardiac Ventricular-Like Organoid Chambers and Tissue Strips from Pluripotent Stem Cells as a Two-Tiered Assay for Inotropic Responses. *Clin. Pharmacol. Ther.* 106, 402–414. doi:10.1002/cpt.1385

Knowles, D. A., Burrows, C. K., Blischak, J. D., Patterson, K. M., Serie, D. J., Norton, N., et al. (2018). Determining the Genetic Basis of Anthracycline-Cardiotoxicity by Molecular Response QTL Mapping in Induced Cardiomyocytes. *Elife* 7, e33480. doi:10.7554/elife.33480

Krischer, J. P., Epstein, S., Cuthbertson, D. D., Goorin, A. M., Epstein, M. L., and Lipshultz, S. E. (1997). Clinical Cardiotoxicity Following Anthracycline Treatment for Childhood Cancer: The Pediatric Oncology Group Experience. *J. Clin. Oncol.* 15, 1544–1552. doi:10.1200/jco.1997.15.4.1544

Krishnaswamy, S., Hao, Q., Al-Rohaimi, A., Hesse, L. M., von Moltke, L. L., Greenblatt, D. J., et al. (2005a). UDP Glucuronosyltransferase (UGT) 1A6 Pharmacogenetics: I. Identification of Polymorphisms in the 5′-Regulatory and Exon 1 Regions, and Association with Human Liver UGT1A6 Gene Expression and Glucuronidation. *J. Pharmacol. Exp. Ther.* 313, 1331–1339. doi:10.1124/jpet.104.081950

Krishnaswamy, S., Hao, Q., Al-Rohaimi, A., Hesse, L. M., von Moltke, L. L., Greenblatt, D. J., et al. (2005b). UDP Glucuronosyltransferase (UGT) 1A6 Pharmacogenetics: II. Functional Impact of the Three Most Common Nonsynonymous UGT1A6 Polymorphisms (S7A, T181A, and R184S). *J. Pharmacol. Exp. Ther.* 313, 1340–1346. doi:10.1124/jpet.104.081968

Ky, B., Vejpongsa, P., Yeh, E. T. H., Force, T., and Moslehi, J. J. (2013). Emerging Paradigms in Cardiomyopathies Associated with Cancer Therapies. *Circ. Res.* 113, 754–764. doi:10.1161/circresaha.113.300218

Leong, S. L., Chaiyakunapruk, N., Tassaneeyakul, W., Arunmanakul, P., Nathisuwan, S., and Lee, S. W. H. (2019). Roles of Pharmacogenomics in Non-anthracycline Antineoplastic-Induced Cardiovascular Toxicities: A Systematic Review and Meta-Analysis of Genotypes Effect. *Int. J. Cardiol.* 280, 190–197. doi:10.1016/j.ijcard.2018.12.049

Li, R. A., Keung, W., Cashman, T. J., Backeris, P. C., Johnson, B. V., Bardot, E. S., et al. (2018). Bioengineering an Electro-Mechanically Functional Miniature Ventricular Heart Chamber from Human Pluripotent Stem Cells. *Biomaterials* 163, 116–127. doi:10.1016/j.biomaterials.2018.02.024

Liang, P., Lan, F., Lee, A. S., Gong, T., Sanchez-Freire, V., Wang, Y., et al. (2013). Drug Screening Using a Library of Human Induced Pluripotent Stem Cell-Derived Cardiomyocytes Reveals Disease-Specific Patterns of Cardiotoxicity. *Circulation* 127, 1677–1691. doi:10.1161/circulationaha.113.001883

Lipshultz, S. E., and Adams, M. J. (2010). Cardiotoxicity after Childhood Cancer: Beginning with the End in Mind. *J. Clin. Oncol.* 28, 1276–1281. doi:10.1200/jco.2009.26.5751

Lundy, S. D., Zhu, W.-Z., Regnier, M., and Laflamme, M. A. (2013). Structural and Functional Maturation of Cardiomyocytes Derived from Human Pluripotent Stem Cells. *Stem Cell Develop.* 22, 1991–2002. doi:10.1089/scd.2012.0490

Magdy, T., Burmeister, B. T., and Burridge, P. W. (2016). Validating the Pharmacogenomics of Chemotherapy-Induced Cardiotoxicity: What is Missing? *Pharmacol. Ther.* 168, 113–125. doi:10.1016/j.pharmthera.2016.09.009

Mannhardt, I., Eder, A., Dumotier, B., Prondzynski, M., Krämer, E., Traebert, M., et al. (2017a). Blinded Contractility Analysis in hiPSC-Cardiomyocytes in Engineered Heart Tissue Format: Comparison with Human Atrial Trabeculae. *Toxicol. Sci.* 158, 164–175. doi:10.1093/toxsci/kfx081

Mannhardt, I., Saleem, U., Benzin, A., Schulze, T., Klampe, B., Eschenhagen, T., et al. (2017b). Automated Contraction Analysis of Human Engineered Heart Tissue for Cardiac Drug Safety Screening. *J. Vis. Exp.*, 55461. doi:10.3791/55461

McAleer, C. W., Long, C. J., Elbrecht, D., Sasserath, T., Bridges, L. R., Rumsey, J. W., et al. (2019). Multi-organ System for the Evaluation of Efficacy and Off-Target Toxicity of Anticancer Therapeutics. *Sci. Transl Med.* 11, eaav1386. doi:10.1126/scitranslmed.aav1386

Mehrotra, S., de Melo, B. A. G., Hirano, M., Keung, W., Li, R. A., Mandal, B. B., et al. (2020). Nonmulberry Silk Based Ink for Fabricating Mechanically Robust Cardiac Patches and Endothelialized Myocardium-on-a-Chip Application. *Adv. Funct. Mater.* 30, 2070079. doi:10.1002/adfm.202070079

Miller, K. D., Siegel, R. L., Lin, C. C., Mariotto, A. B., Kramer, J. L., Rowland, J. H., et al. (2016). Cancer Treatment and Survivorship Statistics, 2016. *CA: A Cancer J. Clin.* 66, 271–289. doi:10.3322/caac.21349

Minotti, G., Cairo, G., and Monti, E. (1999). Role of Iron in Anthracycline Cardiotoxicity: New Tunes for an Old Song? *FASEB J.* 13, 199–212. doi:10.1096/fasebj.13.2.199

Monsuez, J.-J., Charniot, J.-C., Vignat, N., and Artigou, J.-Y. (2010). Cardiac Side-Effects of Cancer Chemotherapy. *Int. J. Cardiol.* 144, 3–15. doi:10.1016/j.ijcard.2010.03.003

Mulrooney, D. A., Yeazel, M. W., Kawashima, T., Mertens, A. C., Mitby, P., Stovall, M., et al. (2009). Cardiac Outcomes in a Cohort of Adult Survivors of Childhood and Adolescent Cancer: Retrospective Analysis of the Childhood Cancer Survivor Study Cohort. *BMJ* 339, b4606. doi:10.1136/bmj.b4606

Nebigil, C. G., and Desaubry, L. (2018). Updates in Anthracycline-Mediated Cardiotoxicity. *Front. Pharmacol.* 9, 1262. doi:10.3389/fphar.2018.01262

Oeffinger, K. C., Mertens, A. C., Sklar, C. A., Kawashima, T., Hudson, M. M., Meadows, A. T., et al. (2006). Chronic Health Conditions in Adult Survivors of Childhood Cancer. *N. Engl. J. Med.* 355, 1572–1582. doi:10.1056/nejmsa060185

Oleaga, C., Bernabini, C., Smith, A. S., Srinivasan, B., Jackson, M., McLamb, W., et al. (2016). Multi-Organ Toxicity Demonstration in a Functional Human *in vitro* System Composed of Four Organs. *Sci. Rep.* 6, 20030. doi:10.1038/srep20030

Pinheiro, E. A., Magdy, T., and Burridge, P. W. (2020). Human *in vitro* Models for Assessing the Genomic Basis of Chemotherapy-Induced Cardiovascular Toxicity. *J. Cardiovasc. Trans. Res.* 13, 377–389. doi:10.1007/s12265-020-09962-x

Polonchuk, L., Chabria, M., Badi, L., Hoflack, J. C., Figtree, G., Davies, M. J., et al. (2017). Cardiac Spheroids as Promising *in vitro* Models to Study the Human Heart Microenvironment. *Sci. Rep.* 7, 7005. doi:10.1038/s41598-017-06385-8

Richards, C. J., Je, Y., Schutz, F. A. B., Heng, D. Y. C., Dallabrida, S. M., Moslehi, J. J., et al. (2011). Incidence and Risk of Congestive Heart Failure in Patients with Renal and Nonrenal Cell Carcinoma Treated with Sunitinib. *J. Clin. Oncol.* 29, 3450–3456. doi:10.1200/jco.2010.34.4309

Roca, L., Diéras, V., Roché, H., Lappartient, E., Kerbrat, P., Cany, L., et al. (2013). Correlation of HER2, FCGR2A, and FCGR3A Gene Polymorphisms with Trastuzumab Related Cardiac Toxicity and Efficacy in a Subgroup of Patients from UNICANCER-PACS04 Trial. *Breast Cancer Res. Treat.* 139, 789–800. doi:10.1007/s10549-013-2587-x

Rowinsky, E. K., McGuire, W. P., Guarnieri, T., Fisherman, J. S., Christian, M. C., and Donehower, R. C. (1991). Cardiac Disturbances during the Administration of Taxol. *J. Clin. Oncol.* 9, 1704–1712. doi:10.1200/jco.1991.9.9.1704

Sagi, J. C., Egyed, B., Kelemen, A., Kutszegi, N., Hegyi, M., Gezsi, A., et al. (2018). Possible Roles of Genetic Variations in Chemotherapy Related Cardiotoxicity in Pediatric Acute Lymphoblastic Leukemia and Osteosarcoma. *BMC Cancer* 18, 704. doi:10.1186/s12885-018-4629-6

Sayed, N., Ameen, M., and Wu, J. C. (2019). Personalized Medicine in Cardio-Oncology: the Role of Induced Pluripotent Stem Cell. *Cardiovasc. Res.* 115, 949–959. doi:10.1093/cvr/cvz024

Scott, E., Hasbullah, J. S., Ross, C. J., and Carleton, B. C. (2018). Reducing Anthracycline-Induced Cardiotoxicity through Pharmacogenetics. *Pharmacogenomics* 19, 1147–1150. doi:10.2217/pgs-2018-0124

Sharma, A., Burridge, P. W., McKeithan, W. L., Serrano, R., Shukla, P., Sayed, N., et al. (2017). High-throughput Screening of Tyrosine Kinase Inhibitor Cardiotoxicity with Human Induced Pluripotent Stem Cells. *Sci. Transl. Med.* 9, eaaf2584. doi:10.1126/scitranslmed.aaf2584

Shin, S. R., Zhang, Y. S., Kim, D.-J., Manbohi, A., Avci, H., Silvestri, A., et al. (2016). Aptamer-Based Microfluidic Electrochemical Biosensor for Monitoring Cell-Secreted Trace Cardiac Biomarkers. *Anal. Chem.* 88, 10019–10027. doi:10.1021/acs.analchem.6b02028

Silverman, L. B., Stevenson, K. E., O'Brien, J. E., Asselin, B. L., Barr, R. D., Clavell, L., et al. (2010). Long-term Results of Dana-Farber Cancer Institute ALL Consortium Protocols for Children with Newly Diagnosed Acute Lymphoblastic Leukemia (1985–2000). *Leukemia* 24, 320–334. doi:10.1038/leu.2009.253

Sirenko, O., Crittenden, C., Callamaras, N., Hesley, J., Chen, Y.-W., Funes, C., et al. (2013). Multiparameter *in vitro* Assessment of Compound Effects on Cardiomyocyte Physiology Using iPSC Cells. *J. Biomol. Screen.* 18, 39–53. doi:10.1177/1087057112457590

Slamon, D., Clark, G., Wong, S., Levin, W., Ullrich, A., and McGuire, W. (1987). Human Breast Cancer: Correlation of Relapse and Survival with Amplification of the HER-2/neu Oncogene. *Science* 235, 177–182. doi:10.1126/science.3798106

Tripaydonis, A., Conyers, R., and Elliott, D. A. (2019). Pediatric Anthracycline-Induced Cardiotoxicity: Mechanisms, Pharmacogenomics, and Pluripotent Stem-Cell Modeling. *Clin. Pharmacol. Ther.* 105, 614–624. doi:10.1002/cpt.1311

Truitt, R., Mu, A., Corbin, E. A., Vite, A., Brandimarto, J., Ky, B., et al. (2018). Increased Afterload Augments Sunitinib-Induced Cardiotoxicity in an Engineered Cardiac Microtissue Model. *JACC: Basic Transl. Sci.* 3, 265–276. doi:10.1016/j.jacbts.2017.12.007

Tukenova, M., Guibout, C., Oberlin, O., Doyon, F., Mousannif, A., Haddy, N., et al. (2010). Role of Cancer Treatment in Long-Term Overall and Cardiovascular Mortality after Childhood Cancer. *J. Clin. Oncol.* 28, 1308–1315. doi:10.1200/jco.2008.20.2267

van Dalen, E. C., van der Pal, H. J. H., Kok, W. E. M., Caron, H. N., and Kremer, L. C. M. (2006). Clinical Heart Failure in a Cohort of Children Treated with Anthracyclines: A Long-Term Follow-Up Study. *Eur. J. Cancer* 42, 3191–3198. doi:10.1016/j.ejca.2006.08.005

Veal, G. J., Cole, M., Chinnaswamy, G., Sludden, J., Jamieson, D., Errington, J., et al. (2016). Cyclophosphamide Pharmacokinetics and Pharmacogenetics in Children with B-Cell Non-hodgkin's Lymphoma. *Eur. J. Cancer* 55, 56–64. doi:10.1016/j.ejca.2015.12.007

Visscher, H., Ross, C. J. D., Rassekh, S. R., Sandor, G. S. S., Caron, H. N., van Dalen, E. C., et al. (2013). Validation of Variants inSLC28A3 and UGT1A6as Genetic Markers Predictive of Anthracycline-Induced Cardiotoxicity in Children. *Pediatr. Blood Cancer* 60, 1375–1381. doi:10.1002/pbc.24505

Wang, X., Sun, C.-L., Quiñones-Lombraña, A., Singh, P., Landier, W., Hageman, L., et al. (2016). CELF4 Variant and Anthracycline-Related Cardiomyopathy: A Children's Oncology Group Genome-wide Association Study. *Jco* 34, 863–870. doi:10.1200/jco.2015.63.4550

Weng, K.-C., Kurokawa, Y. K., Hajek, B. S., Paladin, J. A., Shirure, V. S., and George, S. C. (2020). Human Induced Pluripotent Stem-Cardiac-Endothelial-Tumor-on-a-Chip to Assess Anticancer Efficacy and Cardiotoxicity. *Tissue Eng. C: Methods* 26, 44–55. doi:10.1089/ten.tec.2019.0248

Xu, X., Persson, H. L., and Richardson, D. R. (2005). Molecular Pharmacology of the Interaction of Anthracyclines with Iron. *Mol. Pharmacol.* 68, 261–271. doi:10.1124/mol.105.013383

Zhang, K., Heidrich, F. M., DeGray, B., Boehmerle, W., and Ehrlich, B. E. (2010). Paclitaxel Accelerates Spontaneous Calcium Oscillations in Cardiomyocytes by Interacting with NCS-1 and the InsP3R. *J. Mol. Cell. Cardiol.* 49, 829–835. doi:10.1016/j.yjmcc.2010.08.018

Zhang, S., Liu, X., Bawa-Khalfe, T., Lu, L.-S., Lyu, Y. L., Liu, L. F., et al. (2012). Identification of the Molecular Basis of Doxorubicin-Induced Cardiotoxicity. *Nat. Med.* 18, 1639–1642. doi:10.1038/nm.2919

Conflict of Interest: The authors declare that the research was conducted in the absence of any commercial or financial relationships that could be construed as a potential conflict of interest.

frontiers in Pharmacology

PERSPECTIVE
published: 19 April 2021
doi: 10.3389/fphar.2021.598549

Inflammation as a Risk Factor in Cardiotoxicity: An Important Consideration for Screening During Drug Development

*Chiara Campana[1], Rafael Dariolli[1], Mohamed Boutjdir[2,3,4] and Eric A. Sobie[1]**

[1]Department of Pharmacological Sciences, Icahn School of Medicine at Mount Sinai, New York, NY, United States, [2]Cardiovascular Research Program, VA New York Harbor Healthcare System, Brooklyn, NY, United States, [3]Department of Medicine, Cell Biology and Pharmacology, State University of New York Downstate Medical Center, Brooklyn, NY, United States, [4]Department of Medicine, New York University School of Medicine, New York, NY, United States

OPEN ACCESS

Edited by:
Nicolau Beckmann, Novartis Institutes for BioMedical Research, Switzerland

Reviewed by:
Tamer M. A. Mohamed, University of Louisville, United States
Alberto Aimo, Sant'Anna School of Advanced Studies, Italy
Xin Zhou, University of Oxford, United Kingdom
Elisa Passini, University of Oxford, United Kingdom

****Correspondence:***
Eric A. Sobie
eric.sobie@mssm.edu

Specialty section:
This article was submitted to Cardiovascular and Smooth Muscle Pharmacology, a section of the journal Frontiers in Pharmacology

Received: *25 August 2020*
Accepted: *31 March 2021*
Published: *19 April 2021*

Citation:
Campana C, Dariolli R, Boutjdir M and Sobie EA (2021) Inflammation as a Risk Factor in Cardiotoxicity: An Important Consideration for Screening During Drug Development. Front. Pharmacol. 12:598549. doi: 10.3389/fphar.2021.598549

Numerous commonly prescribed drugs, including antiarrhythmics, antihistamines, and antibiotics, carry a proarrhythmic risk and may induce dangerous arrhythmias, including the potentially fatal Torsades de Pointes. For this reason, cardiotoxicity testing has become essential in drug development and a required step in the approval of any medication for use in humans. Blockade of the hERG K^+ channel and the consequent prolongation of the QT interval on the ECG have been considered the gold standard to predict the arrhythmogenic risk of drugs. In recent years, however, preclinical safety pharmacology has begun to adopt a more integrative approach that incorporates mathematical modeling and considers the effects of drugs on multiple ion channels. Despite these advances, early stage drug screening research only evaluates QT prolongation in experimental and computational models that represent healthy individuals. We suggest here that integrating disease modeling with cardiotoxicity testing can improve drug risk stratification by predicting how disease processes and additional comorbidities may influence the risks posed by specific drugs. In particular, chronic systemic inflammation, a condition associated with many diseases, affects heart function and can exacerbate medications' cardiotoxic effects. We discuss emerging research implicating the role of inflammation in cardiac electrophysiology, and we offer a perspective on how *in silico* modeling of inflammation may lead to improved evaluation of the proarrhythmic risk of drugs at their early stage of development.

Keywords: drug-induced cardiotoxicity, drug-induced arrhythmias, systemic inflammation, cardiac electrophysiology, quantitative systems pharmacology

INTRODUCTION

During drug development, the possibility of cardiotoxicity in the form of drug-induced Torsades de Pointes (TdP) must be evaluated for all new chemical entities. This is assessed by testing for potential block of the rapid delayed rectifier current, I_{Kr}, and by measuring changes to the QT interval in healthy volunteers, under guidelines established by the International Conference on Harmonization and agreed to by regulatory bodies (Food and Drug Administration, HHS, 2005a; 2005b). More recently, initiatives such as CiPA, the Comprehensive *in vitro* Proarrhythmia Assay, aim to combine multiple preclinical measurements for a more complete picture of potential drug-induced arrhythmia (Colatsky et al., 2016; Vicente et al., 2018). Despite these requirements, many approved drugs are associated with isolated instances of TdP, and all drugs are monitored closely through databases such as the FDA Adverse Event Reporting System (Wysowski and Swartz, 2005; Poluzzi et al., 2012). In addition, preclinical efforts at cardiotoxicity testing focus primarily on how drugs influence the electrophysiology of healthy hearts, whereas TdP, when it occurs, is often associated with specific populations of patients, sometimes those with comorbidities (Roden, 2016; El-Sherif et al., 2018). In this perspective we discuss one such comorbidity, systemic inflammation, and argue that a careful consideration of inflammation's effects on ventricular electrophysiology may enable a better understanding of when, and in what patient groups, particular drugs may increase TdP risk.

A PubMed search using the keywords *cardiotoxicity AND inflammation* reveals that 553 papers, of which 119 are reviews, have been published on this topic since 1976. In last 14 months alone, 134 articles were published, indicating increasing interest in the interactions between inflammation and drug-induced cardiac arrhythmias. The advent of Covid-19 provides perhaps the most recent evidence of how systemic inflammation is not only a determinant of disease severity, but also a factor that should be taken into account when choosing the preferred course of therapy (Lazzerini et al., 2020b). Drug repurposing, which has played a role in identifying treatment options for Covid-19 patients, has brought to public attention the intrinsic cardiac risk of some of the existing drugs on the market. Variability in a patient's response to a disease, along with the innate complexity and differences in disease pathophysiology, can serve as obstacles in the establishment of the cardiotoxic risk of a given drug and render it difficult for clinicians to weigh the risk and benefit of therapeutics. In general, patients with underlying cardiac comorbidities, such as structural heart disease, are at higher arrhythmia risk, and factors such as age, electrolyte imbalance, and body weight also have an impact on drug-induced arrhythmia (Heist and Ruskin, 2010; Kannankeril et al., 2010, 2011). More recently, systemic inflammation, which is highly correlated with the occurrence of atrial fibrillation (Lazzerini et al., 2019a) and ventricular arrhythmia, has been implicated as a condition that can increase the risk of adverse cardiac events (Lazzerini et al., 2015b; Korantzopoulos et al., 2018).

An acute inflammatory response begins with activation of the immune system and the production of cytokines and other chemical mediators (Feghali-Bostwick and Wright, 1997; Zhang and An, 2007). Although the mediators that are produced depend on the nature of the inflammatory trigger, their general function is to stimulate target tissues to adjust to the new inflamed condition, including through the recruitment of cellular populations such as neutrophils and macrophages (Medzhitov, 2010; Remick, 2014). The release of cytokines such as interleukin-6 (IL-6), tumor necrosis factor-α (TNF-α) and interleukin-1β (IL-1β) during the inflammatory process can also induce systemic changes that include the production of C-reactive protein (CRP) by the liver and the production of proinflammatory prostaglandins in the brain (Medzhitov, 2010). Because CRP levels correlate with the levels of cytokines, they are utilized as a surrogate marker for monitoring the latter and have been adopted by clinicians to assess disease severity and prognosis (Osman et al., 2006). Inflammation is often triggered by viral and bacterial infections and resolves quickly once the infectious agents have been controlled. However, in the face of a persistent infection or when the inflammatory source is further enhanced through a positive feedback loop, chronic inflammation can arise (Medzhitov, 2010). This can also occur in conditions such as obesity and neurodegenerative disease (Medzhitov, 2010; Nathan and Ding, 2010).

Cytokines that are released during acute and chronic inflammation may influence the function and expression of cardiac ion channels, thereby potentially explaining the increased risk of arrhythmia and sudden cardiac death in the presence of inflammation (Lazzerini et al., 2015b; 2020a). Investigators have begun to uncover the pathophysiology behind this arrhythmogenicity by using patients with chronic inflammatory disorders to better understand the effects of inflammation on specific cardiac ion channels (Alí et al., 2018). In light of this developing research, the term inflammatory cardiac channelopathies has been proposed (Lazzerini et al., 2018; 2019b). For instance, Aromolaran et al. (2018) have recently shown that elevated serum inflammatory markers will inhibit the human ether-à-go-go-related gene (hERG) channel, reducing the rapid delayed rectifier current (I_{Kr}) and leading to action potential (AP) prolongation. This and similar recent results have prompted a consideration of how endogenous inflammation and potential proinflammatory effects of drugs may affect preclinical cardiotoxicity studies.

We propose that evaluating the effects of inflammation on cardiac electrical function is especially important when testing the cardiotoxicity of: 1) drugs that induce inflammation as a side effect, and 2) drugs that are used to treat diseases that are associated with chronic inflammation.

INFLAMMATION AND CARDIOTOXICITY TESTING

Inflammation and the Heart

Acute inflammation is determined by defense mechanisms that activate the immune system and transiently respond to a pathogen, or other triggers, in ways that generally benefit the organism. However, systemic chronic inflammation has a deleterious effect on the body (Medzhitov, 2010). It can be caused by obesity, viral or microbial infection, autoimmune disease, or cancer (Berg and Scherer, 2005; Koene et al., 2016). Heart failure with preserved ejection fraction (HFpEF) is responsible for roughly half of heart failure cases and has a wide variety of underlying causes (Shah et al., 2016; Packer and Kitzman, 2018). Obesity, diabetes and hypertension are common comorbidities in patients with HFpEF, and research in the past decade has recognized their increasingly important role in the pathophysiology of HFpEF, such that an obesity-associated HFpEF phenotype has been defined (Paulus and Tschöpe, 2013; Shah et al., 2016; Packer and Kitzman, 2018).

In the obese HFpEF phenotype, obesity-driven systemic inflammation leads to cardiomyocyte stiffness and interstitial fibrosis that contribute to heart failure development (Paulus and Tschöpe, 2013; Shah et al., 2016; Oh et al., 2019).

With respect to electrophysiology, QT interval is generally prolonged in individuals with systemic inflammation and can be correlated in some instances with CRP levels and the incidence of sudden death (Kazumi et al., 2003; Hussein et al., 2013). For example, patients suffering from rheumatoid arthritis, an autoimmune disease, are at higher risk of experiencing cardiovascular diseases and sudden death (Lazzerini et al., 2015a). In this study, the release of proinflammatory cytokines was one factor that accounted for QT interval prolongation and the risk of sudden death, and the immunosuppressive drug tocilizumab returned the QT interval to a normal value within three months of treatment. Tocilizumab, which binds to the IL-6 receptor, is thought to work by inhibiting both IL-6 signaling and the release of additional cytokines such as TNF-α. The inflammatory pathway common to rheumatoid arthritis and several other conditions leads to structural remodeling of cardiac tissue, inducing fibrosis and coronary atherosclerosis, as well as electrical remodeling that affects the function and the expression of cardiac ion channels. Importantly, the study by Lazzerini et al. (2015a) emphasizes the role of inflammation-induced QT prolongation in precipitating cardiovascular complications often assumed to be secondary to the altered cardiovascular structure.

In isolated cardiomyocytes, the AP is a surrogate for the ECG such that a prolonged cellular AP duration (APD) corresponds to longer QT interval on the ECG, and a higher propensity for early after depolarizations, which can trigger ventricular arrhythmias (Wit, 2018). Because the AP is determined by the balance between inward depolarizing currents and outward hyperpolarizing currents, drugs or genetic mutations that, reduce the magnitude of K^+ currents or increase the magnitude of Ca^{2+} currents can cause an increase in the APD. Although the connection between inflammation and QT prolongation is not completely understood, proinflammatory cytokines TNF-α, IL-6 and IL-1β have been shown to alter both the function of ion channels and their levels of expression, in addition to the cardiovascular structural remodeling caused by inflammation (Lazzerini et al., 2017). We provide a summary of the relevant literature with a focus on the different time scales on which the remodeling occurs.

In terms of direct effects on cardiac ion channels, both IL-6 and TNF-α have been shown to inhibit hERG currents in HEK293 cells (Wang et al., 2004; Aromolaran et al., 2018), and IL-6 both inhibits hERG and prolongs APs in guinea pig hearts (Aromolaran et al., 2018). Acute exposure to IL-1β contributes to increased Ca^{2+} current density and longer APD in guinea pig ventricular cells (Li and Rozanski, 1993). Similarly, Hagiwara et al. (2007) showed that IL-6 rapidly increases Ca^{2+} current density and intracellular Ca^{2+} transients in mouse ventricular cells.

The longer-term effects of these cytokines have also been investigated. Wang et al. (2004) confirmed the proarrhythmic impact of TNF-α in isolated canine cardiomyocytes and showed time-dependent inhibitory effects on I_{Kr} such that APD values after 10 h of exposure were longer than those after 10 min of exposure. IL-6 also reduced hERG expression in HEK293 cells and adult guinea pig ventricular myocytes (Aromolaran et al., 2018). Consistent with these results, Monnerat et al. (2016) showed that rodent and human cells incubated for 24 h with IL-1β had reduced repolarizing transient outward K^+ current (I_{to}), increased Ca^{2+} spark frequency, and increased Ca^{2+}/calmodulin-dependent protein kinase II (CaMKII) oxidation, which in turn intensifies Ca^{2+} leakage from the sarcoplasmic reticulum into the cytosol (Szekely and Arbel, 2018).

Over an even longer period of time, the three cytokines have been determined to alter myocardial contractility, which is consistent with the clinical presentation of chronic inflammation. When administered chronically, IL-6 has been shown to decrease cardiac contractility and induce cardiac hypertrophy in both mouse and human studies (Fontes et al., 2015). Combes et al. (2002) found that neonatal rat cardiac myocytes exposed to IL-1β for three days had reduced amplitude and maximum speed of contraction. Overexpression of TNF-α in mice induced decreased ejection fraction, atrial and ventricular arrhythmias, and heart failure (Feldman et al., 2000; Petkova-Kirova et al., 2006). Underlying these events is a reduction in I_{to} and delayed rectifier currents, accompanied by diminished Kv4.2, Kv4.3 and Kv1.5 protein expression (Petkova-Kirova et al., 2006).

In silico Evaluation of Drug Safety

Decades after the first evidence of drug-induced TdP was discovered during treatment of atrial fibrillation with quinidine (Arthur and Wray, 1964), it is now well established that a wide range of prescription drugs carry a cardiotoxic risk. During drug development in the pharmaceutical industry, a new compound's proarrhythmic potential is investigated early, to attempt to prevent drugs with high cardiotoxicity risk from ultimately entering the market. The most severe forms of acquired arrhythmias are often precipitated by drugs whose mechanism of action involves blockade of I_{Kr}. The proarrhythmic risk associated with these drugs varies between individuals and depends on factors such as age, genetic background, and the presence of comorbidities or concomitant drug treatments (Polak et al., 2015). Due to the extensive usage of some of these medications individually or in combination, even a small proarrhythmic risk can be of concern. Moreover, due to the phenotypic differences among the individuals using these medications, it is difficult but imperative to identify who is at higher risk of developing life-threatening drug-induced arrhythmias.

Although block of I_{Kr}, the so-called "hERG current", has long been considered the simplest way of assessing a compound's cardiotoxic risk, the limitations of this approach have led to newer initiatives such as CiPA (Sager et al., 2014). CiPA proposes to identify reliable proarrhythmia metrics by analyzing how drugs interact with a wide range of ionic channels, and by combining *in vitro* with *in silico* studies (Sager et al., 2014; Colatsky et al., 2016; Li et al., 2020). A multiscale *in silico* approach is adopted to evaluate the effect of channel blockade on the ventricular

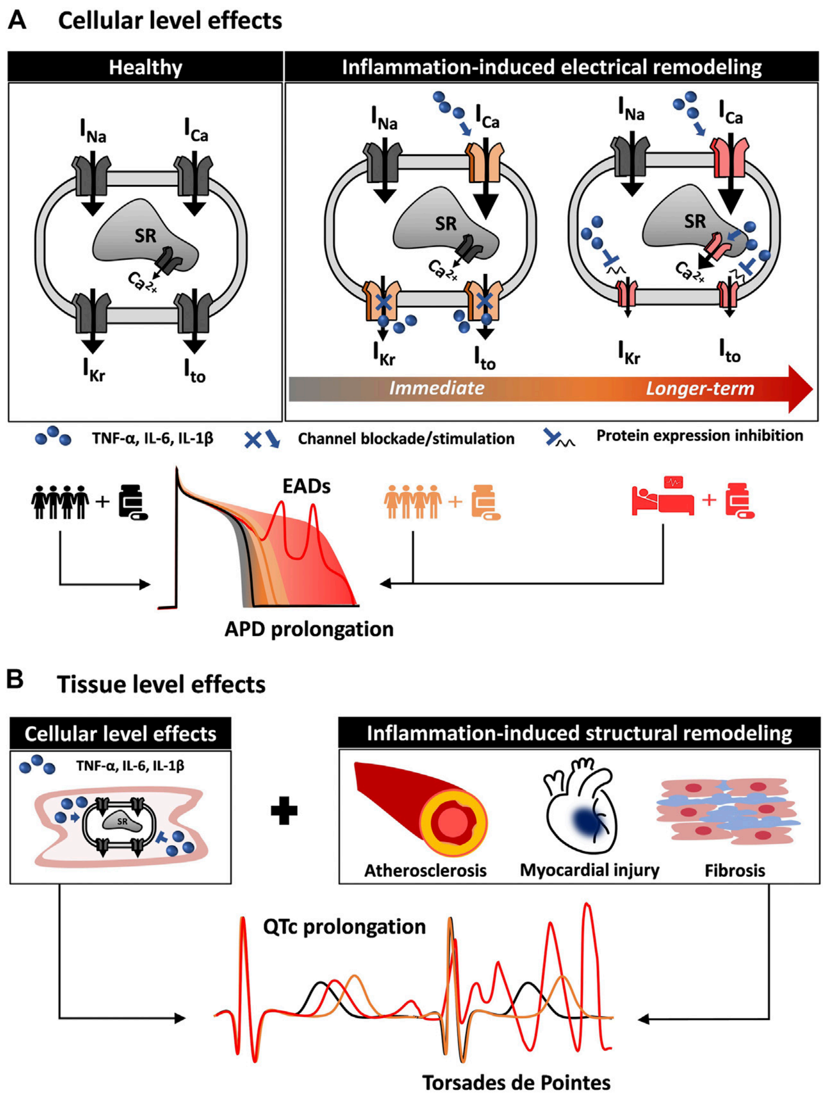

FIGURE 1 | Multiscale quantitative systems pharmacology to integrate inflammation modeling into *in silico* drug safety evaluation. **(A)** Inflammation induces cardiac electrical remodeling. Proinflammatory cytokines can alter cardiac electrophysiology by interacting directly with the cardiac ion channels. By altering the normal function (immediate effect) and expression of cardiac ion channels (longer-term effect), inflammation is a source of variability in the cardiomyocyte response to the administration of drugs. In addition to variability among healthy individuals (black line and gray shaded area), the inflammatory state (orange and red) can profoundly alter the cellular pro-arrhythmia risk metrics normally evaluated in *in silico* drug safety. **(B)** Inflammation affects cardiac tissue pro-arrhythmia risk metrics. Inflammation also contributes to cardiac structural remodeling, affecting cardiac propagation and creating a proarrhythmic substrate. Together with the effects on the single cardiomyocyte, this can result in altered (orange and red) QT interval on the ECG.

cardiomyocyte AP (Li et al., 2019). The *in silico* predictions are then validated in hiPSC-CMs. There has been tremendous progress in expanding the proarrhythmic risk evaluation to different spatial scales and correlating the events happening at the molecular level to the phenomena occurring at the organ level (Yang et al., 2020). The introduction of machine learning approaches and the definition of new metrics other than hERG blockade have helped accomplish a better stratification of drug-induced cardiotoxicity (Lancaster and Sobie, 2016).

While these efforts have certainly improved drug risk prediction, the majority of *in silico* cardiotoxicity studies, which have used models of healthy cardiomyocytes, have largely left unexplored how disease conditions may affect cardiotoxicity predictions (Chi, 2013; Li et al., 2017; Passini et al., 2017; Margara et al., 2020; Yang et al., 2020). Although it is important to study and understand these mechanisms, most drugs are used in individuals whose cardiac electrophysiology differs from that seen in healthy subjects. Models of pathological cardiac electrophysiology have been developed over the years to describe conditions such as heart failure or congenital heart diseases, such as long QT syndromes, caused by cardiac ion channel gene mutations (Niederer et al., 2019).

Some cardiotoxicity studies have also explored the effect of these diseases on *in silico* predictions, recognizing that modeling pre-existing cardiovascular disorders may improve risk stratification (Christophe and Crumb, 2019; Llopis et al., 2019). However, only a limited number of diseases have been modeled, and the field is lacking a comprehensive study evaluating how the response to drugs differs between healthy and diseased human ventricular cardiomyocytes. Since inflammation: 1) underlies or occurs secondarily to many pathologies, and 2) has both direct and indirect effects on multiple cardiac electrophysiology mechanisms, it becomes imperative to explore this emerging role of inflammation in greater detail. We suggest that integrating inflammation in multiscale cardiac electrophysiology modeling would represent a first important step toward disease-specific cardiotoxicity studies.

New Directions in Cardiotoxicity Testing

Multiscale cardiac electrophysiology modeling allows for the study of drug interaction with cardiac ion channels. Several approaches have been previously used to achieve this, including simple pore block models and more complicated Markov chain models (Wiśniowska et al., 2014; Gando et al., 2020). The effects of proinflammatory cytokines on cardiac ion channels, such as the blockade of hERG by IL-6 described by Aromolaran et al. (2018), can be readily incorporated in cardiac electrophysiology modeling to more accurately stratify arrhythmic risk in patients based on their inflammatory state. **Figure 1** shows a schematic of how integrating the effect of comorbidities, in particular inflammation, can alter cellular proarrhythmic markers. The first aspects to be included in *in silico* cardiotoxicity studies would be the direct actions of cytokines on cardiac ion channels combined with the indirect effects caused in myocytes by prolonged cytokine exposure (**Figure 1A**). Although effects of cytokines on certain ion channels have been demonstrated, as described above, it would be important to complement these with measurements of how the cytokines influence action potentials and intracellular [Ca^{2+}] to infer whether additional effects might also contribute. Furthermore as more data become available, effects of cytokines can be incorporated into integrative models that combine electrophysiology and Ca^{2+} signaling with, for instance, cellular energetics (Gauthier et al., 2012) or intracellular signaling (Heijman et al., 2011; Gong et al., 2020). Inclusion of these features would allow for evaluation of how inflammation directly modifies the single cardiomyocyte behavior.

In a second step, structural remodeling can also be integrated into computational analyses if a cardiac tissue is modeled (**Figure 1B**). For instance, inflammation-induced fibrosis affects cardiac propagation, and models of fibroblasts interconnected with cardiac myocytes have been previously implemented (Zeigler et al., 2016). Importantly, hiPSC-CMs can serve as a valuable platform to support the development of accurate models of inflammation-induced electrical remodeling. The effect of many proinflammatory cytokines, alone or in combination, can be evaluated in such systems to inform parameters (such as channel conductance) of *in silico* human models (Yücel et al., 2017). Computational approaches (Gong and Sobie, 2018) have been recently proposed to address the limitations stemming from the immature phenotype of hiPSC-CMs. This can facilitate the translation of recent findings (Yücel et al., 2017) and future discoveries from hiPSC-CMs to human adult cardiomyocytes.

Variability in drug response among healthy individuals is important in drug development and drug cardiotoxicity studies. Cardiac electrophysiological heterogeneity plays an important role in current *in silico* cardiotoxicity studies, and population-based modeling has become an integral aspect of computational cardiac electrophysiology (Sarkar et al., 2012; Britton et al., 2013; Muszkiewicz et al., 2016; Ni et al., 2018). Variability in a healthy population of individuals is typically included in cardiomyocyte models by randomly varying, within a range of physiological values, the ion channels' conductance and gating variables (Sarkar et al., 2012). Age, cardiac disease, and biological sex are important factors that influence electrophysiology (Bednar et al., 2002; Yang et al., 2017), and these can be incorporated into simulations of cardiotoxicity risk (Varshneya et al., 2021). In a computational framework that accounted for inflammation, it would be important to incorporate variability in both the healthy and chronic inflammation populations, since inflammation itself may influence the factors that contribute to arrhythmia risk.

We postulate that in addition to considering variability across populations of healthy individuals, *in silico* cardiotoxicity studies should begin to integrate more detailed modeling of disease pathways. Medications labeled as safe might compromise the cardiac function in patients already at higher risk of cardiac complications because of inherent comorbidities. Although certain disease processes may have little influence, chronic diseases, viral and bacterial infections, and cancer are likely to disturb both normal cardiac function and how the heart interacts with medications. Potentially proarrhythmic drugs, such as the widely prescribed antibiotic clarithromycin, the cancer medication tamoxifen and the tyrosine kinase inhibitor vandetanib, used for treatment of thyroid cancer, are all used in patients with altered electrophysiology. The pathological profile of conditions such as cancer and microbial infections includes increased proinflammatory cytokine levels that, as described in the previous sections, are known to significantly alter many physiological cardiac mechanisms. Considering the impact of inflammation on cardiac ion channel remodeling would be particularly important in these cases and would signify an important step towards incorporating disease modeling into *in silico* drug safety testing.

Despite the complexity of the mechanisms underlying systemic inflammation, it is a phenomenon that should be explored more in depth in the field of computational cardiac electrophysiology. An increasing amount of research has characterized the interplay among systemic inflammation and long QT syndrome and arrhythmogenicity. The multitude of diseases where inflammation plays a role makes it an important process to evaluate in studies of drug response and cardiotoxicity.

DATA AVAILABILITY STATEMENT

The original contributions presented in the study are included in the article/Supplementary Material, further inquiries can be directed to the corresponding author.

AUTHOR CONTRIBUTIONS

CC conceived the manuscript and wrote the initial draft. ES, RD, and MB helped to edit the manuscript.

FUNDING

Research on drug-induced arrhythmias in Dr. Sobie's laboratory is funded by the National Heart Lung and Blood Institute projects U01 HL 136297 and R44HL139248.

REFERENCES

Alí, A., Boutjdir, M., and Aromolaran, A. S. (2018). Cardiolipotoxicity, inflammation, and arrhythmias: role for interleukin-6 molecular mechanisms. *Front. Physiol.* 9, 1866. doi:10.3389/fphys.2018.01866

Aromolaran, A. S., Srivastava, U., Alí, A., Chahine, M., Lazaro, D., El-Sherif, N., et al. (2018). Interleukin-6 inhibition of hERG underlies risk for acquired long QT in cardiac and systemic inflammation. *PLoS One* 13, e0208321. doi:10.1371/journal.pone.0208321

Arthur, S., and Wray, H. (1964). WesleyQuinidine syncope. *Circulation* 30, 17–26. doi:10.1161/01.CIR.30.1.17

Bednar, M. M., Harrigan, E. P., and Ruskin, J. N. (2002). Torsades de pointes associated with nonantiarrhythmic drugs and observations on gender and QTc. *Am. J. Cardiol.* 89, 1316–1319. doi:10.1016/S0002-9149(02)02337-8

Berg, A. H., and Scherer, P. E. (2005). Adipose tissue, inflammation, and cardiovascular disease. *Circ. Res.* 96, 939–949. doi:10.1161/01.RES.0000163635.62927.34

Britton, O. J., Bueno-Orovio, A., Van Ammel, K., Lu, H. R., Towart, R., Gallacher, D. J., et al. (2013). Experimentally calibrated population of models predicts and explains intersubject variability in cardiac cellular electrophysiology. *Proc. Natl. Acad. Sci. USA* 110, E2098–E2105. doi:10.1073/pnas.1304382110

Chi, K. R. (2013). Revolution dawning in cardiotoxicity testing. *Nat. Rev. Drug Discov.* 12, 565–567. doi:10.1038/nrd4083

Christophe, B., and Crumb, W. J. (2019). Impact of disease state on arrhythmic event detection by action potential modelling in cardiac safety pharmacology. *J. Pharmacol. Toxicol. Methods* 96, 15–26. doi:10.1016/j.vascn.2018.12.004

Colatsky, T., Fermini, B., Gintant, G., Pierson, J. B., Sager, P., Sekino, Y., et al. (2016). The comprehensive *in Vitro* proarrhythmia assay (CiPA) initiative - update on progress. *J. Pharmacol. Toxicol. Methods* 81, 15. doi:10.1016/j.vascn.2016.06.002

Combes, A., Frye, C., Lemster, B., Brooks, S., Watkins, S., Feldman, A., et al. (2002). Chronic exposure to interleukin 1β induces a delayed and reversible alteration in excitation-contraction coupling of cultured cardiomyocytes. *Pflugers Arch.* 445, 246–256. doi:10.1007/s00424-002-0921-y

El-Sherif, N., Turitto, G., and Boutjdir, M. (2018). Acquired long QT syndrome and torsade de pointes. *Pacing Clin. Electrophysiol.* 41, 414–421. doi:10.1111/pace.13296

Feghali, C. A., and Wright, T. M. (1997). Cytokines in acute and chronic inflammation. *Front. Biosci.* 2, d12–26. doi:10.2741/A171

Feldman, A. M., Combes, A., Wagner, D., Kadakomi, T., Kubota, T., You Li, Y., et al. (2000). The role of tumor necrosis factor in the pathophysiology of heart failure. *J. Am. Coll. Cardiol.* 35, 537–544. doi:10.1016/s0735-1097(99)00600-2

Fontes, J. A., Rose, N. R., and Čiháková, D. (2015). The varying faces of IL-6: from cardiac protection to cardiac failure. *Cytokine* 74, 62–68. doi:10.1016/j.cyto.2014.12.024

Food and Drug Administration, HHS. (2005a). International conference on harmonisation; guidance on E14 clinical evaluation of QT/QTc interval prolongation and proarrhythmic potential for non-antiarrhythmic drugs; availability. Notice. *Fed. Regist.* 70, 61134–61135. doi:10.1177/009286150503900407

Food and Drug Administration, HHS. (2005b). International conference on harmonisation; guidance on S7B nonclinical evaluation of the potential for delayed ventricular repolarization (QT interval prolongation) by human pharmaceuticals; availability. *Notice. Fed. Regist.* 70, 61133–61134. doi:10.1254/fpj.121.377

Gando, I., Campana, C., Tan, R. B., Cecchin, F., Sobie, E. A., and Coetzee, W. A. (2020). A distinct molecular mechanism by which phenytoin rescues a novel long QT 3 variant. *J. Mol. Cell Cardiol.* 144, 1–11. doi:10.1016/j.yjmcc.2020.04.027

Gauthier, L. D., Greenstein, J. L., and Winslow, R. L. (2012). Toward an integrative computational model of the Guinea pig cardiac myocyte. *Front. Physiol.* 3, 244. doi:10.3389/fphys.2012.00244

Gong, J. Q. X., and Sobie, E. A. (2018). Population-based mechanistic modeling allows for quantitative predictions of drug responses across cell types. *Npj Syst. Biol. Appl.* 4, 1–11. doi:10.1038/s41540-018-0047-2

Gong, J. Q. X., Susilo, M. E., Sher, A., Musante, C. J., and Sobie, E. A. (2020). Quantitative analysis of variability in an integrated model of human ventricular electrophysiology and β-adrenergic signaling. *J. Mol. Cell Cardiol.* 143, 96–106. doi:10.1016/j.yjmcc.2020.04.009

Hagiwara, Y., Miyoshi, S., Fukuda, K., Nishiyama, N., Ikegami, Y., Tanimoto, K., et al. (2007). SHP2-mediated signaling cascade through gp130 is essential for LIF-dependent ICaL, [Ca2+]i transient, and APD increase in cardiomyocytes. *J. Mol. Cell Cardiol.* 43, 710–716. doi:10.1016/j.yjmcc.2007.09.004

Heijman, J., Volders, P. G. A., Westra, R. L., and Rudy, Y. (2011). Local control of β-adrenergic stimulation: effects on ventricular myocyte electrophysiology and Ca2+-transient. *J. Mol. Cell Cardiol.* 50, 863–871. doi:10.1016/j.yjmcc.2011.02.007

Heist, E. K., and Ruskin, J. N. (2010). Drug-induced arrhythmia. *Circulation* 122, 1426–1435. doi:10.1161/CIRCULATIONAHA.109.894725

Hussein, A. A., Gottdiener, J. S., Bartz, T. M., Sotoodehnia, N., DeFilippi, C., See, V., et al. (2013). Inflammation and sudden cardiac death in a community-based population of older adults: the Cardiovascular Health Study. *Heart Rhythm* 10, 1425–1432. doi:10.1016/j.hrthm.2013.07.004

Kannankeril, P. J., Norris, K. J., Carter, S., and Roden, D. M. (2011). Factors affecting the degree of QT prolongation with drug challenge in a large cohort of normal volunteers. *Heart Rhythm* 8, 1530–1534. doi:10.1016/j.hrthm.2011.03.042

Kannankeril, P., Roden, D. M., and Darbar, D. (2010). Drug-induced long QT syndrome. *Pharmacol. Rev.* 62, 760–781. doi:10.1124/pr.110.003723

Kazumi, T., Kawaguchi, A., Hirano, T., and Yoshino, G. (2003). C-reactive protein in young, apparently healthy men: associations with serum leptin, QTc interval, and high-density lipoprotein-cholesterol. *Metabolism* 52, 1113–1116. doi:10.1016/S0026-0495(03)00184-7

Koene, R. J., Prizment, A. E., Blaes, A., and Konety, S. H. (2016). Shared risk factors in cardiovascular disease and cancer. *Circulation* 133, 1104–1114. doi:10.1161/CIRCULATIONAHA.115.020406

Korantzopoulos, P., Letsas, K. P., Tse, G., Fragakis, N., Goudis, C. A., and Liu, T. (2018). Inflammation and atrial fibrillation: a comprehensive review. *J. Arrhythmia* 34, 394–401. doi:10.1002/joa3.12077

Lancaster, M. C., and Sobie, E. (2016). Improved prediction of drug-induced torsades de Pointes through simulations of dynamics and machine learning algorithms. *Clin. Pharmacol. Ther.* 100, 371–379. doi:10.1002/cpt.367

Lazzerini, P. E., Acampa, M., Capecchi, P. L., Fineschi, I., Selvi, E., Moscadelli, V., et al. (2015a). Antiarrhythmic potential of anticytokine therapy in rheumatoid arthritis: tocilizumab reduces corrected QT interval by controlling systemic inflammation. *Arthritis Care Res.* 67, 332–339. doi:10.1002/acr.22455

Lazzerini, P. E., Acampa, M., Laghi-Pasini, F., Bertolozzi, I., Finizola, F., Vanni, F., et al. (2020a). Cardiac arrest risk during acute infections. *Circ. Arrhythmia Electrophysiol.* 13, 113. doi:10.1161/CIRCEP.120.008627

Lazzerini, P. E., Boutjdir, M., and Capecchi, P. L. (2020b). COVID-19, arrhythmic risk, and inflammation. *Circulation* 142, 047293. doi:10.1161/CIRCULATIONAHA.120.047293

Lazzerini, P. E., Capecchi, P. L., El-Sherif, N., Laghi-Pasini, F., and Boutjdir, M. (2018). Emerging arrhythmic risk of autoimmune and inflammatory cardiac channelopathies. *J. Am. Heart Assoc.* 7, e010595. doi:10.1161/JAHA.118.010595

Lazzerini, P. E., Capecchi, P. L., Laghi-Pasini, F., and Boutjdir, M. (2017). Autoimmune channelopathies as a novel mechanism in cardiac arrhythmias. *Nat. Rev. Cardiol.* 14, 521–535. doi:10.1038/nrcardio.2017.61

Lazzerini, P. E., Capecchi, P. L., and Laghi-Pasini, F. (2015b). Long QT syndrome: an emerging role for inflammation and immunity. *Front. Cardiovasc. Med.* 2, 26. doi:10.3389/fcvm.2015.00026

Lazzerini, P. E., Laghi-Pasini, F., Acampa, M., Srivastava, U., Bertolozzi, I., Giabbani, B., et al. (2019a). Systemic inflammation rapidly induces reversible atrial electrical remodeling: the role of interleukin-6-mediated changes in connexin expression. *J Am Heart Assoc.* 8, e011006. doi:10.1161/JAHA.118.011006

Lazzerini, P. E., Laghi-Pasini, F., Boutjdir, M., and Capecchi, P. L. (2019b). Cardioimmunology of arrhythmias: the role of autoimmune and inflammatory cardiac channelopathies. *Nat. Rev. Immunol.* 19, 63–64. doi:10.1038/s41577-018-0098-z

Li, Y.-H., and Rozanski, G. J. (1993). Effects of human recombinant interleukin-1 on electrical properties of Guinea pig ventricular cells. *Cardiovasc. Res.* 27, 525–530. doi:10.1093/cvr/27.3.525

Li, Z., Dutta, S., Sheng, J., Tran, P. N., Wu, W., Chang, K., et al. (2017). Improving the *in silico* assessment of proarrhythmia risk by combining hERG (human ether-à-go-go-related gene) channel-drug binding kinetics and multichannel pharmacology. *Circ. Arrhythm. Electrophysiol.* 10, e004628. doi:10.1161/CIRCEP.116.004628

Li, Z., Garnett, C., and Strauss, D. G. (2019). Quantitative systems pharmacology models for a new international cardiac safety regulatory paradigm: an overview of the comprehensive in vitro proarrhythmia assay *in silico* modeling approach. *CPT Pharmacometrics Syst. Pharmacol.* 8, 371–379. doi:10.1002/psp4.12423

Li, Z., Mirams, G. R., Yoshinaga, T., Ridder, B. J., Han, X., Chen, J. E., et al. (2020). General principles for the validation of proarrhythmia risk prediction models: an extension of the CiPA *in silico* strategy. *Clin. Pharmacol. Ther.* 107, 102–111. doi:10.1002/cpt.1647

Llopis, J., Cano, J., Gomis-Tena, J., Romero, L., Sanz, F., Pastor, M., et al. (2019). *In silico* assay for preclinical assessment of drug proarrhythmicity. *J. Pharmacol. Toxicol. Methods*. 99, 106595. doi:10.1016/j.vascn.2019.05.106

Margara, F., Wang, Z. J., Levrero-Florencio, F., Santiago, A., Vázquez, M., Bueno-Orovio, A., et al. (2021). In-silico human electro-mechanical ventricular modelling and simulation for drug-induced pro-arrhythmia and inotropic risk assessment. *Prog. Biophys. Mol. Biol.* 159, 58. doi:10.1016/j.pbiomolbio.2020.06.007

Medzhitov, R. (2010). Inflammation 2010: new adventures of an old flame. *Cell.* 140, 771–776. doi:10.1016/j.cell.2010.03.006

Monnerat, G., Alarcón, M. L., Vasconcellos, L. R., Hochman-Mendez, C., Brasil, G., Bassani, R. A., et al. (2016). Macrophage-dependent IL-1β production induces cardiac arrhythmias in diabetic mice. *Nat. Commun.* 7, 13344. doi:10.1038/ncomms13344

Muszkiewicz, A., Britton, O. J., Gemmell, P., Passini, E., Sánchez, C., Zhou, X., et al. (2016). Variability in cardiac electrophysiology: using experimentally-calibrated populations of models to move beyond the single virtual physiological human paradigm. *Prog. Biophys. Mol. Biol.* 120, 115–127. doi:10.1016/j.pbiomolbio.2015.12.002

Nathan, C., and Ding, A. (2010). Nonresolving inflammation. *Cell.* 140, 871–882. doi:10.1016/j.cell.2010.02.029

Ni, H., Morotti, S., and Grandi, E. (2018). A heart for diversity: simulating variability in cardiac arrhythmia research. *Front. Physiol.* 9, 958. doi:10.3389/fphys.2018.00958

Niederer, S. A., Lumens, J., and Trayanova, N. A. (2019). Computational models in cardiology. *Nat. Rev. Cardiol.* 16, 100–111. doi:10.1038/s41569-018-0104-y

Oh, A., Okazaki, R., Sam, F., and Valero-Muñoz, M. (2019). Heart failure with preserved ejection fraction and adipose tissue: a story of two tales. *Front. Cardiovasc. Med.* 6, 110. doi:10.3389/fcvm.2019.00110

Osman, R., L'Allier, P. L., Elgharib, N., and Tardif, J.-C. (2006). Critical appraisal of C-reactive protein throughout the spectrum of cardiovascular disease. *Vasc. Health Risk Manag.* 2, 221–237. doi:10.2147/vhrm.2006.2.3.221

Packer, M., and Kitzman, D. W. (2018). Obesity-related heart failure with a preserved ejection fraction. *JACC: Heart Fail.* 6, 633–639. doi:10.1016/j.jchf.2018.01.009

Passini, E., Britton, O. J., Lu, H. R., Rohrbacher, J., Hermans, A. N., Gallacher, D. J., et al. (2017). Human *in silico* drug trials demonstrate higher accuracy than animal models in predicting clinical pro-arrhythmic cardiotoxicity. *Front. Physiol.* 8, 668. doi:10.3389/fphys.2017.00668

Paulus, W. J., and Tschöpe, C. (2013). A novel paradigm for heart failure with preserved ejection fraction. *J. Am. Coll. Cardiol.* 62, 263–271. doi:10.1016/j.jacc.2013.02.092

Petkova-Kirova, P. S., Gursoy, E., Mehdi, H., McTiernan, C. F., London, B., and Salama, G. (2006). Electrical remodeling of cardiac myocytes from mice with heart failure due to the overexpression of tumor necrosis factor-α. *Am. J. Physiology-Heart Circul. Physiol.* 290, H2098–H2107. doi:10.1152/ajpheart.00097.2005

Polak, S., Pugsley, M. K., Stockbridge, N., Garnett, C., and Wiśniowska, B. (2015). Early drug discovery prediction of proarrhythmia potential and its covariates. *AAPS J.* 17, 1025–1032. doi:10.1208/s12248-015-9773-1

Poluzzi, E., Raschi, E., Piccinni, C., and De, F. (2012). Data mining techniques in pharmacovigilance: analysis of the publicly accessible FDA adverse event reporting system (AERS). *Data Min. Appl. Eng. Med.* 12, 131. doi:10.5772/50095

Remick, D. G. (2014). "Systemic inflammation," *Pathobiology of human disease*. Editors L. M. McManus and R. N. Mitchell (San Diego: Academic Press), 315–322. doi:10.1016/B978-0-12-386456-7.01809-8

Roden, D. M. (2016). Predicting drug-induced QT prolongation and torsades de pointes. *J. Physiol.* 594, 2459–2468. doi:10.1113/JP270526

Sager, P. T., Gintant, G., Turner, J. R., Pettit, S., and Stockbridge, N. (2014). Rechanneling the cardiac proarrhythmia safety paradigm: a meeting report from the Cardiac Safety Research Consortium. *Am. Heart J.* 167, 292–300. doi:10.1016/j.ahj.2013.11.004

Sarkar, A. X., Christini, D. J., and Sobie, E. A. (2012). Exploiting mathematical models to illuminate electrophysiological variability between individuals. *J. Physiol.* 590, 2555–2567. doi:10.1113/jphysiol.2011.223313

Shah, S. J., Kitzman, D. W., Borlaug, B. A., van Heerebeek, L., Zile, M. R., Kass, D. A., et al. (2016). Phenotype-specific treatment of heart failure with preserved ejection fraction. *Circulation*. 134, 73–90. doi:10.1161/CIRCULATIONAHA.116.021884

Szekely, Y., and Arbel, Y. (2018). A review of interleukin-1 in heart disease: where do we stand today? *Cardiol. Ther.* 7, 25–44. doi:10.1007/s40119-018-0104-3

Varshneya, M., Irurzun-Arana, I., Campana, C., Dariolli, R., Gutierrez, A., Pullinger, T. K., et al. (2021). Investigational treatments for COVID-19 may increase ventricular arrhythmia risk through drug interactions. *CPT Pharmacometrics Syst. Pharmacol.* 10, 100–107. doi:10.1002/psp4.12573

Vicente, J., Zusterzeel, R., Johannesen, L., Mason, J., Sager, P., Patel, V., et al. (2018). Mechanistic model-informed proarrhythmic risk assessment of drugs: review of the "CiPA" initiative and design of a prospective clinical validation study. *Clin. Pharmacol. Ther.* 103, 54–66. doi:10.1002/cpt.896

Wang, J., Wang, H., Zhang, Y., Gao, H., Nattel, S., and Wang, Z. (2004). Impairment of HERG K+ channel function by tumor necrosis factor-α. *J. Biol. Chem.* 279, 13289–13292. doi:10.1074/jbc.C400025200

Wiśniowska, B., Mendyk, A., Fijorek, K., and Polak, S. (2014). Computer-based prediction of the drug proarrhythmic effect: problems, issues, known and suspected challenges. *Europace* 16, 724–735. doi:10.1093/europace/euu009

Wit, A. L. (2018). Afterdepolarizations and triggered activity as a mechanism for clinical arrhythmias. *Pacing Clin. Electrophysiol.* 41, 883–896. doi:10.1111/pace.13419

Wysowski, D. K., and Swartz, L. (2005). Adverse drug event surveillance and drug withdrawals in the United States, 1969–2002. *Arch. Intern. Med.* 165, 1363–1369. doi:10.1001/archinte.165.12.1363

Yang, P.-C., DeMarco, K. R., Aghasafari, P., Jeng, M.-T., Dawson, J. R. D., Bekker, S., et al. (2020). A computational pipeline to predict cardiotoxicity. *Circ. Res.* 126, 947–964. doi:10.1161/CIRCRESAHA.119.316404

Yang, P.-C., Perissinotti, L. L., López-Redondo, F., Wang, Y., DeMarco, K. R., Jeng, M.-T., et al. (2017). A multiscale computational modelling approach predicts mechanisms of female sex risk in the setting of arousal-induced arrhythmias. *J. Physiol.* 595, 4695–4723. doi:10.1113/JP273142

Yücel, G., Zhao, Z., El-Battrawy, I., Lan, H., Lang, S., Li, X., et al. (2017). Lipopolysaccharides induced inflammatory responses and electrophysiological dysfunctions in human-induced pluripotent stem cell derived cardiomyocytes. *Sci. Rep.* 7, 2935. doi:10.1038/s41598-017-03147-4

Zeigler, A. C., Richardson, W. J., Holmes, J. W., and Saucerman, J. J. (2016). Computational modeling of cardiac fibroblasts and fibrosis. *J. Mol. Cell Cardiol.* 93, 73–83. doi:10.1016/j.yjmcc.2015.11.020

Zhang, J.-M., and An, J. (2007). Cytokines, inflammation, and pain. *Int. Anesthesiol. Clin.* 45, 27–37. doi:10.1097/AIA.0b013e318034194e

Conflict of Interest: The authors declare that the research was conducted in the absence of any commercial or financial relationships that could be construed as a potential conflict of interest.

frontiers in Pharmacology

ORIGINAL RESEARCH
published: 03 August 2021
doi: 10.3389/fphar.2021.680618

High-Throughput Drug Screening System Based on Human Induced Pluripotent Stem Cell-Derived Atrial Myocytes ~ A Novel Platform to Detect Cardiac Toxicity for Atrial Arrhythmias

Yayoi Honda[1,2], *Jun Li*[3,4], *Aya Hino*[4], *Shinji Tsujimoto*[1] *and Jong-Kook Lee*[4]*

[1]*Sumitomo-Dainippon Pharma CO., Ltd., Osaka, Japan,* [2]*Bioanalysis Group, Osaka Laboratory, Technical Solution Headquarters, Sumika Chemical Analysis Service, Ltd., Osaka, Japan,* [3]*Department of Cardiovascular Medicine, Osaka University Graduate School of Medicine, Suita, Japan,* [4]*Department of Cardiovascular Regenerative Medicine, Osaka University Graduate School of Medicine, Suita, Japan*

OPEN ACCESS

Edited by:
Tamer M. A. Mohamed, University of Louisville, United States

Reviewed by:
InKyeom Kim, Kyungpook National University, South Korea
Matthew A. Nystoriak, University of Louisville, United States

***Correspondence:**
Jong-Kook Lee
jlee@cardiology.med.osaka-u.ac.jp

Specialty section:
This article was submitted to Cardiovascular and Smooth Muscle Pharmacology, a section of the journal Frontiers in Pharmacology

Received: *15 March 2021*
Accepted: *13 July 2021*
Published: *03 August 2021*

Citation:
Honda Y, Li J, Hino A, Tsujimoto S and Lee J-K (2021) High-Throughput Drug Screening System Based on Human Induced Pluripotent Stem Cell-Derived Atrial Myocytes ~ A Novel Platform to Detect Cardiac Toxicity for Atrial Arrhythmias. Front. Pharmacol. 12:680618. doi: 10.3389/fphar.2021.680618

Evaluation of proarrhythmic properties is critical for drug discovery. In particular, QT prolongation in electrocardiograms has been utilized as a surrogate marker in many evaluation systems to assess the risk of torsade de pointes and lethal ventricular arrhythmia. Recently, new evaluation systems based on human iPS cell-derived cardiomyocytes have been established. On the other hand, in clinical situations, it has been reported that the incidence of atrial arrhythmias such as atrial fibrillation has been increasing every year, with the prediction of a persistent increase in the near future. As to the increased incidence of atrial arrhythmias, in addition to the increased population of geriatric patients, a wide variety of drug treatments may be related, as an experimental method to detect drug-induced atrial arrhythmia has not been established so far. In the present study, we characterized the atrial-like cardiomyocytes derived from human induced pluripotent stem cells and examined their potential for the evaluation of drug-induced atrial arrhythmia. Atrial-like cardiomyocytes were induced by adding retinoic acid (RA) during the process of myocardial differentiation, and their characteristics were compared to those of RA-free cardiomyocytes. Using gene expression and membrane potential analysis, it was confirmed that the cells with or without RA treatment have atrial or ventricular like cardiomyocytes, respectively. Using the ultra-rapid activating delayed rectifier potassium current (I_{Kur}) channel inhibitor, which is specific to atrial cardiomyocytes, Pulse width duration (PWD) 30cF prolongation was confirmed only in atrial-like cardiomyocytes. In addition, ventricular like cardiomyocytes exhibited an early after depolarization by treatment with rapidly activating delayed rectifier potassium current (I_{Kr}) channel inhibitor, which induces ventricular arrhythmia in clinical situations. Here, we have established a high-throughput drug evaluation system using human iPS cell-derived atrial-like cardiomyocytes. Based on the obtained data, the system might be a valuable platform to detect potential risks for drug-induced atrial arrhythmias.

Keywords: human iPS cell-derived atrial-like cardiomyocytes, nodal-like cardiomyoyctes, atrial arrhythmias, sick sinus syndrome, drug screening

INTRODUCTION

It has been reported that 22% of candidate compounds dropped out at the developmental stage of new drugs and 45% of pharmaceutical products were withdrawn from the market (Watkins, 2011). Therefore, in research and development, it is critical to detect cardiotoxicity during the selection of appropriate compounds for new drugs. In particular, drug-induced torsade de pointes (TdP) has been the most serious concern as it leads to ventricular fibrillation or sudden death.

In western countries, cases of TdP-related death were frequently reported in the late 80s through the early 90s. Several pharmaceutical products were withdrawn from the market because of their risk of inducing TdP in the early 90s (Thomsen et al., 2006; Stockbridge et al., 2013). The International Council for Harmonisation of Technical Requirements for Pharmaceuticals for Human Use (ICH) guidelines for cardiotoxicity evaluation (non-clinical: S7B, clinical: E14), therefore, were enforced to handle these situations, and there have been few examples of product withdrawal due to TdP after the launch of ICH guidelines (Stockbridge et al., 2013). In recent years, human induced pluripotent stem cell-derived cardiomyocytes (hiPSC-CMs) in which ventricular cardiomyocytes are dominant have been commercially available, and multi-facility validation studies using these cells to improve the predictability of drug-induced arrhythmia evaluation have been in progress (Nozaki et al., 2017; Ando et al., 2017).

Cases of not only ventricular but also atrial arrhythmia are also known in clinical situations. Atrial arrhythmia indicates some phenotypes including tachyarrhythmia such as atrial flutter or fibrillation, or bradyarrhythmia such as sick sinus syndrome or atrioventricular block. In tachyarrhythmia, atrial fibrillation occasionally induces cardiac arrest caused by a deterioration of contraction, atrial thrombus formation, and related infarction in organs/tissues. Bradyarrhythmia also causes transient cardiac arrest accompanied by loss of consciousness or cardiac arrest. Although the fatality rate caused by atrial arrhythmia itself is not very high, some lethal diseases originating from atrial arrhythmia are known. The incidence of atrial arrhythmia has increased annually in recent decades (Jensen et al., 2012; Chugh et al., 2014; Schnabel et al., 2015; Lane et al., 2017) and it is predicted that the number of patients will be growing (Jensen et al., 2014; Lane et al., 2017). Aging can be thought of as one of its risk factors, and an aging society might be related to an increase in the number of atrial arrhythmias. Several medicines, such as calcium antagonists, beta-adrenergic blockers, or antipsychotic agents, induce bradyarrhythmia (Edoute et al., 2000; Berry and Hasin, 1978; Johnson et al., 1997; Bordier et al., 2003). Not only aging but also drug treatment may be a trigger for tachyarrhythmia. As the evaluation tools for atria arrhythmia have not been established thus far, we could not confirm the existence of drug-induced atrial arrhythmia itself.

As ventricular cardiomyocytes are dominant in commercially available hiPSC-CMs, atrial arrhythmia might not be detected using these cells. Retinoic acid (RA) is essential in the regulation of cardiac development (Moss et al., 1998). Inhibition of RA synthesis induced the lack of atrial chamber in mouse embryo heart (Xavier-Neto et al., 1999). Hidaka et al.(2003) established a differentiation protocol from mouse embryonic stem (ES) cells to cardiomyocytes, and confirmed that retinoic acid induced atrial cardiomyocytes from ES cells. In recent years, retinoic acid has also been used for inducing atrial cardiomyocyte from human ES/iPS cells Zhang et al. (2011), Gassanov et al. (2008), Lee et al. (2017), and these differentiation methods have been proposed for the application of pathophysiological models of atrial arrhythmia or drug screening for atrial arrhythmia (Devalla et al., 2015; Argenziano et al., 2018; Lemme et al., 2018). In the present study, we obtained a hiPS-derived atrial-like phenotype by supplemented RA during the cardiac mesoderm induction. Accordingly, we tried to examine the acute response to drug administration in the hiPS-CMs with (atrial-like subtype) or without (ventricular-like subtype) treatment of RA.

RESULTS

Cardiac Differentiation Induction From hiPSCs

Undifferentiated hiPSCs were maintained in AK02 medium for 2–3 days until 80% confluency was obtained. Cardiac differentiation was then induced according to the manufacturer's protocol, as shown in **Figure 1A**. To obtain highly purified cardiomyocytes, metabolic selection was performed during post-differentiation, from day 15–26. Cardiomyocyte proportion was quantified by immunostaining with cardiac troponin-T (cTnT). **Figure 1B** shows that the proportion of cTnT-positive cells was over 90% with or without RA treatment (CT 93.9 ± 2.51% vs. AM 96.8 ± 1.81%). The results suggest that RA application did not influence cardiomyocyte differentiation efficiency.

Characteristics of hiPS-Derived Cardiomyocytes With RA Treatment

To further evaluate the gene expression of cardiac subtypes in the control hiPS-CMs (CT) and the RA-treated hiPS-CMs (AM), the cells were co-stained with myosin light chain 2a (MLC-2a: atrial isoform) and myosin light chain 2v (MLC-2v: ventricular isoform) (**Supplementary Figure 1**). An immunofluorescence study showed that the ratio of MLC-2a positive cells and MLC-2v positive cells are comparable in CT (MLC-2a 56.0 ± 2.1% vs. MLC-2v 57.0 ± 2.11%), and the percentage of double-positive cells (MLC-2a$^+$/MLC-2v$^+$) was approximately 40%. In AM (MLC-2a 83.4 ± 0.63%), most cTnT-positive cells were co-positive for MLC-2a, however, very few cTnT-positive cells were found co-positive for MLC-2v (MLC-2v 14.0 ± 2.82%) (**Figures 1B, C**).

To analyze the differences in the functional and electrophysiological properties of atrial and ventricular cardiomyocytes, we assessed multiple parameters of the action potential in CT and AM using a voltage-sensitive dye.

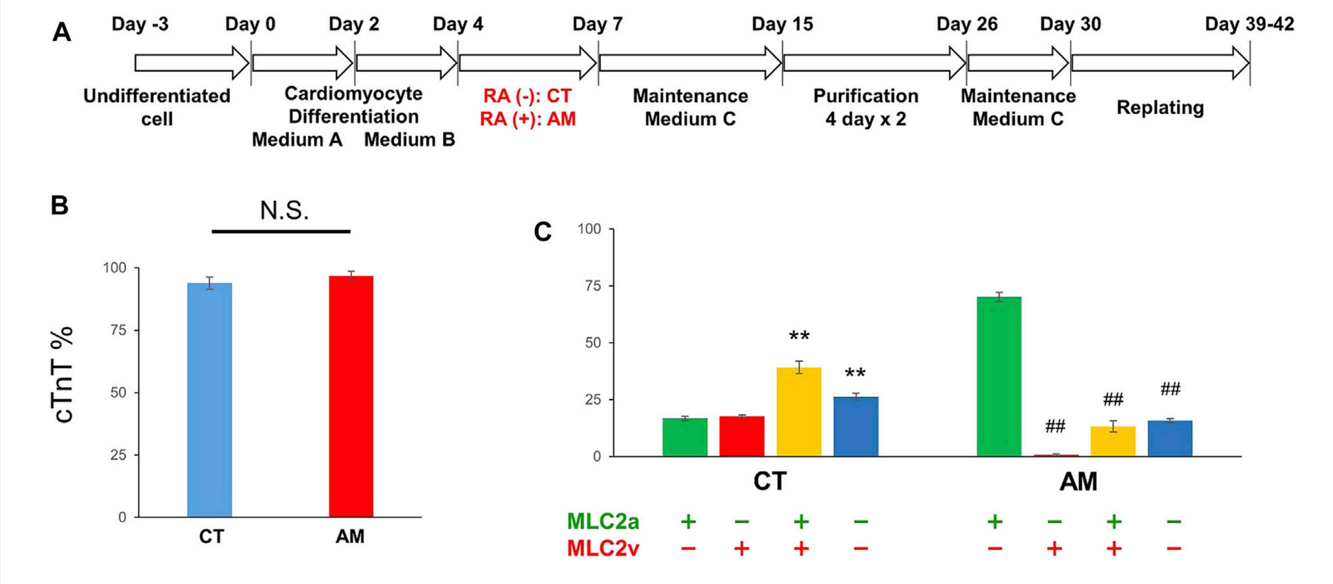

FIGURE 1 | Cardiac differentiation from hiPSCs **(A)** Schematic of the protocol for the differentiation of cardiomyocytes from hiPS cells with (RA (+)) or without RA (RA (–)) treatment **(B)** The ratio of cardiomyocytes quantified by immunostaining with cardiac troponin-T (cTnT). The proportion of cTnT positive cells was 93.91 ± 2.51% in CT (control hiPS-CMs), or 96.79 ± 1.81% in AM (RA-treated hiPS-CMs), respectively (P = N.S.). Error bars represent SD of the mean from the values of independent experiments. $n = 3$. N.S., not significant **(C)** Immunofluorescence analysis of the percentage of MLC2a (atrial isoform) and MLC2v (ventricular isoform) positive expression in the CT and AM. Error bars represent SD of the mean from the values of independent experiments. $^{**}p < 0.01$ for comparison with MLC 2a+/MLC 2v-cardiomyocyte in CT, ##$p < 0.01$ for comparison with MLC 2a+/MLC 2v-cardiomyocyte in AM, $n = 3$.

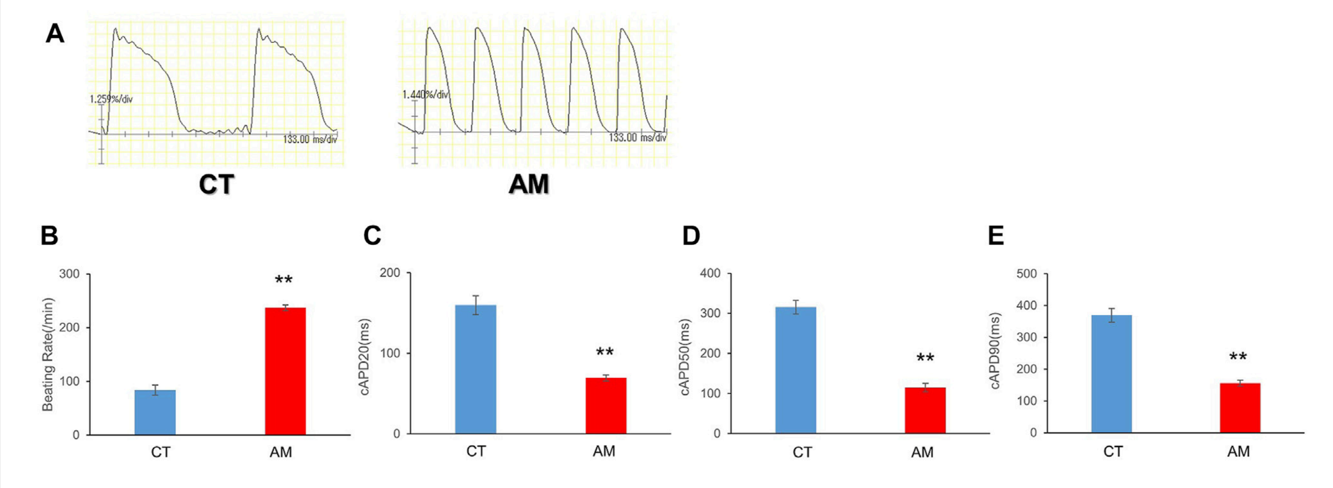

FIGURE 2 | Optical action potential (OAP) of CT (control hiPS-CMs) or AM (RA treatment hiPS-CMs). Representative waveforms for AP of CT or AM. The comparison of AP parameters: beating rate, cAPD20, cAPD50, and cAPD90, between CT and AM. Error bars represent SD of the mean from the values of independent experiments. $^{**}p < 0.01$, $n = 3$.

To examine the electrophysiological properties, we conducted optical mapping of action potentials based on spontaneous beating cardiomyocytes. The AP of AMs displayed a spike-like shape with a steep upslope and downslope, as well as a high frequency, which was more than twice that of CT (**Figures 2A, B**. CT 83.7 ± 9.50/min vs. AM 237 ± 5.20/min). In addition, the action potential duration in AM was significantly shorter than that in CT (**Figures 2C–E**. CT vs. AM: $cAPD_{20}$: 159.8 ± 11.7 vs. 69.8 ± 3.66 ms; $cAPD_{50}$ 315.5 ± 16.93 vs. 114.9 ± 10.7 ms; $cAPD_{90}$ 369.7 ± 21.7 vs. 156.1 ± 9.19 ms).

The above data suggested more atrial-like properties in ATRA-treated AM compared with that of control CT.

High-Throughput Drug Testing Using hiPS-Derived Atrial Myocytes

Using a high-throughput screening system (FDSS/μCell), we assessed the drug toxicity of several experimental drugs on hiPS-derived atrial myocytes as well as control hiPS-derived cardiomyocytes. Membrane potential was used as one of the parameters during the assessment.

After purification, hiPS-derived cardiomyocytes were plated in 96-well plates for downstream drug response assessment using FluoVolt™ Membrane Potential Kit. The results of the analysis of membrane potentials are summarized in **Table 1**. For the proper evaluate the variance of electrophysiological response in CT and AM after drug administration, we have recorded the baseline data of CT and AM respectively (**Supplementary Table 1**). The comparison of variance in the response of drug administration in CT and AM was represented by the percentage of changes based on their baseline values respectively.

hiPS-derived cardiomyocytes without RA (CT) or with RA (AM) were applied with an incremental concentration of I_{Kr} blockers: E-4031, donepezil, and propranolol. The application of E-4031 (0.0003–0.1 μM), donepezil (0.03–10 μM), and propranolol (0.1–100 μM) showed a dose-dependent decrease in beating rate, rising slope, and falling slope of membrane potential in both the CT and the AM (**Figure 3**, **Supplementary Figure 2**). PWD (Pulse width duration) 80cF and PWD30-80 were prolonged as the drug concentration increased. Although under the 0.1 μM E-4031 conditions, both CT and AM showed an increase in membrane potential duration, EAD was elicited in CT (**Figure 3**).

As presented in **Table 2**, E-4031 treatment increased the incidence of EAD in a dose-dependent manner. When treated with 10 μM donepezil on CT, EAD was observed in 2 of 6 cases, while cessation of beating was observed in the remaining 4 cases. However, all of the wells appeared to stop beating in AM under the same dose of donepezil. For the application of propranolol, the CT showed irregular beating or the EAD appeared once the concentration was above 10 μM. Cessation of beating was observed in all cases at a 100 μM dose of propranolol. In the AM, 1 out of 9 samples showed irregular beating at a 10 μM dose of propranolol, and all wells ceased beating at concentrations higher than 30 μM.

With the application of the I_{Ks} channel blocker Chromanol 293B in the range of 0.3–100 μM, CT either AM exhibited a dose-dependent decrease in the rising slope of membrane potential, while an increase in the membrane potential duration was observed (data not shown). When a dose under 100 μM of Chromanol 293B was administered, cessation of beating appeared in 2 of 9 samples in CT and 3 of 12 samples in AM.

To evaluate the response of CT or AM to the I_{Kur} channel blockers, 4-Aminopiridine (4-AP) (0.3–100 μM), DPO-1 (0.01–3 μM), and S9947 (0.03–10 μM) were used within various dose ranges, respectively (**Figure 4**). In AM, the application of 4-AP and DPO-1 exhibited dose-dependent increases in PWD30cF and PWD50cF. S9947 treatment of AM led to a dose-dependent increase in membrane potential duration, and was the highest in PWD30cF. All of the AM samples were arrested after application of 10 μM of S9947, although the half cases were arrested on CT accompanied by a decrease in the amplitude of membrane potential.

Carbachol, which can activate I_{KAch} current, led to a decrease in the beating rate and rising slope of membrane potential in AM; however, no significant difference was observed in the response to CT (**Table 1**). No irregular beating or EAD was elicited on CT either in AM.

As widely used drugs for cardiovascular diseases, the calcium ion channel blocker verapamil and diltiazem, as well as the selective calcium channel activator Bay K8644, were also tested at various concentrations (**Figure 5**, **Supplementary Figure 3**). For CT, verapamil and diltiazem showed dose-dependent increases in beating rate and falling slope of membrane potential. Accordingly, the membrane potential durations decreased, especially for PWD30cF and PWD50cF. However, in AM, except for the dose-dependent increase in the beating rate, no obvious changes were observed in other parameters of membrane potential. At 0.1 μM doses of verapamil and diltiazem, all the AM samples showed cessation of beating. In contrast, Bay K8644 showed a dose-dependent decrease in the falling slope of membrane potential and prolonged membrane potential duration in both CT and AM samples. The CT either AM showed an acute response to Bay K8644, and PWD30 prolonged significantly (**Table 1**).

Carbamazepine treatment in CT led to a decrease in the beating rate and the rising slope of membrane potential, as well as an increase in falling slope and shortened membrane potential duration in a dose-dependent manner (**Figure 6**, **Supplementary Figure 4**). Irregular beating and cessation of beating were induced over application of concentrations above 30 μM. At 100 μM, 11 of 12 cases in CT showed arrest of beating (**Table 2**). In contrast, in AM, no obvious change was observed except a decrease in the rising slope of the membrane potential. However, cessation of beating was observed in half the cases and 5 of 6 cases at concentrations of 30 μM and 100 μM, respectively (**Table 2**).

The effect of phenytoin on CT was characterized by a dose-dependent decrease in the rising slope and an increase in the falling slope of membrane potential (**Figure 6**, **Supplementary Figure 4**). Cessation of beating was elicited when the concentration was higher than 30 μM (**Table 2**). In AM samples, there was also a dose-dependent decrease in the rising slope of membrane potential, though cessation of beating was elicited at the concentration higher than 10 μM. Furthermore, the incidence of cessation of beating increased in a dose-dependent manner (**Table 2**).

DISCUSSION

In the present study, we established a high-throughput drug testing system using human iPS cells derived atrial-like myocytes based on our previous reports (Nakanishi et al., 2019; Hidaka et al., 2003).

The protocol successfully yielded atrial-like myocytes with adequate quality and efficiency, similar to the previous report by (Argenziano et al., 2018).

TABLE 1 | Effects of test compounds in MP of CT or AM. The change scopes of MP parameters are represented by the width of % change.

Drug		Beat Rate	Rising Slope	Falling Slope	PWD30cF	PWD80cF
E-4031	CT	⇓	⬇	⬇	↓	⬆
I_{Kr} inhibition	AM	⇓	↓	⬇		⇑
Chromanol 293B	CT		⇓	↓	⇑	↑
I_{Ks} inhibition	AM		↓		⇑	
4-Aminopridine	CT				↑	
I_{Kur} inhibition	AM				⇑	↑
DPO-1	CT					
I_{Kur} inhibition	AM				⇑	
S9947	CT	⬇	⬇	⇑	⇓	⇓
I_{Kur} inhibition	AM				⬆	⇑
Carbachol	CT					
I_{KAch} activation	AM	↓	↓			
Verapamil	CT	⬆	↓	⬆	⬇	⇓
Cav1.2 inhibition	AM	↑				
Diltiazem	CT	⬆		⬆	⬇	⇓
Cav1.2 inhibition	AM	⇑			↓	
Bay K 8644 (3 min)	CT			↓	↑	↑
Cav1.2 activation	AM		↑	↓	⇑	↑
Propranolol	CT	⬇	⬇	⬇	⇓	⇑
Nav1.5, IKr inhibition	AM	⬇	⬇	⇓		↑
Donepezil	CT	⇓	⇓	⬇		⇑
IKr inhibition	AM	⬇	↓	⬇	↑	⇑
Carbamazepine	CT	⇓	⬇	⇑	↓	↓
	AM		⇓			
Phenytoin	CT		↓	⇑		
	AM		⇓			

Width of % change : ↑↓ 20~30%, ⇑⇓ 30~50%, ⬆⬇ 50%~

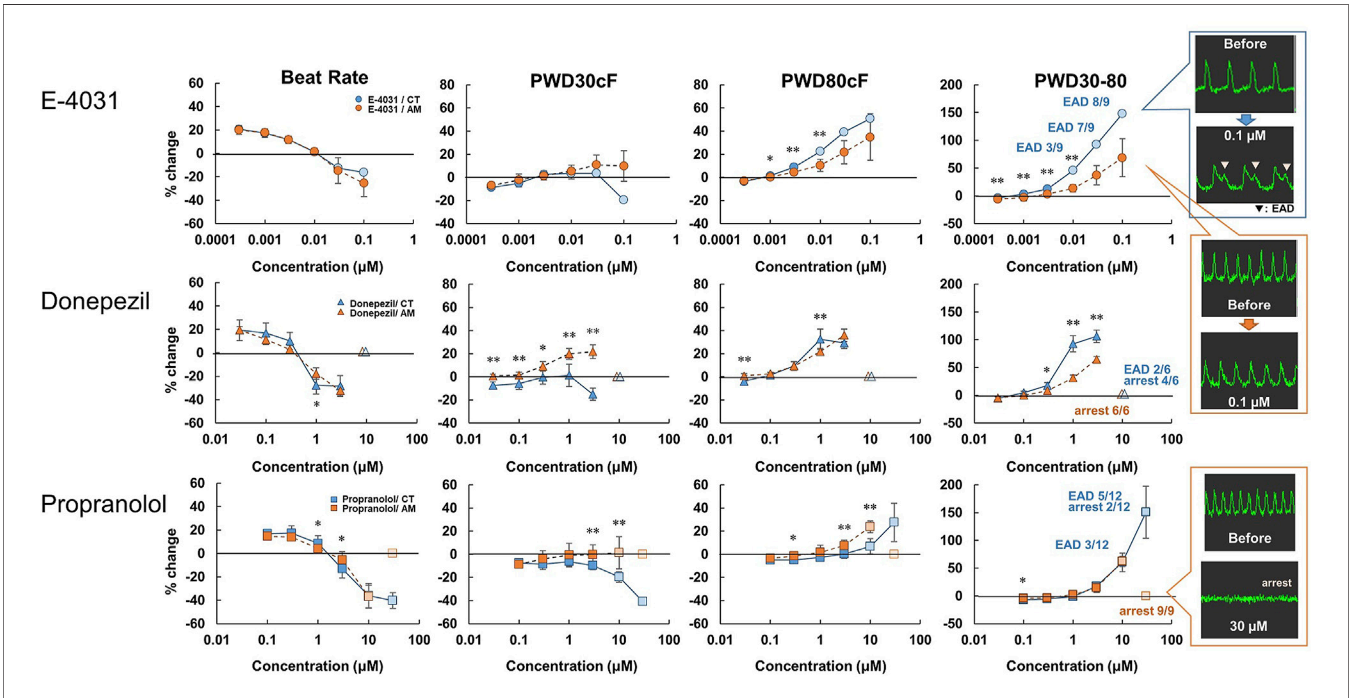

FIGURE 3 | Dose-response of I_{Kr} blockers in CT and AM. CT and AM were treated with various concentrations of E-4031, donepezil, and propranolol, and membrane potential (MP) was analyzed by FDSS/μCell imaging platform. *Y*-axis represents the percentage change from the value before test compound addition. Comparison of MP parameters: beat rate, PWD30cF, PWD80cF, PWD30-80 in CT and AM. Error bars represent SD of the mean from the values of independent experiments. n = 3–12. **p* < 0.05, ***p* < 0.01 for comparison of drug treatment of CT vs. AM (right-most panel) representative waveforms for MP in CT or AM after application of 0.1 μM E-4031. Although both CT and AM showed an increase in membrane potential duration, EAD was elicited in CT. E-4031 data: reuse from the conference paper with permission (Honda, 2020).

In RA-treated myocytes, gene expression levels showed a decrease in ventricle-specific transcription factor IRX4 and an increase in atrium-specific NPPA. On the other hand, those of cardiac ion channels such as Ca^{2+} and K^+ channels, which constitute action potentials, were expressed in both groups, while atrial specific channels such as KCNA5 and KCNJ3 were significantly increased in RA-treated myocytes. These results suggest that RA treatment induces atrial differentiation, similar

TABLE 2 | Effects of test compounds on arrhythmia-like waveforms in CT or AM. The blue frame indicates drug application concentration. Values indicate an incidence of arrhythmia-like waveforms; green column: irregular beat, yellow column: arrest, red column: EAD.

Drug		n	0.0001	0.0003	0.001	0.003	0.01	0.03	0.1	0.3	1	3	10	30	100
			Concentration (μM)												
E-4031	CT	6					50%	83%	83%						
I_{Kr} inhibition	AM	6													
Chromanol 293B	CT	9													22%
I_{Ks} inhibition	AM	12													25%
4-Aminopridine	CT	6													
I_{Kur} inhibition	AM	6													
DPO-1	CT	6													
I_{Kur} inhibition	AM	6													
S9947	CT	6											50%		
I_{Kur} inhibition	AM	6											100%		
Carbachol	CT	9													
I_{KAch} activation	AM	12													
Verapamil	CT	6													
Cav1.2 inhibition	AM	6							100%						
Diltiazem	CT	6													
Cav1.2 inhibition	AM	6									100%				
BayK8644	CT	6													
Cav1.2 activation	AM	6													
Propranolol	CT	3-12											17% 25%	8% 42% 17%	100%
Nav1.5, I_{Kr} inhibition	AM	3-9											11%	100%	100%
Donepezil	CT	6											33% 67%		
I_{Kr} inhibition	AM	6											100%		
Carbamazepine	CT	12												25% 8%	8% 92%
	AM	6												50%	83%
Phenytoin	CT	6												83%	100%
	AM	6											50%	67%	100%

Blue frame shows drug application concentration. Values indicate an incidence of arrhythmia-like waveforms; green column: irregular beat, yellow column: arrest, red column: EAD

to previous reports (Devalla et al., 2015; Argenziano et al., 2018; Lemme et al., 2018; Nakanishi et al., 2005).

The measurement of cardiac action potentials has been used in the research of disease modeling and drug discovery based on hiPS-derived cardiomyocytes, since APs directly recapitulate patients' pathophysiological conditions and reflect the efficacy and cardiotoxicity of pharmacological compounds as drug candidates. Although patch-clamp techniques have been widely used for single-cell-based precise electrophysiological testing, the technique is not suitable for high-throughput screening systems. Thus, in the present study, we employed optical recording using membrane potential dyes (FluoVolt™).

As shown in **Figure 2**, the optical action potentials of CT demonstrated the "plateau" phase, while the shorter action potentials of AM demonstrated a lack of "plateau." This property was recognized as the difference of the ratio APD_{30-40}/ APD_{70-80} in CT (1.30 ± 0.18) and in AM (0.75 ± 0.11) (data not shown). Although the data in the present study was less than the data reported by Argenziano et al. (APD_{30-40}/APD_{70-80}: 0.97 ± 0.12 in CT and AM 0.48 ± 0.0), this may be ascribed to the difference in beating rates (Argenziano et al., 2018).

Based on these properties, hiPS-CTs and hiPS-AMs can be considered stable platforms for electrophysiological testing for drug discovery and development, although the cells may have an immature nature compared to native cardiomyocytes, as reported previously (Feric and Radisic, 2016).

I_{Kr} Blockers

We further verified the feasibility of detecting atrial-specific responses of various pharmacological compounds. In the present study, we examined the effect of E-4031 (an I_{Kr} blocker) on OAP parameters in CT and AM As a result, E-4031 caused dose-dependent increases in PWD80cF and PWD30-80, and a decrease in the rising slope and falling slope in both CT and AM (**Figure 3**, **supplementary Figure 2**). These results are comparable to the previous report by Knobloch stating that I_{Kr} blockers prolonged ventricular repolarization and the atrial refractory period (Knobloch et al., 2002). In addition, it is known that I_{Kr} blockers cause QT prolongation and induce ventricular arrhythmias. Thus, previous papers reported that I_{Kr} blockers showed characteristic proarrhythmic changes in action potentials in ventricular-rich-hiPS-CMs (Ma et al., 2011; Nozaki et al., 2017). In the present study, since EADs were observed in CT but not in AM (**Figure 3**; **Table 2**), induction of proarrhythmic propensity by I_{Kr} blockers in the hiPS-based platform was a ventricular specific phenomenon. Based on this observation, our platform clearly showed the difference between control (induction of arrhythmias) and atrial platform (inhibition of arrhythmias).

Donepezil (Anti-dementia Drug)

Donepezil is a choline esterase inhibitor used to treat Alzheimer's disease and dementia with Lewy bodies, and the drug shows I_{Kr} blocking action with various critical side effects including QT prolongation and lethal ventricular arrhythmias (Kho et al., 2021). Our present data showed that donepezil prolonged the membrane potential duration at a concentration consistent with previous reports 1.3–9.9 μM (Chae et al., 2015) (**Figure 3**). It has been also reported that the drug causes bradyarrhythmias (Rosenbloom et al., 2010; Kuwahata et al., 2021). In the present study, consistent with the

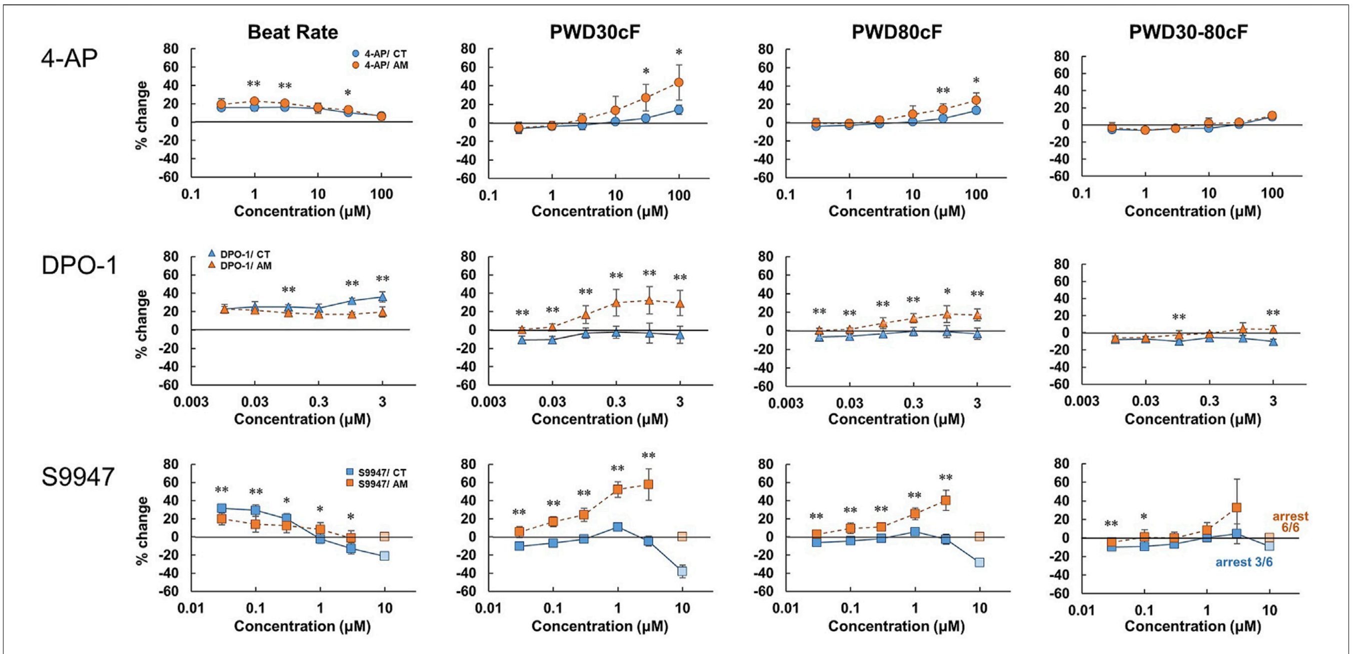

FIGURE 4 | Dose-response of I_{Kur} channel blockers in CT and AM. CT and AM were treated with various concentrations of 4-Aminopiridine (4-AP), DPO-1, and S9947, and MP was analyzed by FDSS/µCell imaging platform. *Y*-axis represents the percentage change from the value before test compound addition. Comparison of MP parameters: beat rate, PWD (Pulse width duration) 30cF, PWD80cF, PWD30-80cF in CT and AM. Error bars represent SD of the mean from the values of independent experiments. n = 6, $^*p < 0.05$, $^{**}p < 0.01$ for comparison of drug treatment of CT vs. AM. DPO-1 data: reuse from the conference paper with permission (Honda, 2020).

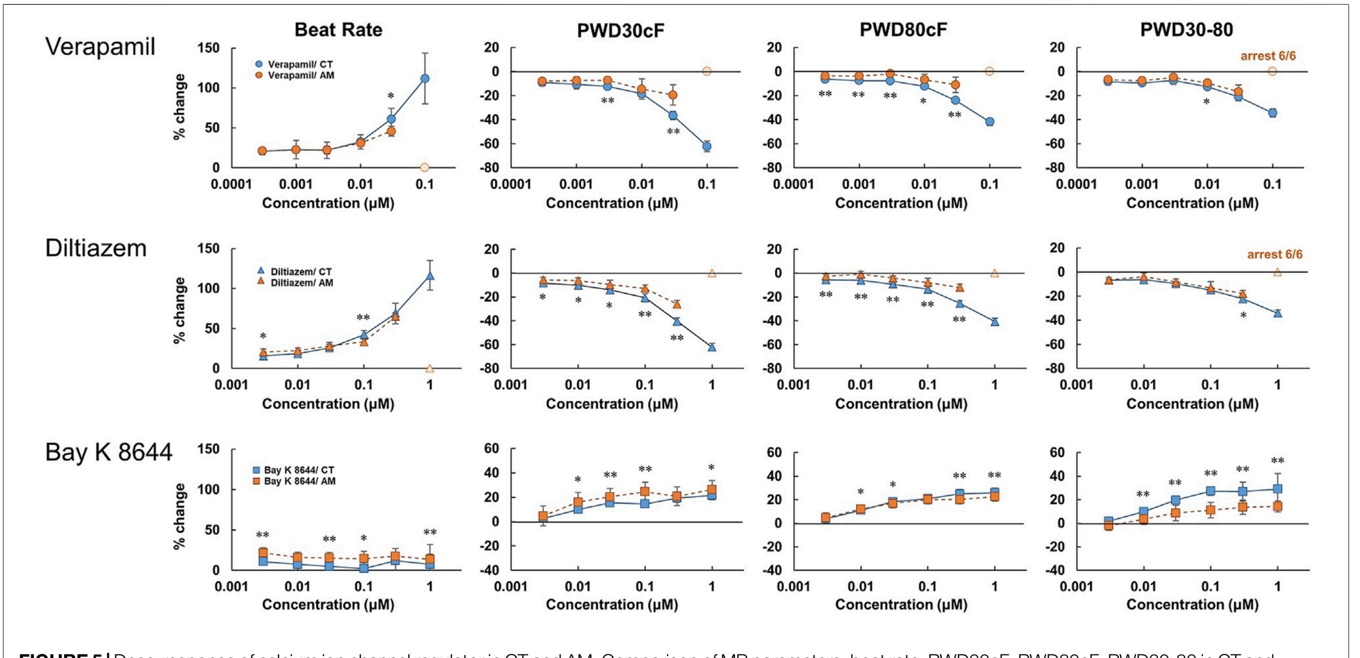

FIGURE 5 | Dose-response of calcium ion channel regulator in CT and AM. Comparison of MP parameters: beat rate, PWD30cF, PWD80cF, PWD30-80 in CT and AM after application of calcium ion channel blocker verapamil and diltiazem, as well as the selective calcium channel activator Bay K 8644. Error bars represent SD of the mean from the values of independent experiments. $n = 6$. $^*p < 0.05$, $^{**}p < 0.01$ for comparison of drug treatment of CT vs. AM. Bay K8644 data: reuse from the conference paper with permission (Honda, 2020).

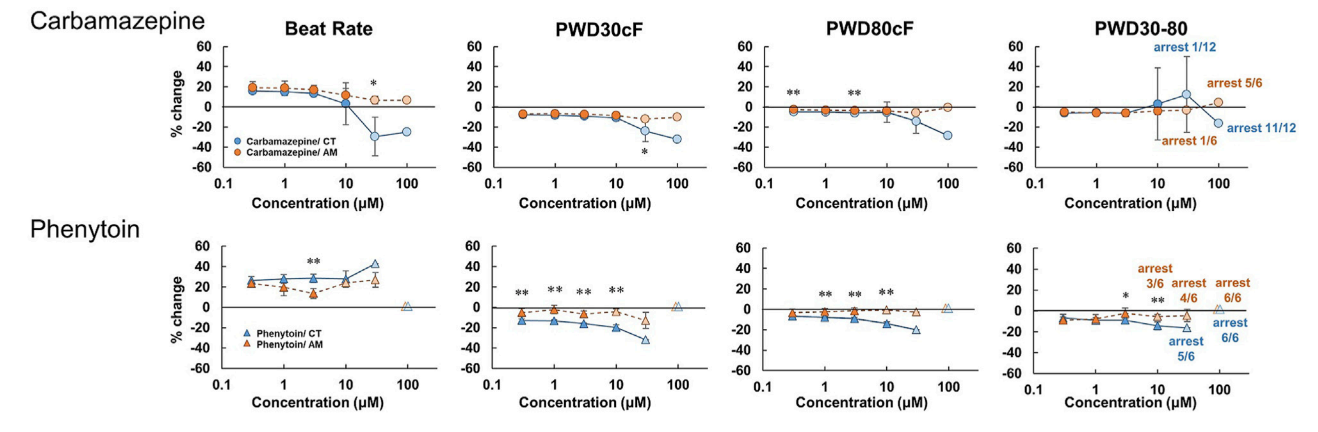

FIGURE 6 | Dose-response of sodium ion channel regulator in CT and AM. Comparison of MP parameters: beat rate, PWD30cF, PWD80cF, PWD30-80 in CT and AM after application of carbamazepine and phenytoin. Error bars represent SD of the mean from the values of independent experiments. n = 6–12. **p* < 0.05, ***p* < 0.01 for comparison of drug treatment of CT vs. AM.

reports, the drug induced the cessation of spontaneous beating in AM and CT at the concentration higher than 30 μM (**Table 2**).

I_{Kur} Blockers

I_{Kur} channels are expressed specifically in the atrium and contribute to atrial repolarization by activating in an ultrarapid manner. I_{Kur} channels have attracted attention because the channel has been considered as a pharmacological target for atrial tachyarrhythmias such as atrial fibrillation (Courtemanche et al., 1999; Nattel et al., 2002). DPO-I, an I_{Kur} inhibitor, showed prolongation of action potentials in human atrial myocytes but not in ventricular myocytes (Lagrutta et al., 2006). In addition, a previous study reported that S9947, another I_{Kur} inhibitor, did not affect ventricular function and porcine ventricular myocytes, but it prolonged the atrial refractory period (Knobloch et al., 2002). In the present study, consistent with the previous reports, DPO-1, S9947, and 4AP (non-selective I_{Kur} inhibitor) showed prolongation in PWD30cF and PWD50cF, but not in CT (**Figure 4**). In addition, our results showed that the KCNA5 gene was more abundantly expressed in AMs than in CT (data not shown). These results suggest that the present system is feasible for detecting the effect of pharmacological compounds on the early repolarization phase through I_{Kur} channels.

Bradyarrhythmias

As for cardiac toxicity, in addition to QT prolongation related to lethal ventricular arrhythmias, life-threatening bradyarrhythmias are also critical rhythm disorders to be avoided. Gene expression patterns in AM suggested that the present system not only shows atrial characteristics but also nodal type cells. Our previous paper reported that retinoic acid-treated hiPS-CMs demonstrated nodal type properties as well as atrial type properties in the gene expression of SHOX2 and HCN4 (Nakanishi et al., 2019). Thus, AM would be useful to detect unexpected electrophysiological action of pharmacological compounds. In the present study, AM demonstrated not only atrial properties but also nodal type, as demonstrated by the increase observed in SHOX2 gene expression and spontaneous beating rates. In this regard, the present system would be useful to detect drug toxicity to induce critical rhythm disorders such as sick sinus syndrome.

I_{KAch} Agonists

I_{KAch} channels are expressed specifically in the atrium as well as I_{Kur}, and contribute to atrial repolarization and resting membrane potentials. The activation of the channel causes shortening and increased dispersion of refractory periods, and these induce atrial reentry following the onset of atrial fibrillation (Liu et al., 1997). In the present study, carbachol, an I_{KAch} agonist, showed a decrease in beating rate and rising slope in AM but not in CT. In the present study, we analyzed the data at the time point (10 min after addition of the drug); however, carbachol caused irregular beats early after application only in AMs (data not shown). This phenomenon suggests that carbachol-induced activation of I_{KAch} led to the increased dispersion of the refractory period, and thus, the optimal analysis time remains to be re-evaluated. In the present system, it is now feasible to evaluate the propensity for drug-induced tachyarrhythmias by comparing the chamber-specific effect of cardiac ion channels of pharmacological compounds.

Ca^{2+} Channel Blockers and Agonist

In the present study, we tested Ca^{2+} channel blockers (verapamil and diltiazem) and an agonist (Bay K 8644). As a result, both verapamil and diltiazem decreased membrane potential duration through the shortening of the plateau phase. On the other hand, Bay K 8644 prolonged membrane potentials, especially PWD30cF in AM as well as in CT. These responses are different from those seen in I_{Kur} blockers, which showed prolongation in AM, but not in CT. In addition, more strikingly, both verapamil and diltiazem caused arrest of spontaneous beating in all the tested samples in the AM at the maximal concentration (**Table 2**). The results may be ascribed to the involvement of nodal type cell type in AMs in which the Ca current plays an important role in generating pacemaker potentials.

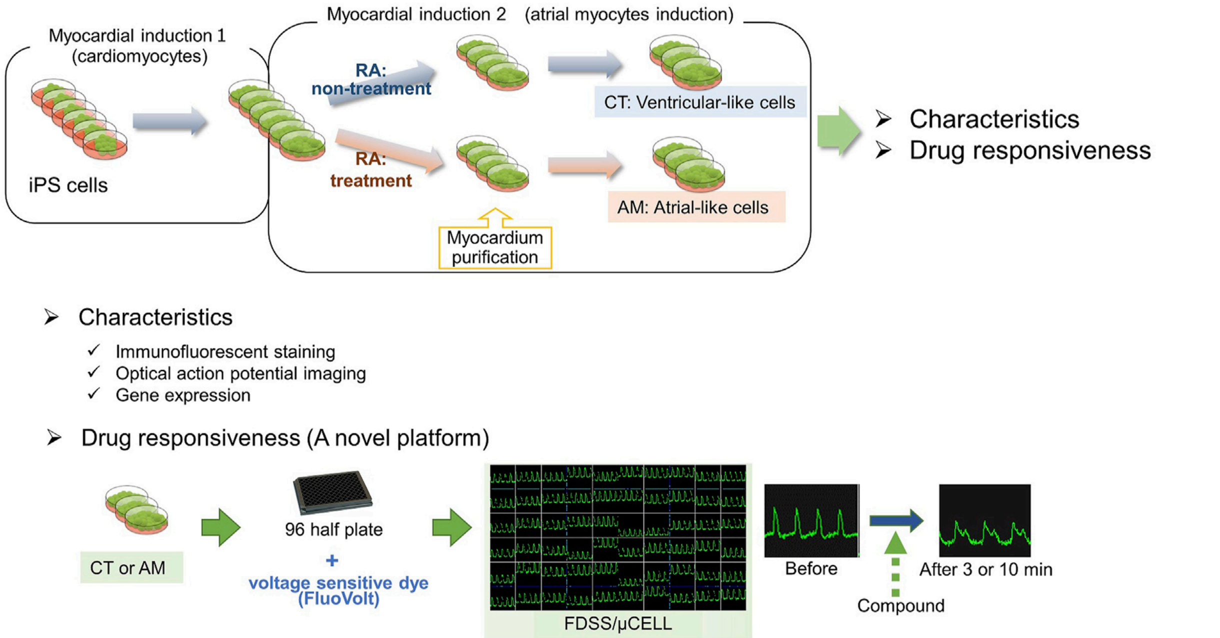

FIGURE 7 | Graphic abstract. In the present study, we generated a hiPS-derived atrial-like phenotype by supplemented RA during the cardiac mesoderm induction. Thereafter, we examined the acute response to several drug administration in the hiPS-CMs with (atrial-like subtype) or without (ventricular-like subtype) treatment of RA by using a high-throughput drug evaluation system, which might be a valuable platform to detect potential risks for drug-induced atrial arrhythmias.

Carbamazepine (Anti-epileptic Drug)

Carbamazepine is an antiepileptic drug that blocks neural Na channels, but the drug is also known to block the cardiac Na^+ channel (Nav1.5) with an IC_{50} of 152.0 μM (Harmer et al., 2011). In the present study, the drug showed a decrease in the rising slope and amplitude of membrane potentials in CT (**Figure 6**, **supplementary Figure 4**). In addition, carbamazepine caused the arrest of spontaneous beating when administered at a dose over 30 μM, more frequently in AM than in CT (**Table 2**). Carbamazepine has been reported to cause a decrease in Vmax and shortening of APD_{50} and APD_{90} in ventricular myocytes of guinea pigs at a concentration of 75 μM (Delaunois et al., 2015). Consistent with the previous study, the effects of carbamazepine on membrane potentials may be attributed to the inhibition of depolarization of ventricular myocytes through blocking of the Nav1.5 current. On the other hand, the membrane potentials of AM showed a decrease in the rising slope only at the maximal concentration. The results may be ascribed to the fact that Ca^{2+} channels, but not Na^+ channels, contribute to membrane potentials mainly in nodal cells, and thus AM were less sensitive to CBZ. The inhibition of the Na^+ current in both atrial-and node-type cells might cause the arrest of spontaneous beating at the maximal concentration.

Phenytoin (Anti-epileptic Drug)

Phenytoin is an antiepileptic drug with neural Na^+ channel blocking action, similar to the action exhibited by carbamazepine. In the present study, phenytoin showed an increase in the falling slope, a slight shortening of membrane potential duration, and arrest of spontaneous beating at concentrations higher than 30 μM in CT, while the drug caused arrests at concentrations higher than 10 μM in AM (**Figure 6**, **supplementary Figure 4**, **Table 2**). These results obtained with phenytoin were similar to those obtained with verapamil and diltiazem. Previous studies reported that phenytoin exhibits an inhibitory action on the cardiac Nav1.5 current and the Cav1.2 current with IC_{50} values of 72.4/120.6 μM and 21.9 μM, respectively Kramer et al., (2013), Harmer et al., (2011), demonstrating that the drug has stronger action on Cav1.2 than Nav1.5. Based on these data, it is conceivable that the results observed with the use of phenytoin in AM may be caused by its heterogenic cellular population including nodal type cells as well as atrial cells.

In the present study, various drugs demonstrated the arrest of spontaneous beatings in AM before the onset of the dysrhythmias in CT, and these results can be explained based on their actions on cardiac ion channels. These results strongly suggest that the detection of drug-induced bradyarrhythmias can be one of the important parameters in addition to the induction of tachyarrhythmias and the velocity/pattern of conduction.

CONCLUSION

We successfully established a platform for human iPS-derived cardiomyocytes with atrial and nodal properties by treatment with retinoic acid (**Figure 7**). Membrane potential-based drug testing on the present platforms would be useful to detect propensities for drug-induced tachyarrhythmias by comparing ventricular and atrial drug responses. In addition, atrial platforms are more sensitive to bradyarrhythmias. This may be achieved with additional parameters for cardiac conduction.

These results suggest that the present evaluation system is useful for developing anti-atrial-arrhythmic drugs as well as for detecting potential risk for drug-induced atrial arrhythmias or rhythm/conduction disturbances.

MATERIALS AND METHODS

The study protocol was approved the Institutional Review Board of Osaka University and all experiments were performed under the guidelines of the Osaka University Gene Modification Experiments Safety Committee.

Cardiac Differentiation of hiPSC-CMs

hiPSCs from a healthy human (RIKEN BRC Cell Bank, Tsukuba, Japan) were subjected to cardiac differentiation using the PSC Cardiomyocyte Differentiation Kit (ThermoFisher SCIENTIFIC). Briefly, undifferentiated hiPSCs were maintained on iMatrix-511 (Nippi, 892,021) in StemFit® AK02N medium (Ajinomoto, AK02N) and passaged enzymatically at 80%–90% confluence.

The hiPSCs were enzymatically dispersed and maintained until 80% confluence with StemFit® AK02N containing 10 μM Y-27632 (Wako, 036-24023). The next day, the culture medium was changed to StemFit® AK02N without Y-27632, which was maintained until the next passage. hiPSCs were seeded on a dish coated with Geltrex LDEV-Free Reduced Growth Factor (ThermoFisher SCIENTIFIC) at 1% concentration in PBS. When the seeded cells reached 80% confluency (day-1), the culture medium was changed to StemFit® AK02N containing Matrigel® (Growth Factor Reduced, Corning, 354,230) at 1% concentration for 24 h. On day0, the culture medium was changed to Medium A (PSC Cardiomyocyte Differentiation Kit, ThermoFisher SCIENTIFIC) containing Matrigel for 48 h. On day2, the culture medium was changed to Medium B (PSC Cardiomyocyte Differentiation Kit, ThermoFisher SCIENTIFIC) for 48 h. On day4, the culture medium was changed to cardiomyocyte maintenance medium (PSC Cardiomyocyte Differentiation Kit, ThermoFisher SCIENTIFIC) supplemented with or without 0.7 μM RA (Sigma Aldrich, R2625) for 72 h. On day 7, the culture medium was changed to cardiomyocyte maintenance medium, and change the medium every 2 days. The cells typically started spontaneous beating around 10 days of initiation of the differentiation protocol. Purification of cardiomyocytes was performed by using a non-glucose medium supplemented with 4 mM lactic acid for 4days/time, performed 2 times (from day 14 to day 18, and from day 21 to day 25), between the 2 times of purifying application, the medium was changed to cardiomyocyte maintenance medium for 72 h (from day 18 to day 21). After purification, the culture was continued in the cardiomyocyte maintenance medium until the functional analysis.

Immunofluorescent Staining

hiPSC-derived cardiomyocytes were fixed with 4% PFA and permeabilized with 0.1% Triton-X in PBS (-) for 15 min at 4°C. Then, the cells were blocked with 5% BSA in PBS (-) for 60 min at room temperature. Primary antibodies were reacted for 24 h at 4°C, and secondary antibodies were reacted for 1 h at room temperature. Nuclei were labeled with Hoechst 33342 (Dojindo, H342). Primary antibodies were anti-Troponin T (clone 13-11) (1:200, Thermo Scientific, MA5-12960), anti-MLC2a (1:200, Synaptic Systems, 311 011), and anti-MLC2v (1:200, ProteinTech, 10906-1-AP). Secondary antibodies were Alexa Fluor 488, donkey anti-mouse IgG (HCL), Alexa Fluor 568, donkey anti-rabbit IgG (HCL), Alexa Fluor 647, donkey anti-mouse IgG (HCL). Fluorescence images were obtained using Operetta high content imaging system (PerkinElmer, Japan) and analyzed using Harmony analysis software (PerkinElmer, Japan).

Optical Action Potential Imaging

hiPSC-CMs were loaded with a voltage-sensitive dye (FluoVolt™ Membrane Potential Kit, F10488, ThermoFisher SCIENTIFIC) for 30 min at RT. The excitation and emission wavelengths were 522 and 535 nm, respectively. Then, 10 μM blebbistatin (Wako, 027-17043), an excitation-contraction uncoupler, was applied to avert motion artifacts. All experiments were performed at 37°C under aerial conditions. Optical action potential (OAP) imaging was acquired at a sampling rate of 5 or 10 ms per frame using the MiCAM02 imaging system (Brainvision, Tokyo, Japan) equipped with a high-speed CMOS camera, alongside field-of-view and spatial resolution, which were 5.76 × 4.8 mm and 30 × 30 μm, respectively. OAP parameters including average CL, $d(-F)/dt_{max}$, and APD, were calculated using OriginPro 8.6J software (LightStone, Tokyo, Japan).

High-Throughput Recording of Membrane Potential Signal Recording

FluoVolt™ Membrane Potential Kit (ThermoFisher SCIENTIFIC, F10488, Massachusetts, United States) was used to measure membrane potentials. The basic procedure was performed in accordance with the manufacturer's instructions. Briefly, the loading dye solution was adjusted with an experimental medium (1% GlutaMAX supplement (ThermoFisher SCIENTIFIC), 1% HEPES (Sigma-Aldrich, Missouri, United States), and 0.001% Pluronic F-127 (Thermo Fisher Scientific) in FluoroBrite DMEM™ (ThermoFisher SCIENTIFIC). After washing the cells twice with the experimental medium, the loading dye solution was added and loaded for 30 min at 37°C. Thereafter, the cells were washed twice with the measurement buffer (1% GlutaMAX supplement, 1% HEPES, 2% fetal bovine serum in FluoroBrite DMEM™). Fluorescence signals representing the membrane potential were measured using FDSS/μCell imaging platform (Hamamatsu Photonics K.K., Hamamatsu, Japan). MP were recorded at excitation and emission stages at wavelengths of 470 and 540 nm, respectively. Measurements were taken during the pre-test, and 10min (except for Bay K 8644, the drug response time was 3 min) post-compound addition. Stock solutions of the test compounds were prepared in 100% DMSO, and serially diluted 1/40 into compound plates for testing (0.5% DMSO was the maximum concentration in all wells). The compounds were automatically pipetted from the compound plate, and 12 μL was loaded in the wells already containing the cells with 48 μL of media.

Recording data were analyzed using Waveform Analysis of Cardiomyocyte Software (Ver.1.2.1J, Hamamatsu Photonics K.K.). Data values for a well were averaged from waveforms that arose during 30 s. The beat rate (BR; beats per minute), waveform amplitude (AMP), and duration at 30, 50, and 80% of decay (PWD30, PWD 50, and PWD 80, respectively) were used as evaluation parameters. PWDs were corrected using the Fridericia formula. PWD30-80 was calculated as the difference between PWD80 and PWD30. Each parameter was calculated as percentage change (%) from the value before test compound addition.

Data Analysis

All data are expressed as mean ± standard deviation (SD). The data were confirmed as normal distribution by the Shapiro-Wilk test. Two independent groups were compared using the Student's t-test for homogeneity variance, and the heteroscedasticity variance by using Welch *t*-test. Multiple groups variance was compared using one-way analysis of variance (ANOVA), followed by Tukey's test. p values of <0.05 were considered statistically significant. Statistical analysis was performed using JMP Pro 14.0 (SAS, Tokyo).

DATA AVAILABILITY STATEMENT

The original contributions presented in the study are included in the article/**Supplementary Material**, further inquiries can be directed to the corresponding author.

ETHICS STATEMENT

The studies involving human participants were reviewed and approved by The Institutional Review Board of Osaka University. The patients/participants provided their written informed consent to participate in this study.

AUTHOR CONTRIBUTIONS

YH, ST, JL and J-KL conceptualized the study, designed and performed the experiments, analyzed the data, and wrote the manuscript. AH analyzed the data, reviewed the manuscript.

FUNDING

This study was supported in part by the Agency for Medical Research and Development, AMED (JP17bm0804008h0001 to J-KL), and Joint Research Grant (Sumitomo-Dainippon Pharma. CO., Ltd).

ACKNOWLEDGMENTS

The authors thank Hiroyuki Nakanishi for technical advice and discussion. The authors are grateful to Mayuko Matsushima, Hideki Yasutake, Yuki Kuramoto and Keiko Miwa for their technical advice and remarks. We would like to thank Editage (www.editage.jp) for language editing. The part of the present study first appeared in the conference paper of the 92nd Annual Scientific Meeting of the Japanese Pharmacological Society [YH. Nihon Yakurigaku Zasshi. 2020; 155(5):303-308]. The permission of the reuse of the contents was granted from the Japanese Pharmacological Society according to the Policies and Publication Ethics of Frontiers (https://www.frontiersin.org/about/policies-and-publication-ethics).

SUPPLEMENTARY MATERIAL

The Supplementary Material for this article can be found online at: https://www.frontiersin.org/articles/10.3389/fphar.2021.680618/full#supplementary-material

REFERENCES

Ando, H., Yoshinaga, T., Yamamoto, W., Asakura, K., Uda, T., Taniguchi, T., et al. (2017). A New Paradigm for Drug-Induced Torsadogenic Risk Assessment Using Human iPS Cell-Derived Cardiomyocytes. *J. Pharmacol. Toxicol. Methods* 84, 111–127. doi:10.1016/j.vascn.2016.12.003

Argenziano, M., Lambers, E., Hong, L., Sridhar, A., Zhang, M., Chalazan, B., et al. (2018). Electrophysiologic Characterization of Calcium Handling in Human Induced Pluripotent Stem Cell-Derived Atrial Cardiomyocytes. *Stem Cel Rep.* 10, 1867–1878. doi:10.1016/j.stemcr.2018.04.005

Berry, E. M., and Hasin, Y. (1978). Propranolol-Induced Dysfunction of the Sinus Node in Wolff-Parkinson-White Syndrome. *Chest* 73, 873–875. doi:10.1378/chest.73.6.873

Bordier, P., Garrigue, S., Barold, S. S., Bressolles, N., Lanusse, S., and Clementy, J. (2003). Significance of Syncope in Patients with Alzheimer's Disease Treated with Cholinesterase Inhibitors. *Europace*. 5 (4), 429-31. doi:10.1016/s1099-5129(03)00080-1

Chae, Y. J., Lee, H. J., Jeon, J. H., Kim, I.-B., Choi, J.-S., and Sung, K.-W. (2015). Effects of Donepezil on hERG Potassium Channels. *Brain Res.* 1597, 77-85. doi:10.1117/12.2081527

Chugh, S. S., Havmoeller, R., Narayanan, K., Singh, D., Rienstra, M., Benjamin, E. J., et al. (2014). Worldwide Epidemiology of Atrial Fibrillation. *Circulation* 129, 837–847. doi:10.1161/CIRCULATIONAHA.113.005119

Courtemanche, M., Ramirez, R. J., and Nattel, S. (1999). Ionic Targets for Drug Therapy and Atrial Fibrillation-Induced Electrical Remodeling: Insights from a Mathematical Model. *Cardiovasc. Res.* 42 (2), 477-489. doi:10.1016/S0008-6363(99)00034-6

Delaunois, A., Colomar, A., Depelchin, B. O., and Cornet, M. (2015). Cardiac Safety of Lacosamide: The Non-clinical Perspective. *Acta Neurol. Scand.* 132, 337–345. doi:10.1111/ane.12413

Devalla, H. D., Schwach, V., Ford, J. W., Milnes, J. T., El-Haou, S., Jackson, C., et al. (2015). Atrial-like Cardiomyocytes from Human Pluripotent Stem Cells Are a Robust Preclinical Model for Assessing Atrial-selective Pharmacology. *EMBO Mol. Med.* 7, 394–410. doi:10.15252/emmm.201404757

Edoute, Y., Nagachandran, P., Svirski, B., and Ben-Ami, H. (2000). Cardiovascular Adverse Drug Reaction Associated with Combined β-Adrenergic and Calcium Entry-Blocking Agents. *J. Cardiovasc. Pharmacol.* 35, 556–559. doi:10.1097/00005344-200004000-00007

Feric, N. T., and Radisic, M. (2016). Maturing Human Pluripotent Stem Cell-Derived Cardiomyocytes in Human Engineered Cardiac Tissues. *Adv. Drug Deliv. Rev.* 96, 110–134. doi:10.1016/j.addr.2015.04.019

Gassanov, N., Er, F., Zagidullin, N., Jankowski, M., Gutkowska, J., and Hoppe, U. C. (2008). Retinoid Acid-Induced Effects on Atrial and Pacemaker Cell Differentiation and Expression of Cardiac Ion Channels. *Differentiation* 76, 971–980. doi:10.1111/j.1432-0436.2008.00283.x

Harmer, A., Valentin, J.-P., and Pollard, C. (2011). On the Relationship between Block of the Cardiac Na+channel and Drug-Induced Prolongation of the QRS Complex. *Br. J. Pharmacol.* 164, 260–273. doi:10.1111/j.1476-5381.2011.01415.x

Hidaka, K., Lee, J. K., Kim, H. S., Ihm, C. H., Iio, A., Ogawa, M., et al. (2003). Chamber-specific Differentiation of Nkx2.5-positive Cardiac Precursor Cells from Murine Embryonic Stem Cells. *FASEB j.* 17, 740–742. doi:10.1096/fj.02-0104fje

Honda, Y. (2020). Availability of a Novel Cardiotoxicity Evaluation System Using Human Induced Pluripotent Stem Cell-Derived Atrial-like Myocytes. *Folia Pharmacol. Jpn.* 155, 303–308. doi:10.1254/fpj.20041

Jensen, M. O., Jogini, V., Borhani, D. W., Leffler, A. E., Dror, R. O., and Shaw, D. E. (2012). Mechanism of Voltage Gating in Potassium Channels. *Science* 336, 229–233. doi:10.1126/science.1216533

Jensen, P. N., Gronroos, N. N., Chen, L. Y., Folsom, A. R., Defilippi, C., Heckbert, S. R., et al. (2014). Incidence of and Risk Factors for Sick Sinus Syndrome in the General Population. *J. Am. Coll. Cardiol.* 64, 531–538. doi:10.1016/j.jacc.2014.03.056

Johnson, C. D., Rivera, H., and Jiménez, J. E. (1997). Carbamazepine-induced Sinus Node Dysfunction. *P. R. Health Sci. J.* 16 (1), 45-9.

Kho, J., Ioannou, A., Mandal, A. K. J., and Missouris, C. G. (2021). Donepezil Induces Ventricular Arrhythmias by Delayed Repolarisation. *Naunyn-schmiedeberg's Arch. Pharmacol.* 394, 559–560. doi:10.1007/s00210-020-02028-4

Knobloch, K., Brendel, J., Peukert, S., Rosenstein, B. x. r., Busch, A., and Wirth, K. (2002). Electrophysiological and Antiarrhythmic Effects of the Novel I Kur Channel Blockers, S9947 and S20951, on Left vs. Right Pig Atrium *In Vivo* in Comparison with the I Kr Blockers Dofetilide, Azimilide, D,l-Sotalol and Ibutilide. *Naunyn Schmiedebergs Arch Pharmacol.* 366, 482–487. doi:10.1007/s00210-002-0599-x

Kramer, J., Obejero-Paz, C. A., Myatt, G., Kuryshev, Y. A., Bruening-Wright, A., Verducci, J. S., et al. (2013). MICE models: Superior to the HERG model in predicting torsade de pointes. *Sci. Rep.* 3, 2100. doi:10.1038/srep02100

Kuwahata, S., Takenaka, T., Motoya, T., Masuda, K., Yonezawa, H., Shinchi, S., et al. (2021). Effect of QT Prolongation in Patients Taking Cholinesterase Inhibitors (Donepezil) for Alzheimer's Disease. *Circ. Rep.* 3, 115–121. doi:10.1253/circrep.CR-20-0115

Lagrutta, A., Wang, J., Fermini, B., and Salata, J. J. (2006). Novel, Potent Inhibitors of Human Kv1.5 K+ Channels and Ultrarapidly Activating Delayed Rectifier Potassium Current. *J. Pharmacol. Exp. Ther.* 317, 1054–1063. doi:10.1124/jpet.106.101162

Lane, D. A., Skjøth, F., Lip, G. Y. H., Larsen, T. B., and Kotecha, D. (2017). Temporal Trends in Incidence, Prevalence, and Mortality of Atrial Fibrillation in Primary Care. *Jaha* 6 (5), e005155. doi:10.1161/JAHA.116.005155

Lee, J. H., Protze, S. I., Laksman, Z., Backx, P. H., and Keller, G. M. (2017). Human Pluripotent Stem Cell-Derived Atrial and Ventricular Cardiomyocytes Develop from Distinct Mesoderm Populations. *Cell Stem Cell* 21, 179–194. doi:10.1016/j.stem.2017.07.003

Lemme, M., Ulmer, B. M., Lemoine, M. D., Zech, A. T. L., Flenner, F., Ravens, U., et al. (2018). Atrial-like Engineered Heart Tissue: An *In Vitro* Model of the Human Atrium. *Stem Cel Rep.* 11, 1378–1390. doi:10.1016/j.stemcr.2018.10.008

Liu, L., and Nattel, S. (1997). Differing Sympathetic and Vagal Effects on Atrial Fibrillation in Dogs: Role of Refractoriness Heterogeneity. *Am. J. Physiol.* 273, H805–H816. doi:10.1152/ajpheart.1997.273.2.H805

Ma, J., Guo, L., Fiene, S. J., Anson, B. D., Thomson, J. A., Kamp, T. J., et al. (2011). High Purity Human-Induced Pluripotent Stem Cell-Derived Cardiomyocytes: Electrophysiological Properties of Action Potentials and Ionic Currents. *Am. J. Physiology-Heart Circulatory Physiol.* 301, H2006–H2017. doi:10.1152/ajpheart.00694.2011

Moss, J. B., Xavier-Neto, J., Shapiro, M. D., Nayeem, S. M., Mccaffery, P., Dräger, U. C., et al. (1998). Dynamic Patterns of Retinoic Acid Synthesis and Response in the Developing Mammalian Heart. *Developmental Biol.* 199, 55–71. doi:10.1006/dbio.1998.8911

Nakanishi, H., Lee, J.-K., Miwa, K., Masuyama, K., Yasutake, H., Li, J., et al. (2019). Geometrical Patterning and Constituent Cell Heterogeneity Facilitate Electrical Conduction Disturbances in a Human Induced Pluripotent Stem Cell-Based Platform: An *In Vitro* Disease Model of Atrial Arrhythmias. *Front. Physiol.* 10, 818. doi:10.3389/fphys.2019.00818

Nakanishi, K., Sudo, T., and Morishima, N. (2005). Endoplasmic Reticulum Stress Signaling Transmitted by ATF6 Mediates Apoptosis during Muscle Development. *J. Cel Biol.* 169, 555–560. doi:10.1083/jcb.200412024

Nattel, S., Khairy, P., Roy, D., Thibault, B., Guerra, P., Talajic, M., et al. (2002). New Approaches to Atrial Fibrillation Management. *Drugs* 62, 2377–2397. doi:10.2165/00003495-200262160-00005

Nozaki, Y., Honda, Y., Watanabe, H., Saiki, S., Koyabu, K., Itoh, T., et al. (2017). CSAHi Study-2: Validation of Multi-Electrode Array Systems (MEA60/2100) for Prediction of Drug-Induced Proarrhythmia Using Human iPS Cell-Derived Cardiomyocytes: Assessment of Reference Compounds and Comparison with Non-clinical Studies and Clinical Information. *Regul. Toxicol. Pharmacol.* 88, 238–251. doi:10.1016/j.yrtph.2017.06.006

Rosenbloom, M. H., Finley, R., Scheinman, M. M., Feldman, M. D., Miller, B. L., and Rabinovici, G. D. (2010). Donepezil-associated Bradyarrhythmia in a Patient with Dementia with Lewy Bodies (DLB). *Alzheimer Dis. Assoc. Disord.* 24, 209–211. doi:10.1097/WAD.0b013e3181b7642b

Schnabel, R. B., Yin, X., Gona, P., Larson, M. G., Beiser, A. S., McManus, D. D., et al. (2015). 50 Year Trends in Atrial Fibrillation Prevalence, Incidence, Risk Factors, and Mortality in the Framingham Heart Study: A Cohort Study. *Lancet* 386 (9989), 154-62. doi:10.1016/S0140-6736(14)61774-8

Stockbridge, N., Morganroth, J., Shah, R. R., and Garnett, C. (2013). Dealing with Global Safety Issues. *Drug Saf.* 36, 167–182. doi:10.1007/s40264-013-0016-z

Thomsen, M. B., Matz, J., Volders, P. G. A., and Vos, M. A. (2006). Assessing the proarrhythmic potential of drugs: Current status of models and surrogate parameters of torsades de pointes arrhythmias. *Pharmacol. Ther.* 112, 150–170. doi:10.1016/j.pharmthera.2005.04.009

Watkins, P. B. (2011). Drug Safety Sciences and the Bottleneck in Drug Development. *Clin. Pharmacol. Ther.* 89, 788–790. doi:10.1038/clpt.2011.63

Xavier-Neto, J., Neville, C. M., Shapiro, M. D., Houghton, L., Wang, G. F., Nikovits, W., et al. (1999). A Retinoic Acid-Inducible Transgenic Marker of Sino-Atrial Development in the Mouse Heart. *Development* 126, 2677–2687. doi:10.1242/dev.126.12.2677

Zhang, Q., Jiang, J., Han, P., Yuan, Q., Zhang, J., Zhang, X., et al. (2011). Direct Differentiation of Atrial and Ventricular Myocytes from Human Embryonic Stem Cells by Alternating Retinoid Signals. *Cell Res* 21, 579–587. doi:10.1038/cr.2010.163

Conflict of Interest: Author YH was employed by the companies Sumitomo Dainippon Pharma Co. Ltd. and Sumika Chemical Analysis Service, Ltd. Author ST was employed by the company Sumitomo Dainippon Pharma Co. Ltd. J-KL and AH belonged to a joint research chair with the companies Sumitomo Dainippon Pharma Co. Ltd., Alpha MED Scientific, Inc. and SCREEN Holdings Co. Ltd.

The remaining authors declare that the research was conducted in the absence of any commercial or financial relationships that could be construed as a potential conflict of interest.

Advantages of publishing in Frontiers

OPEN ACCESS
Articles are free to read for greatest visibility and readership

FAST PUBLICATION
Around 90 days from submission to decision

HIGH QUALITY PEER-REVIEW
Rigorous, collaborative, and constructive peer-review

TRANSPARENT PEER-REVIEW
Editors and reviewers acknowledged by name on published articles

Frontiers
Avenue du Tribunal-Fédéral 34
1005 Lausanne | Switzerland

Visit us: www.frontiersin.org
Contact us: frontiersin.org/about/contact

REPRODUCIBILITY OF RESEARCH
Support open data and methods to enhance research reproducibility

DIGITAL PUBLISHING
Articles designed for optimal readership across devices

FOLLOW US
@frontiersin

IMPACT METRICS
Advanced article metrics track visibility across digital media

EXTENSIVE PROMOTION
Marketing and promotion of impactful research

LOOP RESEARCH NETWORK
Our network increases your article's readership